THE UNIVERSITY OF ADELAIDE

DEPARTMENT OF MECHANICAL ENGINEERING

LIFE CYCLE DESIGN OF DEHUMIDIFIERS IN AIR CONDITIONING

submitted by

Sitaraman Chandra Sekhar, B.E.(Hons)

Thesis for the Degree of Doctor of Philosophy

January 1990

CONTENTS

Summary

The design of dehumidifiers in air conditioning systems has traditionally been based on peak load conditions. Although the peak load criterion is important from the point of view of determining total refrigerating capacity, designs based on peak load alone without due consideration of part loads often fail to satisfy "comfort" conditions at part loads or achieve comfort only by incurring a high energy penalty. Thus, it is very important that dehumidifier design should address the overall perspective of peak and part loads and should maintain the room within the comfort zone over the entire operating demand range. This thesis documents a life cycle design method which satisfies that requirement for dehumidifiers in air conditioning systems.

A prelude to a good design method for dehumidifiers is generalisation - the ability to predict dehumidifier performance with reasonable accuracy at operating conditions other than those which were tested. Hence a fairly extensive testing program was carried out that resulted in the creation of a DATABASE. The most commonly used method of determining the performance of a family of dehumidifier and of selecting a particular dehumidifier for a particular application, known as "The ARI Method" and described in ARI Standard 410 (1981) prepared by the Air Conditioning and Refrigeration Institute of America, was investigated in sufficient detail. The concept of fin efficiency, which is used in the ARI method, is found to be a weak point on the basis of observations of flow through a finned-tube model. An alternative procedure for generalisation, here termed "The Adelaide University (AU) Method" is developed, which avoids some of the weaknesses of the ARI method.

As stated earlier, the primary consideration in the life cycle design of dehumidifiers is to be able to maintain "comfort" conditions in the room over the entire operating range at the expense of minimum energy. In this regard, the "Moisture Staircase" (Sekhar *et al.* 1988) is discussed, which is the phenomenon of thermodynamically adjusting the driving potential for dehumidification between the air and the dehumidifier until the amount of moisture removed from the air at the dehumidifier surface equals the amount of moisture added to the air in the conditioned space. A solution to the inherent problem of "Moisture Staircase" is provided in the form of Low Face Velocity - High Coolant Velocity (LFV/HCV) design methodology (Sekhar *et al.* 1989). The concept of LFV/HCV involves the combination of a low heat transfer coefficient on the air-side and a high heat transfer coefficient on the coolant-side which enables to maintain a low interface temperature and, thereby, enhances dehumidification.

In the LFV/HCV design methodology, it is shown that the "design day" basis for choosing the outside air conditions, as in conventional designs, would be acceptable for peak load but unacceptable for part load which is usually accompanied by a lower dry bulb temperature and a

higher moisture content than the "design day". A means of specifying the outside air condition at part loads (Luxton, Shaw and Sekhar, 1989) is discussed.

The application of the LFV/HCV design methodology is discussed via case studies including an economic appraisal of the LFV/HCV system in one of the case studies. Finally, the thesis is concluded with a discussion on our recent understanding of the human comfort principles which has resulted in the development of "Comfort Integrated LFV/HCV Systems".

Statement of Originality

The material contained in this thesis is original and has not been submitted or accepted for the award of a degree or diploma at any other university. To the best of the author's knowledge and belief, no material which has previously been published or written by another person is included, except when due reference is made in the test of the thesis.

Sitaraman Chandra Sekhar

(January 4, 1990)

Acknowledgements

I wish to express my sincere thanks and gratitude to my supervisors, Professor R.E.Luxton and Dr.A.Shaw, whose unfailing interest, constant encouragement and friendly advice have been instrumental in the developments presented in this thesis. I am grateful to them for the enthusiasm they have displayed throughout the whole project.

To the Departmental staff, thanks are due for their assistance in the preparation of the experimental facilities used for this work, in particular to Mr.E.Browne, Mr.R.Jager, Mr.S.De Ieso, Mr.M.Bethune, Mr.H.Bode and Mr.A.Mittler. I would like to acknowledge the help of Mrs.M.Heslop, Mrs.M.Piccinino, Mrs.C.Unger and Mrs.J.Hughes with several administrative matters at various stages of my work.

Thanks are also due to the members of the staff and my fellow post-graduate students in the Department of Mechanical Engineering for their comments during discussions.

I am indebted to my wife, Nirmala, to my parents in India and to my uncle and aunt in Adelaide for their patience, encouragement and support without which the completion of this thesis would not have been accomplished.

Finally, I wish to acknowledge the award of an Adelaide University Postgraduate Research Grant scholarship and a valuable Grant-In-Aid from the American Society of Heating, Refrigerating and Air-Conditioning Engineers (ASHRAE), believed to be the first such student award made by ASHRAE outside North America.

NOMENCLATURE

A

A	Area, {m^2}
A_o	Total external surface area, $A_o = A_D + A_W$, {m^2}
A_p	Net primary surface area, {m^2}
A_s	Net secondary surface area, {m^2}
A_{ix}	Total cross-sectional flow area inside tubes, {m^2}
A_f	Coil face area, {m^2}
A_i	Total internal coil surface area, {m^2}
A_{min}	Minimum free flow area, {m^2}
A_{cD}	Total "calculated external dry surface area", {m^2}
A_{cW}	Total "calculated external wet surface area", {m^2}
A_c	Total "calculated external surface area", $A_c = A_{cD} + A_{cW}$, {m^2}
A_D	Total external dry surface area, {m^2}
A_W	Total external wet surface area, {m^2}

B

B	Ratio of total external coil surface to the total internal surface, A_o/A_i.

C

C	Coil characteristic $[(R_m + R_w)/(R_{aW}\, c_p)]$, {kg(°C)/kJ}
c	Heat transfer exponent (ARI method), {Dimensionless}
c_1	Heat transfer exponent (AU method), {Dimensionless}
c_p	Air humid specific heat, (A constant value of 1.022 is used to simplify calculation and rating procedure), {kJ/(kg°C)}
c_{pw}	Specific heat capacity of water, {4.187 kJ/(kg.K)}

D

D_i	Tube inside diameter, {mm}
D_o	Tube outside diameter, {mm}
D_f	Equivalent outer diameter of a flat circular plate fin of equal area as that of a rectangular plate fin, {mm}
D_e	Equivalent hydraulic diameter (Gunter and Shaw method), {m}
D_h	Equivalent hydraulic diameter (Kays and London method), {m}

F

F_H	$S_f - D_o$, {mm}
f_a	Air side convective heat transfer coefficient referred to total external surface area, A_o : (a) f_{aD} for dry surface, (b) f_{aW} for wet surface, {W/(m^2°C)}
f_w	Tube side water film heat transfer coefficient referred to total external surface area, {W/(m^2°C)}

G

G	Mass velocity of air, {kg/(s.m^2)}

H

H_f	Coil face height, {mm}
H	Enthalpy of air, {kJ/kg}
H_1	Enthalpy of air at coil entering conditions, {kJ/kg}
H_2	Enthalpy of air at coil leaving conditions, {kJ/kg}
H_1"	Enthalpy of air at entering dew point temperature, {kJ/kg}
H_B	Enthalpy of air at dry wet boundary conditions, {kJ/kg}
H_s	Enthalpy of saturated air at coil surface temperature, t_s, {kJ/kg}
H_{s1}	Enthalpy of saturated air at entering coil surface temperature, t_{s1}, {kJ/kg}
H_{s2}	Enthalpy of saturated air at leaving coil surface temperature, t_{s2}, {kJ/kg}
$H_{\bar{s}}$	Enthalpy of saturated air at effective coil surface temperature, $t_{\bar{s}}$, {kJ/kg}
H_{wm}	Saturated enthalpy at mean water temperature, t_{wm}, {kJ/kg}
H_{sm}	Log mean enthalpy at wetted surface temperature, t_{sm}, {kJ/kg}
H_m	Log mean air enthalpy, {kJ/kg}
ΔH_m	Log mean enthalpy difference.
ΔH	Enthalpy difference.
h_i	Combined coefficient of heat transfer through the outside condensate layer and the tube side water film, {W/(m^2°C)}
h_{cow}	Convective heat transfer coefficient for outside wetted surface, {W/(m^2°C)}
h_{do}	Mass transfer coefficient, {kg/(s m^2)}

I

I_{cl}	Thermal resistance of clothing, {clo}

K

k_f	Fin material thermal conductivity, {W.mm/(m^2 °C)}
k_t	Tube material thermal conductivity, {W.mm/(m^2 °C)}
k	Constant as defined by equation (12.2).

k_d	Constant as defined by equation (12.3).
k_1	Constant in the fan air volume flow equation $Q_{sa} = k_1[(\Delta P)_a]^{0.5}$.
k_2	Constant in the transmission load equation $q_{st} = k_2(t_{amb}-t_a)$.

L

L	Length, {mm}
L_d	Length of the fin in the direction of air flow (Fig A1.1), {mm}
L_c	Length of collar (Fig A1.2), {mm}
L_f	Length of the fin corresponding to the coil face height (Fig A1.1), {mm}
L_t	Fin tube length (Fig A1.1), {mm}
Le	Lewis number = $h_{cow}/(h_{do} \cdot c_p)$, {Dimensionless}

M

m_a	Mass flow rate of air, {kg/s}
m_{sa}	Mass flow rate of suply air, {kg/s}
m''	Slope of saturated air temperature-enthalpy curve at the coil surface temperature, t_s, {kJ/(kg°C)}
m_c	Amount of condensate measured by primary means, {g/s}
m_c'	Amount of condensate by psychrometric calculations, {g/s}

N

N_h	Number of tube holes per fin.
N_t	Number of tubes.
N_f	Number of fins per inch.
N_{fT}	Total number of fins.
N_{tr}	Number of tubes per row.

P

P	Absolute pressure, {kPa}
P_{sa}	Supply air pressure, {Pa}
P_{ra}	Return air pressure, {Pa}
$(\Delta P)_a$	Air pressure drop, {Pa}
Pr	Prandtl number $[(\mu c_p)/k]$, {Dimensionless}

Q

$(Q_a)_{std}$	Air volume flow at ASHRAE standard conditions, {l/s}
$(Q_a)_{act}$	Actual air volume flow, {l/s}
Q_{sa}	Supply air volume flow, {l/s}

q_t	Total heat capacity, {W}
q_s	Sensible heat capacity, {W}
q_{tD}	Dry surface capacity, {W}
q_{tW}	Wetted surface capacity, {W}
q_{st}	Transmission load, {W}
q_{sz}	Zone sensible load, {W}

R

R	Thermal resistance, referred to total external surface area, A_o, {$(m^2 °C)/W$}
R_f	Fin material thermal resistance, {$(m^2 °C)/W$}
R_t	Tube material thermal resistance, {$(m^2 °C)/W$}
R_w	Inside tube water film thermal resistance, {$(m^2 °C)/W$}
R_m	Total metal thermal resistance, $R_m = R_f + R_t$, {$(m^2 °C)/W$}
R_{mD}	Total metal thermal resistance for dry surface, {$(m^2 °C)/W$}
R_{mW}	Total metal thermal resistance for wet surface, {$(m^2 °C)/W$}
R_{aD}	Air film thermal resistance for dry surface, {$(m^2 °C)/W$}
R_{aW}	Air film thermal resistance for wet surface, {$(m^2 °C)/W$}
R_i	Combined thermal resistance for outside condensate layer, metal and inside film, B/h_i, {$(m^2 °C)/W$}
(R_m+R_{ow})	Combined thermal resistance for outside condensate layer and metal, as defined by equation (6.33a), {$(m^2 °C)/W$}
R_{cow}	Wetted surface air film thermal resistance, {$(m^2 °C)/W$}
Re	Reynolds number $[(D_h G)/\mu]$, {Dimensionless}

S

St	Stanton number $[h_{cow}/(G c_p)]$, {Dimensionless}
S_f	Tube spacing in the plane of the fins (Fig A1.1), {mm}
S_r	Tube spacing between rows (Fig A1.1), {mm}
S_1	Tube spacing from the edge of the fin at air entry to the coil (Fig A1.1), {mm}
S_2	Tube spacing from the edge of the fin at air exit from the coil (Fig A1.1), {mm}

T

TLS	Tie line slope $[-(c_p h_i A_i)/(h_{cow} A_o)]$, {kJ/(kg°C)}
t_1	Entering air dry bulb temperature, {°C}
t_2	Leaving air dry bulb temperature, {°C}
t_1'	Entering air wet bulb temperature, {°C}
t_2'	Leaving air wet bulb temperature, {°C}

t_1''	Entering air dew point temperature, {°C}
t_2''	Leaving air dew point temperature, {°C}
t_{s1}	Coil surface temperature at air entry, {°C}
t_{s2}	Coil surface temperature at air exit, {°C}
$\bar{t}_s$	Effective coil surface temperature, {°C}
t_{sm}	Log mean wet surface temperature (obtained from psychrometric chart at H_{sm}), {°C}
t_B	Air dry bulb temperature at dry wet boundary, {°C}
t_{wB}	Tube side water temperature at dry wet boundary, {°C}
t_{w1}	Entering water temperature, {°C}
t_{w2}	Leaving water temperature, {°C}
t_{wm}	Mean water temperature, {°C}
Δt	Temperature difference.
Δt_m	Log mean temperature difference.
t_{ra}	Room air temperature, {°C}
t_{sa}	Supply air temperature, {°C}
$\bar{t}_r$	Mean radiant temperature, {°C}
t_g	Globe temperature, {°C}
t_o	Operative temperature, {°C}
t_{amb}	Outside ambient temperature, {°C}

U

U	Overall heat transfer coefficient referred to total external area, A_o, {W/(m^2°C)}

V

$(V_a)_{std}$	Standard face velocity, {m/s}
$(V_a)_{act}$	Actual face velocity, {m/s}
V_w	Average water velocity inside tubes, {m/s}
V_{rv}	Relative air velocity, {m/s}
v	Specific volume, {m^3/kg}

W

W	Humidity ratio, {kg/kg}
W_w	Water flow rate, {kg/s}
w	Height of equivalent annular fin, {mm}

X

x_b	Fin root radius, {mm}
x_e	Radius of equivalent circular area of a rectangular plate fin ($D_f/2$), {mm}

Y

Y_f	Fin thickness (Fig A1.2), {mm}
y	Ratio of water temperature rise to air enthalpy drop, {(kg°C)/kJ}

GREEK SYMBOLS

μ	Dynamic viscosity, {Pa.s}
η	Total surface effectiveness.
ϕ	Fin efficiency.
ρ_{std}	Standard density of moist air, {1.204 kg/m^3}
ρ_{act}	Actual density of moist air at the psychrometric conditions, {kg/m^3}
ρ_{sa}	Density of supply air, {kg/m^3}
ρ_w	Standard density of water, {1000 kg/m^3 = 1 kg/litre}
θ	Louvre angle.

List of Tables

List of Figures

Chapter 1

AN INTRODUCTION TO THE OVERALL SYSTEM DESIGN OF DEHUMIDIFIERS

The dehumidifier is the most important component in the entire air conditioning system. Thermodynamically the dehumidifier, by itself will offset the sensible and latent heat loads in the proportion in which they occur, from peak to minimum part load. The psychrometric state of the conditioned air at the end of this process should ideally be that which satisfies the requirements of the process or the occupants of the room.[1] Failure to achieve the desired state directly was not a serious problem before the energy crisis since the design objective could be obtained by overcooling and reheating. Today this proposition is no longer acceptable and either insufficient dehumidification or excessively cold temperatures are particularly evident during part load conditions in both CAV and VAV systems. Although there is some flexibility in the range within which the humidity of a space may be allowed to vary from the design condition, a commonly occurring set of circumstances can cause the performance to deteriorate into the non-acceptable range.

Consider the dehumidification requirements when any or several of the following conditions occur :

a) During part load the sensible heat load reduces while the latent heat load remains constant or increases.

b) During part load the dew point temperature of the outside air is higher than at peak design load.

c) In a VAV system the humidity in the room is not controlled. The thermostat senses that a part load condition exists but the population density of the building is constant.

d) There is a high ventilation load.

e) A single air-handling unit with a single dehumidifier is employed to serve an entire floor of an office building as a multi-zone unit.

1/ The term "room" is used throughout this thesis to designate the conditioned space or an average of several spaces which form a "zone", regardless of the function of the space or spaces.

In each case a steeper coil condition curve than that required at peak load is necessary. In (a) the sensible heat ratio reduces. In (b) the mixture of outside and return air is at a higher dew point temperature. In (c) again the sensible heat ratio is decreased and in both (c) and (d) as VAV flow reduces the ventilation load must remain the same. Thus if at peak load 15 % outside air is required, then at 50 % part load 30 % outside air is necessary to meet the ventilation load. Again a steeper coil condition curve is required. In (e) the air handling unit responds to some weighted average of the zone conditions and, if there is any variation in humidity within a zone or between zones, spaces with the higher humid loads can be under served. It is apparent that to satisfy psychrometric requirements under the above conditions, which can occur simultaneously, is a most demanding heat and mass transfer design problem.

Traditionally dehumidifier design has been based on the peak load alone. Although the importance of the peak load criterion is recognised, design based on the peak load alone without due consideration of part loads often fails to satisfy comfort conditions at part loads (Gupta et al, 1987) or achieves comfort only by incurring a high energy penalty. It is strongly recommended that dehumidifier design should address the overall perspective of peak and part loads and should maintain the room within the comfort zone over the entire operating demand range. This leads to the life cycle design method for dehumidifiers in air-conditioning systems the evolution of which is documented in this thesis.

The thesis begins with a brief historical review of dehumidifier design, a summary of conventions concerning face velocity (the velocity of air as it approaches the inlet face of the dehumidifier) and a discussion of the concept of fin efficiency, which is seen as being a weak point in the mixture of theory and empiricism on which the design of dehumidifiers is presently based. The most commonly used method of determining the performance of a family of dehumidifiers and of selecting a particular dehumidifier for a particular application, known as "The ARI Method" and described in Standard 410 (1981) prepared by the Air Conditioning and Refrigeration Institute of America, is then described and assessed in detail. An alternative procedure, here termed "The Adelaide University (AU) Method", which avoids some of the weaknesses of the ARI method, is offered in Chapter 6. The AU method is based on an extensive program of testing, described in Chapter 8, in the unique controlled environment wind tunnel described in Chapter 7.

Computerised coil selection programs developed for the ARI and the AU methods are discussed in Chapters 5 and 6 respectively. Based on a critical comparison of the predictions of the two programs with actual test results, tabulated in Appendix 5, the AU method is preferred and used for selecting the Low Face Velocity/High Coolant Velocity (LFV/HCV) coils in the case studies in Chapter 11. The LFV/HCV concept is described in Chapter 9 and the design methodology, evolved from this concept is presented in Chapter 10. The LFV/HCV design methodology addresses the

overall perspective of peak and part loads and strives to maintain comfortable conditions in the room at all times. Recent understanding of the human comfort principles has resulted in the development of "Comfort Integrated LFV/HCV Systems" which is discussed in Chapter 12.

Chapter 2

HISTORICAL REVIEW OF DEHUMIDIFIER DESIGN

2.1 Introduction

An important aspect of the design of dehumidifiers is the accurate prediction of their performance for a given set of operating conditions. Whilst a long term goal is to be able to calculate fully the flow through a dehumidifier from the governing equations, at the present time, a good method of performance prediction can only result from an accurate and detailed experimental study of dehumidifiers combined with the formulation of a physically sound interpretation of the complicated thermodynamic, heat transfer and fluid flow processes.

Despite the complex geometry, the determination of cooling coil performance is relatively simple when the air is sensibly cooled on a dry coil surface if reliable average heat transfer coefficients are available. However, the majority of cooling coil applications require dehumidification as well. This requirement considerably complicates the problem, as both heat and mass transfer must be considered.

When the surface temperature of a coil is below the dew point temperature of the air, water vapour in the air is condensed and both heat and mass are transferred to the coil surface. In a cooling coil, the air dry and wet bulb temperatures and the coolant temperatures vary as the air is being cooled. Consequently, the coil surface temperatures also vary throughout the coil. The major difficulty in the accurate prediction of dehumidifying coil performance lies in the determination of this varying surface temperature.

The Air-conditioning and Refrigeration Institute of America (ARI) has specified a standard basic method by which the performance of cooling and dehumidifying coils may be rated in the air face velocity range of 1.02m/s - 4.06m/s (200 ft/min - 810 ft/min). The ARI method of evaluating the cooling coil performance will be considered in detail later in this thesis, but at this point it is pertinent to review the background to the assumptions concerning the wet surface performance of coils used in the method. It is evident from Fig 5.1, which ignores the geometric complexities of the typical tube and plate-fin dehumidifier, that wet surface performance prediction is not a simple problem. The following two quotations dating from the mid-1970's are indicative of the state of the art even today :

> *"The present state-of-the-art does not afford a clear relationship between sensible heat transfer coefficients and combined heat and mass transfer coefficients; and it is not known when the analogy is true and when it is not." (McQuiston, F.C., 1976).*

"Unfortunately, the amount of heat transfer, mass transfer and friction factor data published in the open literature for a given configuration is very limited and the data available for condensing of water from the air for a specific heat exchanger are almost nonexistant." (Tree, David R. and Helmer, Wayne A., 1976).

The second of these quotations suggests that the authors may have suspected that manufacturers have substantial data sets which have not beeen published in the open literature. While this is probably correct, experience with at least one major manufacturer's coil rating and selection program suggests that it depends primarily on the ARI method into which all major manufacturers and many leading researchers had input. It is therefore reasonable to presume that the ARI method is representative of the state of the art. Some important contributions to the evolution of this art are briefly summarised below.

2.2 Goodman (1938)

Goodman defined an overall enthalpy potential by multiplying the temperature potential between the coil surface and the refrigerant by a factor with the dimensions of specific heat. This factor he defined as the average of the values obtained from experiments over a range of surface temperatures. While the overall enthalpy potential is a valuable aid to conceptual thinking, its detailed application can introduce inaccuracies which are inherent since the actual surface temperature varies spatially. Goodman's method also fails to account for the effect of dehumidification on the fin efficiency.

2.3 Brown (1954)

Brown extended Goodman's (1938) approach by establishing an enthalpy potential between the tube surface and the air and using a trial and error calculation to find an effective tube surface temperature. Although this method takes into account the effect of dehumidification on the fin efficiency, it requires an intricate iterative solution to obtain results of acceptable accuracy as the fin efficiency is dependent on the mean temperature of the fins.

2.4 Heating and Cooling Coil Manufacturer's Association (HCCMA 1955)

An overall potential is defined between the air dry bulb and the refrigerant temperature by applying an "adjustment factor" to the air-side coefficient. This factor is the ratio of total to sensible heat. Since both the potential and the adjustment factor are functions of the final dry bulb temperature, the method is extremely sensitive to inaccuracies in the air dry bulb temperature determination.

2.5 Ware and Hacha (1960)

Ware and Hacha calculated the amount of wet surface required to perform a given duty and compared this with an experimental determination of the amount of surface required for the same duty. The heat transfer coefficients used were derived from sensible heat transfer (dry coil) tests. They found that the calculated and empirically determined areas were within 2.5% of each other and concluded that sensible heat transfer coefficients can be used for predicting the wet surface performance.

2.6 McElgin and Wiley (1940)

McElgin and Wiley adopted a dual potential method; an enthalpy potential from the air to the wetted surface and a temperature potential from the surface through the fins and tubes to the water. As the ARI method is fundamentally based on this approach, it will be discussed in detail in subsequent chapters.

2.7 Myers (1967)

The aim of the project undertaken by R.J.Myers was to determine the effect of dehumidification on the air-side heat transfer coefficient for a finned-tube coil. He observed that the heat transfer coefficients obtained from the wet surface tests were two to ten percent higher than those obtained from the dry surface tests when both were correlated using the maximum mass velocity within the coil. For the same air flow rate the maximum mass velocity within the coil is eight percent more for the wet surface tests than for the dry surface tests due to the reduction in the free flow area caused by the water film on the surface.

Chapter 3

STANDARD AND ACTUAL FACE VELOCITIES

Since the specific volume of air varies appreciably, it is recommended to analyse the performance of dehumidifiers using the mass of air instead of the volume. However, volume values are required for selecting coils, fans and ducts. A traditional practice in the air-conditioning industry is the use of volume values based on measurement at ASHRAE standard conditions. The standard value is 1.204 kg of dry air/m^3 (0.83 m^3/kg of dry air) which corresponds to approximately 16°C at saturation and 21°C, dry at 101.4 kPa.

As described later in Chapter 8, the actual volume flow rate is measured by the venturi in the unique closed cycle thermal environment wind tunnel and consequently the Database is in terms of actual volumes for all the empirical tests. In the analysis of these tests by the ARI (Air-conditioning and Refrigeration Institute) and the AU (Adelaide University) methods, the actual volume flow has been used as input to the relevant data reduction computer programs. However, as the ARI method uses standard volumes and standard face velocity the actual inputs are translated to the required standard forms before entering the main ARI programs.

The ARI Method

The actual volume flow, $(Q_a)_{act}$, is the input to the data reduction program "ARI DATA REDUCTION". The standard volume flow, $(Q_a)_{std}$, is then obtained as follows:

Actual mass flow rate = Standard mass flow rate

$$(Q_a)_{act}\ \rho_{act} = (Q_a)_{std}\ \rho_{std} \qquad (3.1)$$

where $\rho_{act} = \dfrac{1 + W_1}{v_1}$, $\rho_{std} = 1.204$ kg/m^3 ,

W_1 = Humidity ratio at entering air condition

and v_1 = Specific volume at entering air condition.

Thus

$$(Q_a)_{std} = \frac{(Q_a)_{act}\ \rho_{act}}{1.204} \ . \qquad (3.2)$$

The standard face velocity is then given by

$$(V_a)_{std} = \frac{(Q_a)_{std}}{\text{Face Area}} \quad . \qquad (3.3)$$

The standard face velocity plays an important role in the development of air film thermal resistances as will be described in detail in Chapter 5.

The coil performance prediction **"ARI GENERALISATION PROGRAM"** can accept either the actual or the standard volume flow although the program is fundamentally structured to use $(V_a)_{std}$ to be consistent with the requirements of the ARI method. If actual volume flow is the input, the actual density and thus the actual mass flow is computed and then the equivalent standard volume flow is obtained.

The above two programs are described in detail in Chapter 5.

The AU Method

The actual volume flow is the input to the data reduction program **"TLS BY LEWIS NUMBER CORRELATION"** and the mass flow rate is obtained by considering the actual density. It will also be apparent from the data reduction procedures described in Chapter 6 that the mass flow rate is used consistently throughout the analysis. The determination of $(V_a)_{std}$ or $(V_a)_{act}$ does not play an important role in the determination of the heat and mass transfer coefficients as it is the mass velocity contained in the Reynolds and Stanton numbers which is significant.

The **"ADELAIDE UNIVERSITY (AU) COIL SELECTION PROGRAM"** is fundamentally structured to use the mass flow rather than the volume flow. However, it can accept either the actual or the standard volume flow and computes the mass flow rate using the relevant (actual or standard) density. Both the standard and the actual face velocities are given in the output of the program.

The above two programs are described in detail in Chapter 6.

Chapter 4
FIN EFFICIENCY

4.1 Introduction

In a conventional heat exchanger which employs primary surface alone, heat is transferred from one fluid to another through a metallic wall and, under the given constraints, the rate of heat flow is directly proportional to the extent of the wall surface and to the temperature difference between one fluid and the adjacent surface. In the case of an extended surface heat exchanger, the use of fins on the primary surface, extending into one of the fluids, increases the total surface for heat transfer and it might be expected that the rate of heat flow per unit of basic surface would increase in direct proportion. However, the surface temperature of these fins must vary if they are to conduct heat to the primary surface. Due to the increasing cross-sectional area of the fins with increasing radius from the primary tube surfaces, the temperature gradient decreases so that the fin temperature rapidly approaches the temperature of the surrounding fluid and hence the effectiveness of the fin surface approaches zero. Thus the net increase of heat flow is considerably less than would be anticipated on the basis of surface area alone. A conventional dehumidifier, employing primary and secondary surfaces is an example of such extended surface heat transfer. The cylindrical tubes, constituting the primary surface, have coolant medium flowing through them and the secondary surfaces (fins) extend into the air stream.

It is thus apparent that a unit of fin surface will be less effective than a unit of primary surface when a fin and its primary surface are exposed to a uniform thermal environment. The fin efficiency is defined as the ratio of the actual heat dissipation of a fin to its ideal heat dissipation if the entire fin surface is at the same temperature as the base. In other words, it is the ratio of the average temperature difference between the air and the fin surface to that between the air and the base surface.

4.2 Determination of Fin Efficiency

The fin efficiency, ϕ, is obtained from a mathematical analysis by Gardner (1945) which is based on the following assumptions:

a) The heat flow and temperature distribution throughout the fin are independent of time, *i.e.* the heat flow is steady.

b) The fin material is homogeneous and isotropic.

c) There are no heat sources in the fin itself.

d) The heat flow to or from the fin surface at any point is directly proportional to the temperature difference between the surface at that point and the surrounding fluid.

e) The thermal conductivity of the fin is constant.

f) The heat transfer coefficient is the same over all the fin surface.

g) The temperature of the surrounding fluid is uniform.

h) The temperature of the base of the fin is uniform.

i) The fin thickness is sufficiently small compared to its height for temperature gradients normal to the surface to be neglected.

j) The heat transferred through the outermost edge of the fin is negligible compared to that passing through the sides.

A second order differential equation is obtained for the temperature gradient through the fin element. The mathematical analysis involves the reduction of this equation to the form of the second order Bessel equation leading to a solution in terms of Bessel functions.

For a continuous plate fin, the outside radius, x_e, considered to give a fin surface area equivalent to the area of an axisymmetric (annular) fin is given by

$$\pi x_e^2 = L_f L_d / N_t \quad ,$$

$$\text{or} \quad x_e = \left[\frac{(L_f L_d)}{\pi N_t} \right]^{0.5} \quad , \qquad (4.1)$$

where L_f is the length of the fin corresponding to the height of the dehumidifier, L_d is the length of the fin in the direction of air flow and N_t is the total number of tubes. A further discussion on equation (4.1) can be found in Section A2.1, Appendix 2, where x_e is replaced by r_c in the AU method.

The fin root radius, x_b, is given by

$$x_b = \frac{D_o + 2Y_f}{2} \quad , \qquad (4.2)$$

where D_o is the tube outside diameter and Y_f is the thickness of the fin.

The height of the equivalent annular fin, w, is given by

$$w = x_e - x_b \quad . \qquad (4.3)$$

The fin efficiency, ϕ, is obtained from the following equation in terms of Bessel functions :

$$\phi = \frac{2}{U_b\left[1 - (U_e/U_b)^2\right]} \left[\frac{I_1(U_b) - \beta K_1(U_b)}{I_o(U_b) + \beta K_o(U_b)}\right] , \qquad (4.4)$$

where $\beta = \dfrac{I_1(U_e)}{K_1(U_e)}$,

$$U_b = \frac{w}{(x_e/x_b - 1)} \sqrt{\frac{2f_{aD}}{ky_f}} ,$$

$$f_{aD} = \frac{1}{R_{aD}} ,$$

and $U_e = (x_e/x_b)U_b$.

The total surface effectiveness, η, by definition is given by :

$$\eta = \frac{\phi A_s + A_p}{A_o} . \qquad (4.5)$$

where A_p is the net primary surface area, A_s is the net secondary surface area and A_o is the total external surface area.

The total metal thermal resistance, R_m, to heat flow through the external fins and the primary tube wall is given by

$$R_m = R_f + R_t . \qquad (4.6)$$

where R_f and R_t are the thermal resistance of the material of the fin and the tube respectively.

$$R_t = \frac{B\, D_i}{2\, k_t} \left[\ln \frac{D_o}{D_i}\right] . \qquad (4.7)$$

where D_i is the inside diameter of the tube, B is the ratio of the total external surface area to the total internal surface area and k_t is the thermal conductivity of the material of the tube.

The variable fin thermal resistance for a dry surface, R_f, based on total external surface effectiveness, is given by

$$R_f = \left[\frac{1 - \eta}{\eta} \right] R_{aD} \qquad (4.8)$$

where R_{aD} is the air film thermal resistance for a dry surface.

The above equations (4.4), (4.5) and (4.8) for the determination of fin efficiency, total surface effectiveness and the variable fin thermal resistance are used in the ARI method. This is discussed in detail in Chapter 5. Note that the values of fin efficiency are those which were obtained by Gardner (1945) on the basis of the assumptions outlined earlier. Our recent understanding of the thermodynamics and the fluid mechanics of an extended surface dehumidfier lead us to suspect the validity of Gardner's assumption that the heat transfer coefficient is the same over the entire fin surface. Subsequent studies made by Gilbert (1987), involving the measurement of local heat transfer coefficients in a finned-tube model revealed the following distinct regions :

a) A region of high heat transfer coefficient due to the laminar vortices formed at the junctions between the tubes and the plates.
b) A region of moderate heat transfer coefficient between adjacent tubes in a given row.
c) A region of almost negligible heat transfer coefficient between rows in the shadow of the tubes.

The observations made by Gilbert is discussed further in Chapter 9.

Note also that the above expressions for fin efficiency and the fin thermal resistance was originally derived by Gardner for a dry surface. The value of the air film thermal resistance for wet surface, R_{aW}, is modified by a factor of m''/c_p to yield

$$f_{aW} = \frac{m''/c_p}{R_{aW}}$$

and the same expression [equation (4.4)] is used to determine the fin efficiency for a wet surface. m" is the slope of the saturated air temperature - enthalpy curve at the coil surface temperature and c_p is the specific heat of moist air.

The AU method, essentially developed for wet coils, avoids the use of fin efficiency and surface effectiveness and obtains the various heat and mass transfer coefficients directly from actual test results without resorting to any of the "theoretical" curves required in the ARI method.

Chapter 5

THE AIR CONDITIONING AND REFRIGERATION INSTITUTE (ARI) METHOD

5.1 The Fundamentals of the Method

The ARI (1981) approach employs a dual potential method wherein the transfer of heat from the warm moist air to the cold dehumidifier surface, and subsequently through the fins and the tubes to the coolant inside the tubes is analysed by dividing the process into two distinct steps :

a)Heat and mass transfer from the air to the wetted surface;
b)Heat transfer from the surface through the fins and tubes to the coolant within the tubes.

In the actual experimental investigation of dehumidifiers a chilled water system was used that consisted of the refrigeration unit and a chiller. Therefore the term "coolant" in this chapter and elsewhere in this thesis should be considered as chilled water.

The basic theory of the ARI method is as presented by McElgin and Wiley (1940). The total heat transferred from the air as it passes over an element of wetted surface of area dA_o (Fig 5.1) is given by

$$dq_t = \frac{(H - H_s)\, dA_o}{R_{aW}\, c_p} \quad . \qquad (5.1)$$

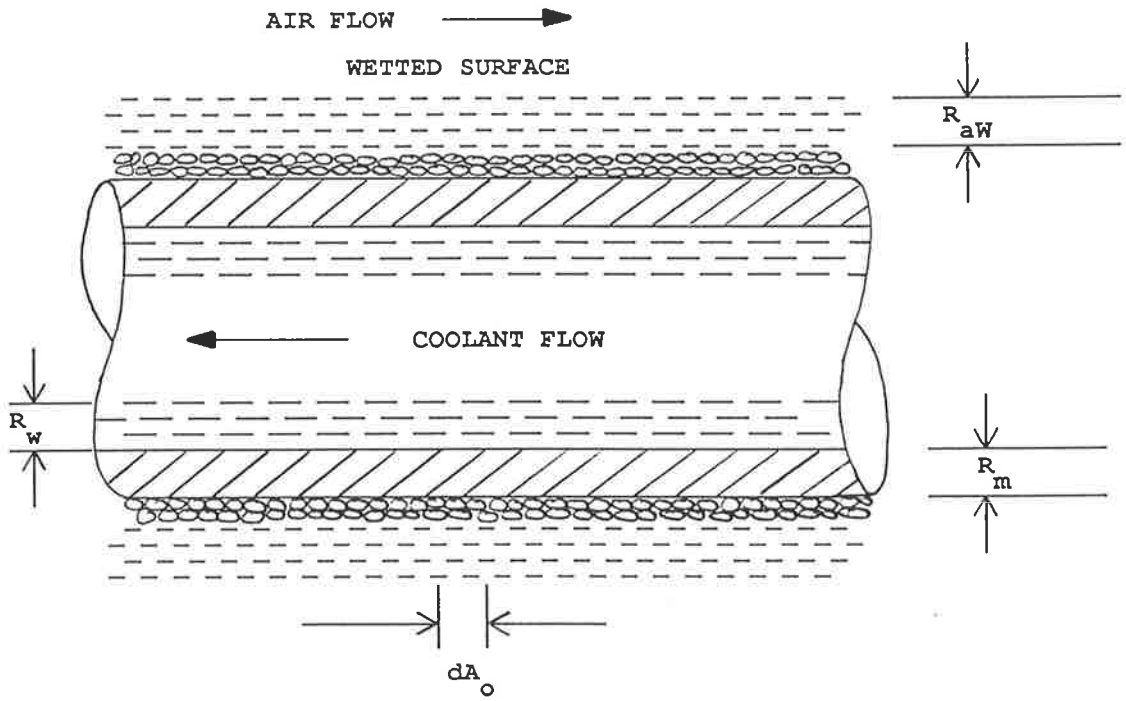

Fig 5.1 : An element of wetted surface and the various component resistances in the ARI method.

This equation, originally derived by Merkel (1927), combines sensible heat transfer due to temperature difference and latent heat transfer due to vapour pressure difference into a single equation which states that the rate of simultaneous sensible and latent heat flow depends upon the difference between the total heat of the air flowing over the surface and the total heat corresponding to saturation at the surface temperature.

The total heat transferred from the element of area dA_o through the fins and the tubes to the water is given by

$$dq_t = \frac{(t_s - t_w)\, dA_o}{R} \quad , \qquad (5.2)$$

where R is defined as the composite resistance to heat flow imposed by the fins (R_f), the tubes (R_t) and the internal water film (R_w).

Substituting $R = R_f + R_t + R_w$ in (5.2) and equating it to (5.1) yields

$$\frac{(t_s - t_w)}{(H - H_s)} = \frac{(R_f + R_t + R_w)}{R_{aW}\, c_p} = C \quad . \qquad (5.3)$$

C is the "Coil Characteristic", defined in terms of the individual thermal resistances.

Equation (5.3) is essentially of the same form as that originally derived by Goodman (1936).

It is, however, to be noted that the effect of the droplets, or the film of water condensed from the air on the surface, is not directly considered in the above analysis.

The ADELAIDE UNIVERSITY (AU) method, discussed in Chapter 6, is used for the fully wet and for the wet portion of partially dry coils. Application of the ARI method for fully dry and for the dry portion of partially dry coils is discussed in the following sections and in the process, its application to coil selection for conventional system is discussed.

5.2 Data Reduction

The overall thermal resistance data from empirical tests of coils must be assigned to the various component resistances. This reduction, as prescribed by ARI Standard 410-81 is outlined in the present section. A computer program **"ARI DATA REDUCTION"**, coded in Turbo-Pascal, encodes

the procedure for determination of the air film thermal resistances, R_{aD} and R_{aW}, for dry and wet surfaces respectively. It is necessary to obtain R_{aD} before evaluating R_{aW} as R_{aW} requires an iterative process with initial values being those for a dry surface. A schematic representation of the flow chart to reduce the dry and wet surface test data is shown in Fig 5.2. This chart could be interpreted as an "unpacking the mysteries of ARI Standard 410-81." A minimum of four dry and wet tests at four different standard air face velocities is required by the ARI standard. The tests must cover the entire rating range of air speed in approximately equally spaced velocity increments on a logarithmic scale.

The ratio of air-side sensible heat to total heat is given by

$$\frac{q_s}{q_t} = \frac{c_p (t_1 - t_2)}{(H_1 - H_2)} \quad . \tag{5.4}$$

This ratio is used as an index to identify the type of analysis required for determining coil performance:

a)If $q_s/q_t < 0.95$, the tests are wet and a further criterion of $q_s/q_t < 0.75$ is used for fully wet tests.

b)If $q_s/q_t \geq 0.95$, the tests are presumed to be fully dry.

5.2.1 Analysis of Sensible Cooling Tests

As mentioned earlier, the determination of cooling coil performance is relatively simple when the air is sensibly cooled on a dry surface. The reduction of dry empirical test data to obtain dry heat transfer coefficients follows the following procedure.

As discussed in Chapter 4, the total metal thermal resistance, R_{mD}, to heat flow through the external fins and the primary tube wall is given by

$$R_{mD} = R_f + R_t \quad , \tag{5.5}$$

where

$$R_t = \frac{B\, D_i}{2\, k_t} \left[\ln \frac{D_o}{D_i} \right] \quad . \tag{5.6}$$

The variable fin thermal resistance, R_f, based on total external surface effectiveness, is given by

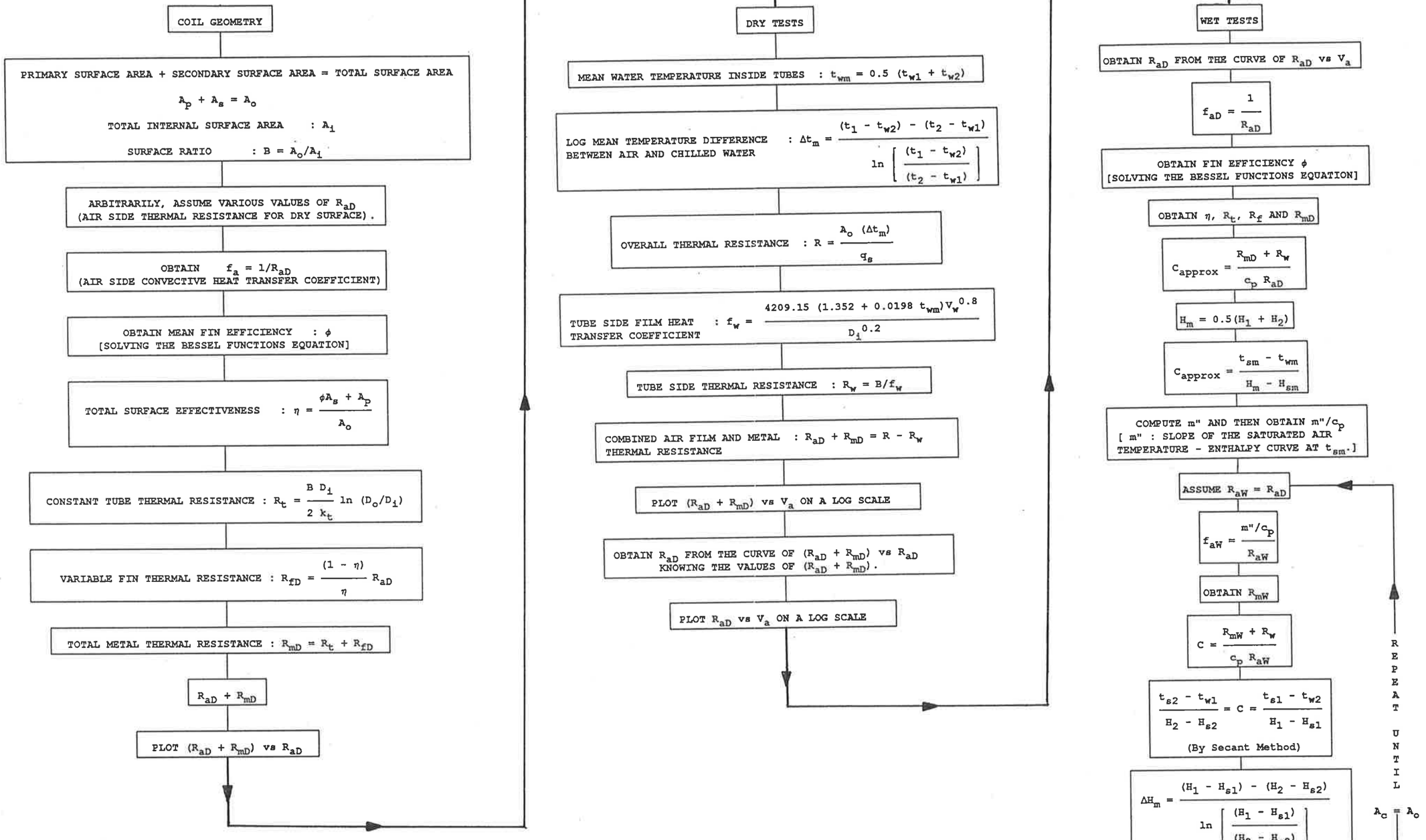

Fig 5.2 : Flow chart for the computer program "ARI DATA REDUCTION".

$$R_f = \left[\frac{1 - \eta}{\eta} \right] R_{aD} \quad . \qquad (5.7)$$

Also as discussed in Chapter 4, the fin efficiency, ϕ, is obtained from the following equation in terms of Bessel functions :

$$\phi = \frac{2}{U_b\left[1 - (U_e/U_b)^2 \right]} \left[\frac{I_1(U_b) - \beta K_1(U_b)}{I_o(U_b) + \beta K_o(U_b)} \right] \quad , \qquad (5.8)$$

where $\beta = \dfrac{I_1(U_e)}{K_1(U_e)}$,

$$U_b = \frac{w}{(x_e/x_b - 1)} \sqrt{\frac{2f_{aD}}{ky_f}} \quad ,$$

$$f_{aD} = \frac{1}{R_{aD}} \quad ,$$

$$U_e = (x_e/x_b)U_b$$

and $$\eta = \frac{\phi A_s + A_p}{A_o} \quad , \qquad (5.9)$$

where $A_o = A_s + A_p$.

By arbitrarily assuming various values of R_{aD}, a graph of $(R_{aD} + R_{mD})$ vs R_{aD} can be plotted on rectilinear coordinates.

It is important to note that equation (5.5) and the development of the above curve do not require any test data other than that on which the expression for ϕ was based [Gardner (1945)].

The actual determination of R_{mD} and the development of the curve will be presented in Chapter 8 as part of the discussion of the results and analysis of the empirical tests.

The overall thermal resistance, R, is determined from the following variation of Newton's law of cooling :

$$R = \frac{A_o (\Delta t_m)}{q_s} \quad , \tag{5.10}$$

$$\text{where } \Delta t_m = \frac{(t_1 - t_{w2}) - (t_2 - t_{w1})}{\ln\left[\frac{(t_1 - t_{w2})}{(t_2 - t_{w1})}\right]} \quad . \tag{5.11}$$

Δt_m is the log mean temperature difference between air and chilled water.

For water coils employing smooth, plain internal tube walls, the tube-side water film heat transfer coefficient, f_w, is determined from McAdams (1954) equation

$$f_w = \frac{4209.15(1.352 + 0.0198\, t_{wm})(V_w)^{0.8}}{(D_i)^{0.2}} \quad , \tag{5.12}$$

where t_{wm} = mean water temperature inside the tubes = 0.5 (t_{w1} + t_{w2}).

Equation (5.12) is applicable for tube-side Reynolds numbers exceeding 3100.

The tube-side film thermal resistance, R_w, is given by

$$R_w = B/f_w \quad . \tag{5.13}$$

The surface ratio, B, is included in the above equation for consistency to base the resistance on the total external surface area, A_o.

The combined air film and metal thermal resistance, (R_{aD} + R_{mD}), is then given by

$$R_{aD} + R_{mD} = R - R_w \quad . \tag{5.14}$$

The values of R_{aD} for each of the four dry tests are obtained from the curve of (R_{aD} + R_{mD}) vs R_{aD} which was developed earlier. With the known values of (R_{aD} + R_{mD}) determined from equation (5.14), the values of R_{aD} may be obtained.

The application rating curve of a chilled water sensible heat coil, R_{aD} vs $(V_a)_{std}$, may then be plotted on logarithmic coordinates. The actual development of this curve is presented in Chapter 8 during discussion of the empirical tests.

5.2.2 Analysis of Cooling and Dehumidifying Tests

The purpose of this test series is to establish the validity under wetted surface conditions of the air-side heat transfer coefficients, f_a, as determined for dry surface tests in Section 5.2.1. According to the ARI method, adjustments may or may not be required, depending upon the particular design and arrangement of the heat transfer surface. An important criterion of this test series is that each test should be performed under fully wetted surface conditions with the entire air-side surface actively condensing moisture. This operating condition exists when the air-side surface temperature, at all positions throughout the coil, is below the entering air dew point temperature. The following range of variables are specified by ARI for the above criterion to be fulfilled:

Entering water temperature, t_{w1} = 1.7 to 12.8°C,

Entering wet bulb depression, $t_1 - t_1' \geq 3.3$°C,

Air sensible heat ratio, $q_s/q_t \leq 0.75$,

$t_2' - t_{w1} \geq 2.8$°C.

These requirements may be interpreted as a fairly reasonable means of ensuring that a fully wet test is being performed.

The water side film heat transfer coefficient, f_w, is determined by employing McAdams equation. The value of R_{aD} at the known face velocity, $(V_a)_{std}$, is obtained from the curve of R_{aD} vs $(V_a)_{std}$, developed in Section 5.2.1. The air-side heat transfer coefficient, f_{aD}, is given by

$$f_{aD} = 1/R_{aD} \quad . \tag{5.15}$$

Assuming a dry surface, the total metal thermal resistance, R_{mD}, is obtained from equation (5.5), developed in Section 5.2.1. The values of f_{aD}, as determined by equation (5.15), are used in obtaining the values of R_{mD}.

The coil characteristic is given by equation (5.3), which is written as

$$C = \frac{R_m + R_w}{c_p R_{aW}} \tag{5.3a}$$

$$\text{and} \quad C = \frac{t_s - t_w}{H - H_s} \quad . \tag{5.3b}$$

An approximate value of C is initially obtained by using the empirically determined values of R_{mD}, R_w and R_{aD}.

After expressing H_s in terms of t_s, the Secant method of numerical iteration is employed to obtain an approximate mean surface temperature, t_{sm}, using known values of H_m, t_{wm} and C_{approx}.

The approximate air-side heat transfer multiplier, m''/c_p, may then be obtained once m'' has been evaluated. Here m'' is the slope of the saturated air temperature - enthalpy curve at the approximate mean coil surface temperature.

The air film thermal resistance for a wet surface, R_{aW}, is determined by the following trial-and-error procedure.

An initial value of R_{aW} is assumed to be that of R_{aD}. The approximate air-side wetted surface heat transfer coefficient, f_{aW}, is then given by

$$f_{aW} = \frac{m''/c_p}{R_{aW}} \quad . \qquad (5.16)$$

The total metal thermal resistance under wetted surface condition, R_{mW}, is obtained from equation (5.5).

The coil characteristic, C, is obtained from equation (5.3) :

$$C = \frac{R_{mW} + R_w}{c_p R_{aW}} \quad . \qquad (5.3c)$$

Using known values of H_1, t_{w2}, H_2, t_{w1} and C, the air side entering and leaving temperatures, t_{s1} and t_{s2} for the wetted surface are obtained by the Secant method of numerical iteration. The saturated air enthalpies, H_{s1} and H_{s2}, are then determined and the log mean enthalpy difference, ΔH_m, is computed from

$$\Delta H_m = \frac{(H_1 - H_{s1}) - (H_2 - H_{s2})}{\ln\left[\frac{(H_1 - H_{s1})}{(H_2 - H_{s2})}\right]} \quad . \qquad (5.17)$$

The "calculated external surface area", A_c, is given by

$$A_c = \frac{c_p \, R_{aW} \, q_t}{\Delta H_m} \quad . \qquad (5.18)$$

The assumed value of R_{aW} is the actual value of the wetted surface air film thermal resistance if the total "calculated external surface area", A_c, is equal to the actual total external surface area A_o. This is achieved by means of an iterative process employing the Secant method. The cooling and dehumidifying coil application rating curve, R_{aW} vs $(V_a)_{std}$, is then plotted on logarithmic coordinates. The actual determination of R_{aW} and the development of this curve are presented in Chapter 8 as part of the analysis of experimental data.

5.3 The Generalisation Process

The process of generalisation involves the prediction of the leaving conditions at any operating condition other than laboratory testing conditions. The values of R_{aD} and R_{aW} obtained by the method described in the previous section are used in the generalisation process. It is to be noted that the process of generalisation is valid only for coils of similar physical geometry to those used for obtaining the application ratings. However, the ARI Standard provides a means of extending the process of generalisation by performing a series of dry and wet tests on single and multiple row coils having different fin densities. The generalisation is further extended over a range of chilled water velocities by the use of McAdams equation (1954).

For a coil of a known geometry, the leaving conditions for any entry condition are predicted by a trial-and-error method, assuming different values of the total heat quantity, q_t. A computer program **"ARI GENERALISATION PROGRAM"** has been coded in Turbo-Pascal to predict the performance of coils according to ARI Standard 410-81. A schematic representation of the flow chart of the above program is shown in Fig 5.3.

The basic input/output format of the program is as follows:

Input Data :

- Coil dimensions (height and length)
- Entering air dry bulb temperature
- Entering air dew point temperature
- Air volume flow
- Entering water temperatrure
- Water velocity
- Circuiting

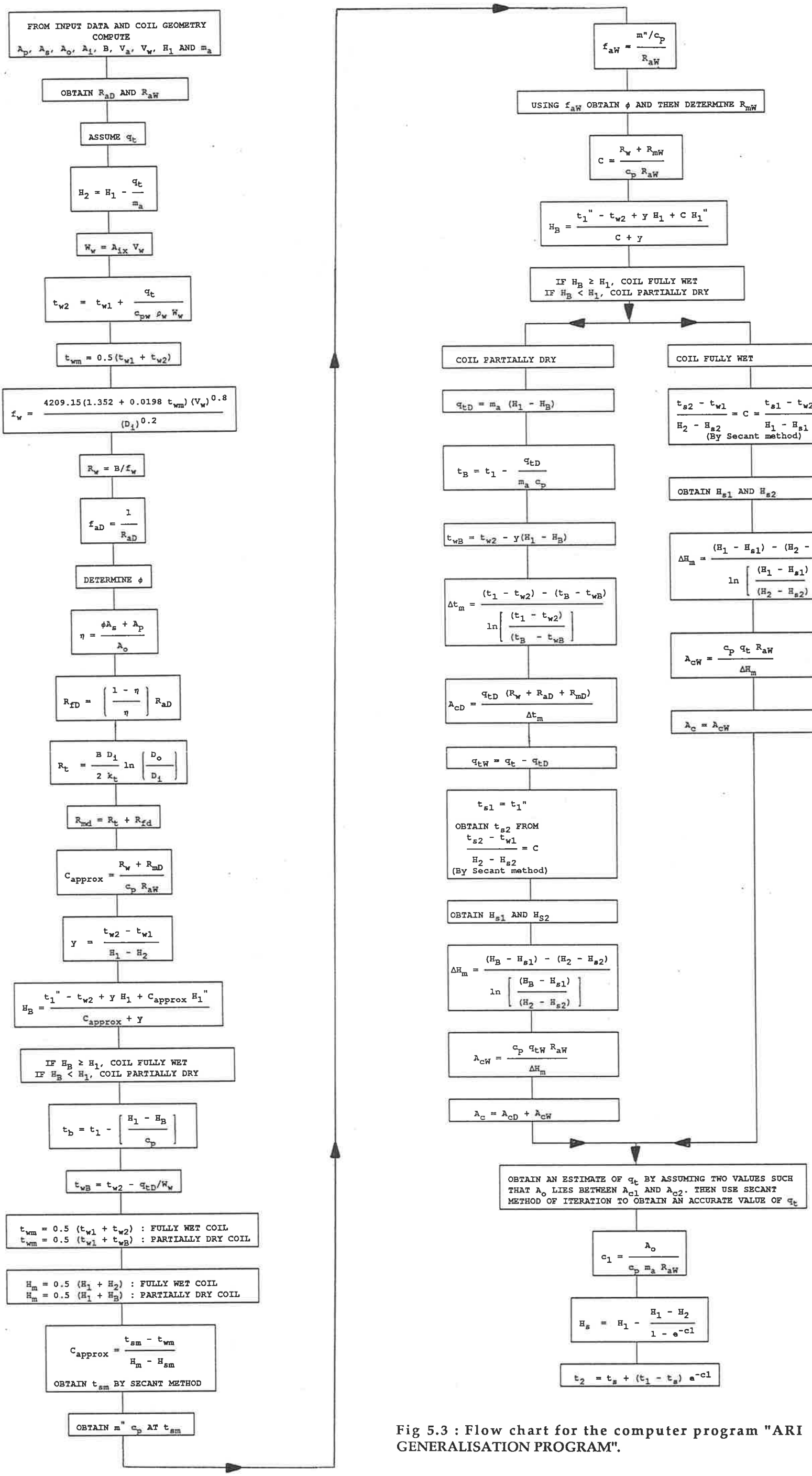

Fig 5.3 : Flow chart for the computer program "ARI GENERALISATION PROGRAM".

Rows

Fin density.

Output Data :

Leaving air dry bulb temperature

Leaving air dew point temperature

Water temperature rise

Cooling capacity.

Having chosen a coil of a given geometry, the various physical parameters such as A_F, A_o and A_{ix} are computed. The standard face velocity, $(V_a)_{std}$, is determined from the known standard volume air flow through the coil. The entering air dry and wet bulb temperatures and the entering water temperature and velocity are known. The values of R_{aD} and R_{aW} are obtained from the curves of R_{aD} vs $(V_a)_{std}$ and R_{aW} vs $(V_a)_{std}$ at the standard face velocity $(V_a)_{std}$.

The actual total heat capacity of the coil is determined by an iterative process using the relationships

$$q_t = q_{tD} + q_{tW} \quad , \tag{5.19a}$$

$$q_{tD} = \frac{A_D \, \Delta t_m}{R} \quad , \tag{5.19b}$$

$$q_{tW} = \frac{A_W \, \Delta H_m}{c_p \, R_{aW}} \tag{5.19c}$$

and $$A_o = A_D + A_W \quad , \tag{5.19d}$$

where q_{tD} and q_{tW} are the heat capacities and A_D and A_W are the external surface areas of the dry and wet portions of a coil respectively.

By assuming a value of q_t, the "calculated surface areas", A_{cD} and A_{cW} are determined. The total "calculated surface area" is then

$$A_c = A_{cD} + A_{cW} \quad . \tag{5.19e}$$

If this calculated value A_c does not equal the true value A_o, the assumed value of q_t is revised and the calculation process is repeated. For the correct value of q_t,

$$A_c = A_{cD} + A_{cW} = A_o \quad . \tag{5.19f}$$

5.3.1 Details of the Iterative Process to Predict the Total Heat Capacity and the Leaving Enthalpy

An initial value of the total heat transfer to the coolant, q_t, is assumed and the leaving air enthalpy, H_2, is determined from

$$H_2 = H_1 - \frac{q_t}{m_a} \quad . \tag{5.20}$$

The water volume flow rate is given by

$$W_w = A_{ix} V_w \quad . \tag{5.21}$$

The leaving water temperature may then be calculated from

$$t_{w2} = t_{w1} + \frac{q_t}{c_{pw} \rho_w W_w} \quad , \tag{5.22}$$

where

ρ_w = Density of water = 1 kg/litre.

c_{pw} = Specific heat capacity of water = 4.187 kJ/(kgK)

The water-side film heat transfer coefficient, f_w, is obtained from equation (5.12). That is

$$f_w = \frac{4209.15(1.352 + 0.0198\, t_{wm})(V_w)^{0.8}}{(D_i)^{0.2}} \quad , \tag{5.12}$$

where $t_{wm} = 0.5(t_{w1} + t_{w2})$.

The tube side thermal resistance is obtained from equation (5.13),

$$R_w = B/f_w \quad . \tag{5.13}$$

The total metal thermal resistance, R_{mD}, is obtained from equation (5.5).

An approximate value of the coil characteristic, C_{approx}, is initially obtained from equation (5.3) by using the values of R_{mD}, R_w and R_{aD}. Thus

$$C_{approx} = \frac{R_w + R_{mD}}{c_p R_{aW}} \quad . \tag{5.3d}$$

The air-stream enthalpy at the consequent dry-wet boundary is given by

$$H_B = \frac{t_1'' - t_{w2} + y H_1 + C_{approx} H_1''}{C_{approx} + y} \quad , \tag{5.23}$$

where the ratio of the tube-side temperature difference to the air enthalpy difference, y, is given by

$$y = \frac{t_{w2} - t_{w1}}{H_1 - H_2} \quad . \tag{5.24}$$

If $H_B \geq H_1$, the entire coil surface area is wet and A_D=0. The wetted surface area A_W alone is calculated for this condition. If $H_B < H_1$, a portion of the coil surface is operating dry and for this condition, the dry (A_D) and wetted (A_W) surface areas are separately calculated.

As described in Section 5.2.2, the Secant method of numerical iteration is employed to obtain an approximate "mean" (effective) surface temperature, t_{sm}, using known values of H_m, t_{wm} and C_{approx}.

The approximate air-side heat transfer multiplier, m''/c_p, is then obtained after evaluating m'', the slope of the saturated air temperature - enthalpy curve at the approximate mean coil surface temperature.

The air dry bulb temperature at the dry-wet boundary is given by

$$t_B = t_1 - \left[\frac{H_1 - H_B}{c_p}\right] \tag{5.25}$$

and the cold water tube-side temperature at the dry-wet boundary by

$$t_{wB} = t_{w2} - \left[\frac{q_{tD}}{W_w}\right] \quad . \tag{5.26}$$

The mean tube-side temperatures may then be calculated for the wet portion of a partially dry coil from

$$t_{wm} = 0.5(t_{w1} + t_{wB}) \qquad (5.27a)$$

and for a fully wet coil from

$$t_{wm} = 0.5(t_{w1} + t_{w2}) \quad . \qquad (5.27b)$$

The mean air enthalpy for the wet portion of a partially dry coil is

$$H_{sm} = 0.5(H_1 + H_B) \qquad (5.28a)$$

and for a fully wet coil is

$$H_{sm} = 0.5(H_1 + H_2) \quad . \qquad (5.28b)$$

The approximate mean surface temperature for a fully wet coil or for the wet portion of a partially dry coil is then determined using C_{approx} (from equation (5.3d)), t_{wB} (from equation (5.26)) and H_{wB} (from equation (5.28)).

The air-side heat transfer multiplier for the wet surface is obtained using the approximate mean surface temperature determined above. This value of m''/c_p is used in determining f_{aW}, which is obtained from equation (5.16); thus

$$f_{aW} = \frac{m'' / c_p}{R_{aW}} \quad . \qquad (5.16)$$

The wet surface fin efficiency is obtained from equation (5.8) using the above value of f_{aW}. It is to be noted here that equation (5.8) was developed by Gardner for a dry surface. By introducing a factor of m''/c_p (equation (5.16)), the same equation (5.8) is now used to obtain the fin efficiency for a wet surface.

R_{mW} is then determined from equation (5.5).

The final value of the coil characteristic for the wetted surface is determined from equation (5.3) which is written as

$$C = \frac{R_w + R_{mW}}{c_p R_{aW}} \quad . \tag{5.3e}$$

The air enthalpy at the boundary is again computed as

$$H_B = \frac{t_1'' - t_{w2} + yH_1 + C H_1''}{C + y} \quad , \tag{5.29}$$

where C is given by equation (5.3e).

If H_B (from equation 5.29) < H_1, the surface is partially dry.

If H_B (from equation 5.29) ≥ H_1, the surface is fully wet.

Partially Dry Coils

The capacity of the dry portion of the coil is

$$q_{tD} = m_a (H_1 - H_B) \quad , \tag{5.30}$$

where H_B is determined from equation (5.29).

The air dry bulb temperature at the boundary, t_B, is given by

$$t_B = t_1 - \frac{q_{tD}}{m_a c_p} \quad . \tag{5.31}$$

The tube-side temperature, t_{wB}, at boundary is

$$t_{wB} = t_{w2} - y(H_1 - H_B) \quad , \tag{5.32}$$

where H_B is determined from equation (5.29).

The logarithmic mean temperature difference, Δt_m, for the dry portion of coil is

$$\Delta t_m = \frac{(t_1 - t_{w2}) - (t_B - t_{wB})}{\ln\left[\frac{(t_1 - t_{w2})}{(t_B - t_{wB})}\right]} \quad . \tag{5.33}$$

The "calculated external dry surface area" for the dry portion of the coil is

$$A_{cD} = \frac{q_{tD}\,(R_w + R_{aD} + R_{mD})}{\Delta t_m} \quad , \tag{5.34}$$

where Δt_m is determined from equation (5.33).

The capacity of the wet portion of the coil is then

$$q_{tW} = q_t - q_{tD} \quad . \tag{5.35}$$

It is apparent that for the wet portion of a partially dry coil, $t_{s1} = t_1$".

Knowing t_{w1}, H_2 and C, the wetted surface temperature at air exit, t_{s2} is obtained from equation (5.3b) using the Secant method.

The enthalpies of the saturated air, H_{s1} and H_{s2}, at t_{s1} and t_{s2} respectively are then determined and the logarithmic mean enthalpy difference, ΔH_m, between the air stream and the wetted surface is

$$\Delta H_m = \frac{(H_B - H_{s1}) - (H_2 - H_{s2})}{\ln\left[\frac{(H_B - H_{s1})}{(H_2 - H_{s2})}\right]} \quad , \tag{5.36}$$

where H_B is determined from equation (5.29).

The "calculated external wetted surface area" is then

$$A_{cW} = \frac{c_p \, q_{tW}}{\Delta H_m \, h_{cow}} \quad , \tag{5.37}$$

The total "calculated external surface area" is given by

$$A_c = A_{cD} + A_{cW} \quad . \tag{5.38}$$

The calculation is then repeated successively until $A_c = A_o$.

Fully Wet Coils

The capacity of the fully wet coil is the same as the assumed value of q_t.

The wetted surface temperatures at air entry and exit, t_{s1} and t_{s2} respectively are obtained from equation (5.3b) using the Secant method. Equation (5.3b) is rewritten as

$$C = \frac{t_{s1} - t_{w2}}{H_1 - H_{s1}} \tag{5.3b}$$

$$\text{and} \quad C = \frac{t_{s2} - t_{w1}}{H_2 - H_{s2}} \quad , \tag{5.3b}$$

where C is obtained from equation (5.3e).

The enthalpies of the saturated air, H_{s1} and H_{s2}, at t_{s1} and t_{s2} respectively are then determined and the logarithmic mean enthalpy difference, ΔH_m, between the air stream and the wetted surface is determined for fully wet coils by the following procedure :

$$\Delta H_m = \frac{(H_1 - H_{s1}) - (H_2 - H_{s2})}{\ln \left[\frac{(H_1 - H_{s1})}{(H_2 - H_{s2})} \right]} \quad . \tag{5.39}$$

The "calculated external wetted surface area" is then obtained from

$$A_{cW} = \frac{c_p \, R_{aW} \, q_{tW}}{\Delta H_m} \quad . \tag{5.40}$$

The total "calculated external surface area" A_c is equal to A_{cW}.

The actual value of q_t is the assumed value of the total heat capacity when the total "calculated external surface area" of a fully wet coil, A_c, (as for the partially dry coil) is equal to the actual total external surface area, A_o.

5.3.2 Prediction of Leaving Dry Bulb Temperature

The equation for the leaving dry bulb temperature is fully derived as part of the detailing of the Adelaide University (AU) Method in the corresponding section of Chapter 6.

The following equations could be written for the total and the sensible heat capacities of the coil :

$$dq_t = \frac{1}{R_{aW}\, c_p} (H - H_s^-)\, dA_o \qquad (5.1)$$

and $$dq_s = \frac{1}{R_{aW}} (t - t_s^-)\, dA_o \quad . \qquad (5.41)$$

Also $$dq_t = m_a\, dH \qquad (5.42)$$

and $$dq_s = m_a\, c_p\, dt \quad . \qquad (5.43)$$

Equating (5.1) to (5.42) and (5.41) to (5.43) and integrating for a constant effective surface temperature gives

$$\ln\left[\frac{H_2 - H_s^-}{H_1 - H_s^-}\right] = -\frac{A_o}{c_p\, m_a\, R_{aW}} = \ln\left[\frac{t_2 - t_s^-}{t_1 - t_s^-}\right] , \qquad (5.44)$$

where $$c = \frac{A_o}{c_p\, m_a\, R_{aW}} \quad . \qquad (5.45)$$

c is the heat transfer exponent defined by equation (5.45).

It is to be noted that the ARI Standard 410-81 prescribes the value of R_{aD} to be used in the above heat transfer exponent expressed by equation (5.45). As a result of evaluating many thoroughly documented sets of test results, the writer has found that the accuracy of the ARI procedure is greatest if R_{aW} is used in evaluating c, rather than R_{aD} as stated by the ARI Standard 410-81. This appears to give a better and more logical representation of the actual wetted surface performance.

Substituting equation (5.45) in equation (5.44) and then rearranging gives

$$e^{-c} = \frac{H_2 - \bar{H}_s}{H_1 - \bar{H}_s} = \frac{t_2 - \bar{t}_s}{t_1 - \bar{t}_s} \quad , \tag{5.46}$$

The saturated air enthalpy corresponding to the effective coil surface temperature is therefore

$$\bar{H}_s = H_1 - \left[\frac{H_1 - H_2}{1 - e^{-c}}\right] \quad , \tag{5.47}$$

and the leaving air dry bulb temperature, t_2, is

$$t_2 = \bar{t}_s + (t_1 - \bar{t}_s)\, e^{-c} \quad . \tag{5.48}$$

Chapter 6

THE ADELAIDE UNIVERSITY (AU) METHOD

6.1 The Fundamentals of the Method

Fundamentally the AU method employs

(a) an enthalpy potential for the total heat and mass transfer from the warm moist air to the cold dehumidifier surface and

(b) a temperature potential for the pure heat transfer from the wetted dehumidifier surface through the fins and the tubes to the coolant water "film".

Although the basic methodologies of the AU and the ARI methods appear to be similar, there are pertinent differences. The ARI method does not consider directly the effect of the layer of condensate on the outside surface of the fins and the tubes, while the AU method, through the process employed to obtain the heat and mass transfer coefficients, accounts for the effect of this outside condensate layer. The AU method avoids the use of fin efficiency and fin effectiveness and obtains the various heat and mass transfer coefficients directly from empirical test results without resorting to any of the "theoretical" curves required in the ARI method. The empirical test results are, therefore, central to the development of the AU method. The unique controlled environment heat and mass transfer tunnel in the Department of Mechanical Engineering at The University of Adelaide has facilitated the accumulation of some extremely accurate test results. These have laid the foundation for the development of the AU method for evaluating dehumidifying coil performance. The research and testing facility is discussed in detail in Chapter 7. The AU method aims to represent to the best of present understanding the physical phenomena occurring in a dehumidifier. The fundamental insights gained from extensive work in the unique testing system lends confidence to the view that the fundamental approach of the AU method for the present places it ahead of other methods of coil performance evaluation.

It is to be noted that the AU method has been particularly developed for a fully wet or for the wet portion of a partially dry coil. The ARI method, which appears to give reasonably good predictions for dry coils, has been adopted for fully dry or for the dry portion of a partially dry coil.

In the manner of McElgin and Wiley (1940), the overall process of enthalpy transfer from the air stream to the coolant may be divided into two parts; a combined heat and mass transfer from the air to the condensate surface followed by a pure heat transfer process through the condensate, fin, and tube wall to the coolant. The relevant thermodynamic transfer relations may be summarised in terms of transfer across an enthalpy potential followed by transfer across a temperature potential. The relevant equations are as follows.

The enthalpy potential equation for the transfer of heat and mass from the warm moist air to an incremental area dA_o of the cold dehumidifier surface is given by

$$dq_t = \frac{h_{cow}}{c_p} (H - H_s)\, dA_o \quad , \qquad (6.1)$$

where h_{cow} is the convective heat transfer coefficient for outside wetted surface in $W/(m^2 ℃)$, H is the enthalpy of moist air and H_s is the enthalpy of saturated air at coil surface temperature t_s.

The temperature potential equation for the transfer of heat from the wetted surface through the outside condensate layer, fins and tubes to the bulk flow of chilled water inside the tubes is given by

$$dq_t = h_i \left[\frac{A_o}{A_i} \right] (t_s - t_w)\, dA_o \quad , \qquad (6.2)$$

where h_i is the combined coefficient of heat transfer through the outside condensate layer, metal and the tube side water "film" in $W/(m^2 ℃)$, t_s is the coil surface temperature and t_w is the chilled water temperature.

Note that equation (6.2) relates to pure heat transfer and is independent of phase change processes.

Equations (6.1) and (6.2) are two equations for the same quantity dq_t and may therefore be equated. Thus

$$\frac{H_s - H}{t_s - t_w} = - \frac{c_p\, h_i\, A_i}{h_{cow}\, A_o} \quad , \qquad (6.3)$$

which ratio is defined as the Tie Line Slope (TLS) because it progressively represents the slope of a line, the Coil Condition Curve (CCC), from the entering to the leaving air conditions on the psychrometric chart (Kusuda, 1957). Note that TLS has the dimensions of a "modified" or "effective" specific heat. It is at this point that the AU analysis departs from that of McElgin and Wiley (1940).

The Lewis relationship is given by

$$Le = \frac{h_{cow}}{h_{do}\, c_p} \simeq 1 \quad , \qquad (6.4)$$

where h_{do} is the mass transfer coefficient in kg/(s m^2).

Kusuda (1965) recommends a value of 0.9 for the Lewis number. This has been found by Kusuda and others to be more representative of air/water vapour mixtures. Hence 0.9 will be assumed for the Lewis number in equation (6.4). An expression for h_{cow} may now be written

$$h_{cow} = 0.9\ h_{do}\ c_p \qquad (6.4a)$$

and substituted into equation (6.3) to yield

$$\frac{H_s - H}{t_s - t_w} = -\frac{c_p\ h_i\ A_i}{0.9\ h_{do}\ A_o} \equiv TLS \quad . \qquad (6.5)$$

Knowing the empirical test results for q_t, A_i and Δt_m, h_i is first obtained by using the pure heat transfer equation

$$q_t = h_i\ A_i\ \Delta t_m \quad . \qquad (6.6)$$

The log mean temperature difference, Δt_m, is evaluated from the outside condensate layer on the wetted surface through the fins and tubes to the water "film" inside the tubes.

Knowing the value of TLS, h_{do} and h_{cow} are obtained from equations (6.5) and (6.4a) respectively.

It is thus apparent that the determination of TLS plays an important role in the development of the AU method. The TLS is obtained by a computer based analytical method which is described in detail in Section 6.2. It may also be obtained by a graphical construction of the Coil Condition Curve (CCC) on the Psychrometric Chart, as suggested by Kusuda (1957) and subsequently adopted by Shaw (1979) in his development of the Low Face Velocity (LFV) method of air conditioning. A Surface Temperature Determination Line is superimposed on a conventional Psychrometric Chart by plotting a temperature scale at right angles to the enthalpy scale. The Surface Temperature Determination Line could be viewed as the pivot point about which the superimposed temperature ordinate can be transferred to the coordinates of the conventional Psychrometric Chart. This is achieved by means of the lines of constant enthalpy which are common to both the conventional Psychrometric Chart and the superimposed temperature-enthalpy plot. The value of the TLS from

the construction of the CCC on such a modified Psychrometric Chart is obtained by means of a trial and error process. However, once the correct value of TLS is obtained by Kusuda's method, the same construction facilitates the direct determination of the wetted surface temperatures at entry and exit to the dehumidifier.

The analysis which underpins the AU method for evaluating the performance of dehumidifying coils is discussed and the procedure is specified by means of flow charts in the following sections of this chapter.

6.2 Data Reduction

A computer program **"TLS BY LEWIS NUMBER CORRELATION"** has been developed for analysing empirical test data to obtain the various heat and mass transfer coefficients outlined in this section. The program, coded in Turbo-Pascal, determines the value of TLS by an iterative process which is terminated when the required value of the Lewis number is obtained. As discussed in the previous section, a Lewis number of 0.9 is taken as the basis for relating the heat and the mass transfer coefficients in air-water vapour mixtures. The heat and mass transfer coefficients determined by this method are employed in the generalisation process which is described in detail in Section 6.3.

6.2.1 Determination of the Tie Line Slope (TLS) by Lewis Number Correlation

A flow chart of the computer program **"TLS BY LEWIS NUMBER CORRELATION"** is presented in Fig 6.1. The iterative process described in Fig 6.1 is accomplished numerically by the "Secant Method". The procedure in detail is as follows :

We assume a value of TLS. The coil characteristic is then given by

$$C = -\frac{1}{TLS} \quad . \tag{6.7}$$

The sensible and latent heat capacities can be expressed by

$$q_s = m_a \, c_p \, [\, t_1 - t_2 \,] \quad , \tag{6.8}$$

$$q_l = m_a \, h_{fg} \, [\, W_1 - W_2 \,] \quad . \tag{6.9}$$

The surface temperatures at air entry and exit, t_{s1} and t_{s2} may be obtained from equation (5.3b). For convenience all equations are repeated here within the sequence for the present chapter.

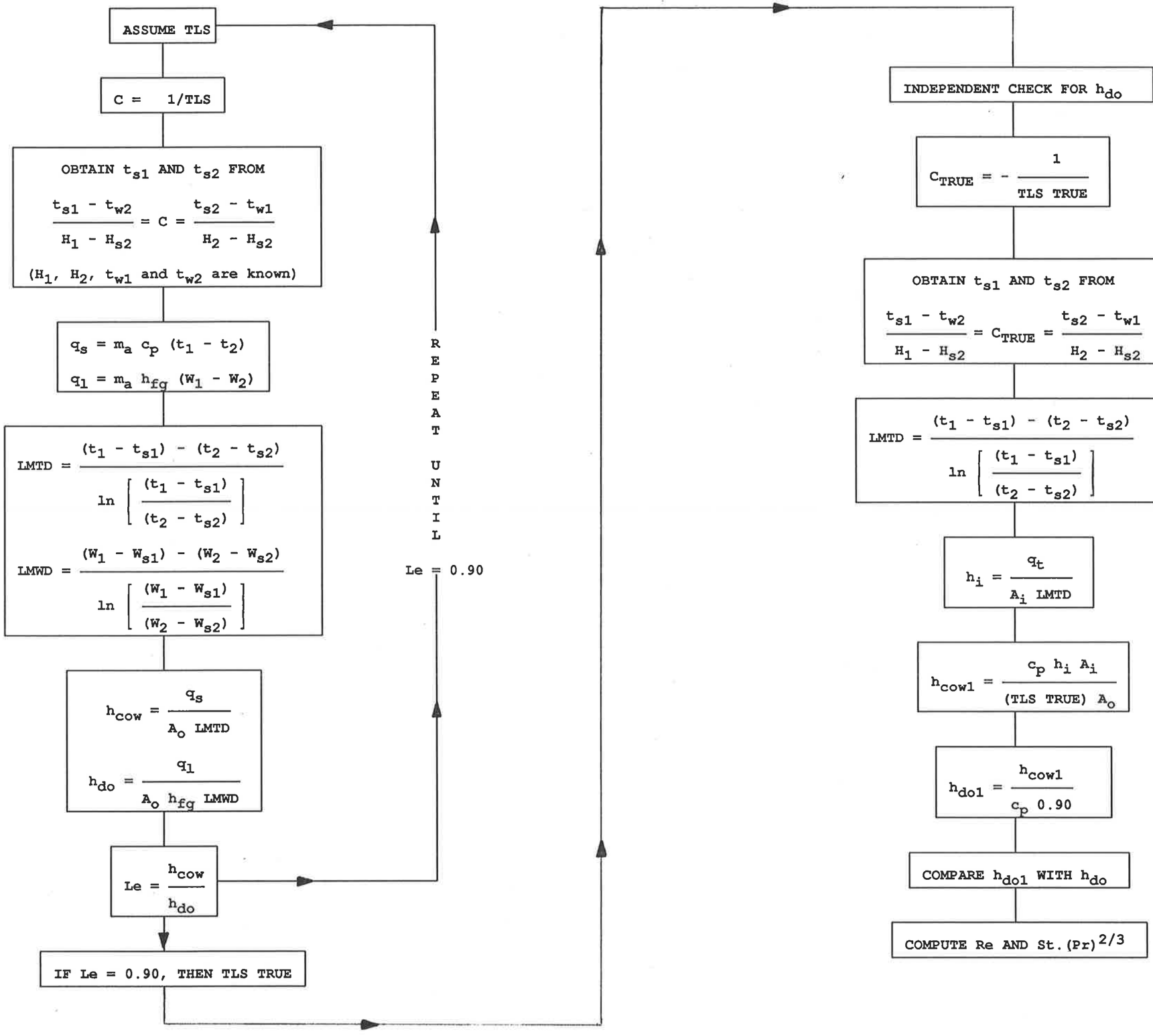

Fig 6.1 : Flow chart for the computer program "TLS BY LEWIS NUMBER CORRELATION".

$$\frac{t_{s1} - t_{w2}}{H_1 - H_{s1}} = C \qquad (6.10a)$$

and $$\frac{t_{s2} - t_{w1}}{H_2 - H_{s2}} = C \quad . \qquad (6.10b)$$

In equations (6.10a) and (6.10b), H_{s1} and H_{s2} can be expressed in terms of t_{s1} and t_{s2} respectively. The Secant Method of numerical iteration is then employed to obtain t_{s1} and t_{s2}. The entering and leaving conditions, H_1, t_{w1} and H_2, t_{w2} are known in the above equations.

The humidity ratios, W_{s1} and W_{s2} are obtained at t_{s1} and t_{s2} respectively. The log mean temperature difference (LMTD) and log mean humidity ratio difference (LMWD) are then given by

$$LMTD = \frac{(t_1 - t_{s1}) - (t_2 - t_{s2})}{\ln\left[\frac{(t_1 - t_{s1})}{(t_2 - t_{s2})}\right]} \qquad (6.11)$$

and $$LMWD = \frac{(W_1 - W_{s1}) - (W_2 - W_{s2})}{\ln\left[\frac{(W_1 - W_{s1})}{(W_2 - W_{s2})}\right]} \qquad (6.12)$$

respectively.

The convective heat transfer coefficient for the outside wetted surface, h_{cow} and the mass transfer coefficient, h_{do} are given by

$$h_{cow} = \frac{q_s}{A_o \; LMTD} \quad , \qquad (6.13)$$

$$h_{do} = \frac{q_l}{A_o \; h_{fg} \; LMWD} \quad . \qquad (6.14)$$

The Lewis number is then

$$Le = \frac{h_{cow}}{c_p \; h_{do}} \quad . \qquad (6.15)$$

The numerical iteration is continued until the Lewis number as computed by equation (6.15) is equal to 0.90. The corresponding value of TLS, denoted as TLS_{true} is taken as the correct TLS.

An independent check is available for the computed value of h_{do}. Using TLS_{true}, the corresponding values of t_{s1} and t_{s2} are obtained from equations (6.10a) and (6.10b) respectively. The log mean temperature difference between the outside wetted surface and the tube side water "film" is

$$\Delta t_m = \frac{(t_{s1} - t_{w2}) - (t_{s2} - t_{w1})}{\ln\left[\frac{(t_{s1} - t_{w2})}{(t_{s2} - t_{w1})}\right]} \qquad (6.16)$$

and the corresponding heat transfer coefficient h_i is

$$h_i = \frac{q_t}{A_i \, \Delta t_m} \quad . \qquad (6.17)$$

On the air side, h_{cow} and h_{do} are then

$$h_{cow} = \frac{c_p \, h_i \, A_i}{TLS_{true} \, A_o} \qquad (6.18)$$

and $$h_{do} = \frac{h_{cow}}{c_p \, 0.9} \quad . \qquad (6.19)$$

This calculation of h_{do} may then be compared with the value of h_{do} obtained from equation (6.14).

The values of h_{cow} for different air face velocities are represented as a logarithmic plot of $St(Pr)^{2/3}$ vs Re where the definition of Reynolds number is as follows.

6.2.2 Determination of the Reynolds Number

Kays and London (1984) define a Reynolds number based on an equivalent flow passage hydraulic diameter, $4r_h$. This is expressed in dimensionless terms as

$$\frac{4 \, r_h}{L} = \frac{D_h}{L} = 4 \, \frac{A_{min}}{A_o} \qquad (6.20)$$

where

L = Flow length of the heat exchanger

A_{min} = Minimum free flow area

A_o = Total heat transfer area

D_h = Hydraulic diameter as defined by Kays and London.

For flow normal to tube banks, L is an equivalent flow length measured from the leading edge of the first tube row to the leading edge of a tube row that would follow the last tube row, were another tube row present.

Another method for determining this equivalent hydraulic diameter is that suggested by Gunter and Shaw (1945), wherein the equivalent volumetric diameter is defined as

$$D_e = \frac{4 \text{ (Free volume of tube bundle)}}{\text{(Outside surface area of the tubes)}} \quad . \qquad (6.21)$$

The equivalent diameter used in the present analysis for the AU method is that used by Kays and London. It is important to understand that the choices of length scale represented by the above expressions are intended primarily to provide a scale which is consistent for coils of given configuration but varying flow length, in terms of number of rows, and between coils of different configurations, e.g. fin densities or tube spacing. The actual number which emerges from this process does not necessarily have any significance in terms of the fluid mechanics of the air flow through the coil, as shown by Gilbert (1987). Despite the clear statement by Kays and London (1984) that the air flow through the coils they studied is laminar, there is an almost universal belief within the air conditioning industry that the flow is turbulent. A further discussion on this matter can be found in Chapter 9.

The procedure for evaluating the equivalent hydraulic diameter according to equations (6.20) and (6.21) is detailed in Appendix 2. The hydraulic diameter, D_e is first derived according to the Gunter and Shaw method. This is followed by the derivation of the hydraulic diameter, D_h according to the definition of Kays and London. Imperial units are used partly to enable comparison with the data of Kays and London (1984), which are given in imperial units, but also because the air-conditioning industry has not yet fully adopted S.I. units. The values of D_h and D_e as computed from equations (6.20) and (6.21) for the MULLER coil are mutually compared and also compared with the equivalent diameter of Fig 10.92 in Kays and London (1984) which is reproduced as Fig A2.3 in Appendix 2. The determination of D_e according to equation (6.21) for the Muller coils is

summarised in Table 6.1 and their comparison with D_h according to equation (6.20) and that of the data quoted by Kays and London is presented in Table 6.2. Table 6.2 is a reproduction of Table A2.1 from Appendix 2.

The mass velocity, sometimes referred to as the cut-off velocity, is given by G = Mass flow rate / Minimum flow area, *i.e.*

$$G = \frac{m_a}{A_{min}} \quad . \tag{6.22}$$

The minimum free flow area, A_{min} in m^2 is given by

$$A_{min} = L_f \, L_t \, 10^{-6} - A_{metal} \quad , \tag{6.23}$$

where A_{metal} is the total metal cross sectional area across the face in a direction normal to the air flow and L_f and L_t are in millimetres.

The mass velocity is then

$$G = \frac{m_a}{(L_f \, L_t - A_{metal}) \, 10^{-6}} \quad . \tag{6.24}$$

The Reynolds number is

$$Re = \frac{D_e \, G}{\mu} \quad , \tag{6.25}$$

where $\mu = 0.018 \times 10^{-3}$ Pa.s.

Substituting the values of D_e, G and μ in equation (6.25), we have

$$Re = \frac{276.67 \times 10^6 \, m_a}{(L_f \, L_t - A_{metal})} \tag{6.26}$$

Free volume of tube bundle	$0.843in^3$
Outside surface area of tubes	$11.5814in^2$
Equivalent hydraulic diameter	0.02426ft ($7.396x10^{-3}m$)

Table 6.1 : **Equivalent hydraulic diameter for Muller (thesis) coils according to Gunter/Shaw method**

	Muller coil (Gunter/Shaw) D_e	Muller coil (Kays/London) D_h	K & L coil (Kays/London) D_h
Tube outside diameter	0.625" (15.875mm)	0.625" (15.875mm)	0.676" (17.17mm)
Fin density	6.18 per inch (243 per m)	6.18 per inch (243 per m)	7.75 per inch (305 per m)
Tube spacing in the plane of the fins	1.5" (38.1mm)	1.5" (38.1mm)	1.5" (38.1mm)
Tube spacing between coil rows	1.38" (35.05mm)	1.38" (35.05mm)	1.75" (44.45mm)
Equivalent hydraulic diameter	0.02426ft ($7.396x10^{-3}m$)	0.0163ft ($4.98x10^{-3}m$)	0.0114ft ($3.48x10^{-3}m$)

Table 6.2 : Comparison of equivalent hydraulic diameter

where m_a is in kg/s and L_f and L_t are in mm.

Equations (6.23), (6.24) and (6.26) are derived in Appendix 2.

6.2.3 Determination of the Stanton.(Prandtl)$^{2/3}$ Number

The product St.(Pr)$^{2/3}$ is given by

$$St.(Pr)^{2/3} = \left[\frac{h_{cow}}{G\ c_p} \right] \left[\frac{\mu\ c_p}{k} \right]^{2/3} \quad . \qquad (6.27)$$

Substituting the various values in consistent units in the equations for the Stanton and Prandtl numbers, we have Pr = 0.7217, and with G from equation (6.24) equation (6.27) becomes

$$St.(Pr)^{2/3} = \frac{0.79035 \times 10^{-9}\ h_{cow}\ (L_f\ L_t - A_{metal})}{m_a} \quad . \qquad (6.28)$$

The units of m_a are kg/s and L_f and L_t are in mm. Details of the calculation of Prandtl number and equation (6.28) can be found in Appendix 2.

A plot of St.(Pr)$^{2/3}$, as obtained from equation (6.28), vs Re, as obtained from equation (6.26), is the application rating curve for the AU method and is employed in the generalisation process described in detail in Section 6.3.

Computer printouts of the program **"TLS BY LEWIS NUMBER CORRELATION"** indicating the various heat and mass transfer coefficients and the actual development of the dimensionless expression of St(Pr)$^{2/3}$ vs Re are presented in Chapter 8 during discussion of the results and analysis of empirical tests.

6.2.4 Determination of the Empirical Constant

The combined resistance to heat transfer through outside condensate layer, metal and tube-side water "film" can be expressed as

$$R_i = R_w + (R_m + R_{ow}) \quad . \qquad (6.29)$$

The convective heat transfer coefficient of the tube-side water "film" is obtained from McAdams equation

$$f_w = \frac{4209.15(1.352 + 0.0198\ t_{wm})(V_w)^{0.8}}{(D_i)^{0.2}} \quad , \qquad (6.30)$$

where the numerical values are consequential upon the choice of units. Here t_{wm} is in °C, V_w is in m/s and D_i in mm.

The tube-side water "film" thermal resistance is then given by

$$R_w = \frac{B}{f_w} \quad , \qquad (6.31)$$

where B is the ratio of the total external surface area to the total internal surface area.

The combined thermal resistance for the outside condensate layer, metal and tube-side water "film" is then given by

$$R_i = \frac{B}{h_i} \quad . \qquad (6.32)$$

Having determined R_i and R_w, the empirical constant is obtained from equation (6.29), *i.e.*

$$(R_m + R_{ow}) = R_i - R_w \quad . \qquad (6.29a)$$

The determination of the empirical constant, $(R_m + R_{ow})$ is demonstrated in Chapter 8 during discussion of the results and the analysis of the empirical tests.

6.3 The Generalisation Process

The process of generalisation involves the prediction at any operating condition of a dehumidifying coil of the leaving conditions, such as leaving enthalpy and leaving dry bulb temperature, based on interpolation or extrapolation from the derivations of heat and mass transfer coefficients available from specific empirical tests. The availability of an apparently unique testing facility at The University of Adelaide has allowed the development of an extensive data bank of accurate empirical

test results. From this database the process of generalisation has been developed to predict the performance of coils. This has been further extended and developed into a coil selection program which can be used to select a coil for a given air conditioning application. This computer program **"ADELAIDE UNIVERSITY (AU) COIL SELECTION PROGRAM"**, coded in Turbo-Pascal, encapsulates the processs of generalisation discussed here.

The basic input/output format of the coil selection program is as follows :

Input Data :

- Coil dimensions (height and length)
- Entering air dry bulb temperature
- Entering air dew point temperature
- Air volume flow
- Entering water temperature
- Water quantity
- Circuiting
- Rows
- Fin density.

Output Data :

- Leaving air dry bulb temperature
- Leaving air dew point temperature
- Water temperature rise
- Cooling capacity.

As mentioned earlier in Section 6.1, the reduction of test data described in Sections 6.1 and 6.2 has been developed for fully wet coils. Consequently, the development of $St(Pr)^{2/3}$ vs Re curves has been based on data from tests in which the coil surface has been actively condensing moisture. Nevertheless the determination of heat and mass transfer coefficients from such tests does enable the performance prediction for a partially dry coil provided the dry-wet boundary condition is established. The procedure for establishing the dry-wet boundary condition has been accepted as that described in the ARI method. Having determined the boundary condition, the ARI method is then used for the dry portion of the coil and the AU method is used for the wet portion of the coil. The ARI method is also employed when the coil is fully dry. As discussed earlier, the analysis of a coil is relatively simple when only heat transfer is involved as is the case when the coil is performing dry.

A flow chart of the program **"ADELAIDE UNIVERSITY (AU) COIL SELECTION PROGRAM"** is shown in Fig 6.2.

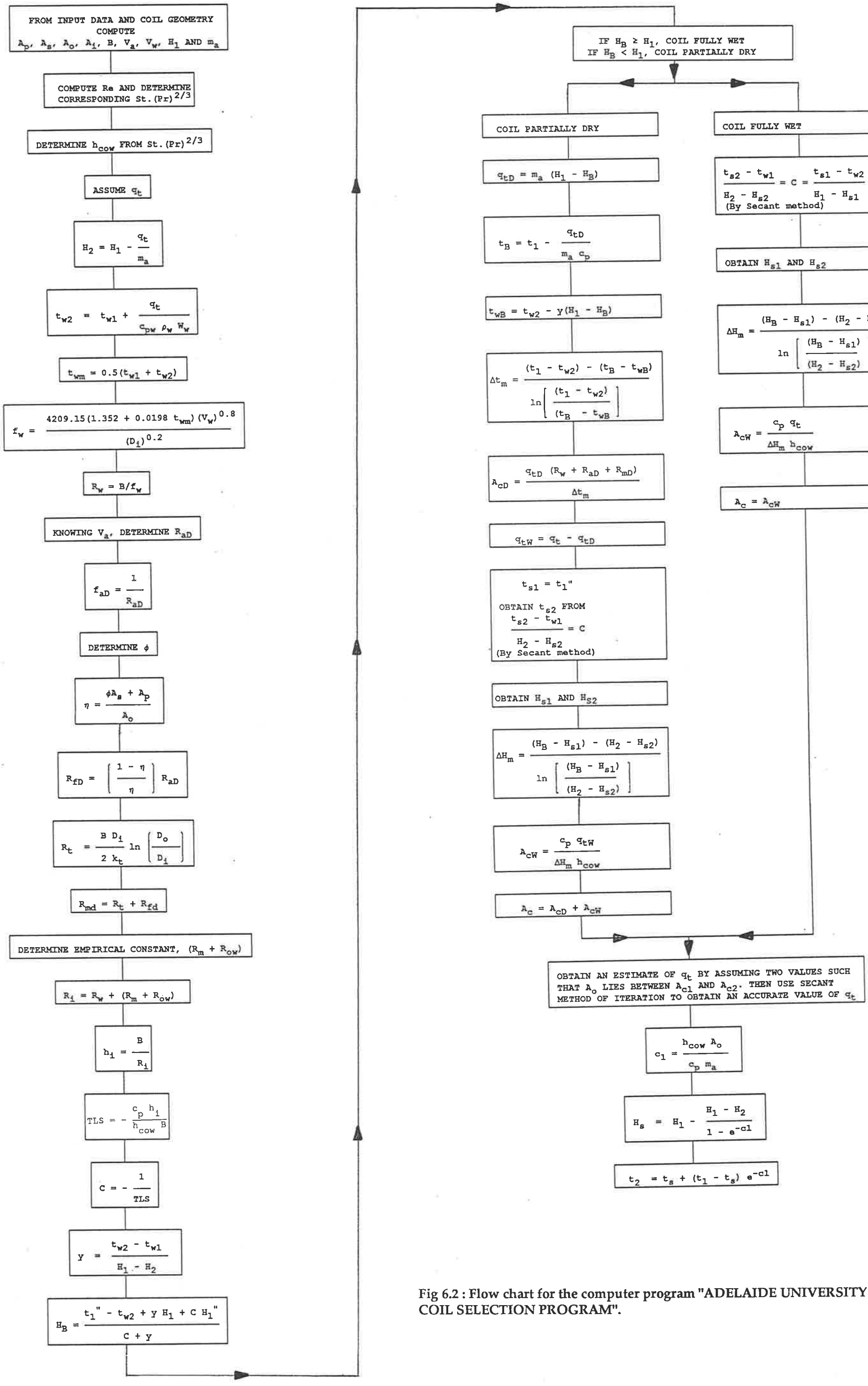

Fig 6.2 : Flow chart for the computer program "ADELAIDE UNIVERSITY (AU) COIL SELECTION PROGRAM".

It is to be noted that most of the empirical tests were performed with the circuiting of the chilled water arranged so that half the number of tubes in the first row were fed. This arrangement is referred to as "half-circuiting". In the generalisation this can be extrapolated to any other circuiting by considering the length of the flow path through the coil. This requires only a small modification to the input of the program. For a different circuiting arrangement, an equivalent half-circuiting is obtained by suitable alterations to the height and length of the coil. Thus, the equivalent half-circuited coil would have the same frontal area as the coil required with the different circuiting arrangement but the frontal dimensions would be different. This implies that a reduction in height would be accompanied by an increase in the length of the coil. However, the length of run of the chilled water is kept the same in both the arrangements. As an example, the computer simulation of a 1/3 circuited coil (*i.e.* one third of the number of tubes in the first row fed) with length, L and height, H would be as follows:

$$\text{Length} = \frac{3}{2} \text{ L}$$

$$\text{Height} = \frac{2}{3} \text{ H}$$

Equivalent circuiting = Half .

Tests of a four-row coil with quarter circuiting (one fourth of the number of tubes in the first row fed) were performed. These are compared with the performance predicted by the computer program through the use of the above modifications. The comparison is presented in Chapter 8 as part of the discussion and analysis of results, but for the present it may be stated that the prediction is extremely good.

Having chosen a coil of a given geometry, the various physical parameters such as face area A_F, total external surface area A_o and total internal surface area A_{ix} are computed. The standard and the actual face velocities are determined from the known volumetric air flow through the coil. The dry and wet bulb temperatures of the entering air and the entering water temperature and its velocity in the tubes are known.

The actual total heat capacity of the coil is determined by an iterative process using the following equations :

$$q_t = q_{tD} + q_{tW} \quad , \tag{6.33a}$$

$$q_{tD} = \frac{A_D \, \Delta t_m}{R} \quad , \tag{6.33b}$$

$$q_{tW} = \frac{A_W \, \Delta H_m \, h_{cow}}{c_p} \quad , \tag{6.33c}$$

$$A_o = A_D + A_W \quad . \tag{6.33d}$$

By assuming a value of q_t for the total heat transfer rate, the "calculated surface areas", A_{cD} and A_{cW} are determined. The "total calculated surface area" is then given by

$$A_c = A_{cD} + A_{cW} \quad . \tag{6.33e}$$

For the correct value of q_t,

$$A_c = A_{cD} + A_{cW} = A_o \tag{6.33f}$$

and the iteration proceeds until this is achieved.

6.3.1 Description of the Iterative Process to Predict the Total Heat Capacity and the Leaving Enthalpy

An initial value of the total heat transfer, q_t, to the coolant is assumed and the leaving air enthalpy, H_2, is determined from

$$H_2 = H_1 - \frac{q_t}{m_a} \quad . \tag{6.34}$$

The water volume flow rate is given by

$$W_w = A_{ix} \, V_w \tag{6.35}$$

and the leaving water temperature is given by

$$t_{w2} = t_{w1} + \frac{q_t}{c_{pw}\,\rho_w\,W_w} \quad , \qquad (6.36)$$

where,

ρ_w = Density of water = 1 kg/litre;

c_{pw} = Specific heat capacity of water = 4.187 kJ/(kg K).

The mean water temperature in the coil is assumed to be given by

$$t_{wm} = 0.5\ (t_{w1} + t_{w2}) \quad . \qquad (6.37)$$

The water-side "film" heat transfer coefficient, f_w, is obtained from McAdams equation *i.e.*

$$f_w = \frac{4209.15(1.352 + 0.0198\ t_{wm})\,(V_w)^{0.8}}{(D_i)^{0.2}} \quad . \qquad (6.30)$$

The tube side thermal resistance is

$$R_w = \frac{B}{f_w} \quad , \qquad (6.31)$$

where we recall that B is the ratio of the total external surface area to the total internal surface area of the coil.

The Reynolds number Re is determined and the value of $St(Pr)^{2/3}$ is obtained from the plot of $St(Pr)^{2/3}$ vs Re. Knowing $St(Pr)^{2/3}$, the value of h_{cow} is determined. The application rating curve, R_{aD} vs $(V_a)_{std}$, as developed by the ARI method is used for dry coils and for determining the dry-wet boundary condition. The value of R_{aD} is obtained from the plot of R_{aD} vs $(V_a)_{std}$. The dry coil analysis and the determination of the dry-wet boundary condition is the same as that described in Chapter 5 and is briefly reviewed here.

The total metal thermal resistance is given by

$$R_{mD} = R_t + R_{fD} \quad . \qquad (6.38)$$

The combined thermal resistance R_i for the outside condensate layer, metal and inside "film", is given by

$$R_i = R_w + \text{empirical constant} \quad . \tag{6.39}$$

The empirical constant used in equation (6.39) is that obtained from equation (6.29a), described in Section 6.2.2.

The combined coefficient of heat transfer through the outside condensate layer, metal and the tube-side "film" h_i is then given by

$$h_i = \frac{B}{R_i} \quad . \tag{6.40}$$

The tie line slope is then

$$TLS = - \frac{c_p \, h_i}{h_{cow} \, B} \tag{6.41}$$

and

$$C = - \frac{1}{TLS} \quad , \tag{6.42}$$

where C is the coil characteristic.

The air-stream enthalpy at the dry-wet boundary is given by

$$H_B = \frac{t_1'' - t_{w2} + y \, H_1 + C \, H_1''}{C + y} \quad , \tag{6.43}$$

where H_1'' is the enthalpy of the air at the entering dew point temperature, t_1''.

If $H_B \geq H_1$ the entire coil surface area is wet and A_D=0. Only the wetted surface area, A_W, is calculated for this condition. If $H_B < H_1$, a portion of the coil surface is operating dry and for this condition, the dry (A_D) and the wetted (A_W) surface areas are separately calculated.

Partially dry coils

The capacity of the dry portion of the coil is

$$q_{tD} = m_a (H_1 - H_B) \quad , \tag{6.44}$$

where H_B is determined from equation (6.43).

The air dry bulb temperature at the boundary, t_B, is given by

$$t_B = t_1 - \frac{q_{tD}}{m_a c_p} \quad . \tag{6.45}$$

The tube-side temperature at the boundary, t_{wB}, is

$$t_{wB} = t_{w2} - y(H_1 - H_B) \quad , \tag{6.46}$$

where H_B is determined from equation (6.43).

The logarithmic mean temperature difference, Δt_m, for dry portion of the coil is

$$\Delta t_m = \frac{(t_1 - t_{w2}) - (t_B - t_{wB})}{\ln\left[\frac{(t_1 - t_{w2})}{(t_B - t_{wB})}\right]} \quad . \tag{6.47}$$

The "calculated external surface area" for the dry portion of the coil is

$$A_{cD} = \frac{q_{tD} (R_w + R_{aD} + R_{mD})}{\Delta t_m} \quad , \tag{6.48}$$

where Δt_m is determined from equation (6.47).

The capacity of the wet portion of the coil is then given by

$$q_{tW} = q_t - q_{tD} \quad . \tag{6.49}$$

It is apparent that for the wet portion of a partially dry coil, $t_{s1} = t_1''$.

The wetted surface temperature at air exit, t_{s2} is obtained from equation (6.10b) using the Secant method.

The enthalpies of the saturated air, H_{s1} and H_{s2}, at t_{s1} and t_{s2} respectively are then determined and the logarithmic mean enthalpy difference, ΔH_m, between the air stream and the wetted surface is then

$$\Delta H_m = \frac{(H_B - H_{s1}) - (H_2 - H_{s2})}{\ln\left[\frac{(H_B - H_{s1})}{(H_2 - H_{s2})}\right]} \quad , \qquad (6.50)$$

where H_B is determined from equation (6.43).

The "calculated external wetted surface area" is then obtained from

$$A_{cW} = \frac{c_p \, q_{tW}}{\Delta H_m \, h_{cow}} \qquad (6.51)$$

and the total "calculated external surface area" is given by

$$A_c = A_{cD} + A_{cW} \quad . \qquad (6.52)$$

Fully wet coils

The capacity of the fully wet coil is necessarily the assumed value of q_t.

The wetted surface temperatures at air entry and exit, t_{s1} and t_{s2} respectively, are obtained from equations (6.10a) and (6.10b) using the Secant method.

The enthalpies of the saturated air, H_{s1} and H_{s2}, at t_{s1} and t_{s2} respectively are then determined and the logarithmic mean enthalpy difference, ΔH_m, between the air stream and the wetted surface is determined from

$$\Delta H_m = \frac{(H_1 - H_{s1}) - (H_2 - H_{s2})}{\ln\left[\frac{(H_1 - H_{s1})}{(H_2 - H_{s2})}\right]} \quad . \qquad (6.53)$$

The "calculated external wetted surface area" is then obtained from equation (6.51). Thus

$$A_{cW} = \frac{c_p \, q_{tW}}{\Delta H_m \, h_{cow}} \quad . \qquad (6.51)$$

The total "calculated external surface area" A_c is equal to A_{cW}.

The assumed value of q_t is the actual value of the total heat capacity if the total "calculated external surface area" of a partially dry coil or a fully wet coil, A_c, is equal to the actual total external surface area, A_o. This is achieved by means of an iterative process employing the Secant method.

6.3.2 Prediction of Leaving Dry Bulb Temperature

An equation for determining the leaving dry bulb temperature, t_2, from known values of t_1, H_1, H_2 and h_{cow}, is derived in this section.

The total heat capacity is given by

$$dq_t = m_a \, dH \quad . \qquad (6.54)$$

Equation (6.1) is rewritten as

$$dq_t = \frac{h_{cow}}{c_p} (H - H_{\bar{s}}) \, dA_o \quad , \qquad (6.1a)$$

where $H_{\bar{s}}$ = Saturated enthalpy of wetted surface at constant effective surface temperature, $t_{\bar{s}}$.

From equations (6.54) and (6.1a),

$$\frac{dH}{(H - H_{\bar{s}})} = \frac{h_{cow}}{c_p \, m_a} dA_o \quad .$$

Integrating the above equation for a constant $t_{\bar{s}}$ gives

$$\ln (H_1 - H_{\bar{s}}) - \ln (H_2 - H_{\bar{s}}) = \frac{A_o \, h_{cow}}{c_p \, m_a} ,$$

$$\text{or} \quad \ln \left[\frac{H_2 - H_{\bar{s}}}{H_1 - H_{\bar{s}}} \right] = - \frac{h_{cow}}{c_p \, m_a} A_o$$

and hence

$$\frac{H_2 - H_{\bar{s}}}{H_1 - H_{\bar{s}}} = e^{-c_1} \qquad (6.55)$$

$$\text{where} \qquad c_1 = \frac{h_{cow} \, A_o}{c_p \, m_a} . \qquad (6.56)$$

Here c_1 is the heat transfer exponent defined by equation (6.56).

The sensible heat capacity of the wetted surface is expressed as

$$dq_s = h_{cow} (t - t_{\bar{s}}) \, dA_o . \qquad (6.57)$$

$$\text{Also} \quad dq_s = m_a \, c_p \, dt . \qquad (6.58)$$

From equations (6.57) and (6.58),

$$\frac{dt}{(t - t_{\bar{s}})} = \frac{h_{cow}}{m_a \, c_p} dA_o .$$

Integrating the above equation for a constant $t_{\bar{s}}$ gives

$$\ln (t_1 - t_{\bar{s}}) - \ln (t_2 - t_{\bar{s}}) = \frac{h_{cow}}{m_a \, c_p} A_o$$

$$\text{or} \quad \ln\left[\frac{t_2 - \bar{t_s}}{t_1 - \bar{t_s}}\right] = -\frac{h_{cow}}{m_a c_p} A_o$$

and hence

$$\left[\frac{t_2 - \bar{t_s}}{t_1 - \bar{t_s}}\right] = e^{-c_1} \quad . \tag{6.59}$$

From equation (6.55),

$$\bar{H_s} = H_1 - \frac{H_1 - H_2}{1 - e^{-c_1}} \quad .$$

From this equation $\bar{t_s}$ may be determined after expressing $\bar{H_s}$ in terms of $\bar{t_s}$.

Thus, from equation (6.59),

$$t_2 = \bar{t_s} + (t_1 - \bar{t_s})\, e^{-c_1} \quad . \tag{6.60}$$

Chapter 7

THE CLOSED CYCLE THERMAL ENVIRONMENT WIND TUNNEL

7.1 The Test Facility

The unique closed cycle thermal environment wind tunnel, located in the Holden Laboratory of the Department of Mechanical Engineering at the University of Adelaide, is central to the accumulation of the empirical test results that constitute the Database on which the method of evaluating the performance of dehumidifying coils is founded. A photograph of the test facility is presented in Fig 7.1 and a schematic illustration of the same is given in Fig 7.2. In this test facility, temperature and humidity conditions appropriate to most parts of the world can be established. The flow of air and coolant through the test facility can be varied and accurately measured. The flexibility of this test facility, coupled with its capacity to maintain steady state, steady flow conditions, renders it ideal for determining the actual performance of cooling and dehumidifying coils. The test coils can either be chilled water or direct expansion refrigerant coils, as currently used in the air-conditioning industry. The Database project employed chilled water coils. The test facility consists of an Air cycle, a Refrigeration cycle and a Chilled Water cycle.

The closed system can simulate over a wide range and can maintain constant almost any air-on temperature and humidity condition, air face velocity, chilled water velocity and chilled water temperature despite changes in the external laboratory conditions. This is a significant advantage over most conventional open cycle testing facilities, such as that specified by ARI and ASHRAE for use with ARI Standard 410-81. It is to be noted that the ARI method refers to an open testing system that renders the collection of accurate empirical test results over a comprehensive range of conditions extremely difficult, if not impossible.

The duct work of the test facility extends almost the entire length of the Holden Laboratory. This ensures that the air is uniformly mixed at all critical measuring stations.

7.1.1 The Air Cycle

The air cycle comprises the following main components :

Variable Speed Fan : A single inlet centrifugal fan with eddy current drive enables the circulation of the air within the ductwork. The eddy current drive facilitates a wide range of air flow rates to be established, up to a maximum fan speed of 3000 rpm. The maximum flow rate is dependent on the size of the coil and the depth of the rows.

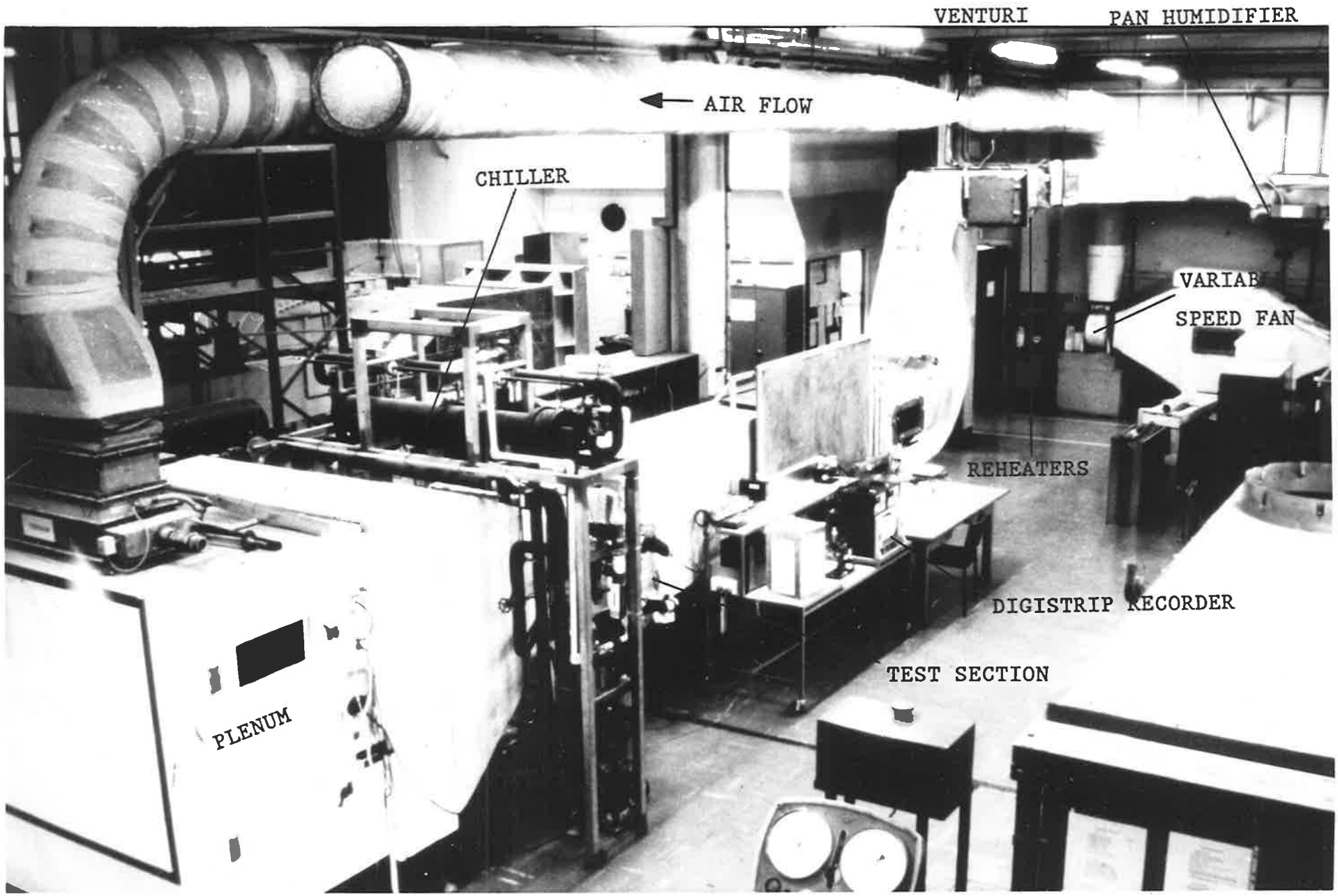

Fig 7.1 : The closed cycle thermal environment wind tunnel

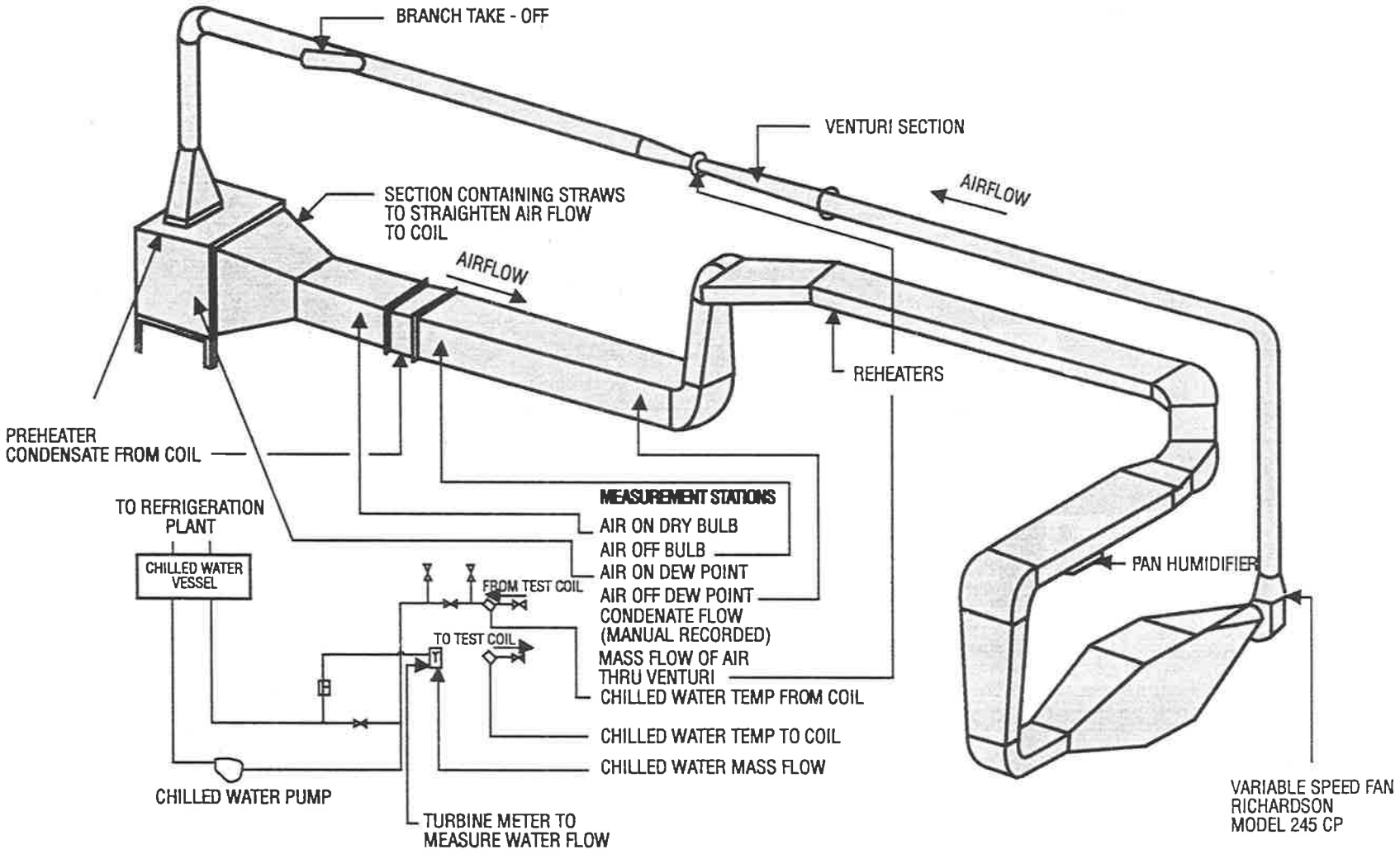

Fig 7.2 : A schematic diagram of the closed cycle thermal environment wind tunnel.

Venturi : The venturi section is designed according to ISO standards, which incorporate British Standards, and enables accurate measurement of air flow through the apparatus during tests.

Test Coil Section : The test coil section is removable to facilitate the installation of coils to be tested. This section can accommodate coils with various aspect ratios up to a maximum size of 760x760mm. Coil sizes of 229x760, 457x760, 533x760, 610x760 and 457x373 have been used in the Database project. The variations in height (or number of tubes in the face of the coil) were accommodated without introducing air flow disturbances by means of fairing plates both upstream and downstream of the test section. The variations in length were obtained by baffling the inactive portions of the coil.

The test section is preceded by a contraction, with an area ratio of between 8:1 and 26:1 depending on the face area of the coil under test. A honeycomb and screen section packed with drinking straws removes any axial swirl from the air stream entering the dehumidifier and establishes a consistent length scale for the turbulence in the flow.

The downstream section of the dehumidifier is immediately followed by a windmill to ensure thorough mixing of the air leaving the dehumidifier before the downstream measuring station.

Reheater section : The reheater section consists of electric heating elements that are automatically controlled to return the air from the air-off condition after the test coil to the selected air-on dry bulb temperature condition. The controller for the reheater can be operated in either automatic or manual mode and a wattmeter, installed on the instrument panel, measures the rate of heat supplied by the electric elements.

The Pan Humidifier : The pan humidifier contains a large quantity of water which is heated by automatically controlled electric elements. The air is humidified in this section from the air-off dew point temperature to the required air-on dew point temperature. The controller for the pan humidifier can be operated in either automatic or manual mode and a wattmeter, installed on the instrument panel, measures the rate of heat supplied to the water in the pan humidifier.

7.1.2 The Refrigeration Cycle

The refrigeration cycle, using Freon (R-12) as the refrigerant has a refrigeration capacity of approximately 10 KW and comprises a variable speed compressor, a water cooled condenser and an evaporator.

7.1.3 The Chilled Water Cycle

The chilled water cycle essentially consists of two chilled water pumps in parallel and the necessary piping arrangements and valves for the circulation of water through the test coil and the evaporator. Flow measuring devices, namely a turbinemeter and a flowmeter, are installed in the chilled water circuit for measuring the flow of chilled water through the test coil.

7.2 Instrumentation

The test facility is equipped with high quality instrumentation which has proved to give a high degree of reliability in the measurement of the various parameters during coil tests. A DIGISTRIP RECORDER is used to record the measured quantities and these records are transferred directly to a PC disk via a serial interface.

7.2.1 Temperature

The locations of the platinum resistance thermometer probes used to measure the five most important temperatures are as follows:

TEMPERATURE	LOCATION
Entering chilled water	Before the supply manifold of dehumidifier
Leaving chilled water	After the return manifold of dehumidifier
Entering air dry bulb	Outlet of contraction upstream of dehumidifier
Leaving air dry bulb	After the windmill downstream of dehumidifier
Condensate	Dehumidifier drain

The accuracy of these instruments is of the order of $\pm 0.05\,^{\circ}C$. The above temperature probes are calibrated against an authorised mercury-in-glass thermometer at least once a fortnight.

7.2.2 Humidity

Mirror dew point hygrometers are used for the measurement of entering and leaving air dew point temperatures. These are amongst the most accurate and reliable instruments available for humidity measurements.

In the mirror dew point type of hygrometer, a smooth mirror surface is thermo-electrically cooled until confusion of a reflected light beam indicates that dew or frost has begun to form. The condensing surface is then accurately maintained in vapour pressure equilibrium with the surrounding air by means of a feed-back control circuit. The equilibrium surface temperature is the dew point temperature by definition. The accuracy of the hygrometer is ±0.3°C.

7.2.3 Chilled Water Flow

A turbinemeter is used for the measurement of chilled water flow through the coil. The turbinemeter provides flow measurement over a wide range with an accuracy of ±0.5 percent. A Kent variable gap flowmeter provides a visual backup.

7.2.4 Air Flow

A venturi, manufactured in accordance with British Standard Code BS 1042 : 1967, is used for the measurement of air flow and forms an integral part of the closed cycle thermal environment wind tunnel. This method of measurement is based on Bernoulli's relationship between the pressure energy and the kinetic energy of a flow in the absence of dissipation. Pressure tappings are distributed around the circumference of the venturi tube and are connected to a piezometer ring. The differential pressure is sensed by a capacitance-type differential pressure transducer in which a measuring diaphragm moves relative to fixed plates and changes in capacitance are detected by an oscillator or bridge circuit.

The accuracy of the differential pressure transducer is ±0.5% of reading.

7.2.5 Backup Measurements

In order to preserve a high standard of reporting of data, a second independent means of measurement is employed wherever possible to substantiate the data. For example, as described in Section 8.1.2 of Chapter 8, a primary measurement of the mass flow rate of condensate is used as a check on the change in the measured humidity ratio across a dehumidifier being investigated. Although the basic measurements used in the analysis are recorded on the DIGISTRIP RECORDER by the instruments described earlier in this section, backup measurements as described below, form an integral part of each test performed.

Multi Point Recorder Charts : Two twenty-four point temperature recorders are mounted on the instrument panel. These were originally installed to record temperatures during tests of Direct Expansion (DX) coils. With chilled water coils, while Freon cycle temperatures are useful for trouble-shooting, only the following air-side temperature records are of direct relevance :

Entering dry bulb temperature.
Entering dew-point temperature.
Temperature of water in the pan humidifier.

These temperatures are also the inputs to the control system of the apparatus. The dry bulb temperature recorder employs resistance bulb sensors while the dew point temperature and the pan humidifier water temperature recorder employs thermocouples. The sensor for entering dry bulb temperature is located in the duct immediately before the plenum chamber (*i.e.* upstream of the dehumidifier). The sensor for dew-point temperature (Lithium Chloride - cavity temperature instrument) is located immediately after the pan humidifier and the sensor for the temperature of the water in the pan humidifier is located in the pan humidifier itself.

Assman Psychrometers : The Assman Psychrometers with electrically driven fans are installed within the air cycle, upstream and downstream of the dehumidifier for the measurement of dry and wet bulb temperatures. The upstream Assman Psychrometer is placed in the plenum chamber, near the window in the plenum door through which it may be read. The downstream Assman Psychrometer is placed in the duct, again near the window, downstream of the test section.

Condensate Measurement : A primary measurement of the moisture condensed by the dehumidifier during each test was obtained by collecting and measuring the condensate over a given time period. This is correlated with the change in humidity ratio as indicated on the psychrometric chart by plotting the entering and leaving air conditions and the air mass flow rate.

Inclined Manometer: The pressure differential through the air flow venturi is measured by an inclined manometer and compared with that determined from a differential pressure transducer.

Flowmeter: A variable gap flow measuring device is located in the chilled water circuit to measure the flow of chilled water through the dehumidifier.

Hygrothermograph: The dry bulb temperature and the relative humidity is recorded on a 24-hour chart which is located in a plant-growth plenum downstream of the pan humidifier and upstream of the fan. This chart is basically used as an indication of the thermal stability of the system.

7.3 Test Procedure and Data Accumulation

After the closed cycle thermal environment wind tunnel is started, the system takes between two and three hours to attain thermal equilibrium. In the actual recording of data from a test, the procedures as set forth in ASHRAE Standard 33-78 and ARI Standard 410-81 have been used as guidelines to ensure that the system is in thermal equilibrium. The test apparatus referred to in the ASHRAE Standard is an open cycle system which is strongly influenced by ambient conditions. The testing facility at The University of Adelaide is a closed cycle system which is independent of ambient conditions. Accordingly, closer tolerances over a relatively shorter test period provide a better indication of system stability. Each test in the present research project is in accordance with the requirements of the ASHRAE Standard during a period of 30 minutes after thermal equilibrium is attained. Thus, in addition to satisfying the ASHRAE Standard requirements it is further required that much tighter conditions be satisfied for at least 10 consecutive minutes during the 30 minute test (Table A4.1, Appendix 4). These tighter conditions are :

a) No individual dry bulb temperature reading to vary by more than 0.05 °C from the average dry bulb temperature reading.
b) No individual dew point temperature reading to vary by more than 0.1 °C from the mean dew point temperature reading.
c) No individual chilled water temperature reading to vary by more than 0.05 °C from the average chilled water temperature reading.
d) The chilled water flow rate to vary by not more than 1% of the average flow rate.

The average value of the readings over the test period is used in the reduction of test data to determine the heat and mass transfer coefficients of the coil.

After the system has attained thermal equilibrium, a personal computer which is interfaced with the DIGISTRIP RECORDER is used for logging the test data in machine-readable form with a logging interval of one minute throughout the whole of the 30 minute duration of the test. During the test, a data sheet is also completed with all the relevant details. A minimum of four condensate mass readings is recorded and the average is used for comparison with ΔW, as obtained from psychrometric calculations. At least one set of upstream and downstream Assman psychrometer readings are recorded for comparison with the DIGISTRIP recordings of dew point and dry bulb temperatures.

The test data which is logged on the personal computer is stored on floppy disks for subsequent analysis and archiving.

An archive of all individual test backups such as the multi point recorder charts, the DIGISTRIP recording, the Hygrothermograph chart and the data sheet is also maintained. This archive is classified to allow easy identification and correlation of any test recorded on the floppy disk with its corresponding backup.

Chapter 8

RESULTS AND ANALYSIS

8.1 Database

In this section the processing of the raw test data to obtain the various psychrometric properties from each test is detailed. A means of checking the internal consistency of each test to ensure a high standard of the Database is presented.

8.1.1 Database test results

As discussed in Chapter 7, the raw test data is stored on a floppy disk and analysed after the experiment. Initially a Lotus 123 spreadsheet analysis was adopted to obtain the various psychrometric properties of each test but later a program called "TESTP" was coded in Turbo-Pascal to replace the spreadsheet method. "TESTP" was found to be more suitable than Lotus due to the ease with which the psychrometric properties of a large number of tests could be obtained relatively quickly. Another important factor in favour of the "TESTP" program was to be consistent

Results of TEST-P analysis

INPUT DATA			OUTPUT		
Title	:	H72B:W3953	air volume flow (cms)	:	0.212
edb (°C)	:	33.61	air mass flow (kg/s)	:	0.242
edp (°C)	:	20.27	water flow rate (lps)	:	1.06
ldb (°C)	:	22.85	entering enthalpy (kJ/kg)	:	71.91
ldp (°C)	:	17.22	leaving enthalpy (kJ/kg)	:	54.12
ewt (°C)	:	7.01	specific volume (m^3/kg)	:	0.890
lwt (°C)	:	7.83	enthalpy change (delta H)	:	17.78
digistrip water (volts)	:	1.745	water side capacity (kw)	:	3.632
digistrip air (volts)	:	0.120	air side capacity (kw)	:	4.297
barometric pressure ("Hg)	:	30.17	sensible heat factor	:	0.62
actual condensate (g/s)	:	0.67	ratio of water/air cap.	:	0.85
height of face (m)	:	0.457	est. condensate (g/kg)	:	0.64
length of face (m)	:	0.760	act/est condensate	:	1.05
rows	:	1	coil face area (sq.m)	:	0.347
No. of tubes high	:	12	face velocity (m/s)	:	0.61
No. of tubes fed	:	6	water velocity (m/s)	:	1.01
			measured water temp.rise	:	0.82

Table 8.1 : A sample output of the computer program "TESTP".

with the ARI and the AU data reduction and generalisation programs, all of which are coded in Turbo-Pascal. A sample output of "TESTP" is presented in Table 8.1. The program evaluates and uses average values over the entire test period in its calculations of psychrometric parameters. The following inputs to the program are provided from the test data :

entering and leaving dry bulb temperatures (edb and ldb),
entering and leaving dew point temperatures (edp and ldp),
entering and leaving water temperatures (ewt and lwt),
air and water volume flow rates,
actual condensate measurement,
the coil frontal dimensions,
rows,
number of tubes high and
number of tubes fed.

The program then computes the following outputs :

entering and leaving air enthalpies,
change in enthalpy (ΔH),
entering specific volume,
sensible and total air-side capacities,
water-side capacity,
sensible heat ratio,
measured and corrected water temperature rises,
coil face area,
face velocity,
water velocity,
theoretical estimate of moisture removal,
the ratio of water to air side capacities and
the ratio of actual condensate measured to theoretically estimated moisture removal.

The computer program "TESTP" evaluates the basic psychrometric properties and details of the calculations involved in the program can be found in Appendix 3.

A sample of the archive of the tests is presented in Appendix 4. Tables A4.1 and A4.2 of Appendix 4 are respectively samples of the Digistrip recording and the data sheet. Typical backup data such as Honeywell recorder charts and the hygrothermograph chart are illustrated in Figs A4.1 - A4.3 in Appendix 4. Unless data is as stable as that illustrated in these figures, a test is regarded as unsatisfactory and is excluded from the data base. It is apparent in Fig A4.1 that point number 23 on the Honeywell recorder chart, the entering air dry bulb temperature, is stable during the test.

Similarly, it is apparent from the Honeywell recorder chart in Fig A4.2 that the entering air dew point temperature represented by point number 24 and the water temperature in the pan humidifier represented by point numbers 1, 7, 13 and 19 are also stable during the test. The stability of the system is further indicated by the hygrothermograph chart recording in Fig A4.3.

Each test is identified by a unique code having the format shown below.

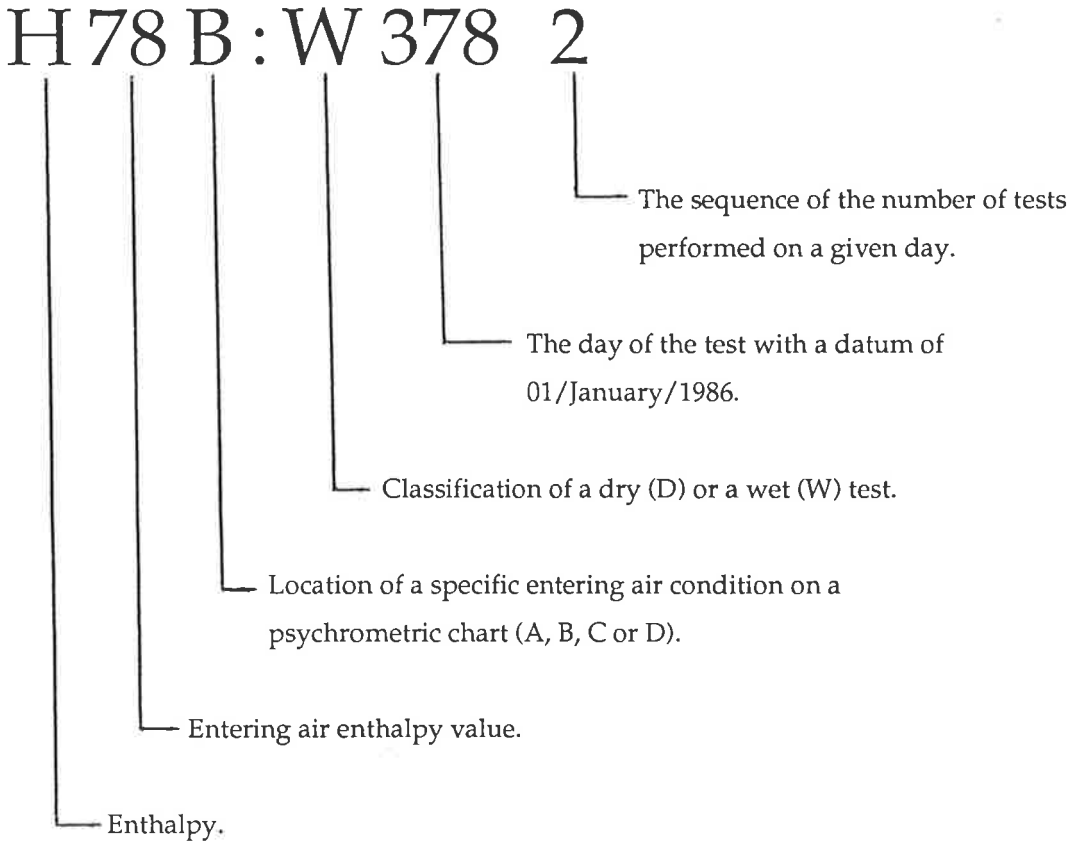

The test data recorded by the Digistrip recorder consists of the temperatures converted via calibration data to degrees Celsius and the flow measurements in volts. The actual volume flow rate of air is calculated from the venturi equation appropriate to the particular dimensions of the venturi in the test apparatus,

$$(Q_a)_{act} = 0.04 \left[1 - 0.692\left[\frac{\Delta p}{P}\right]\right] \left[\frac{\Delta p}{\rho_{act}}\right]^{0.5} \qquad (8.1)$$

where

$(Q_a)_{act}$ = actual volume flow rate in m^3/s

Δp = pressure differential across venturi in Pa

P = atmospheric pressure in Pa

ρ_{act} = actual density of moist air in kg/m^3.

The density of moist air is given by

$$\rho = \frac{1 + W}{v} \qquad (8.2)$$

where W and v are the humidity ratio and the specific volume at the entering air condition, in consistent units.

To facilitate the interpretation of the data in terms used commonly in the air conditioning industry a conversion factor is used to convert Δp to millimetres (mm) of water. Similarly, a conversion factor is used to convert the water flow recording to litres per second (lps).

8.1.2 Standard of Data Accumulation

In the search for a means of predicting heat and mass transfer coefficients in a situation in which one must face a wide spectrum of variations of design conditions combined with multitudinous arrangements of compact heat exchangers leading to combinations of conditions and heat exchangers which approach the infinite, it is essential to address the task in a manner which maximises the use of well established fundamental relationships so that data from a limited range of tests can be extrapolated to the broad area which is not tested. For example, the enthalpy potential theory provides an excellent basis for developing the heat and mass transfer coeffients. A theoretical correlation of the physical process of condensation in a heat exchanger, for which the rate is measured absolutely, is another relationship on which one can rely in developing the heat and mass transfer coefficients. In this section, it is shown that the above two fundamental relationships are consistently satisfied by the data accumulated. It is claimed that this ensures the high standard and reliability of the empirical test results. An example of the empirical test results of a 1-row coil obtained from **"TESTP"** is shown in Table 8.2.

Adherence to enthalpy potential theory

The combined driving force for the transfer of heat and mass between unsaturated air and a wetted surface is the "enthalpy potential". This concept is fundamental in predicting the performance of cooling coils. The following equations must be satisfied to confirm the adherence of the empirical tests to the enthalpy potential. Thus

$$\Delta H = H_1 - H_2 \qquad (8.3)$$

$$\Delta(\Delta H) = (\Delta H)_A - (\Delta H)_B \qquad (8.4)$$

Results of TEST-P analysis

INPUT DATA								
Title	H78A:W3852	H78A:W3791	H78A:W3762	H78A:W3802	H78B:W3853	H78B:W3782	H78B:W3761	H78B:W3803
edb (°C)	28.98	29.01	28.92	28.98	35.28	35.44	35.66	35.49
edp (°C)	24.23	24.13	24.21	24.30	22.04	22.03	21.92	22.13
ldb (°C)	19.22	21.01	22.92	24.22	21.29	23.59	26.02	27.80
ldp (°C)	17.74	19.11	20.71	21.79	16.83	18.10	19.47	20.47
ewt (°C)	7.03	7.04	7.02	7.05	7.03	7.06	7.05	7.11
lwt (°C)	7.49	7.58	7.76	8.00	7.47	7.61	7.81	8.06
digistrip water (volts)	2.790	2.815	2.815	2.815	2.820	2.815	2.810	2.815
digistrip air (volts)	0.050	0.112	0.333	0.820	0.054	0.112	0.333	0.822
barometric pressure ("Hg)	29.85	30.26	30.13	30.14	29.85	30.13	30.13	30.14
actual condensate (g/s)	1.06	1.25	1.57	1.87	0.79	0.91	1.02	1.11
height of face (m)	0.457	0.457	0.457	0.457	0.457	0.457	0.457	0.457
length of face (m)	0.760	0.760	0.760	0.760	0.760	0.760	0.760	0.760
rows	1	1	1	1	1	1	1	1
No. of tubes high	12	12	12	12	12	12	12	12
No. of tubes fed	6	6	6	6	6	6	6	6
OUTPUT								
air volume flow (cms)	0.136	0.203	0.351	0.550	0.143	0.205	0.354	0.557
air mass flow (kg/s)	0.157	0.235	0.405	0.636	0.162	0.233	0.401	0.630
water flow rate (lps)	1.69	1.71	1.71	1.71	1.71	1.71	1.70	1.71
entering enthalpy (kJ/kg)	77.88	77.61	77.76	78.09	78.14	78.28	78.21	78.60
leaving enthalpy (kJ/kg)	51.48	56.27	62.00	66.09	51.75	56.70	62.23	66.42
specific volume (m^3/kg)	0.882	0.882	0.882	0.882	0.897	0.898	0.898	0.898
enthalpy change (delta H)	26.40	21.34	15.76	12.00	26.39	21.57	15.99	12.17
$delta(H)_A - delta(H)_B$	**0.01**	**-0.23**	**-0.23**	**-0.17**				
water side capacity (kw)	3.257	3.858	5.287	6.788	3.149	3.930	5.420	6.788
air side capacity (kw)	4.145	5.014	6.384	7.631	4.264	5.020	6.411	7.672
sensible heat factor	0.38	0.38	0.39	0.41	0.54	0.56	0.62	0.65
ratio of water/air cap.	0.79	0.77	0.83	0.89	0.74	0.78	0.85	0.88
est. condensate (g/kg)	1.01	1.21	1.52	1.77	0.76	0.86	0.95	1.05
act/est condensate	1.05	1.03	1.03	1.06	1.04	1.06	1.07	1.06
coil face area (sq.m)	0.347	0.347	0.347	0.347	0.347	0.347	0.347	0.347
face velocity (m/s)	0.39	0.59	1.01	1.58	0.41	0.59	1.02	1.60
water velocity (m/s)	1.61	1.63	1.63	1.63	1.63	1.63	1.62	1.63
measured water temp.rise	0.46	0.54	0.74	0.95	0.44	0.55	0.76	0.95
corrected water temp.rise	0.59	0.70	0.89	1.07	0.56	0.70	0.89	1.07

Table 8.2 : An example of the test results of a 1-row coil illustrating the adherence of the tests to the enthalpy potential.

A sample representation of two points each with a specific enthalpy of 78 kJ/kg is given on a psychrometric chart in Fig 8.1. If, for a given coil configuration and chilled water conditions, tests are performed at a given air face velocity from two different points on the same enthalpy line (such as H_{1A} and H_{1B} in Fig 8.1), the leaving conditions should in the absence of error or spurious effects lie on the same enthalpy line (such as H_{2A} and H_{2B} in Fig 8.1). This is substantially corroborated by the observation that equation (8.4) has been consistently satisfied to a tolerance within 0.5kJ/kg. It is thus seen that a high standard of empirical test results is achieved from the testing facility in spite of the varying nature of the several thermodynamic parameters measured within a complex compact heat exchanger.

Theoretical correlation of moisture condensation

It is apparent that the condensation of moisture from warm moist air in its passage across a dehumidifer involves a combination of both sensible and latent heat transfer. Although the individual rates of transfer of heat and mass under a given set of constraints may be different, as stated earlier, the net transport mechanism is governed by the overall enthalpy potential. Hence, it is evident that an essential relationship must exist between the mass of condensate collected per unit time and the change in the psychrometric state of the air as it passes through the coil. Close adherence to this requirement coupled with an excellent adherence to the overall enthalpy potential allows strong assertion of the reliability of the wide range of data accumulated during experiments on this truly complex set of physical phenomena.

The amount of moisture condensed from the air on the heat exchanger surface is measured by collecting the condensate over a certain time period (Table A4.2, Appendix 4). For any given test, this is compared with the theoretical estimate of condensate derived from the psychrometric calculations shown below.

Amount of condensate m_c (By psychrometric calculations) $= \Delta W \, m_a$, (8.5)

where $\Delta W = W_1 - W_2$.

Amount of condensate measured by primary means = m_c'.

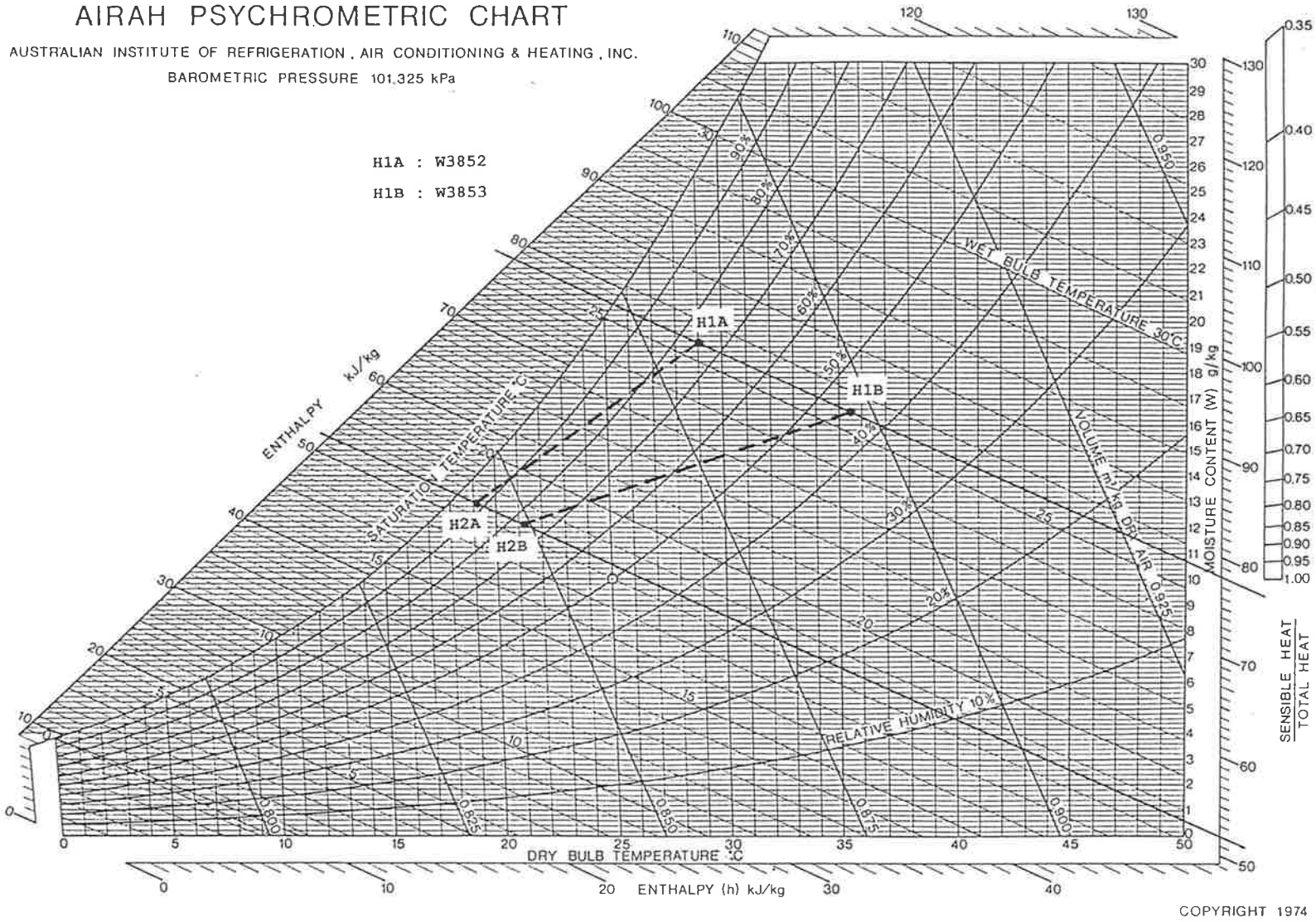

Fig 8.1 : A sample representation of two test points on the same enthalpy line on a psychrometric chart to illustrate the enthalpy potential theory.

$$\frac{\text{Amount of condensate by psychrometric calculations}}{\text{Amount of condensate measured by primary means}} = \frac{m_c}{m_c'}$$

$$= \left[1 + \frac{\epsilon}{m_c'} \right] \qquad (8.6)$$

where W_1 = Humidity ratio at entering air condition,

W_2 = Humidity ratio at leaving air condition,

m_a = Mass flow rate of air,

and ϵ = $m_c - m_c'$.

The various tests performed have indicated the deviation ϵ / m_c' as given by equation (8.6) is less than 0.1. Thus the value of ϵ / m_c' is a reliable check on the change in the humidity ratio, ΔW, across a dehumidifier.

Determination of total heat quantity

An accurate heat balance between the air and water sides has not been possible due to difficulties encountered in measuring extremely low water temperature rise accurately. The specified accuracy of the platinum resistance probes used for the measurement of entering and leaving chilled water temperatures is ±0.05°C and the change in chilled water temperature is of the order of 0.5 to 3°C. Thus the potential error could be as high as ±10%. It is evident that the chilled water temperature measurements could lead to erroneous results, if used to define differences between inlet and outlet flows when water temperature rises are extremely low. This situation is inherent in the tests described in this thesis. A good correlation of $\underline{\Delta W}$ values, as indicated earlier, requires also good accuracy in the mass flow of air as measured by the Venturi. In view of the good $\underline{\Delta(\Delta H)}$ values, the total quantity of heat, q_t, has been determined from the air-side and is considered to be sufficiently accurate for use in the analyses.

8.2 Data Reduction - ARI Method

The theory behind the ARI method of data reduction has already been developed in Chapter 5. The actual determination of the various air film thermal resistances is presented in this section. Fig 8.2 is a plot of $(R_{aD} + R_{mD})$ vs R_{aD} which is used during data reduction of only dry tests of 1, 2 and 4-row coils. As already stated in Chapter 5, the development of the curve in Fig 8.2 does not require any test data other than that on which the expression for ϕ was based [Gardner (1945)]. The analysis of a single row coil is presented first followed by that of 2- and 4-row coils.

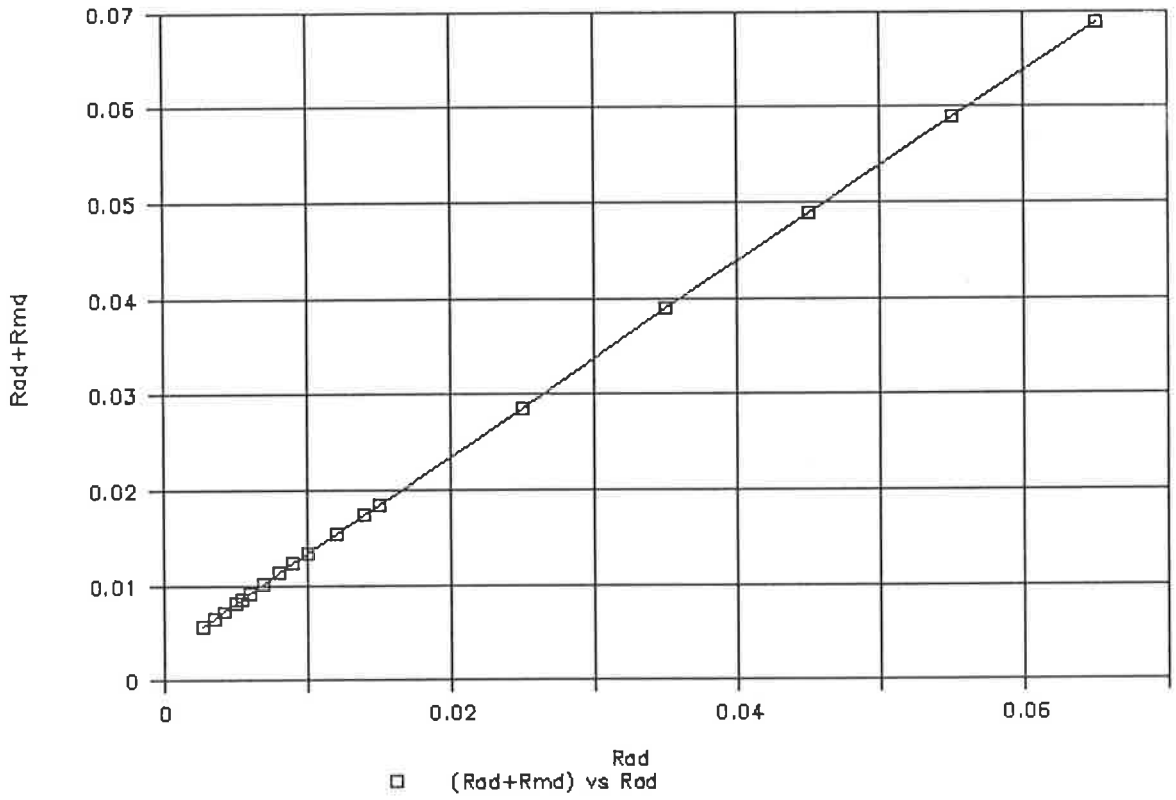

Fig 8.2 : Plot of $(R_{aD} + R_{mD})$ vs R_{aD} used in the analysis of dry tests of 1, 2 and 4-row coils.

This ARI data reduction program is used to analyse the empirical test results { FULLY DRY OR FULLY WET } to obtain the values of Rad and Raw of a Muller 1, 2 or 4 Row, 6FPI, half circuited coil.
ANALYSIS OF A FULLY DRY TEST

Input:							
TEST CODE			D2904	D2892	D2891	D2901	D2902	D2903
ENTERING DRY BULB TEMP	(°C)		54.90	44.63	50.70	48.74	34.30	29.80
ENTERING DEW POINT TEMP	(°C)		11.90	13.75	19.20	9.50	4.75	3.40
LEAVING DRY BULB TEMP	(°C)		30.65	31.00	39.15	39.65	28.07	25.00
LEAVING DEW POINT TEMP	(°C)		11.90	13.75	19.20	9.50	4.75	3.40
ENTERING WATER TEMP	(°C)		14.90	11.30	17.15	18.74	8.74	7.60
WATER TEMPERATURE RISE	(°C)		0.50	0.65	0.84	0.87	0.80	0.81
ACTUAL AIR FLOW	(lps)		141.00	278.00	435.00	570.00	738.00	952.00
WATER VELOCITY	(m/s)		1.70	1.50	1.50	1.50	1.50	1.50
NUMBER OF TUBES FED			6	6	6	6	6	6
COIL HEIGHT	(mm)		457.00	457.00	457.00	457.00	457.00	457.00
COIL LENGTH	(mm)		760.00	760.00	760.00	760.00	760.00	760.00
NUMBER OF ROWS			1	1	1	1	1	1
Output:								
COIL FACE AREA	(sq.m)		0.35	0.35	0.35	0.35	0.35	0.35
STANDARD FACE VELOCITY	(m/s)		0.36	0.74	1.13	1.49	2.03	2.65
WATER FLOW	(lps)		1.78	1.57	1.57	1.57	1.57	1.57
ENTERING ENTHALPY	(kJ/kg)		77.45	69.95	86.91	67.84	47.90	42.12
LEAVING ENTHALPY	(kJ/kg)		52.82	56.08	75.07	58.62	41.61	37.28
REFRIGERATING CAPACITY	(kW)		3.72	4.26	5.57	5.73	5.31	5.35
SENSIBLE CAPACITY	(kW)		3.66	4.18	5.43	5.66	5.26	5.31
TOTAL THERMAL RES (R)		(sq.m°C)/W	0.0384	0.0333	0.0271	0.0238	0.0227	0.0198
INS.FILM HEAT TRANS.RES (Rw)		(sq.m°C)/W	0.0021	0.0024	0.0022	0.0022	0.0024	0.0025
AIR FILM THERM RES DRY SUR.(Rad)		(sq.m°C)/W	0.0331	0.0277	0.0215	0.0184	0.0169	0.0140
LOG(Va)			-0.44	-0.13	0.05	0.17	0.31	0.42
LOG(Rad)			-1.48	-1.56	-1.67	-1.74	-1.77	-1.85

Table 8.3 : Printout of the program "ARI DATA REDUCTION". Results of 1-row coil dry tests over a range of face velocities.

This ARI data reduction program is used to analyse the
empirical test results { FULLY DRY OR FULLY WET } to
obtain the values of Rad and Raw of a Muller 1, 2 or 4
Row, 6FPI, half circuited coil.
ANALYSIS OF A FULLY WET TEST

Input:

TEST CODE		H66B:W3881	H66B:W3741	H66B:W3771	H66B:W3752	H66B:W3751
ENTERING DRY BULB TEMP	('C)	31.00	31.12	31.03	30.80	30.90
ENTERING DEW POINT TEMP	('C)	18.95	18.76	18.80	18.85	18.72
LEAVING DRY BULB TEMP	('C)	19.00	20.80	22.85	24.20	25.00
LEAVING DEW POINT TEMP	('C)	14.70	15.62	16.84	17.60	17.90
ENTERING WATER TEMP	('C)	7.00	7.10	7.00	7.00	7.10
WATER TEMPERATURE RISE	('C)	0.45	0.55	0.70	0.83	0.90
ACTUAL AIR FLOW	(lps)	136.00	202.00	350.00	551.00	728.00
WATER VELOCITY	(m/s)	1.63	1.61	1.63	1.63	1.62
NUMBER OF TUBES FED		6	6	6	6	6
COIL HEIGHT (mm)		457.00	457.00	457.00	457.00	457.00
COIL LENGTH (mm)		760.00	760.00	760.00	760.00	760.00
NUMBER OF ROWS		1	1	1	1	1

Output:

COIL FACE AREA	(sq.m)	0.35	0.35	0.35	0.35	0.35
STANDARD FACE VELOCITY	(m/s)	0.38	0.56	0.97	1.52	2.01
WATER FLOW	(lps)	1.71	1.69	1.71	1.71	1.70
ENTERING ENTHALPY	(kJ/kg)	66.15	65.85	65.84	65.72	65.53
LEAVING ENTHALPY	(kJ/kg)	45.47	48.95	53.36	56.28	57.72
REFRIGERATING CAPACITY	(kW)	3.24	3.93	5.03	5.99	6.55
FIN EFFICIENCY		0.81	0.78	0.73	0.67	0.64
AIR SIDE HEAT TRANS.MULTIPLIER	(m"/cp)	2.35	2.42	2.53	2.62	2.69
INS.FILM HEAT TRANS.RES (Rw)	(sq.m'C)/W	0.0024	0.0024	0.0023	0.0023	0.0024
TUBE MATERIAL THERMAL RES (Rt)	(sq.m'C)/W	0.00002	0.00002	0.00002	0.00002	0.00002
FIN MATERIAL THERMAL RES (Rfw)	(sq.m'C)/W	0.0035	0.0034	0.0034	0.0033	0.0032
TOTAL METAL THERM RES (Rmw)	(sq.m'C)/W	0.0035	0.0034	0.0034	0.0033	0.0033
AIR FILM THERM RES WET SUR.(Raw)	(sq.m'C)/W	0.0395	0.0324	0.0252	0.0202	0.0176
COIL CHARACTERISTIC (C)	(kg'C)/kJ	0.1470	0.1794	0.2290	0.2843	0.3257
TIE LINE SLOPE (TLS = -1/C)	kJ/(kg'C)	-6.80	-5.57	-4.37	-3.52	-3.07
LOG(Va)		-0.43	-0.25	-0.01	0.18	0.30
LOG(Raw)		-1.40	-1.49	-1.60	-1.70	-1.76

Table 8.4 : Printout of the program "ARI DATA REDUCTION". Results of 1-row coil wet tests over a range of face velocities.

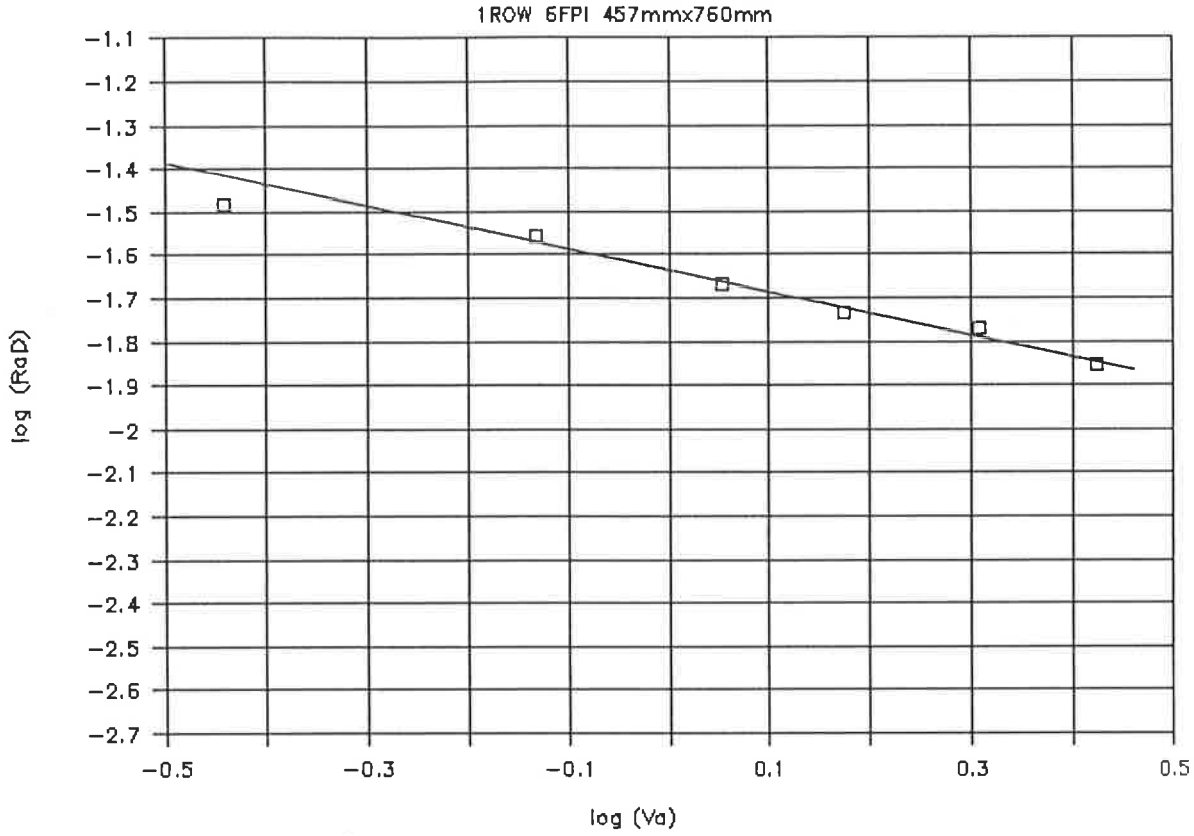

Fig 8.3 : Application rating curve, $\log(R_{aD})$ vs $\log(V_a)_{std}$, for 1-row sensible heat coil.

t_1=31°C t_1"=18.8°C t_{w1}=7°C V_w=1.6m/s

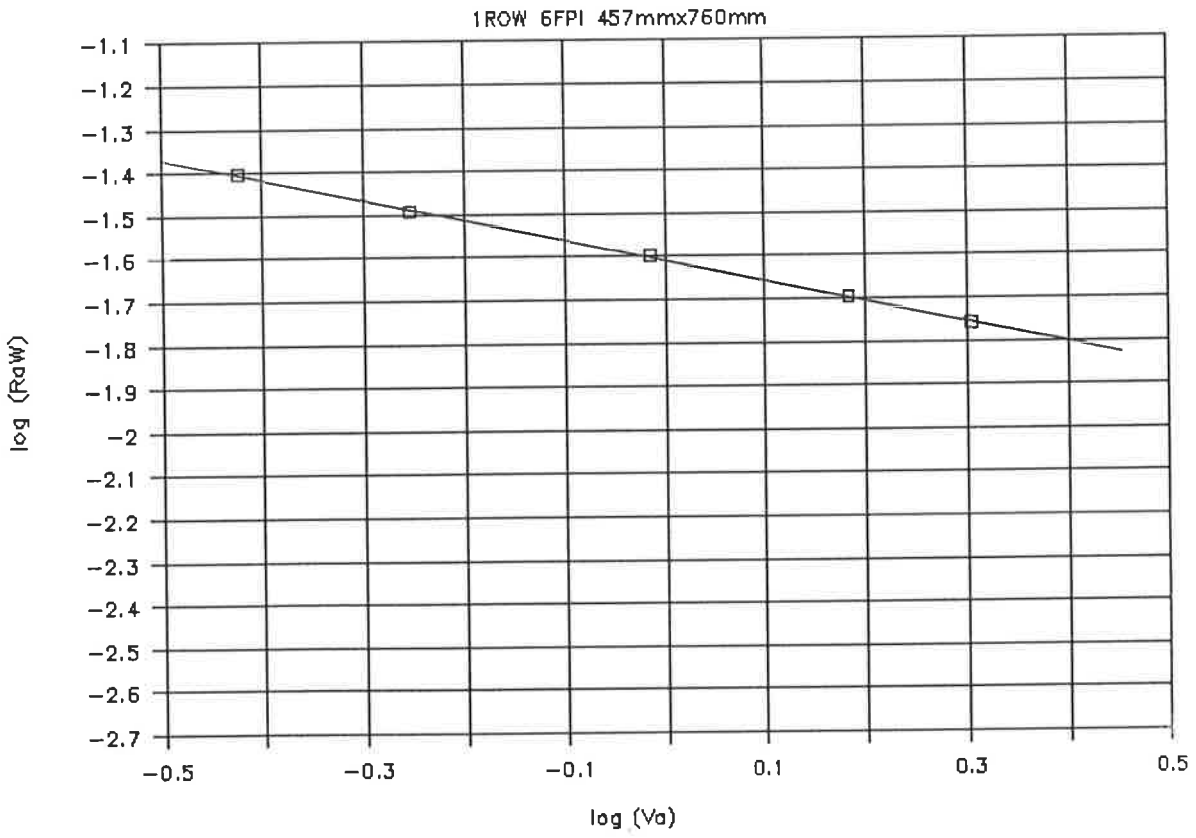

Fig 8.4 : Application rating curve, $\log(R_{aW})$ vs $\log(V_a)_{std}$, for 1-row dehumidifying coil.

This ARI data reduction program is used to analyse the
empirical test results { FULLY DRY OR FULLY WET } to
obtain the values of Rad and Raw of a Muller 1, 2 or 4
Row, 6FPI, half circuited coil.
ANALYSIS OF A FULLY DRY TEST

Input:

TEST CODE			D6102	D6101	D6103	D6111
ENTERING DRY BULB TEMP	(°C)		42.60	43.80	44.10	43.60
ENTERING DEW POINT TEMP	(°C)		14.40	18.50	11.90	7.40
LEAVING DRY BULB TEMP	(°C)		23.00	28.70	31.00	31.70
LEAVING DEW POINT TEMP	(°C)		14.40	18.50	11.90	7.40
ENTERING WATER TEMP	(°C)		12.40	16.70	18.15	18.50
WATER TEMPERATURE RISE	(°C)		1.12	1.42	1.50	1.59
ACTUAL AIR FLOW	(lps)		175.00	292.00	362.00	420.00
WATER VELOCITY	(m/s)		1.58	1.60	1.60	1.61
NUMBER OF TUBES FED			3	3	3	3
COIL HEIGHT	(mm)		229.00	229.00	229.00	229.00
COIL LENGTH	(mm)		760.00	760.00	760.00	760.00
NUMBER OF ROWS			2	2	2	2

Output:

COIL FACE AREA	(sq.m)		0.17	0.17	0.17	0.17
STANDARD FACE VELOCITY	(m/s)		0.93	1.54	1.92	2.23
WATER FLOW	(lps)		0.83	0.84	0.84	0.84
ENTERING ENTHALPY	(kJ/kg)		68.99	78.26	66.48	60.07
LEAVING ENTHALPY	(kJ/kg)		49.03	62.80	53.17	48.04
REFRIGERATING CAPACITY	(kW)		3.88	4.99	5.33	5.61
SENSIBLE CAPACITY	(kW)		3.81	4.87	5.25	5.55
TOTAL THERMAL RES (R)		(sq.m°C)/W	0.0262	0.0201	0.0187	0.0176
INS.FILM HEAT TRANS.RES (Rw)		(sq.m°C)/W	0.0022	0.0021	0.0021	0.0021
AIR FILM THERM RES DRY SUR.(Rad)		(sq.m°C)/W	0.0207	0.0147	0.0133	0.0122
LOG(Va)			-0.03	0.19	0.28	0.35
LOG(Rad)			-1.68	-1.83	-1.87	-1.91

Table 8.5 : Printout of the program "ARI DATA REDUCTION". Results of 2 row coil dry tests over a range of face velocities.

This ARI data reduction program is used to analyse the
empirical test results { FULLY DRY OR FULLY WET } to
obtain the values of Rad and Raw of a Muller 1, 2 or 4
Row, 6FPI, half circuited coil.
ANALYSIS OF A FULLY WET TEST

Input:

TEST CODE		H66C:W5401	H66C:W5471	H66C:W5262	H66C:W6051
ENTERING DRY BULB TEMP	(°C)	28.57	28.95	28.82	29.07
ENTERING DEW POINT TEMP	(°C)	19.70	19.85	19.64	19.80
LEAVING DRY BULB TEMP	(°C)	12.45	14.07	16.24	18.40
LEAVING DEW POINT TEMP	(°C)	11.24	12.65	14.39	16.20
ENTERING WATER TEMP	(°C)	6.94	7.03	7.00	6.94
WATER TEMPERATURE RISE	(°C)	0.78	0.96	1.30	1.66
ACTUAL AIR FLOW	(lps)	149.00	201.00	343.00	271.00
WATER VELOCITY	(m/s)	1.62	1.61	1.62	1.60
NUMBER OF TUBES FED		6	6	6	3
COIL HEIGHT (mm)		457.00	457.00	457.00	229.00
COIL LENGTH (mm)		760.00	760.00	760.00	760.00
NUMBER OF ROWS		2	2	2	2

Output:

COIL FACE AREA	(sq.m)	0.35	0.35	0.35	0.17
STANDARD FACE VELOCITY	(m/s)	0.41	0.56	0.95	1.50
WATER FLOW	(lps)	1.70	1.69	1.70	0.84
ENTERING ENTHALPY	(kJ/kg)	65.37	66.12	65.49	66.12
LEAVING ENTHALPY	(kJ/kg)	33.39	37.10	42.13	47.58
REFRIGERATING CAPACITY	(kW)	5.53	6.75	9.29	5.82
FIN EFFICIENCY		0.78	0.75	0.68	0.62
AIR SIDE HEAT TRANS.MULTIPLIER (m"/cp)		2.32	2.39	2.51	2.65
INS.FILM HEAT TRANS.RES (Rw)	(sq.m°C)/W	0.0024	0.0024	0.0023	0.0024
TUBE MATERIAL THERMAL RES (Rt)	(sq.m°C)/W	0.00002	0.00002	0.00002	0.00002
FIN MATERIAL THERMAL RES (Rfw)	(sq.m°C)/W	0.0034	0.0034	0.0033	0.0032
TOTAL METAL THERM RES (Rmw)	(sq.m°C)/W	0.0034	0.0034	0.0033	0.0032
AIR FILM THERM RES WET SUR.(Raw)	(sq.m°C)/W	0.0312	0.0275	0.0198	0.0162
COIL CHARACTERISTIC (C)	(kg°C)/kJ	0.1862	0.2111	0.2902	0.3536
TIE LINE SLOPE (TLS = -1/C)	kJ/(kg°C)	-5.37	-4.74	-3.45	-2.83
LOG(Va)		-0.38	-0.25	-0.02	0.18
LOG(Raw)		-1.51	-1.56	-1.70	-1.79

Table 8.6 : Printout of the program "ARI DATA REDUCTION". Results of 2 row coil wet tests over a range of face velocities.

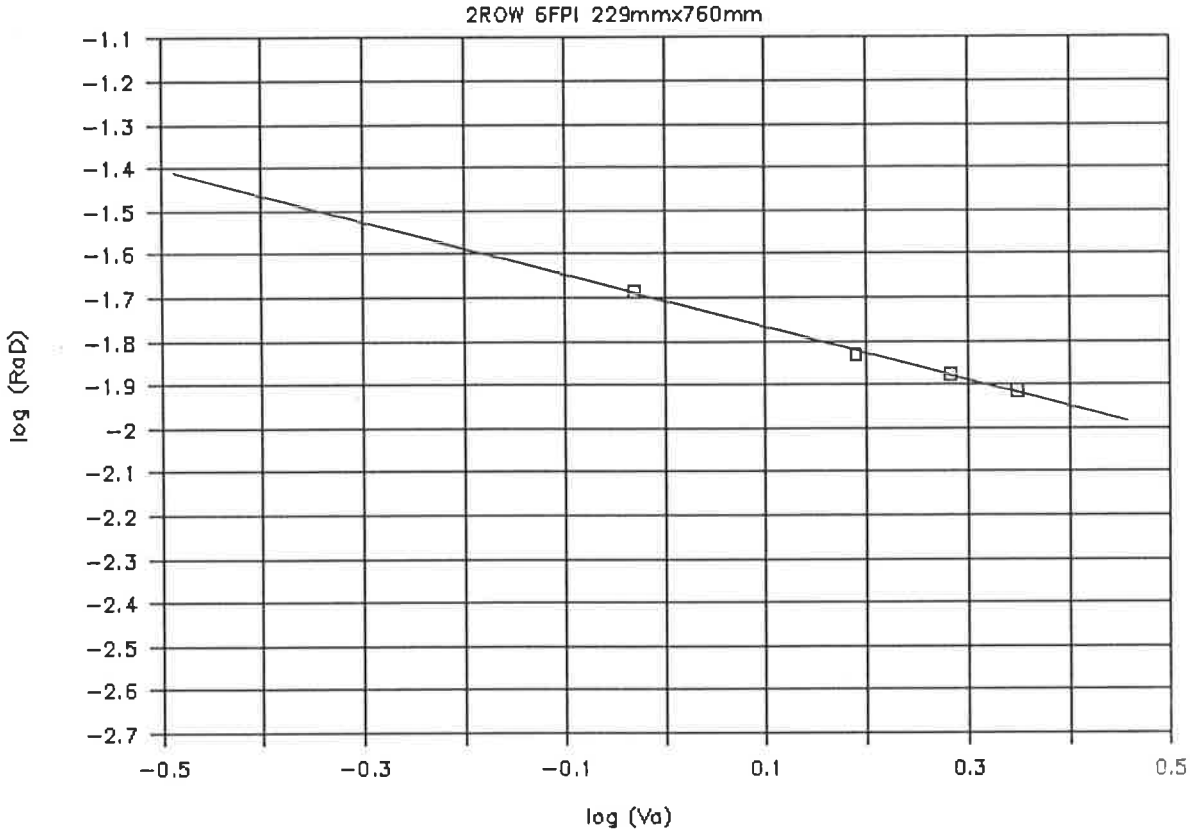

Fig 8.5 : Application rating curve, $\log(R_{aD})$ vs $\log(V_a)_{std}$, for 2-row sensible heat coil.

t_1=29°C t_1"=19.7°C t_{w1}=7°C V_w=1.6m/s

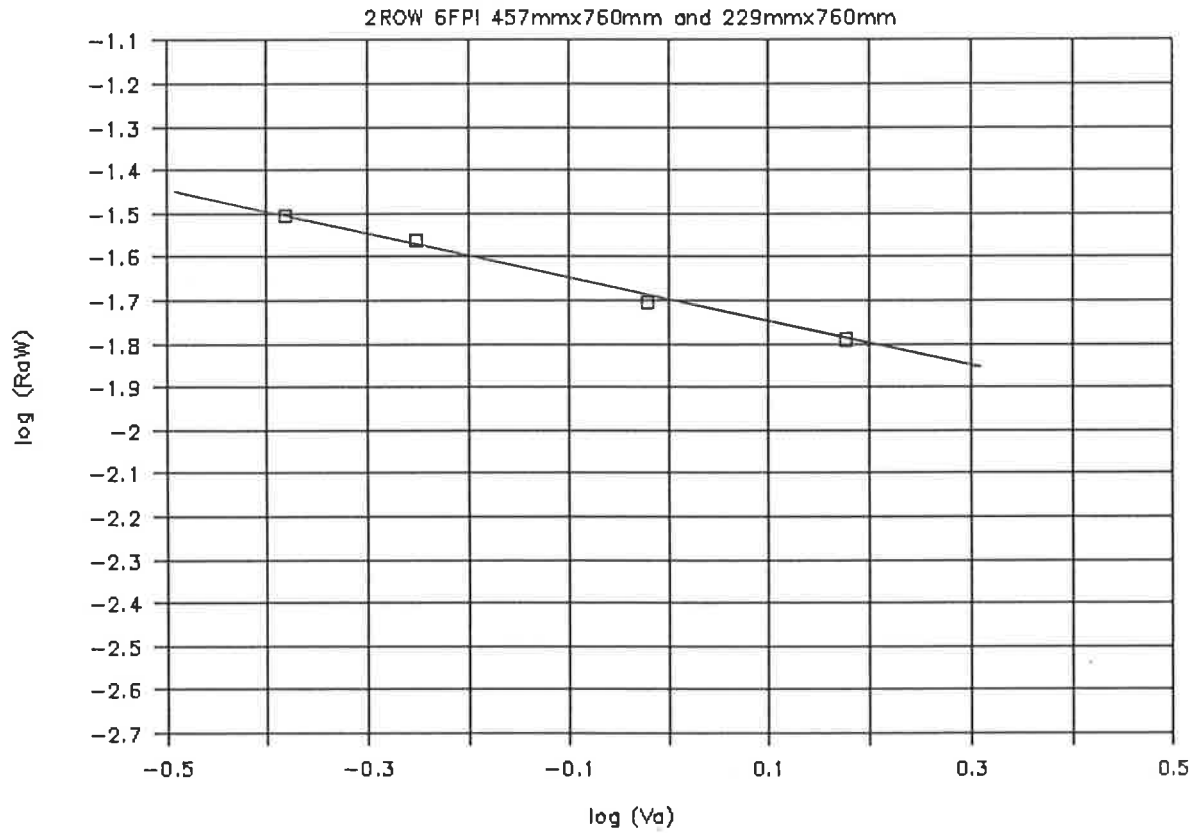

Fig 8.6 : Application rating curve, $\log(R_{aW})$ vs $\log(V_a)_{std}$, for 2-row dehumidifying coil.

This ARI data reduction program is used to analyse the
empirical test results { FULLY DRY OR FULLY WET } to
obtain the values of Rad and Raw of a Muller 1, 2 or 4
Row, 6FPI, half circuited coil.
ANALYSIS OF A FULLY DRY TEST

Input:					
TEST CODE			D6571	D6542	D6541
ENTERING DRY BULB TEMP	(°C)		35.70	37.25	37.70
ENTERING DEW POINT TEMP	(°C)		11.30	16.30	18.30
LEAVING DRY BULB TEMP	(°C)		18.40	20.30	22.00
LEAVING DEW POINT TEMP	(°C)		11.30	16.30	18.30
ENTERING WATER TEMP	(°C)		15.70	16.40	17.60
WATER TEMPERATURE RISE	(°C)		0.51	0.73	0.90
ACTUAL AIR FLOW	(lps)		184.00	268.00	354.00
WATER VELOCITY	(m/s)		1.64	1.64	1.64
NUMBER OF TUBES FED			6	6	6
COIL HEIGHT	(mm)		457.00	457.00	457.00
COIL LENGTH	(mm)		373.00	373.00	373.00
NUMBER OF ROWS			4	4	4
Output:					
COIL FACE AREA	(sq.m)		0.17	0.17	0.17
STANDARD FACE VELOCITY	(m/s)		1.02	1.48	1.95
WATER FLOW	(lps)		1.72	1.72	1.72
ENTERING ENTHALPY	(kJ/kg)		57.07	67.02	71.58
LEAVING ENTHALPY	(kJ/kg)		39.51	49.71	55.50
REFRIGERATING CAPACITY	(kW)		3.67	5.24	6.41
SENSIBLE CAPACITY	(kW)		3.62	5.13	6.26
TOTAL THERMAL RES (R)		(sq.m°C)/W	0.0251	0.0206	0.0171
INS.FILM HEAT TRANS.RES (Rw)		(sq.m°C)/W	0.0021	0.0021	0.0020
AIR FILM THERM RES DRY SUR.(Rad)		(sq.m°C)/W	0.0197	0.0152	0.0118
LOG(Va)			0.01	0.17	0.29
LOG(Rad)			-1.71	-1.82	-1.93

Table 8.7 : Printout of the program "ARI DATA REDUCTION". Results of 4-row coil dry tests over a range of face velocities.

This ARI data reduction program is used to analyse the
empirical test results { FULLY DRY OR FULLY WET } to
obtain the values of Rad and Raw of a Muller 1, 2 or 4
Row, 6FPI, half circuited coil.
ANALYSIS OF A FULLY WET TEST

Input:

TEST CODE		:	H66B:W6471	H66B:W6461	H66B:W6441
ENTERING DRY BULB TEMP	(°C)	:	31.00	31.20	31.06
ENTERING DEW POINT TEMP	(°C)	:	18.76	18.70	18.84
LEAVING DRY BULB TEMP	(°C)	:	9.63	10.95	12.60
LEAVING DEW POINT TEMP	(°C)	:	9.42	10.75	12.50
ENTERING WATER TEMP	(°C)	:	7.00	7.00	7.00
WATER TEMPERATURE RISE	(°C)	:	0.65	0.97	1.30
ACTUAL AIR FLOW	(lps)	:	105.00	172.00	265.00
WATER VELOCITY	(m/s)	:	1.61	1.61	1.62
NUMBER OF TUBES FED		:	6	6	6
COIL HEIGHT (mm)		:	457.00	457.00	457.00
COIL LENGTH (mm)		:	373.00	373.00	373.00
NUMBER OF ROWS		:	4	4	4

Output:

COIL FACE AREA	(sq.m)	:	0.17	0.17	0.17
STANDARD FACE VELOCITY	(m/s)	:	0.59	0.97	1.49
WATER FLOW	(lps)	:	1.69	1.69	1.70
ENTERING ENTHALPY	(kJ/kg)	:	65.72	65.80	65.96
LEAVING ENTHALPY	(kJ/kg)	:	28.10	31.19	35.38
REFRIGERATING CAPACITY	(kW)	:	4.55	6.85	9.33
FIN EFFICIENCY		:	0.76	0.68	0.60
AIR SIDE HEAT TRANS.MULTIPLIER	(m"/cp)	:	2.32	2.42	2.54
INS.FILM HEAT TRANS.RES (Rw)	(sq.m°C)/W	:	0.0024	0.0024	0.0023
TUBE MATERIAL THERMAL RES (Rt)	(sq.m°C)/W	:	0.00002	0.00002	0.00002
FIN MATERIAL THERMAL RES (Rfw)	(sq.m°C)/W	:	0.0034	0.0033	0.0032
TOTAL METAL THERM RES (Rmw)	(sq.m°C)/W	:	0.0034	0.0033	0.0032
AIR FILM THERM RES WET SUR.(Raw)	(sq.m°C)/W	:	0.0283	0.0188	0.0140
COIL CHARACTERISTIC (C)	(kg°C)/kJ	:	0.2054	0.3070	0.4057
TIE LINE SLOPE (TLS = -1/C)	kJ/(kg°C)	:	-4.87	-3.26	-2.46
LOG(Va)		:	-0.23	-0.01	0.17
LOG(Raw)		:	-1.55	-1.73	-1.85

Table 8.8 : Printout of the program "ARI DATA REDUCTION". Results of 4-row coil wet tests over a range of face velocities.

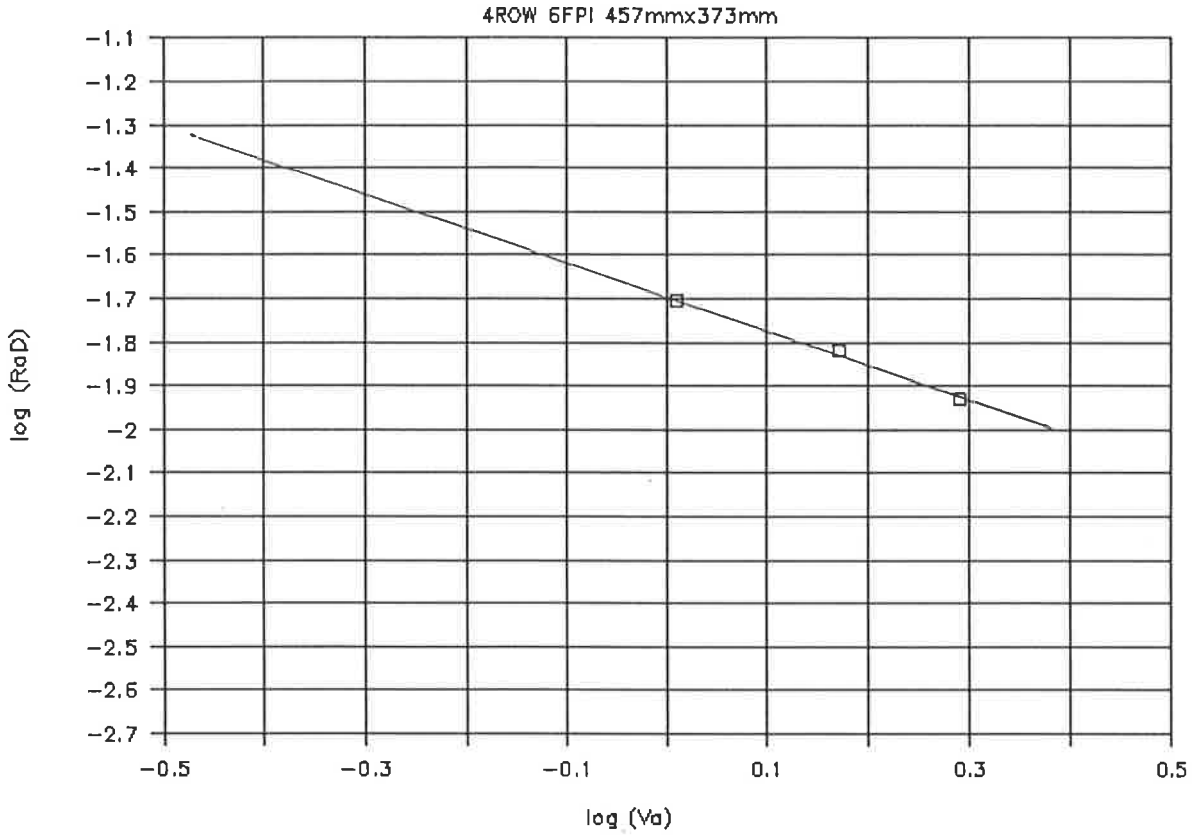

Fig 8.7 : Application rating curve, $\log(R_{aD})$ vs $\log(V_a)_{std}$, for 4-row sensible heat coil.

t_1=31°C t_1"=18.8°C t_{w1}=7°C V_w=1.6m/s

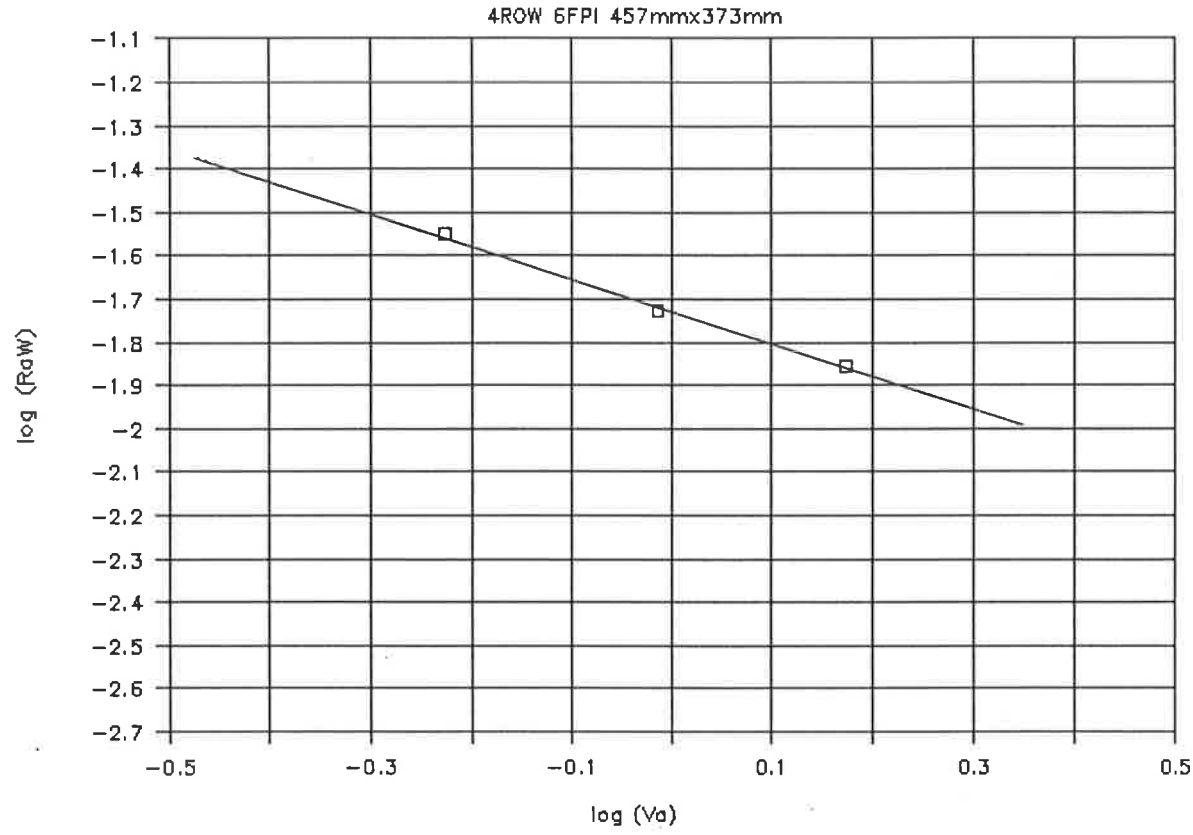

Fig 8.8 : Application rating curve, $\log(R_{aW})$ vs $\log(V_a)_{std}$, for 4-row dehumidifying coil.

8.2.1 Single Row Coil

Computer printouts of the program "ARI DATA REDUCTION" for dry tests are presented in Table 8.3 and the values of the logarithm of the dry air side thermal resistance, log R_{aD}, are plotted against the logarithm of the air face velocity, log V_a, in Fig 8.3. A linear relationship is observed and the empirical expression for the dry coil application rating curve may be determined to be

$$R_{aD} = 0.024x(V_a)^{-0.486} \quad . \tag{8.7}$$

Computer printouts for wet tests are presented in Table 8.4 and the values of log R_{aW} are plotted against log V_a in Fig 8.4. Once again a linear relationship is observed and the resulting empirical expression for the wet coil application rating curve is found to be

$$R_{aW} = 0.025x(V_a)^{-0.485} \quad . \tag{8.8}$$

In the above equations and similar equations elsewhere in this thesis, it should be noted that the variance of the least squares fit of the straight line relationships to the data effectively limit the number of figures in the coefficients and exponents which are significant.

8.2.2 Two Row Coil

Computer printouts of the program "ARI DATA REDUCTION" for dry and wet tests are presented in Tables 8.5 and 8.6 respectively. The plots of (log R_{aD} vs log V_a) and (log R_{aW} vs log V_a) are presented in Figs 8.5 and 8.6 respectively. Both the plots reveal linear relationships and the following empirical expressions are determined for the dry and wet coil application rating curves :

$$R_{aD} = 0.02x(V_a)^{-0.605} \tag{8.9}$$

and $$R_{aW} = 0.02x(V_a)^{-0.508} \quad . \tag{8.10}$$

8.2.2 Four Row Coil

Computer printouts of the program "ARI DATA REDUCTION" for dry and wet tests are presented in Tables 8.7 and 8.8 respectively. The plots of (log R_{aD} vs log V_a) and (log R_{aW} vs log V_a) are presented in Figs 8.7 and 8.8 respectively. Both the plots have linear relationships and the following empirical expressions are determined for the dry and wet coil application rating curves :

$$R_{aD} = 0.02x(V_a)^{-0.796} \tag{8.11}$$

and $$R_{aW} = 0.019x(V_a)^{-0.758} \quad . \tag{8.12}$$

8.3 Data Reduction - AU Method

The theory behind the AU method of data reduction has been developed in Chapter 6. The actual determinations of the various heat and mass transfer coefficients are presented in this section. As discussed earlier, the computer program "TLS BY LEWIS NUMBER CORRELATION" is used to obtain h_i, h_{cow}, TLS, Re and St.$(Pr)^{2/3}$ for fully wet tests.

8.3.1 One Row Coil

Examples of the printouts from the program **"TLS BY LEWIS NUMBER CORRELATION"** are presented in Tables 8.9 - 8.13. The values of $\log[St.(Pr)^{2/3}]$ vs $\log(Re)$ are plotted in Figs 8.9 - 8.13 for tests of a fully wet 1-row coil. Each Table comprises tests over a range of face velocities for a given entering air condition, given entering water temperature and set water velocity. A comparison for different entering air conditions and different water velocities is available from Tables 8.9, 8.10 and 8.11 and Figs 8.9, 8.10 and 8.11, while a comparison of different entering air conditions at a constant water velocity is obtained from Tables 8.10, 8.12 and 8.13 and Figs 8.10, 8.12 and 8.13. A linear relationship between $\log[St.(Pr)^{2/3}]$ and $\log(Re)$ is obtained from these plots and it is concluded that for a coil of a given physical geometry, h_{cow} depends only on Re (or face velocity) and is independent of the entering air condition or the tube-side conditions. It is to be noted here that a consistent line is drawn for the plots of Figs 8.9 - 8.13 and any minor deviation of the points from this line indicates the deviation of the value of h_{cow} as obtained from the actual test results.

The equation of the observed relationship between $St.(Pr)^{2/3}$ and Reynolds number can be determined from the assembled data. The values of $\log[St.(Pr)^{2/3}]$ and $\log(Re)$ from Table 8.12 are used and the following empirical relation is obtained :

$$St.(Pr)^{2/3} = 0.23(Re)^{-0.383} \qquad (8.13)$$

Equation (8.13) is used in the generalisation process to obtain the value of h_{cow} for a single row coil.

As discussed in Section 6.2.2, the empirical constant $(R_m + R_{ow})$ is obtained as the difference between R_i and R_w. The values of $(R_m + R_{ow})$ for the above tests are tabulated in Table 8.14.

The values of h_i used in Table 8.14 are used from Tables 8.9 - 8.13. As discussed in Section 6.2.2, the McAdams equation is used to compute R_w. A graph of $(R_m + R_{ow})$ vs R_{cow} is plotted in Fig 8.14 and the resulting best fit lines are

$$(R_m + R_{ow}) = \frac{0.0975}{h_{cow}} + 0.0041 \quad \text{for } h_{cow} > 50 \qquad (8.14a)$$

$$\text{and} \quad (R_m + R_{ow}) = \frac{0.0182}{h_{cow}} + 0.0056 \quad \text{for } h_{cow} \leq 50 \qquad (8.14b)$$

TLS determined by an iterative process
of correlating Lewis number :
INPUTS TO THE PROGRAM

Test Code	:H66B:W4061	H66B:W4062	H66B:W4063	H66B:W4081	H66B:W4082
Entering dry bulb temp (°C) :	31.06	31.00	31.02	31.05	31.01
Entering dew point temp (°C) :	18.78	18.80	18.77	18.77	18.79
Leaving dry bulb temp (°C) :	19.30	21.13	23.29	24.58	25.40
Leaving dew point temp (°C) :	14.88	15.92	17.00	17.83	18.12
Entering water temp (°C) :	6.99	7.00	7.00	6.98	6.98
Corrected water temp rise :	0.71	0.84	1.05	1.25	1.36
Air volume flow (lps) :	139.0	202.0	350.0	551.0	729.0
Number of rows :	1	1	1	1	1
OUTPUT FROM THE PROGRAM					
Air face velocity (m/s) :	0.40	0.58	1.01	1.59	2.10
Entering surface temp (°C) :	14.69	15.57	16.61	17.84	18.11
Leaving surface temp (°C) :	11.05	12.26	13.84	15.51	16.07
TLS :	-3.55	-2.89	-2.24	-1.62	-1.50
hi [W/(sq.m°C)] :	1371.1	1355.2	1429.9	1417.0	1500.8
hcow[qs/(Ao LMTD)][W/(sq.m°C)] :	29.92	36.50	49.95	70.25	80.52
hdo[ql/(Ao LMWD)][kg/(s sq.m)] :	32.43	39.57	54.14	76.15	87.29
Le [hcow/(hdo cp)] :	0.90	0.90	0.90	0.90	0.90
hcow1[cp hi Ai/(TLS Ao)] :	31.13	37.83	51.32	70.65	80.48
hdo1 [hcow1/(0.9 cp)] :	33.75	41.00	55.63	76.58	87.24
Reynolds number :	227.0	329.9	571.6	899.8	1190.6
Stanton(Prandtl)$^{2/3}$:	0.0285	0.0239	0.0189	0.0169	0.0146
log(Re) :	2.36	2.52	2.76	2.95	3.08
log[St(Pr)$^{2/3}$] :	-1.55	-1.62	-1.72	-1.77	-1.84

Table 8.9 : Printout of the program "TLS BY LEWIS NUMBER CORRELATION". Results of 1-row coil spanning a range of face velocities with a specific entering air condition having an enthalpy of 66kJ/kg and a chilled water velocity of 1m/s.

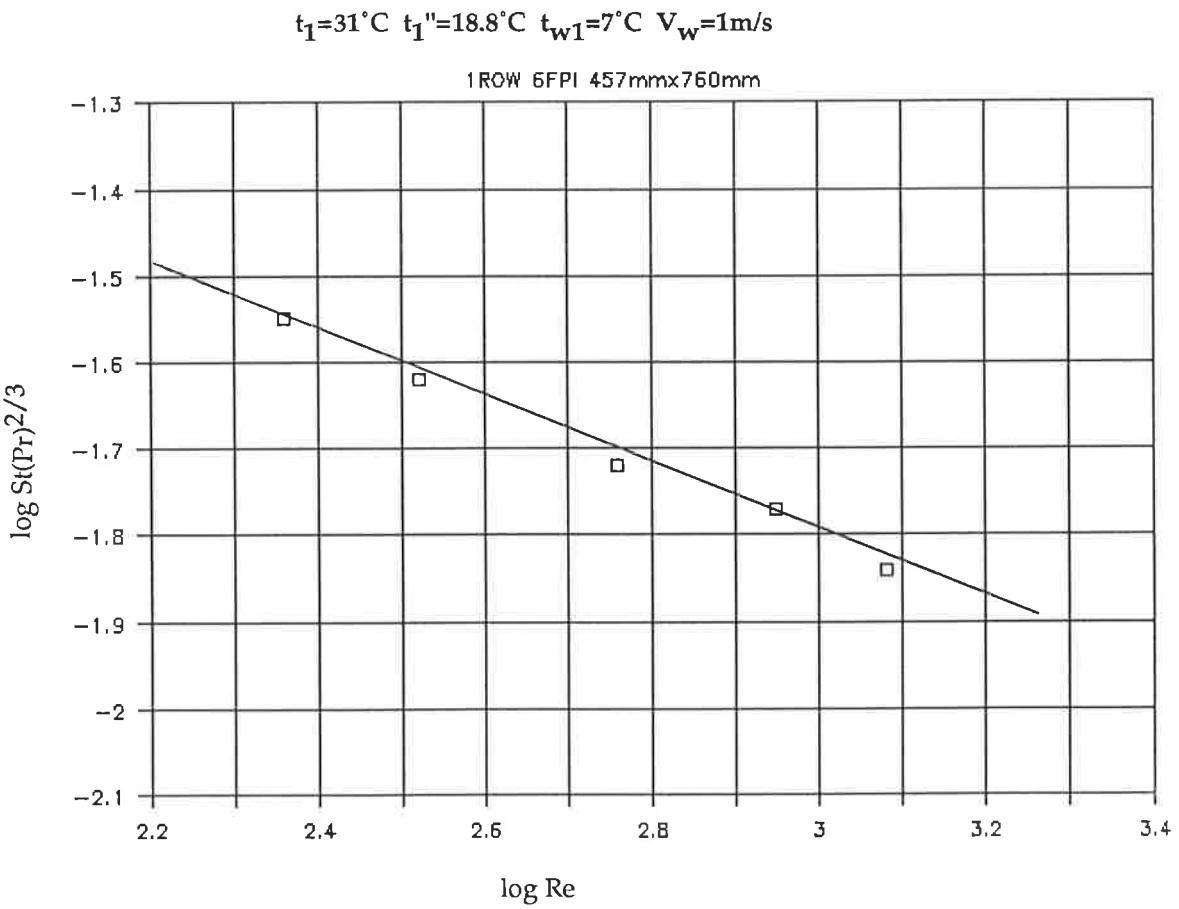

Fig 8.9 : Plot of log[St(Pr)$^{2/3}$] against logRe for the values in Table 8.9.

TLS determined by an iterative process
of correlating Lewis number :
INPUTS TO THE PROGRAM

Test Code	:H72B:W3862	H72B:W3781	H72B:W3772	H72B:W3842	H72B:W3841
Entering dry bulb temp (°C)	: 33.63	33.64	33.69	33.60	33.62
Entering dew point temp (°C)	: 20.37	20.33	20.29	20.27	20.33
Leaving dry bulb temp (°C)	: 20.33	22.39	24.64	26.20	27.09
Leaving dew point temp (°C)	: 15.69	16.85	18.07	18.93	19.40
Entering water temp (°C)	: 6.99	7.07	7.02	7.05	7.04
Corrected water temp rise	: 0.52	0.63	0.79	0.95	1.03
Air volume flow (lps)	: 140.0	206.0	348.0	555.0	731.0
Number of rows	: 1	1	1	1	1
OUTPUT FROM THE PROGRAM					
Air face velocity (m/s)	: 0.40	0.59	1.00	1.60	2.10
Entering surface temp (°C)	: 15.23	16.27	17.58	18.67	19.26
Leaving surface temp (°C)	: 11.26	12.64	14.48	16.10	17.02
TLS	: -3.83	-3.10	-2.31	-1.78	-1.54
hi [W/(sq.m°C)]	: 1511.2	1513.5	1552.5	1612.4	1641.7
hcow[qs/(Ao LMTD)][W/(sq.m°C)]	: 30.34	37.74	52.44	71.45	84.89
hdo[ql/(Ao LMWD)][kg/(s sq.m)]	: 32.89	40.91	56.85	77.45	92.02
Le [hcow/(hdo cp)]	: 0.90	0.90	0.90	0.90	0.90
hcowl[cp hi Ai/(TLS Ao)]	: 31.74	39.32	54.17	72.91	85.80
hdol [hcowl/(0.9 cp)]	: 34.40	42.62	58.72	79.03	93.01
Reynolds number	: 226.5	333.3	562.9	898.1	1182.7
Stanton(Prandtl)$^{2/3}$	: 0.0290	0.0245	0.0201	0.0172	0.0155
log(Re)	: 2.36	2.52	2.75	2.95	3.07
log[St(Pr)$^{2/3}$]	: -1.54	-1.61	-1.70	-1.76	-1.81

Table 8.10 : Printout of the program "TLS BY LEWIS NUMBER CORRELATION". Results of 1-row coil spanning a range of face velocities with a specific entering air condition having an enthalpy of 72kJ/kg and a chilled water velocity of 1.6m/s.

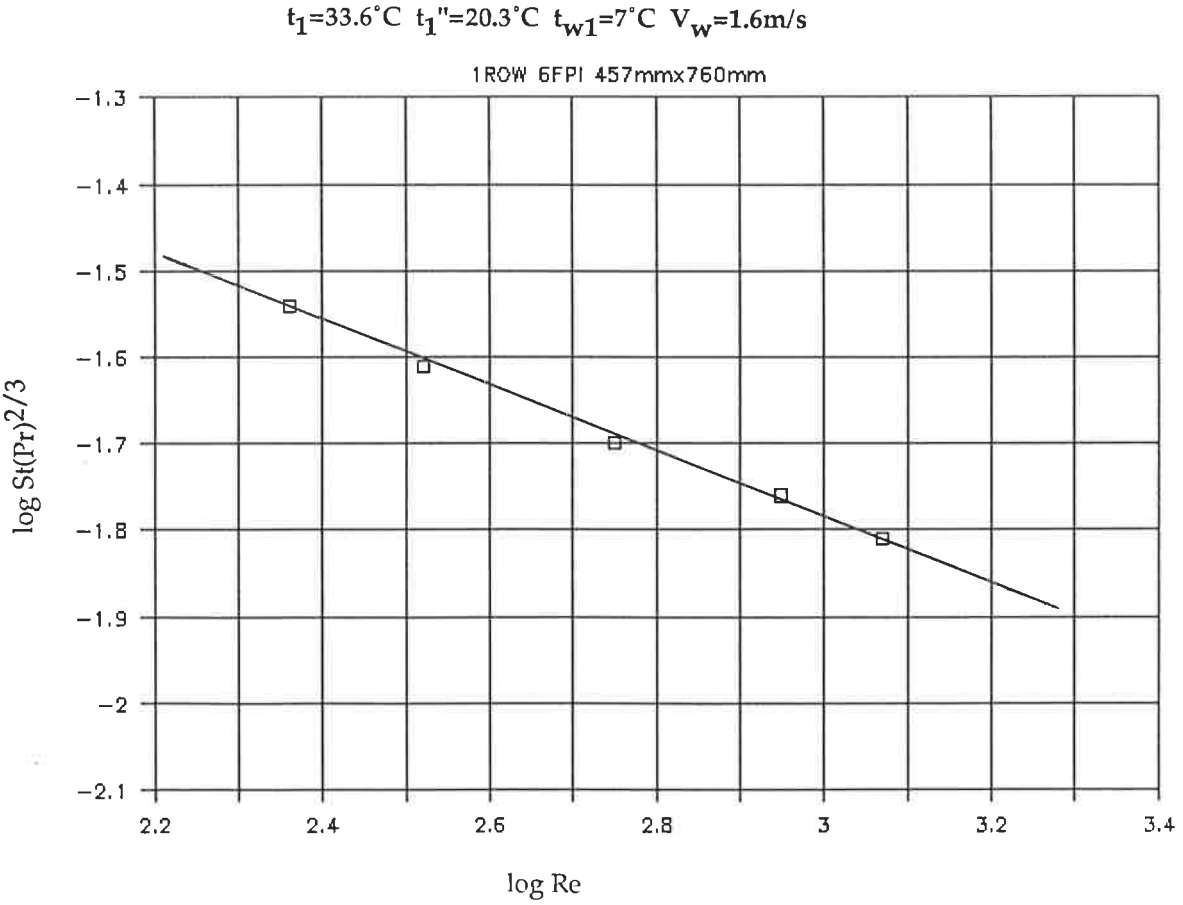

Fig 8.10 : Plot of log[St(Pr)$^{2/3}$] against logRe for the values in Table 8.10.

TLS determined by an iterative process
of correlating Lewis number :
INPUTS TO THE PROGRAM

Test Code	:H78B:W4161	H78B:W4191	H78B:W4192	H78B:W4193
Entering dry bulb temp (°C)	35.48	35.52	35.54	35.54
Entering dew point temp (°C)	21.98	21.90	22.01	22.05
Leaving dry bulb temp (°C)	21.30	23.60	26.08	27.66
Leaving dew point temp (°C)	16.69	17.92	19.41	20.34
Entering water temp (°C)	7.01	7.03	7.01	7.05
Corrected water temp rise	0.43	0.51	0.66	0.80
Air volume flow (lps)	140.0	205.0	354.0	559.0
Number of rows	1	1	1	1
OUTPUT FROM THE PROGRAM				
Air face velocity (m/s)	0.40	0.59	1.02	1.61
Entering surface temp (°C)	16.05	16.97	18.59	19.78
Leaving surface temp (°C)	11.71	13.09	15.28	17.00
TLS	-3.87	-3.22	-2.35	-1.83
hi [W/(sq.m°C)]	1533.4	1545.1	1591.7	1692.4
hcow[qs/(Ao LMTD)][W/(sq.m°C)]	30.41	36.85	52.37	72.08
hdo[ql/(Ao LMWD)][kg/(s sq.m)]	32.96	39.95	56.77	78.13
Le [hcow/(hdo cp)]	0.90	0.90	0.90	0.90
hcow1[cp hi Ai/(TLS Ao)]	31.94	38.61	54.51	74.34
hdo1 [hcow1/(0.9 cp)]	34.63	41.85	59.09	80.58
Reynolds number	224.9	329.3	568.6	897.9
Stanton(Prandtl)$^{2/3}$	0.0292	0.0242	0.0199	0.0173
log(Re	2.35	2.52	2.75	2.95
log[St(Pr)$^{2/3}$]	-1.53	-1.62	-1.7	-1.76

Table 8.11 : Printout of the program "TLS BY LEWIS NUMBER CORRELATION". Results of 1-row coil spanning a range of face velocities with a specific entering air condition having an enthalpy of 78kJ/kg and a chilled water velocity of 2.2m/s.

t_1=35.5°C t_1"=22°C t_{w1}=7°C V_w=2.2m/s

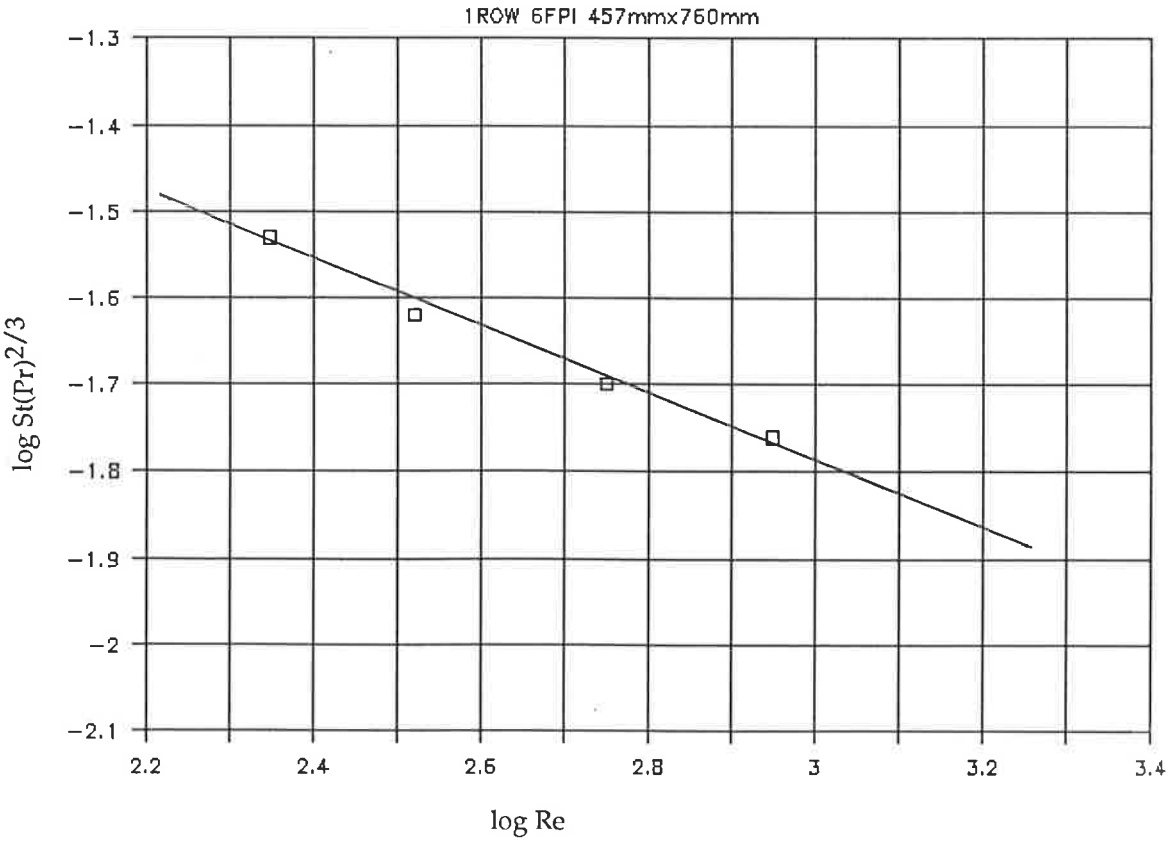

Fig 8.11 : Plot of log[St(Pr)$^{2/3}$] against logRe for the values in Table 8.11.

TLS determined by an iterative process
of correlating Lewis number :
INPUTS TO THE PROGRAM

Test Code	:H66B:W3881	H66B:W3741	H66B:W3771	H66B:W3752	H66B:W3751
Entering dry bulb temp (°C) :	31.00	31.12	31.03	30.81	30.90
Entering dew point temp (°C) :	18.95	18.76	18.80	18.85	18.72
Leaving dry bulb temp (°C) :	18.98	20.80	22.85	24.20	25.03
Leaving dew point temp (°C) :	14.70	15.62	16.84	17.62	17.89
Entering water temp (°C) :	7.07	7.10	7.02	7.00	7.13
Corrected water temp rise :	0.45	0.55	0.70	0.83	0.92
Air volume flow (lps) :	136.0	202.0	350.0	551.0	728.0
Number of rows :	1	1	1	1	1
OUTPUT FROM THE PROGRAM					
Air face velocity (m/s) :	0.39	0.58	1.01	1.59	2.10
Entering surface temp (°C) :	14.26	15.11	16.46	17.35	17.75
Leaving surface temp (°C) :	10.77	11.89	13.68	15.03	15.73
TLS :	-3.90	-3.17	-2.26	-1.78	-1.60
hi [W/(sq.m°C)] :	1496.9	1525.3	1537.8	1596.1	1675.0
hcow[qs/(Ao LMTD)][W/(sq.m°C)] :	29.61	37.32	53.25	70.75	83.43
hdo[ql/(Ao LMWD)][kg/(s sq.m)] :	32.10	40.45	57.72	76.69	90.44
Le [hcow/(hdo cp)] :	0.90	0.90	0.90	0.90	0.90
hcow1[cp hi Ai/(TLS Ao)] :	30.91	38.76	54.82	72.15	84.22
hdo1 [hcow1/(0.9 cp)] :	33.50	42.02	59.42	78.21	91.29
Reynolds number :	222.1	329.8	571.6	900.4	1189.4
Stanton(Prandtl)$^{2/3}$:	0.0288	0.0245	0.0201	0.0170	0.0152
log(Re) :	2.35	2.52	2.76	2.95	3.08
log[St(Pr)$^{2/3}$] :	-1.54	-1.61	-1.70	-1.77	-1.82

Table 8.12 : Printout of the program "TLS BY LEWIS NUMBER CORRELATION". Results of 1-row coil spanning a range of face velocities with a specific entering air condition having an enthalpy of 66kJ/kg and a chilled water velocity of 1.6m/s.

t_1=31°C t_1"=18.8°C t_{w1}=7°C V_w=1.6m/s

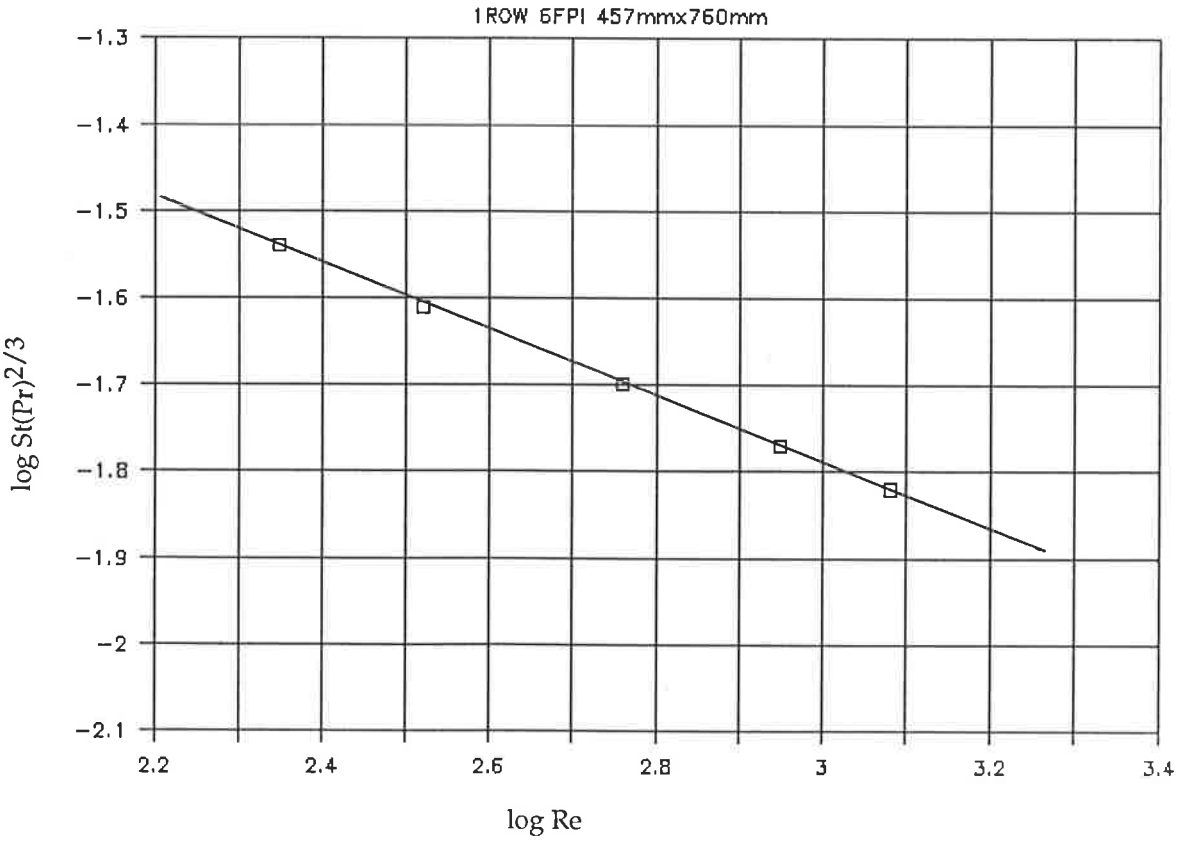

Fig 8.12 : Plot of log[St(Pr)$^{2/3}$] against logRe for the values in Table 8.12.

TLS determined by an iterative process
of correlating Lewis number :

INPUTS TO THE PROGRAM					
Test Code	:	H78B:W3853	H78B:W3782	H78B:W3761	H78B:W3803
Entering dry bulb temp (°C)	:	35.28	35.44	35.66	35.49
Entering dew point temp (°C)	:	22.04	22.03	21.92	22.13
Leaving dry bulb temp (°C)	:	21.29	23.59	26.02	27.80
Leaving dew point temp (°C)	:	16.83	18.10	19.47	20.47
Entering water temp (°C)	:	7.03	7.06	7.05	7.11
Corrected water temp rise	:	0.60	0.70	0.90	1.07
Air volume flow (lps)	:	143.0	205.0	354.0	557.0
Number of rows	:	1	1	1	1
OUTPUT FROM THE PROGRAM					
Air face velocity (m/s)	:	0.41	0.59	1.02	1.60
Entering surface temp (°C)	:	16.40	17.38	19.03	19.93
Leaving surface temp (°C)	:	11.91	13.35	15.60	17.12
TLS	:	-3.67	-3.06	-2.18	-1.83
hi [W/(sq.m°C)]	:	1507.3	1495.5	1535.6	1655.3
hcow[qs/(Ao LMTD)][W/(sq.m°C)]	:	31.47	37.63	54.80	70.48
hdo[ql/(Ao LMWD)][kg/(s sq.m)]	:	34.11	40.79	59.40	76.41
Le [hcow/(hdo cp)]	:	0.90	0.90	0.90	0.90
hcow1[cp hi Ai/(TLS Ao)]	:	33.05	39.39	56.77	72.66
hdo1 [hcow1/(0.9 cp)]	:	35.82	42.70	61.54	78.77
Reynolds number	:	229.9	329.4	568.4	894.8
Stanton(Prandtl)$^{2/3}$	:	0.0296	0.0247	0.0208	0.017
log(Re)	:	2.36	2.52	2.75	2.95
log[St(Pr)$^{2/3}$]	:	-1.53	-1.61	-1.68	-1.77

Table 8.13 : Printout of the program "TLS BY LEWIS NUMBER CORRELATION". Results of 1-row coil spanning a range of face velocities with a specific entering air condition having an enthalpy of 78kJ/kg and a chilled water velocity of 1.6m/s.

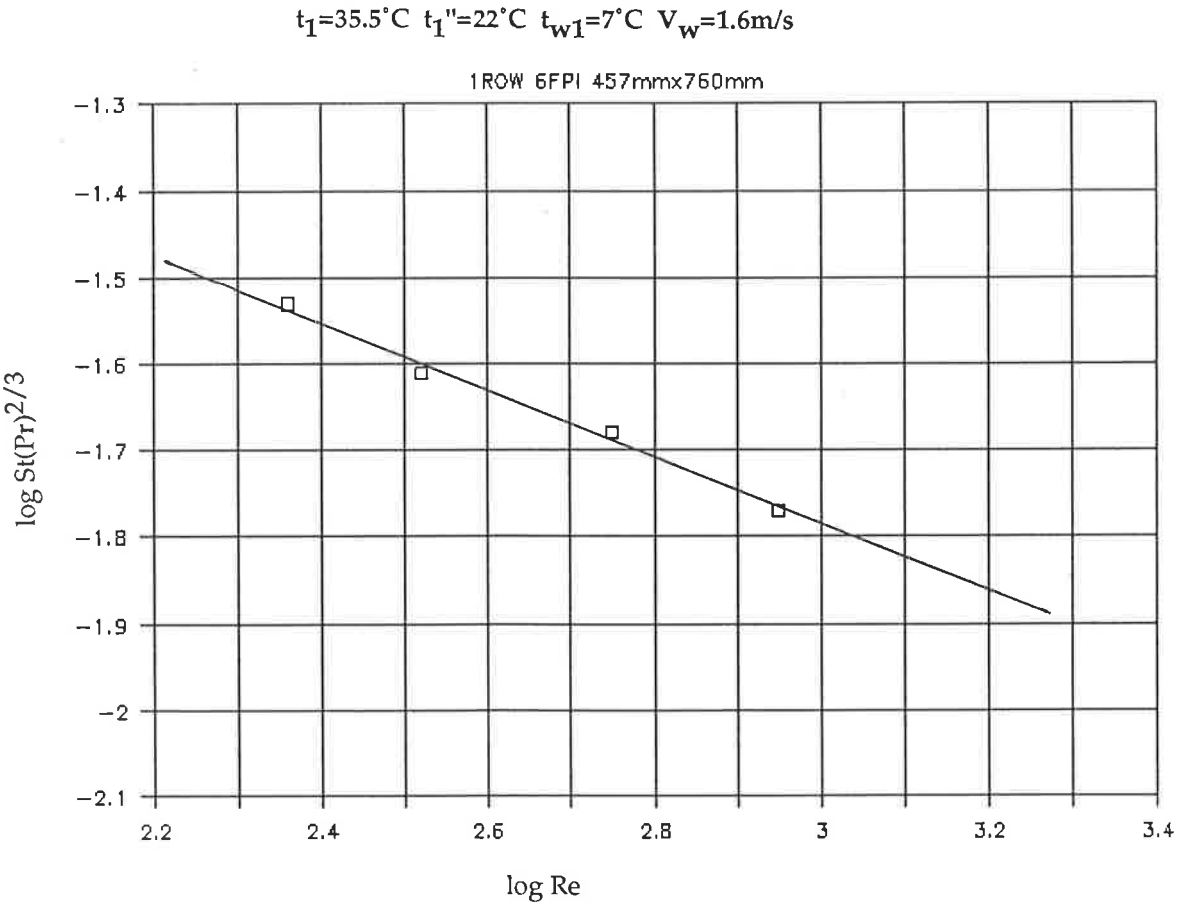

Fig 8.13 : Plot of log[St(Pr)$^{2/3}$] against logRe for the values in Table 8.13.

Face Vel.	Items	Water velocity 1.0m/s H66B	1.6m/s H72B	2.2m/s H78B	1.6m/s H66B	1.6m/s H78B
	Test code	W4061	W3862	W4161	W3881	W3853
	h_i	1371	1511	1533	1497	1507
0.4m/s	R_i	0.0093	0.0084	0.0083	0.0085	0.0085
	R_w	0.0034	0.0023	0.0018	0.0023	0.0023
	$(R_m + R_{ow})$	0.0059	0.0061	0.0065	0.0062	0.0062
	Test code	W4062	W3781	W4191	W3741	W3782
	h_i	1355	1513	1545	1525	1496
0.6m/s	R_i	0.0094	0.0084	0.0082	0.0083	0.0085
	R_w	0.0034	0.0023	0.0018	0.0023	0.0023
	$(R_m + R_{ow})$	0.006	0.0061	0.0064	0.006	0.0062
	Test code	W4063	W3772	W4192	W3771	W3761
	h_i	1429	1553	1592	1538	1536
1.0m/s	R_i	0.0089	0.0082	0.0080	0.0083	0.0083
	R_w	0.0034	0.0023	0.0018	0.0023	0.0023
	$(R_m + R_{ow})$	0.0055	0.0059	0.0062	0.006	0.006
	Test code	W4081	W3842	W4193	W3752	W3803
	h_i	1417	1612	1692	1596	1655
1.6m/s	R_i	0.0090	0.0079	0.0075	0.0080	0.0077
	R_w	0.0034	0.0023	0.0018	0.0023	0.0023
	$(R_m + R_{ow})$	0.0056	0.0056	0.0057	0.0057	0.0054
	Test code	W4082	W3841	-	W3751	-
	h_i	1500	1642	-	1675	-
2.1m/s	R_i	0.0085	0.0078	-	0.0076	-
	R_w	0.0034	0.0023	-	0.0023	-
	$(R_m + R_{ow})$	0.0051	0.0055	-	0.0053	-

Table 8.14 : Values of the empirical constant $(R_m + R_{ow})$ for the 1-row coil.

1-Row Coil

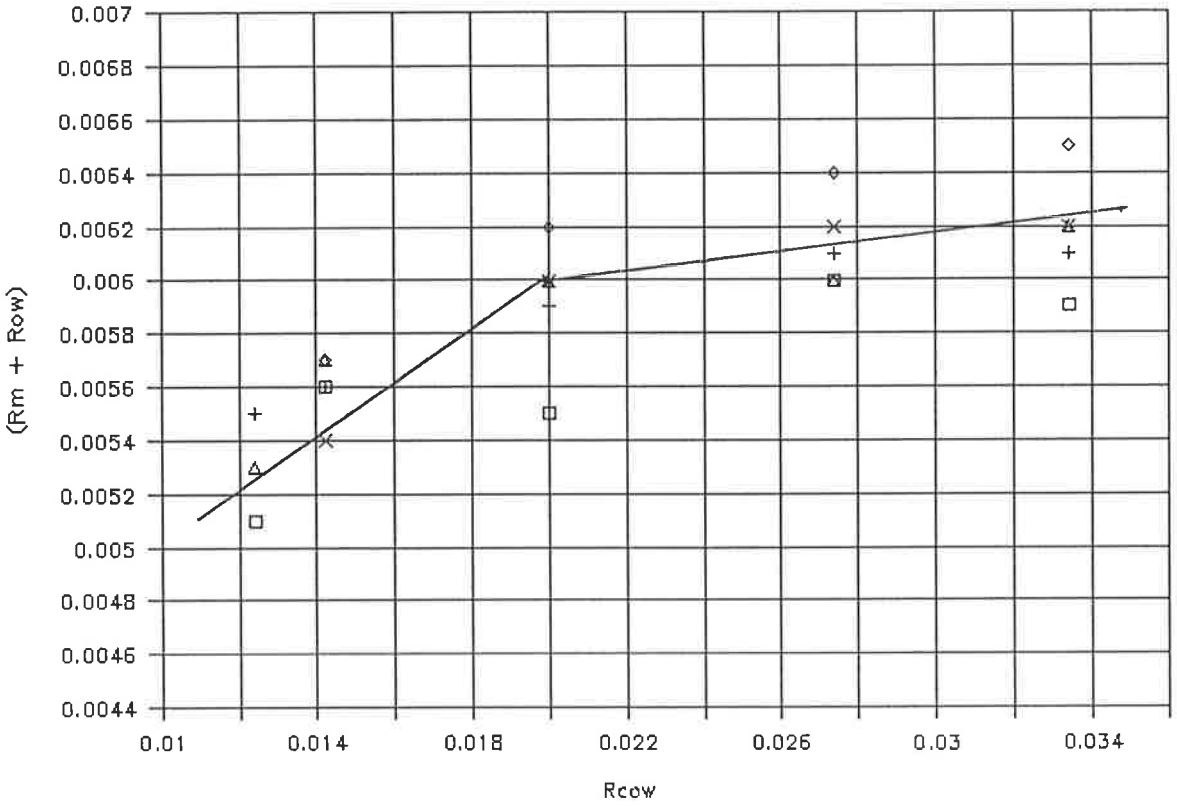

□ H66B WV=1.0m/s
+ H72B WV=1.6m/s
x H78B WV=1.6m/s
Δ H66B WV=1.6m/s
◇ H78B WV=2.2m/s

Fig 8.14 : A plot of ($R_m + R_{ow}$) against R_{cow} ($1/h_{cow}$) for a 1-row coil over a range of face velocities for different entering air conditions and water velocities.

It is to be noted that ($R_m + R_{ow}$) is only a weak function of h_{cow} and consequently equations (8.14a) and (8.14b) are expected to give ($R_m + R_{ow}$) to sufficient degree of accuracy.

An important conclusion from Table 8.14 is the evaluation of h_i over a range of water velocities. It is apparent that h_i is dependent primarily on the tube-side film resistance, R_w, and is not significantly affected by the air-side operating conditions. Thus, h_i can be obtained by using McAdams equation and the above empirical constant.

The value of ($R_m + R_{ow}$) as determined from equation (8.14a) or (8.14b) is used in the generalisation process to compute h_i for a single row coil. The value of h_{cow} is obtained from $St.(Pr)^{2/3}$ determined from equation (8.13). The Tie Line Slope, TLS and the coil characteristic, C, can then be computed to be used in the prediction of the leaving enthalpy and the leaving dry bulb temperature. The process of generalisation has been discussed in detail in Chapter 6.

8.3.2 Two Row Coil

Tables 8.15 - 8.18 contain computer printouts of the program "TLS BY LEWIS NUMBER CORRELATION" for fully wet tests of a 2-row coil. The values of $\log[St.(Pr)^{2/3}]$ vs log(Re) are plotted in Figs 8.15 - 8.18. As in the case of 1-row coil, each of the Tables 8.15 - 8.18 comprises tests over a range of face velocities for a given entering air condition, entering water temperature and water velocity. Having investigated a comprehensive range of operating conditions for a 1-row coil both on the air and the water sides, the test matrix for the 2-row coil was subsequently investigated. Having developed the ability to predict h_i over a range of water velocities for the 1-row coil, the 2-row coil tests were performed at a fixed water velocity of 1.6m/s. A comparison of the performance for different entering air conditions but with a fixed water velocity is obtained from Tables 8.15 - 8.18 and Figs 8.15 - 8.18. A linear relationship between $\log[St.(Pr)^{2/3}]$ and log(Re) is obtained from these plots and it is concluded again that for a coil of a given physical geometry, h_{cow} depends only on Re (or face velocity) and is independent of the entering air conditions and/or the tube-side conditions. This result is important as it verifies the fundamental separation of the transfer path into an enthalpy transfer process followed linearly by a sensible transfer process, in the manner of McElgin and Wiley (1940).

The equation of the dimensionless expression of $St.(Pr)^{2/3}$ vs Re may now be determined. The values of $\log[St.(Pr)^{2/3}]$ and log(Re) are used from Table 8.18 to yield

$$St.(Pr)^{2/3} = 0.108(Re)^{-0.256} \qquad (8.15)$$

Equation (8.15) is used in the generalisation process to obtain the value of h_{cow} for a two row coil.

TLS determined by an iterative process
of correlating Lewis number :
INPUTS TO THE PROGRAM

Test Code	:H66B:W5311	H66B:W5202	H66B:W6041
Entering dry bulb temp (°C)	: 30.90	30.64	30.99
Entering dew point temp (°C)	: 18.95	18.75	18.97
Leaving dry bulb temp (°C)	: 14.46	16.68	18.96
Leaving dew point temp (°C)	: 12.52	14.24	16.28
Entering water temp (°C)	: 6.95	6.97	7.00
Corrected water temp rise	: 0.98	1.28	1.63
Air volume flow (lps)	: 211.0	344.0	279.0
Number of rows	: 2	2	2
OUTPUT FROM THE PROGRAM			
Air face velocity (m/s)	: 0.61	0.99	1.60
Entering surface temp (°C)	: 14.47	15.95	17.81
Leaving surface temp (°C)	: 9.38	10.98	13.30
TLS	: -3.91	-2.69	-1.74
hi [W/(sq.m°C)]	: 1967.7	1888.5	1757.2
hcow[qs/(Ao LMTD)][W/(sq.m°C)]	: 38.93	54.91	81.62
hdo[ql/(Ao LMWD)][kg/(s sq.m)]	: 42.20	59.53	88.48
Le [hcow/(hdo cp)]	: 0.90	0.90	0.90
hcow1[cp hi Ai/(TLS Ao)]	: 40.54	56.48	80.95
hdo1 [hcow1/(0.9 cp)]	: 43.94	61.23	87.75
Reynolds number	: 344.7	562.5	907.7
Stanton(Prandtl)$^{2/3}$	: 0.0244	0.0211	0.0194
log(Re)	: 2.54	2.75	2.96
log[St(Pr)$^{2/3}$]	: -1.61	-1.68	-1.71

Table 8.15 : Printout of the program "TLS BY LEWIS NUMBER CORRELATION". Results of 2-row coil spanning a range of face velocities with a specific entering air condition having an enthalpy of 66kJ/kg and a chilled water velocity of 1.6m/s.

t_1=31°C t_1"=18.8°C t_{w1}=7°C V_w=1.6m/s

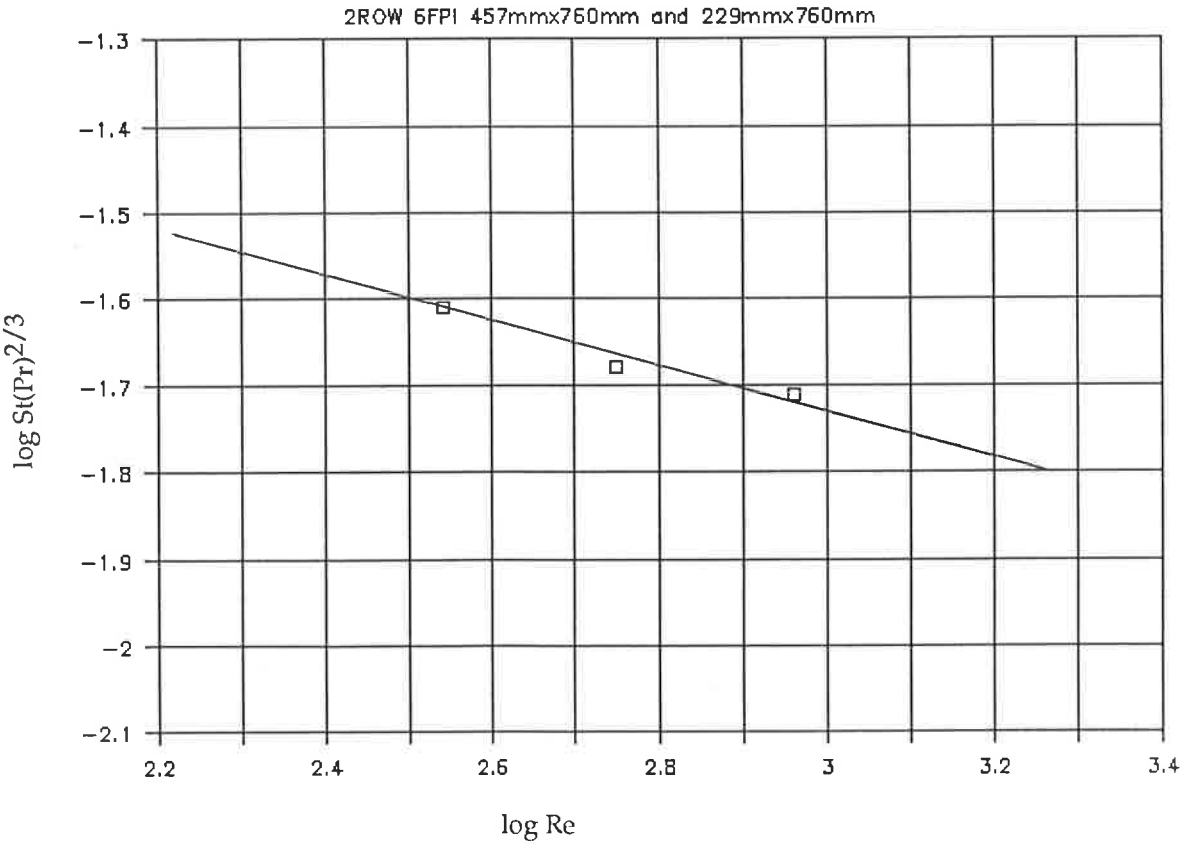

Fig 8.15 : Plot of log[St(Pr)$^{2/3}$] against logRe for the values in Table 8.15.

TLS determined by an iterative process
of correlating Lewis number :

INPUTS TO THE PROGRAM				
Test Code	:	H72B:W5281	H72B:W5312	H72B:W6081
Entering dry bulb temp (°C)	:	33.63	33.65	33.64
Entering dew point temp (°C)	:	20.38	20.22	20.28
Leaving dry bulb temp (°C)	:	13.38	15.18	20.18
Leaving dew point temp (°C)	:	11.69	13.04	17.01
Entering water temp (°C)	:	7.04	6.93	7.03
Corrected water temp rise	:	0.87	1.07	1.87
Air volume flow (lps)	:	146.0	203.0	274.0
Number of rows	:	2	2	2
OUTPUT FROM THE PROGRAM				
Air face velocity (m/s)	:	0.42	0.58	1.57
Entering surface temp (°C)	:	13.88	15.13	18.62
Leaving surface temp (°C)	:	8.63	9.52	13.57
TLS	:	-5.58	-4.14	-1.98
hi [W/(sq.m°C)]	:	2191.9	1992.6	1912.6
hcow[qs/(Ao LMTD)][W/(sq.m°C)]	:	30.17	37.14	77.16
hdo[ql/(Ao LMWD)][kg/(s sq.m)]	:	32.71	40.26	83.64
Le [hcow/(hdo cp)]	:	0.90	0.90	0.90
hcowl[cp hi Ai/(TLS Ao)]	:	31.62	38.76	77.67
hdol [hcowl/(0.9 cp)]	:	34.28	42.02	84.20
Reynolds number	:	236.2	328.4	883.1
Stanton(Prandtl)$^{2/3}$	:	0.0276	0.0244	0.0189
log(Re)	:	2.37	2.52	2.95
log[St(Pr)$^{2/3}$]	:	-1.56	-1.61	-1.72

Table 8.16 : Printout of the program "TLS BY LEWIS NUMBER CORRELATION". Results of 2-row coil spanning a range of face velocities with a specific entering air condition having an enthalpy of 72kJ/kg and a chilled water velocity of 1.6m/s.

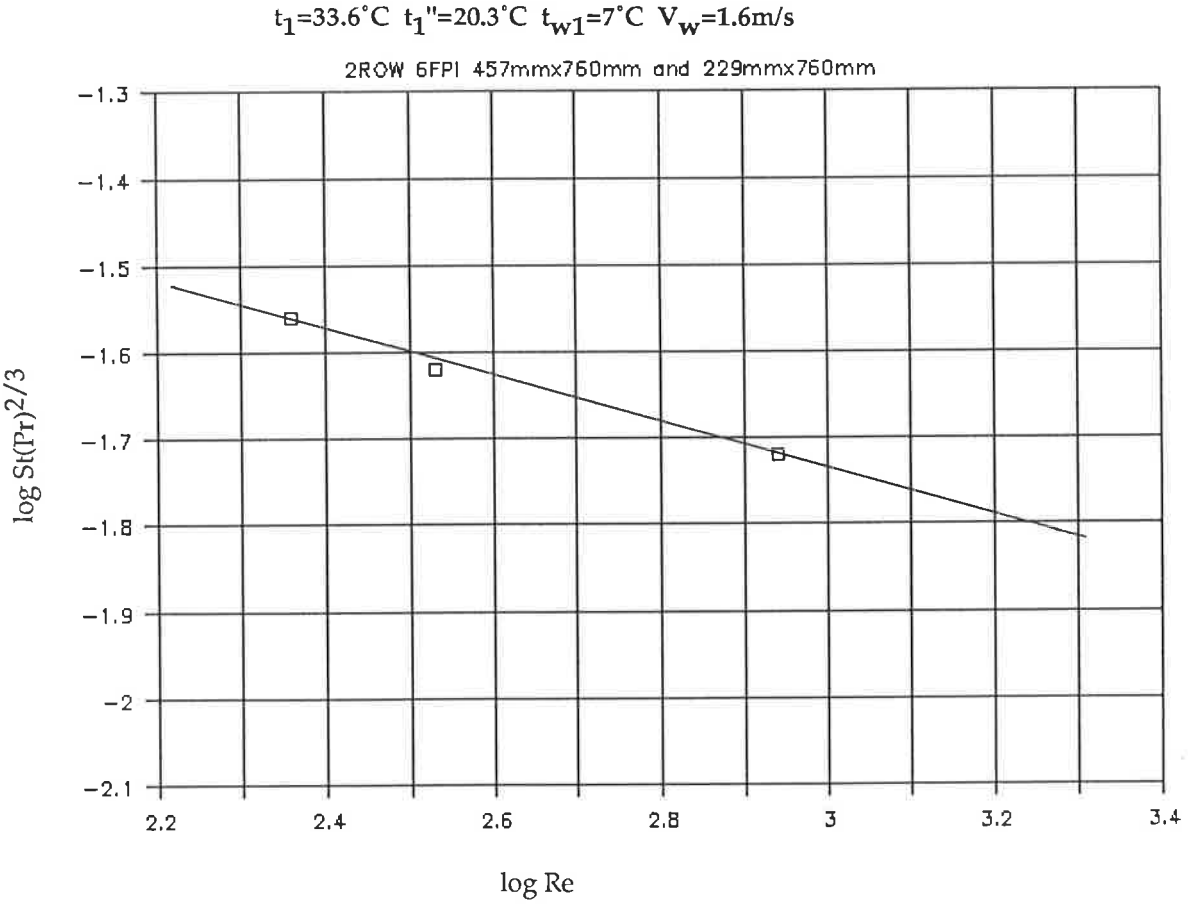

Fig 8.16 : Plot of log[St(Pr)$^{2/3}$] against logRe for the values in Table 8.16.

TLS determined by an iterative process
of correlating Lewis number :
INPUTS TO THE PROGRAM

Test Code	:H78B:W5271	H78B:W5351	H78B:W6082
Entering dry bulb temp (°C)	35.51	35.36	35.57
Entering dew point temp (°C)	22.04	22.02	22.04
Leaving dry bulb temp (°C)	13.64	16.24	21.35
Leaving dew point temp (°C)	12.02	14.13	18.25
Entering water temp (°C)	6.95	6.98	6.99
Corrected water temp rise	0.96	1.23	2.10
Air volume flow (lps)	143.0	213.0	275.0
Number of rows	2	2	2
OUTPUT FROM THE PROGRAM			
Air face velocity (m/s)	0.41	0.61	1.58
Entering surface temp (°C)	14.25	16.34	20.03
Leaving surface temp (°C)	8.56	10.07	14.45
TLS	-6.08	-3.99	-1.92
hi [W/(sq.m°C)]	2344.1	1978.7	1900.6
hcow[qs/(Ao LMTD)][W/(sq.m°C)]	29.51	38.08	78.21
hdo[ql/(Ao LMWD)][kg/(s sq.m)]	31.99	41.27	84.78
Le [hcow/(hdo cp)]	0.90	0.90	0.90
hcowl[cp hi Ai/(TLS Ao)]	31.07	39.94	79.41
hdol [hcowl/(0.9 cp)]	33.68	43.29	86.08
Reynolds number	229.7	342.3	879.9
Stanton(Prandtl)$^{2/3}$	0.0278	0.0240	0.0192
log(Re)	2.36	2.53	2.94
log[St(Pr)$^{2/3}$]	-1.56	-1.62	-1.72

Table 8.17 : Printout of the program "TLS BY LEWIS NUMBER CORRELATION". Results of 2-row coil spanning a range of face velocities with a specific entering air condition having an enthalpy of 78kJ/kg and a chilled water velocity of 1.6m/s.

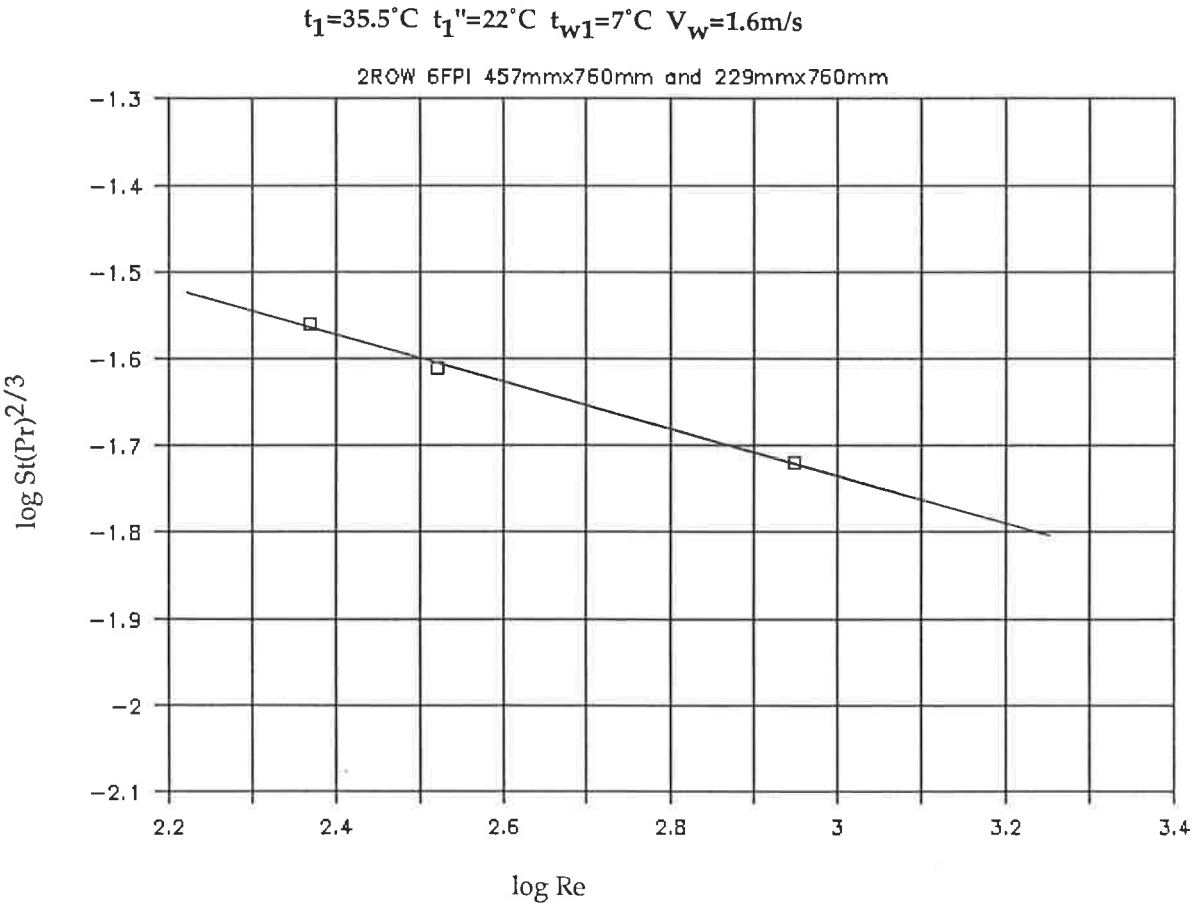

Fig 8.17 : Plot of log[St(Pr)$^{2/3}$] against logRe for the values in Table 8.17.

TLS determined by an iterative process
of correlating Lewis number :
INPUTS TO THE PROGRAM

Test Code	:H66C:W5401	H66C:W5471	H66C:W5262	H66C:W6051
Entering dry bulb temp (°C)	: 28.57	28.95	28.82	29.07
Entering dew point temp (°C)	: 19.69	19.85	19.64	19.77
Leaving dry bulb temp (°C)	: 12.45	14.07	16.24	18.40
Leaving dew point temp (°C)	: 11.24	12.65	14.39	16.19
Entering water temp (°C)	: 6.94	7.03	6.99	6.94
Corrected water temp rise	: 0.78	0.96	1.30	1.66
Air volume flow (lps)	: 149.0	201.0	343.0	271.0
Number of rows	: 2	2	2	2
OUTPUT FROM THE PROGRAM				
Air face velocity (m/s)	: 0.43	0.58	0.99	1.56
Entering surface temp (°C)	: 12.85	14.50	16.01	17.61
Leaving surface temp (°C)	: 8.33	9.39	10.96	12.98
TLS	: -5.69	-3.93	-2.68	-1.83
hi [W/(sq.m°C)]	: 2255.9	1933.0	1928.1	1828.6
hcow[qs/(Ao LMTD)][W/(sq.m°C)]	: 30.31	37.67	55.45	78.03
hdo[ql/(Ao LMWD)][kg/(s sq.m)]	: 32.86	40.83	60.11	84.59
Le [hcow/(hdo cp)]	: 0.90	0.90	0.90	0.90
hcow1[cp hi Ai/(TLS Ao)]	: 31.93	39.59	57.87	80.23
hdo1 [hcow1/(0.9 cp)]	: 34.61	42.92	62.74	86.97
Reynolds number	: 245.2	330.3	564.0	886.9
Stanton(Prandtl)$^{2/3}$	: 0.0267	0.0246	0.0213	0.0190
log(Re)	: 2.39	2.52	2.75	2.95
log[St(Pr)$^{2/3}$]	: -1.57	-1.61	-1.67	-1.72

Table 8.18 : Printout of the program "TLS BY LEWIS NUMBER CORRELATION". Results of 2-row coil spanning a range of face velocities with a specific entering air condition having an enthalpy of 66kJ/kg and a chilled water velocity of 1.6m/s.

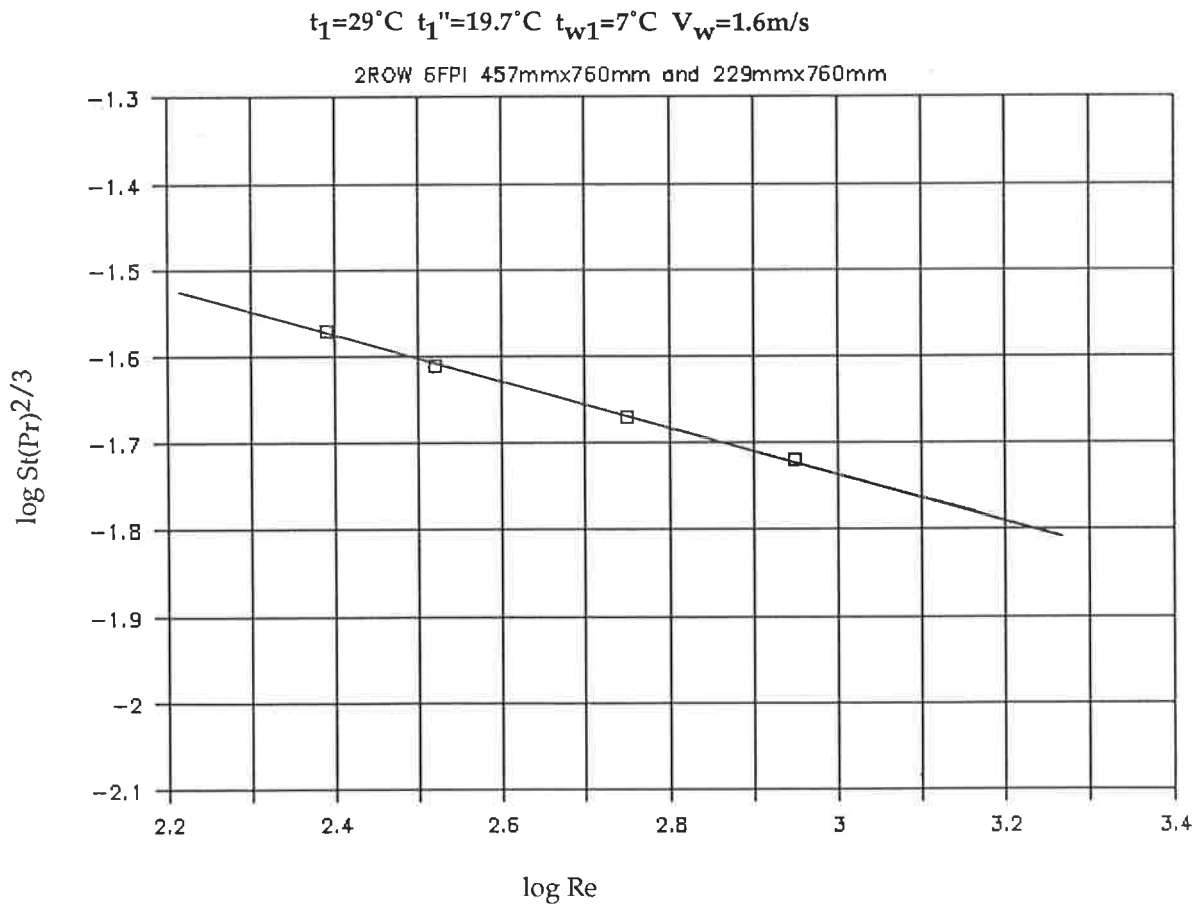

Fig 8.18 : Plot of log[St(Pr)$^{2/3}$] against logRe for the values in Table 8.18.

Face Vel.	Items	Water velocity 1.6m/s H66B	1.6m/s H72B	1.6m/s H78B	1.6m/s H66C
	Test code	-	W5281	W5271	W5401
	h_i	-	2192	2344	2256
0.4m/s	R_i	-	0.0058	0.0054	0.0056
	R_w	-	0.0023	0.0023	0.0023
	$(R_m + R_{ow})$	-	0.0035	0.0031	0.0033
	Test code	W5311	W5312B	W5351	W5471
	h_i	1968	1993	1979	1933
0.6m/s	R_i	0.0065	0.0064	0.0064	0.0066
	R_w	0.0023	0.0023	0.0023	0.0023
	$(R_m + R_{ow})$	0.0042	0.0041	0.0041	0.0043
	Test code	W5202	-	-	W5262
	h_i	1888	-	-	1928
1.0m/s	R_i	0.0067	-	-	0.0066
	R_w	0.0023	-	-	0.0023
	$(R_m + R_{ow})$	0.0044	-	-	0.0043
	Test code	W6041	W6081	W6082	W6051
	h_i	1757	1913	1901	1829
1.6m/s	R_i	0.0072	0.0067	0.0067	0.0070
	R_w	0.0023	0.0023	0.0023	0.0023
	$(R_m + R_{ow})$	0.0049	0.0044	0.0044	0.0047

Table 8.19 : Values of the empirical constant $(R_m + R_{ow})$ for the 2-row coil.

2-Row Coil

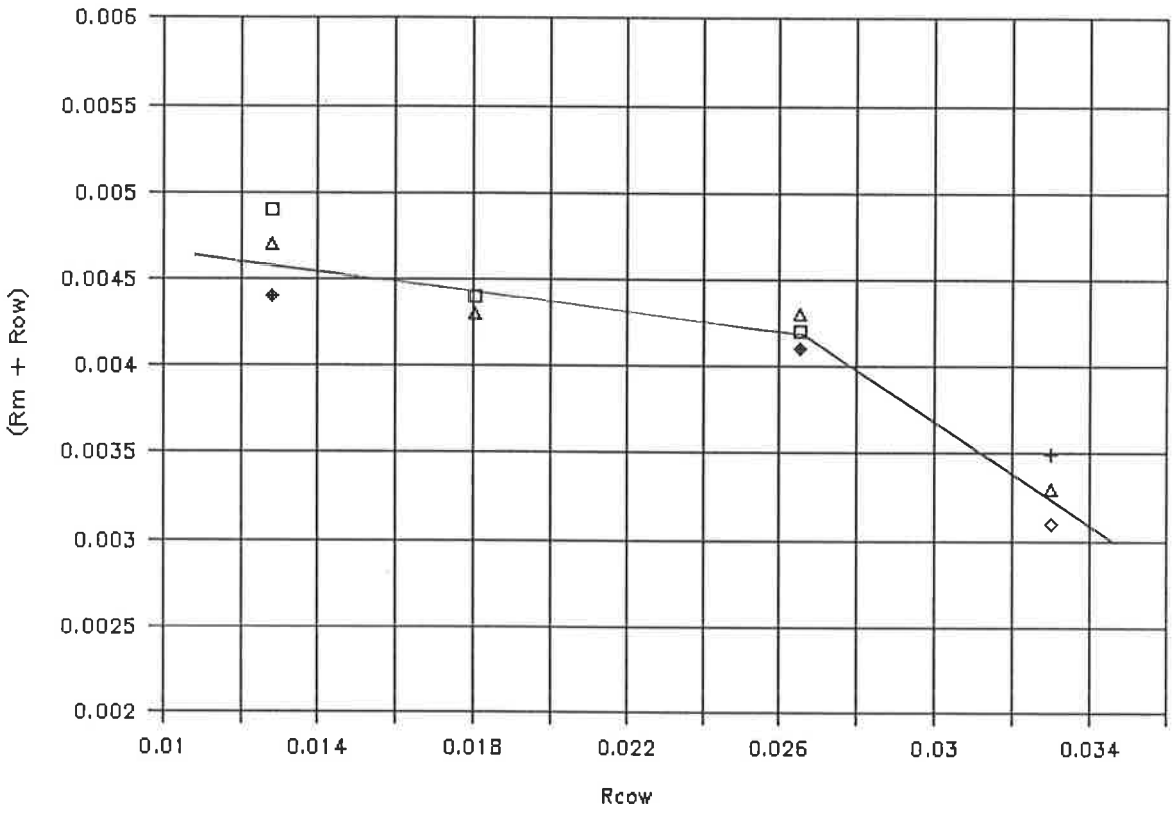

Δ H66C WV=1.6m/s
□ H66B WV=1.6m/s
+ H72B WV=1.6m/s
◇ H78B WV=1.6m/s

Fig 8.19 : A plot of ($R_m + R_{ow}$) against R_{cow} ($1/h_{cow}$) for a 2-row coil over a range of face velocities for different entering air conditions and water velocities.

The empirical constant for the two row coil is determined from the values of $(R_m + R_{ow})$ for the above tests as tabulated in Table 8.19. The values of h_i in Table 8.19 are from Tables 8.15 - 8.18 and the McAdams equation is used to compute R_w. The empirical constant $(R_m + R_{ow})$ as a function of $(1/h_{cow})$ is plotted in Fig 8.19 and the resulting best fit lines are

$$(R_m + R_{ow}) = -\frac{0.02}{h_{cow}} + 0.0048 \qquad \text{for } h_{cow} > 55 \qquad (8.16a)$$

and $$(R_m + R_{ow}) = -\frac{0.15}{h_{cow}} + 0.0082 \qquad \text{for } h_{cow} \leq 55 \qquad (8.16b)$$

As stated earlier, $(R_m + R_{ow})$ is only a weak function of h_{cow}. Consequently equations (8.16a) and (8.16b) are expected to determine $(R_m + R_{ow})$ to a reasonable accuracy. These equations are used in the generalisation process to compute h_i for the two row coil.

8.3.3 Four Row Coil

Tables 8.20 and 8.21 contain computer printouts of the program "TLS BY LEWIS NUMBER CORRELATION" for fully wet tests of a 4-row deep coil. The values of $\log[St.(Pr)^{2/3}]$ vs $\log(Re)$ are plotted in Figs 8.20 and 8.21. The test matrix for the 4-row coil was considerably reduced due to capacity limitations on the compressor. Each Table comprises tests over a range of face velocities for given tube-side conditions. A comparison of different entering air conditions for a given water velocity is obtained from Tables 8.20 and 8.21 and Figs 8.20 and 8.21. A linear relationship is obtained, and as in the case of one and two row coils, h_{cow} depends only on Re (or face velocity) and is independent of the entering air conditions or tube-side conditions.

The equation of the dimensionless expression of $St.(Pr)^{2/3}$ vs Re is fundamental to the AU method. The values of $\log[St.(Pr)^{2/3}]$ and $\log(Re)$ are used from Table 8.20 to yield the empirical relation

$$St.(Pr)^{2/3} = 0.085(Re)^{-0.22} \qquad (8.17)$$

Equation (8.17) is used in the generalisation process to obtain the value of h_{cow} for a four row coil.

The values of $(R_m + R_{ow})$ for the 4-row coil tests are tabulated in Table 8.22 and a graph of $(R_m + R_{ow})$ vs $(1/h_{cow})$ is plotted in Fig 8.22. The following equation may be obtained from Fig 8.22 :

$$(R_m + R_{ow}) = \frac{0.05}{h_{cow}} + 0.0031 \qquad (8.18)$$

TLS determined by an iterative process of correlating Lewis number :				
INPUTS TO THE PROGRAM				
Test Code	:H66B:W6471	H66B:W6461	H66B:W6441	
Entering dry bulb temp (°C)	:	31.02	31.19	31.06
Entering dew point temp (°C)	:	18.76	18.69	18.84
Leaving dry bulb temp (°C)	:	9.63	10.95	12.59
Leaving dew point temp (°C)	:	9.42	10.75	12.51
Entering water temp (°C)	:	7.02	7.01	7.01
Corrected water temp rise	:	0.65	0.97	1.31
Air volume flow (lps)	:	105.0	172.0	265.0
Number of rows	:	4	4	4
OUTPUT FROM THE PROGRAM				
Air face velocity (m/s)	:	0.62	1.01	1.55
Entering surface temp (°C)	:	14.27	15.43	16.81
Leaving surface temp (°C)	:	7.92	8.66	9.90
TLS	:	-3.91	-3.03	-2.22
hi [W/(sq.m°C)]	:	1893.2	2120.1	2140.4
hcow[qs/(Ao LMTD)][W/(sq.m°C)]	:	37.68	55.06	77.96
hdo[ql/(Ao LMWD)][kg/(s sq.m)]	:	40.85	59.68	84.51
Le [hcow/(hdo cp)]	:	0.90	0.90	0.90
hcowl[cp hi Ai/(TLS Ao)]	:	39.00	56.26	77.71
hdol [hcowl/(0.9 cp)]	:	42.28	60.98	84.24
Reynolds number	:	349.4	572.0	881.7
Stanton(Prandtl)$^{2/3}$	:	0.0233	0.0208	0.0191
log(Re)	:	2.54	2.75	2.95
log[St(Pr)]$^{2/3}$	:	-1.63	-1.68	-1.72

Table 8.20 : Printout of the program "TLS BY LEWIS NUMBER CORRELATION". Results of 4-row coil spanning a range of face velocities with a specific entering air condition having an enthalpy of 66kJ/kg and a chilled water velocity of 1.6m/s.

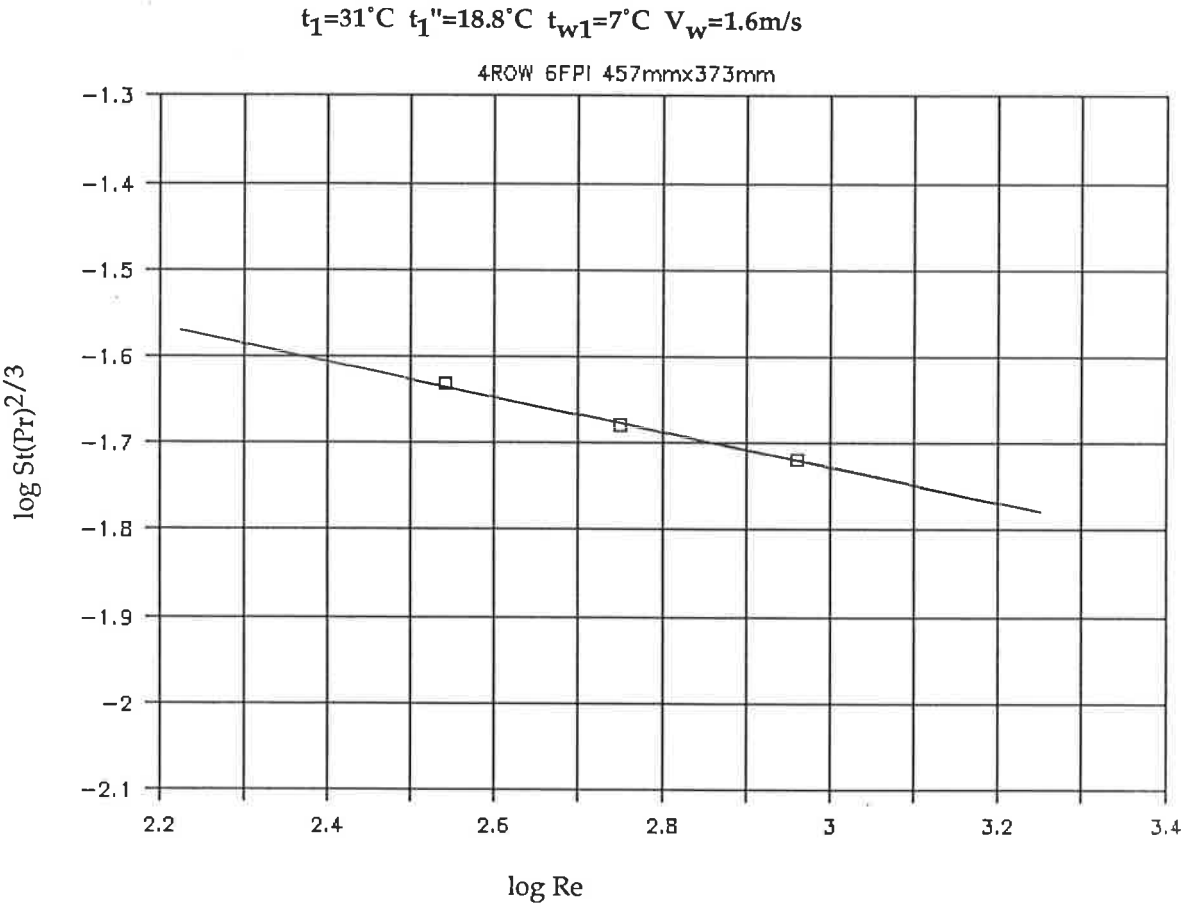

Fig 8.20 : Plot of log[St(Pr)$^{2/3}$] against logRe for the values in Table 8.20.

TLS determined by an iterative process of correlating Lewis number :				
INPUTS TO THE PROGRAM				
Test Code	:	H66C:W6472	H66C:W6462	H66C:W6452
Entering dry bulb temp (°C)	:	28.97	29.00	29.06
Entering dew point temp (°C)	:	19.70	19.76	19.79
Leaving dry bulb temp (°C)	:	9.60	10.84	12.63
Leaving dew point temp (°C)	:	9.40	10.79	12.60
Entering water temp (°C)	:	7.00	7.02	7.10
Corrected water temp rise	:	0.65	0.98	1.32
Air volume flow (lps)	:	105.0	172.0	265.0
Number of rows	:	4	4	4
OUTPUT FROM THE PROGRAM				
Air face velocity (m/s)	:	0.62	1.01	1.55
Entering surface temp (°C)	:	14.30	15.93	17.16
Leaving surface temp (°C)	:	7.90	8.77	10.09
TLS	:	-3.88	-2.70	-2.05
hi [W/(sq.m°C)]	:	1900.8	2023.3	2083.5
hcow[qs/(Ao LMTD)][W/(sq.m°C)]	:	37.61	58.16	79.84
hdo[ql/(Ao LMWD)][kg/(s sq.m)]	:	40.77	63.04	86.55
Le [hcow/(hdo cp)]	:	0.90	0.90	0.90
hcowl[cp hi Ai/(TLS Ao)]	:	39.42	60.44	81.81
hdol [hcowl/(0.9 cp)]	:	42.74	65.52	88.68
Reynolds number	:	351.6	575.9	887.0
Stanton(Prandtl)$^{2/3}$	:	0.0231	0.0218	0.0195
log(Re)	:	2.55	2.76	2.95
log[St(Pr)$^{2/3}$]	:	-1.64	-1.66	-1.71

Table 8.21 : Printout of the program "TLS BY LEWIS NUMBER CORRELATION". Results of 4-row coil spanning a range of face velocities with a specific entering air condition having an enthalpy of 66kJ/kg and a chilled water velocity of 1.6m/s.

t_1=29°C t_1"=19.7°C t_{w1}=7°C V_w=1.6m/s

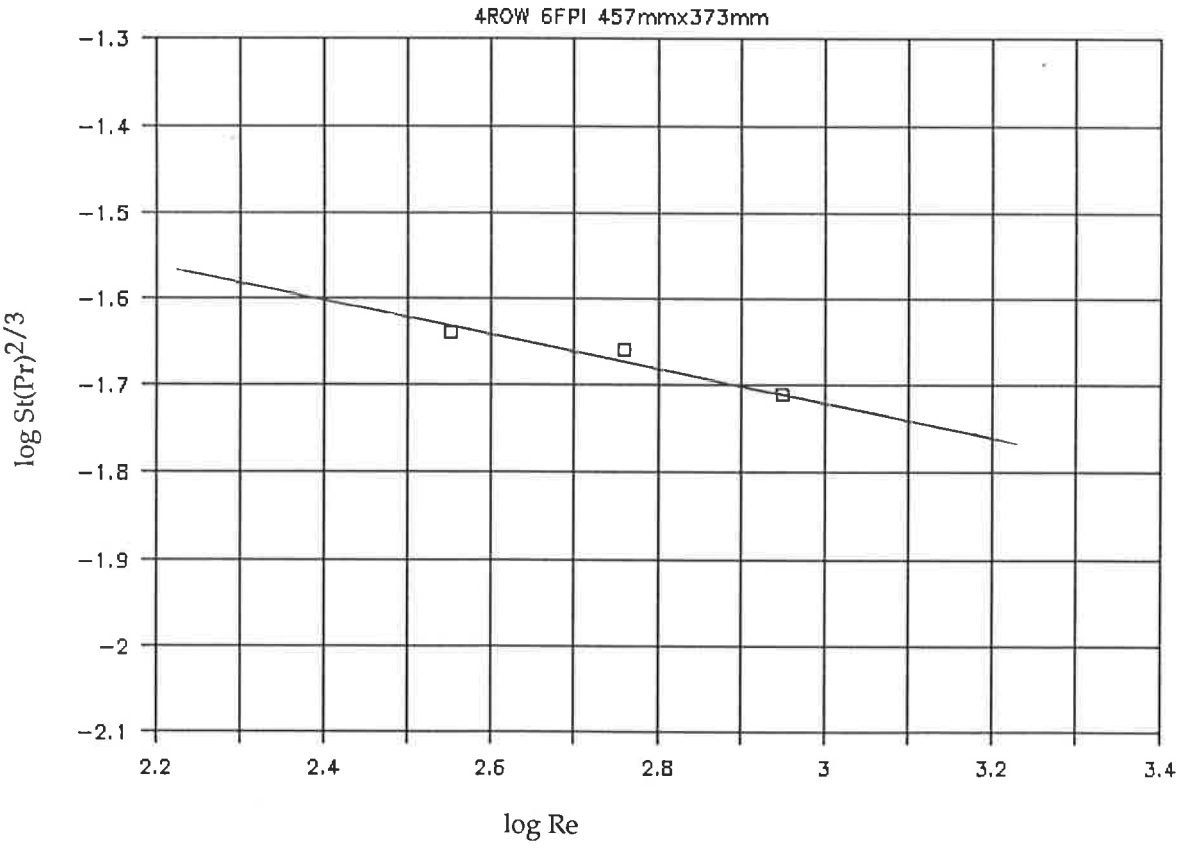

Fig 8.21 : Plot of log[St(Pr)$^{2/3}$] against logRe for the values in Table 8.21.

Face Vel.	Items	Water velocity 1.6m/s H66B	1.6m/s H66C
	Test code	W6471	W6472
	h_i	1893	1901
0.6m/s	R_i	0.0067	0.0067
	R_w	0.0023	0.0023
	$(R_m + R_{ow})$	0.0044	0.0044
	Test code	W6461	W6462
	h_i	2120	2023
1.0m/s	R_i	0.006	0.0063
	R_w	0.0023	0.0023
	$(R_m + R_{ow})$	0.0037	0.0040
	Test code	W6441	W6452
	h_i	2140	2084
1.6m/s	R_i	0.0059	0.0061
	R_w	0.0023	0.0023
	$(R_m + R_{ow})$	0.0036	0.0038

Table 8.22 : Values of the empirical constant $(R_m + R_{ow})$ for the 4-row coil.

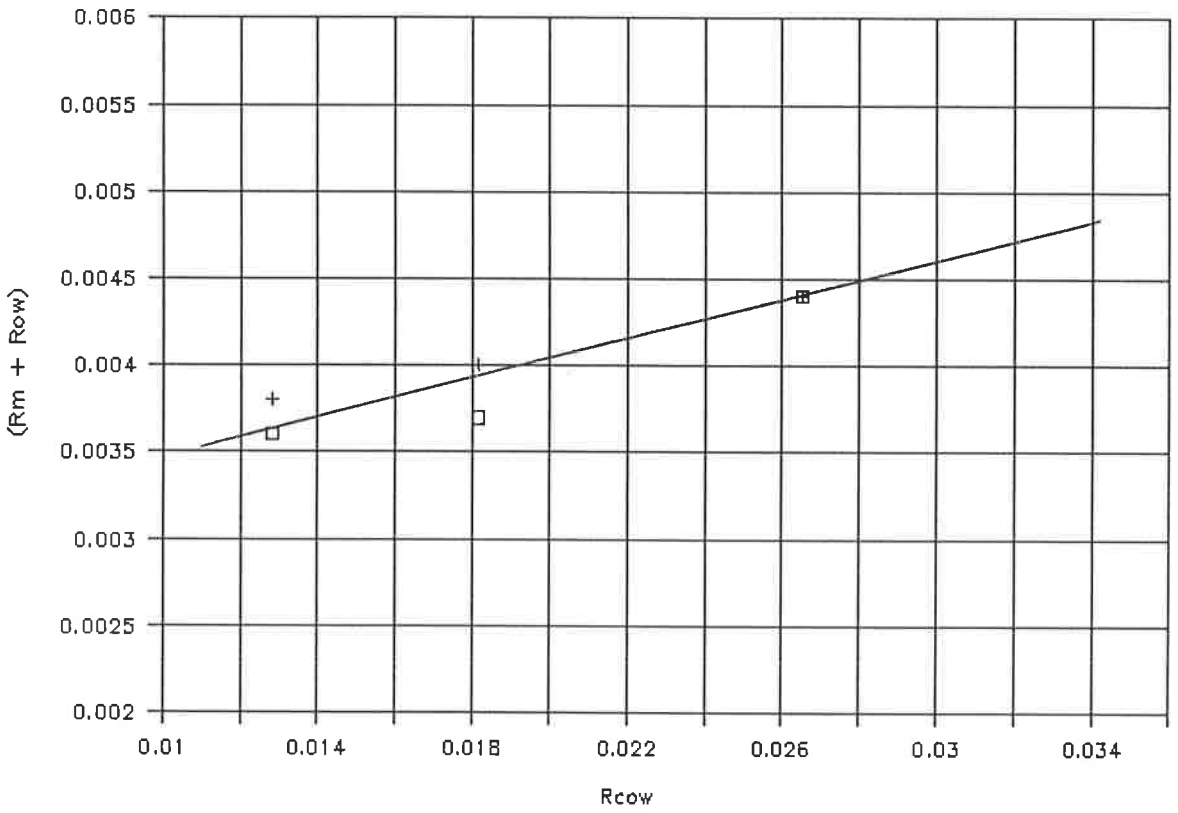

Fig 8.22 : A plot of ($R_m + R_{ow}$) against R_{cow} ($1/h_{cow}$) for a 4-row coil over a range of face velocities for different entering air conditions and water velocities.

The empirical constant as determined from equation (8.18) is used in the generalisation process to compute h_i for 4-row coil.

8.4 The ARI and the AU Generalisations - A Discussion

The theories on which the ARI and the AU methods of generalisation are based have been discussed in Chapters 5 and 6 respectively. The **"ARI GENERALISATION PROGRAM"** and the **"AU COIL SELECTION PROGRAM"** have been developed to predict the performance of coils by the two methods. Examples of the computer printouts of these two programs are presented in Tables A5.1 through A5.5 and A5.1a through A5.5a in Appendix 5. Tables A5.1 - A5.5 consist of the output of the **"AU COIL SELECTION PROGRAM"** followed by the corresponding output of the **"TESTP"** program. Tables A5.1a - A5.5a consist of the output of the **"ARI GENERALISATION PROGRAM"** followed by the corresponding output of the **"TESTP"** program. Thus a direct comparison of the predictions of coil performance by the ARI and the AU methods with the actual test results is obtained. For example, Tables A5.1 and A5.1a give a comparison of the AU and the ARI predictions of the same series of tests with actual test results. It is to be noted that none of the tests from the Tables above has been used in the data reduction process described in Sections 8.2 and 8.3. Thus there can be no circularity in this comparison of predictive capability.

Tables A5.1 - A5.3 and A5.1a - A5.3a give a comparison of the performance prediction with the actual results for the 1-row coil. Tables A5.4 and A5.4a pertain to the 2-row coil and Tables A5.5 and A5.5a pertain to the 4-row coil. Table A5.5 also involves a coil with a different circuiting arrangement from that actually tested. The modifications of the prediction method needed to accommodate different circuiting arrangements has been discussed in Chapter 6. In Table A5.5, a quarter circuiting was used for the actual (**"TESTP"**) while the simulated circuiting in the program **"AU COIL SELECTION PROGRAM"** provides an equivalent half-circuiting.

A detailed comparison of these predictions reveals that the leaving dry bulb and leaving dew point temperatures predicted by the AU method are closer to the empirical test results than are those predicted by the ARI method. It may be argued that the differences between the ARI predictions and the empirical test results are too insignificant to cause concern in the unprecise field of air-conditioning. However, the trend of deviations observed in the ARI generalisations is of remarkable consistency, and, as will be shown in Chapter 9, could lead to room moisture ratios which are much higher than intended in the dehumidifier design. It is observed that the ARI method tends to predict a lower dew point temperature than that found in the empirical tests and this deviation appears to be more significant in the case of a 1-row coil than a 2- or 4- row coil. It is also observed that the lower dew point temperature is accompanied by a higher dry bulb temperature than in the empirical tests.

The ARI predictions deviate more from the test results as the face velocity increases. A possible reason for this is that the air-side convective heat transfer coefficient is higher at high face velocities and this results in lower values of both the mean fin efficiency, ϕ and the surface effectiveness, η. A lower value of ϕ is indicative of an increase in the approximate fin resistance, R_{fD} and hence in the total metal thermal resistance, R_{mD}. The situation is further aggravated by the presence of the condensate layer. The ARI method uses a factor m''/c_p to relate the wet fin efficiency to the wet fin thermal resistance, R_{fW}, where m" is the slope of the saturated air temperature - enthalpy curve at the mean surface temperature, Brown (1954).

It is reasonable to conclude that a low estimate of fin efficiency will result in an underestimate of the coil characteristic, C, and hence the prediction of a lower mean interface temperature than that which actually exists. The lower mean interface temperature will result in the prediction of a lower dew point temperature than is found in the actual tests.

The above deviation in the ARI method has been observed for a coil having six fins per inch. Although the coils of other fin densities have not yet been investigated, it would be reasonable to presume that a similar trend prevails. Hence it may be concluded that, on balance, the AU method, being the more soundly based, is to be preferred. Hence the **"AU COIL SELECTION PROGRAM"** is used for the selection of LFV/HCV coils in the case studies to be discussed in Chapter 11.

Chapter 9

THE PHYSICAL BASIS FOR THE LFV/HCV METHOD OF AIR CONDITIONING

In this chapter are outlined some of the misconceptions prevalent in the traditional approach to dehumidifier design and, in the process, the key features of the new Low Face Velocity - High Coolant Velocity (LFV/HCV) method are highlighted. As stated in Chapter 1, the procedure for the life cycle design of dehumidifiers has evolved from the method of air conditioning which combines low face velocity (LFV) in the air stream with high coolant velocity (HCV) inside the tubes of the dehumidifier.

9.1 The Low Face Velocity (LFV) Concept

It is conventional practice for architects to attempt to minimise the size of the plant rooms as such rooms are not rentable space. Hence the consulting engineers must fight for every square metre and hence must press suppliers of equipment to even smaller sizes of plant. The air handling unit is no exception and hence "high" velocity systems tend to have set "the bottom line" for AHU size below which the engineer will not yield to the architect. This has led to conventional AHU design being dictated by the cross sectional area of the preselected air-conditioning cabinet, which presumes a coil face velocity of about 2.5m/s. A face velocity below 2m/s at design conditions is rare. The choice of face velocity is often justified by the suggestion that airstream velocity and coolant velocity are not of primary importance in air-conditioning system design. The findings of Shaw (1979 a, b and 1982 a, b,) contradict this as they indicate that simultaneous heat and mass transfer performance is considerably influenced by the airstream velocity through the minimum free flow area of the dehumidifier. This particular result has important consequences, as indicated below.

A primary aim when designing an air conditioning system is to offset simultaneously the sensible and latent heat loads of the space in the precise ratio in which they occur. The relative rates at which the cooling and dehumidifiying coil removes moisture and reduces the dry bulb temperature of the air passing through it determine the progressive slope of the coil condition curve (CCC) from the "air-on" condition to the "air-off" condition, when plotted on a psychrometric chart. In humid climates or other situations where the latent heat loads in the space are comparable with the sensible loads, this slope must be steep. However there are thermodynamic constraints on the slope and the shape of the CCC. At all points along its length the local tangent must intersect the saturation line at a temperature which is greater than, or in the limit equal to, the local temperature of the coil surface. A consequence of this is that the curvature must be concave downwards. The local slope of

the CCC is a function of the time for which the air has been in contact with the surface and it is apparent that this is a function of the air-flow velocity. In the limit of zero air velocity all the air reaches a state of equilibrium with the coil surface and the CCC becomes a straight line connecting the state points defining the air-on and the coil surface conditions.

Clearly it would be both impractical and is unnecessary to use zero air flow velocity through the coil, so the design objective is to ensure that as much of the air as possible contacts the coil surface for long enough to approach a condition of equilibrium with it. The mixture of this air with the air which has "by-passed" the surface determines the state of the air leaving the coil; that is, the air-off condition. Conventional wisdom has been to aim for high rates of heat and mass transfer at the coil surface and to ensure that as much of the air as possible actually contacts the surface. Both of these aims suggest that a high degree of turbulence in the air flow through the coil and a long air flow passage would be desirable. Hence it has become standard practice to use a relatively high air velocity through a deep coil. The air flow velocity is characterized by the coil face velocity V_a, defined as the volume flow rate Q divided by the face area of the coil A_f. The high face velocity implies a small face area requires deep coils to maximise exposure of the air to the surface and to accommodate the necessary heat transfer surface area. Such a design accords with the requirement of small cabinets. Hence it is found that coils have, typically, 4 to 6 or even 8 rows of depth and employ face velocities in the range 2.25m/s to 3.0m/s. The unwanted consequence is that they present a significant flow resistance and so require a high power consumption by the fan.

In normal circumstances, high Reynolds numbers result in turbulent flow and high heat and mass transfer coefficients. But this situation does not apply to a dehumidifier. Contrary to the almost universal assumption that the relevant Reynolds number for the air flow in a tube and plate-fin heat exchanger is that based on the equivalent hydraulic diameter (see Section 6.2.2, Chapter 6) and the "cut off" velocity through the smallest section between tubes, the controlling length dimension for the flow is the width of the channel between the fins. The Reynolds number based on this characteristic length is lower than that based on hydraulic mean diameter and is much lower than that required for turbulent flow to exist. It has been shown conclusively by Gilbert (1987) that even at a face velocity of 4m/s through a dehumidifier with low fin density the air flow is laminar. Figs 9.1 and 9.2 are reproduced from Gilbert (1987) and show that even the vortices which form at the junctions between the tubes and the plates, and which dominate the heat transfer on the fins, are laminar vortices. Gilbert also showed that the strength of these vortices decreases as fin density increases. It is important to note that the effective Reynolds number decreases as fin density increases (Appendix 2).

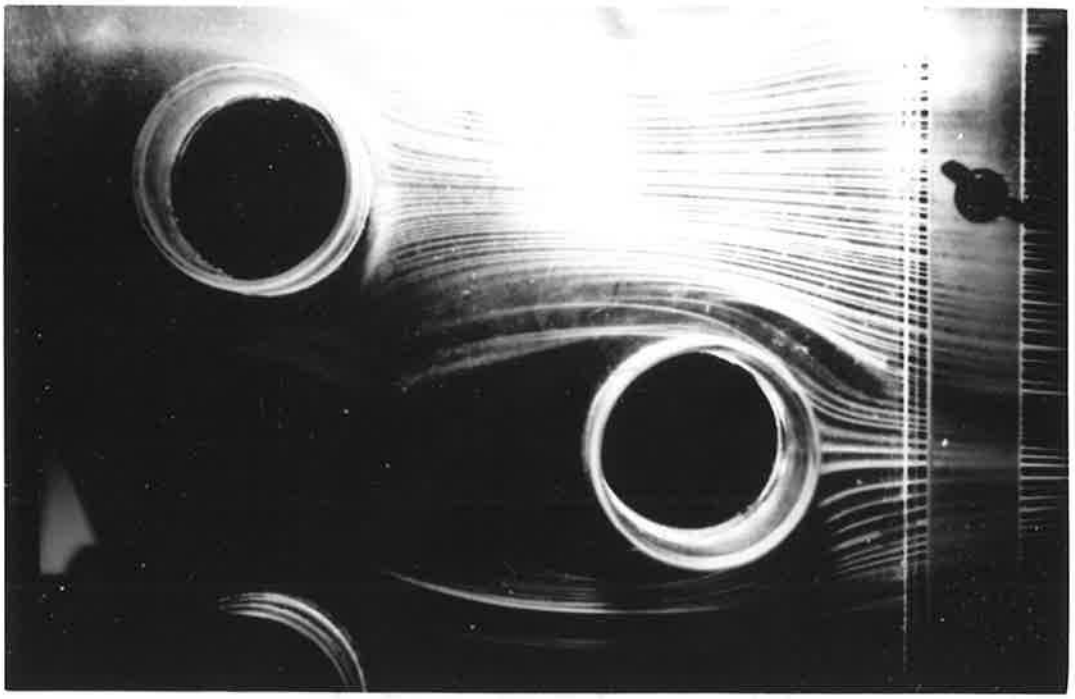

Fig 9.1 : Flow through the staggerred two row model exchanger - Tube view, 4m/s, 6 fins per inch.

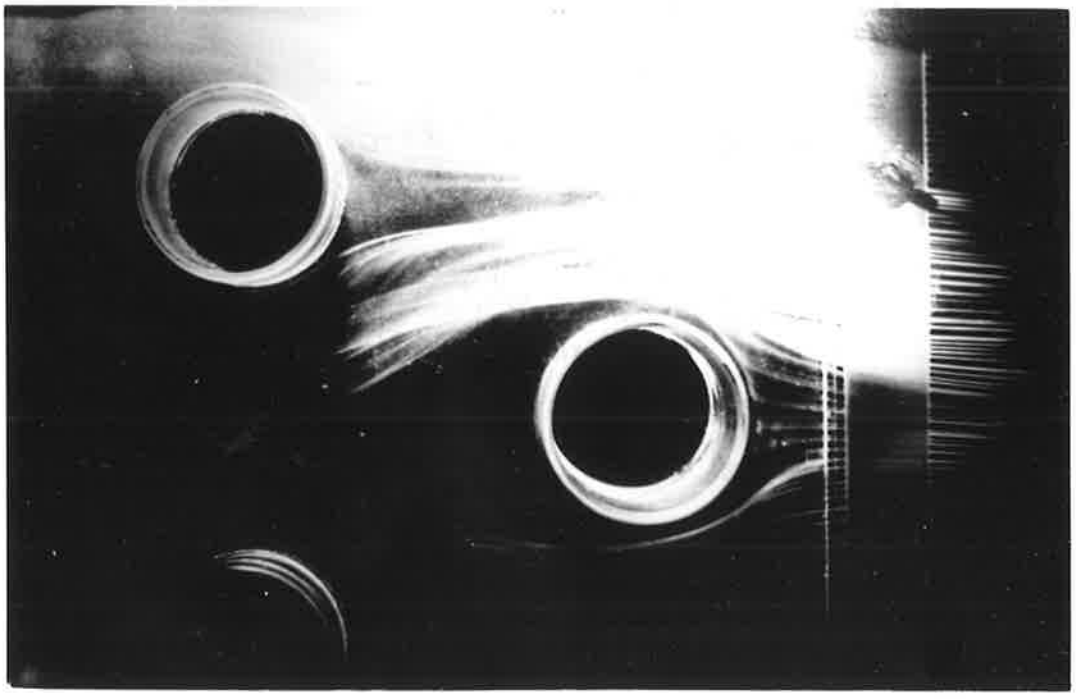

Fig 9.2 : Flow through the staggerred two row model exchanger - Tube view, 4m/s, 8 fins per inch.

9.2 The Low Face Velocity - High Coolant Velocity (LFV-HCV) Concept

The conventional means of controlling the capacity of a given air-conditioning system is by control of the volume flow rate of coolant through the dehumidifier. As the sensible cooling loads are reduced, the flow of coolant is also reduced. It will be shown in Section 9.4 that the part load situation in the life cycle of a dehumidifier is characterised by a higher latent cooling load relative to sensible cooling load than that at the design (peak) load. This implies that the dehumidifier must be capable of increasing dehumidification as sensible cooling demand decreases. We show below that a high coolant velocity is essential for better dehumidification. It then becomes apparent that, at part load, conventional control by reducing the coolant velocity is counter to the basic requirement for good dehumidification.

A "LOW FACE VELOCITY" is typically less than half of the "conventional face velocity" of 2.25m/s to 3m/s. The ratio of dehumidification to sensible cooling is determined by the temperature of the interface between the air passing through the coil passages and the wetted film covering the primary and secondary surface areas. It is apparent that dehumidification will be enhanced by a lower interface temperature. As an illustration, the complex heat and mass transfer problem is simplified to the idealised situation of a one-dimensional heat transfer problem through a perfectly conducting interface between two flowing fluids, one hot and the other cold. In Fig 9.3, t_h represents the temperature of the hot fluid and t_c that of the cold fluid. The interface temperature is represented by t_s. The heat transfer coefficients on the hot and cold fluid sides are h_h and h_c respectively. Let the sensible heat transfer rate between the two fluids be denoted by $\dot{q}$. Thus

$$\dot{q} = h_h A (t_h - t_s) \qquad (9.1)$$

and $$\dot{q} = h_c A (t_s - t_c) \qquad (9.2)$$

where A = heat transfer surface area.

From equations (9.1) and (9.2), we have

$$(t_h - t_s) = \frac{h_c}{h_h} (t_s - t_c)$$

or $$\frac{t_s - t_c}{t_h - t_c} = \frac{1}{1 + \left[\frac{h_c}{h_h}\right]} \qquad (9.3)$$

Equation (9.3) represents the dimensionless interfacial temperature and illustrates the basis of the LFV-HCV concept. The temperature of the interface decreases as the ratio of the heat transfer coefficient on the cold (coolant) side to that on the hot (air) side, h_c/h_h, increases.

The driving force for condensation is the difference between the dew point temperature of the air and the interface temperature. Hence, a large condensation driving force for a given dew point temperature requires a low surface temperature which in turn requires, as stated above, a low heat transfer coefficient on the air side and a high heat transfer coefficient on the coolant side. A low air side heat transfer coefficient is achieved by a low face velocity (LFV) and a high coolant side heat transfer coefficient by a high coolant velocity (HCV).

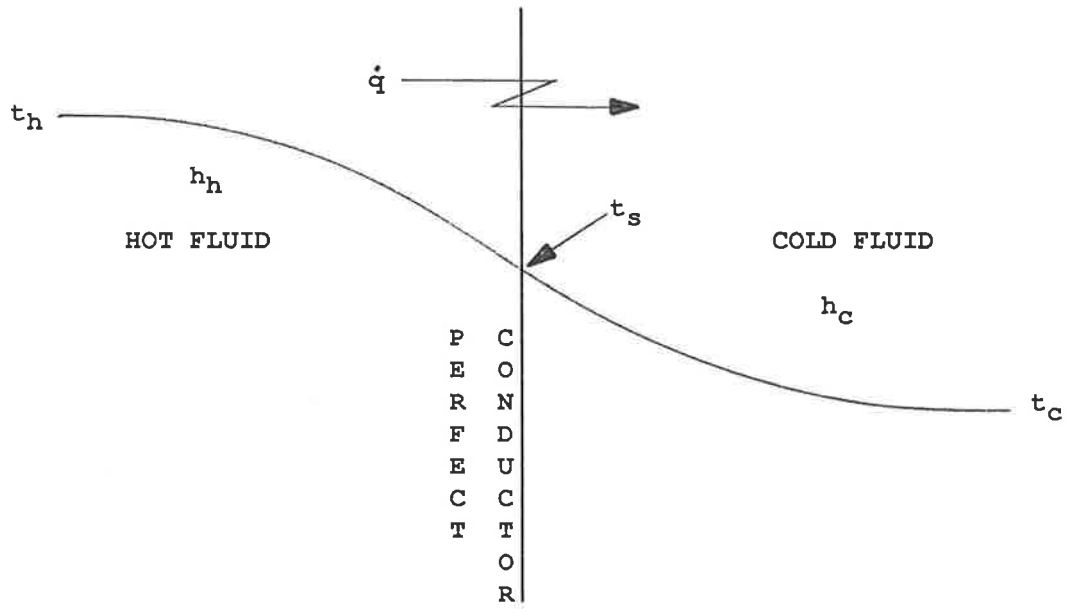

Fig 9.3 : An idealised situation of a one-dimensional heat tranfser problem through a perfectly conducting interface between two flowing fluids.

9.3 The Nature of the Condensate Layer on the Outside Wetted Surface

It is traditionally believed that condensation occurs in the form of a film on the primary and the secondary surfaces of a dehumidifying coil. It is further believed, as observed in the hypothesis of McElgin and Wiley (1940) which is used in the ARI method, that the film has no significant effect on the performance of the dehumidifier.

A brief review of the process of condensation is shown in Fig 9.4. In the case of condensation on heat exchanger surfaces, the physical properties of the surface material and of the vapour mixture, as well as the fluid-dynamical conditions of the vapour flow, determine whether the initially formed condensate drops will remain as drops or spread into a film covering the surface. The former occurs

when the cohesive forces within the liquid exceed the adhesive forces between the liquid and the surface and the latter occurs when the adhesive forces exceed the cohesive forces. This can be expressed in relation to the contact angle between the drop and the surface. The term "dropwise" condensation refers to drops with a contact angle larger than 90 degrees, which corresponds to a virtually non-wetted surface, as shown in Fig 9.4 (a). "Droplike" condensation, shown in Fig 9.4 (b), denotes the mode where the contact angle of a drop is equal to or smaller than 90 degrees and the surface is partially wetted. In the case of "filmwise" condensation, as shown in Fig 9.4 (c), the contact angle is zero degrees and the surface is fully wetted.

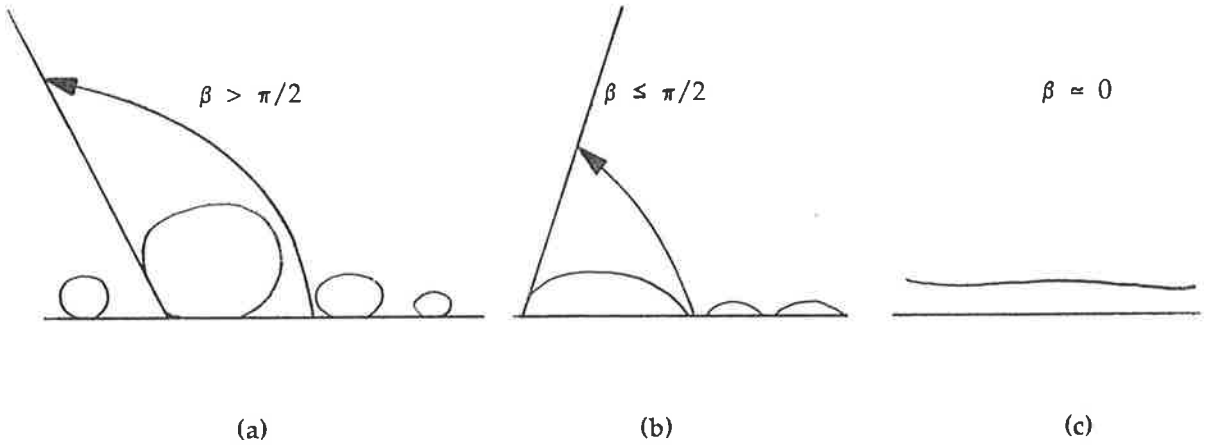

(a) - "DROPWISE" condensation on non-wetted surface.
(b) - "DROPLIKE" condensation on partially wetted surface.
(c) - "FILMWISE" condensation on fully wetted surface.

Fig 9.4 : Modes of condensation process.

Some interesting observations have been made by Anne Schroeder-Lanz (1989) at The University of Adelaide. These are presented in the form of photographs of an operating dehumidifying coil in Figs 9.5 - 9.10. A dry fin and tube dehumidifier is shown in Fig 9.5. It is generally believed that special treatments are required on the condensing surface to obtain dropwise condensation; otherwise filmwise condensation occurs. Yet the preliminary photographs of a dehumidifying coil operating in the low face velocity regime indicate that, even without particular attention to condensing surface, the condensate definitely does not form a film, but forms as drops of different shapes and sizes (Fig 9.9 and 9.10).

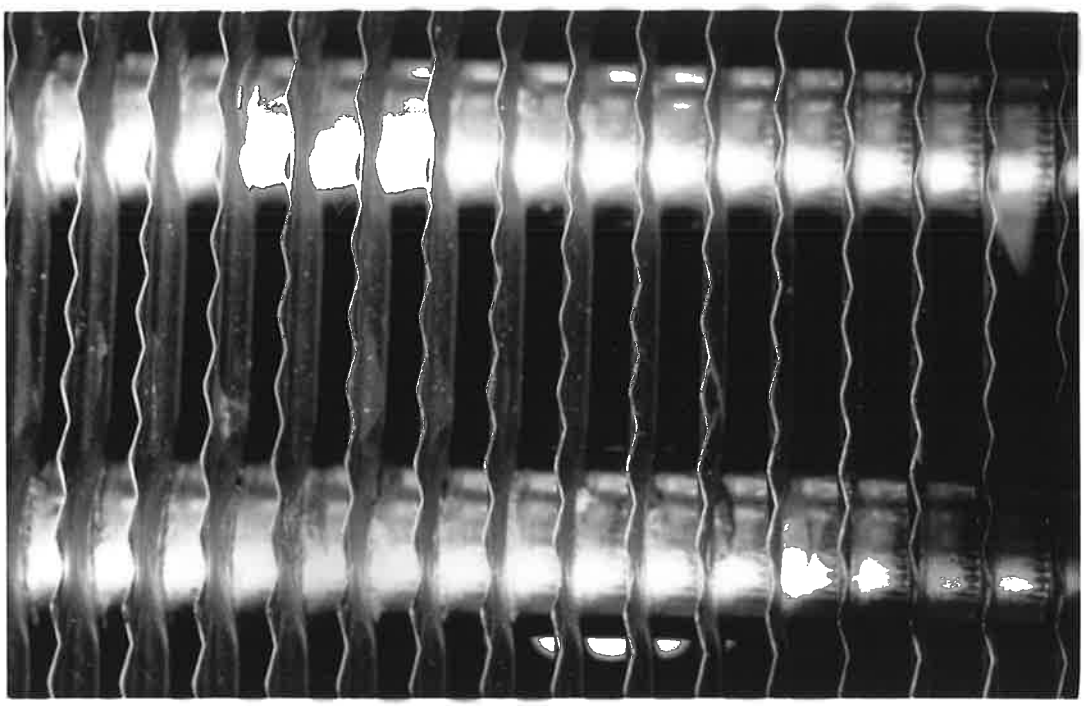

Fig 9.5 : A dry finned-tube coil.

Fig 9.6 : Filmwise condensation on a bare copper tube coil.

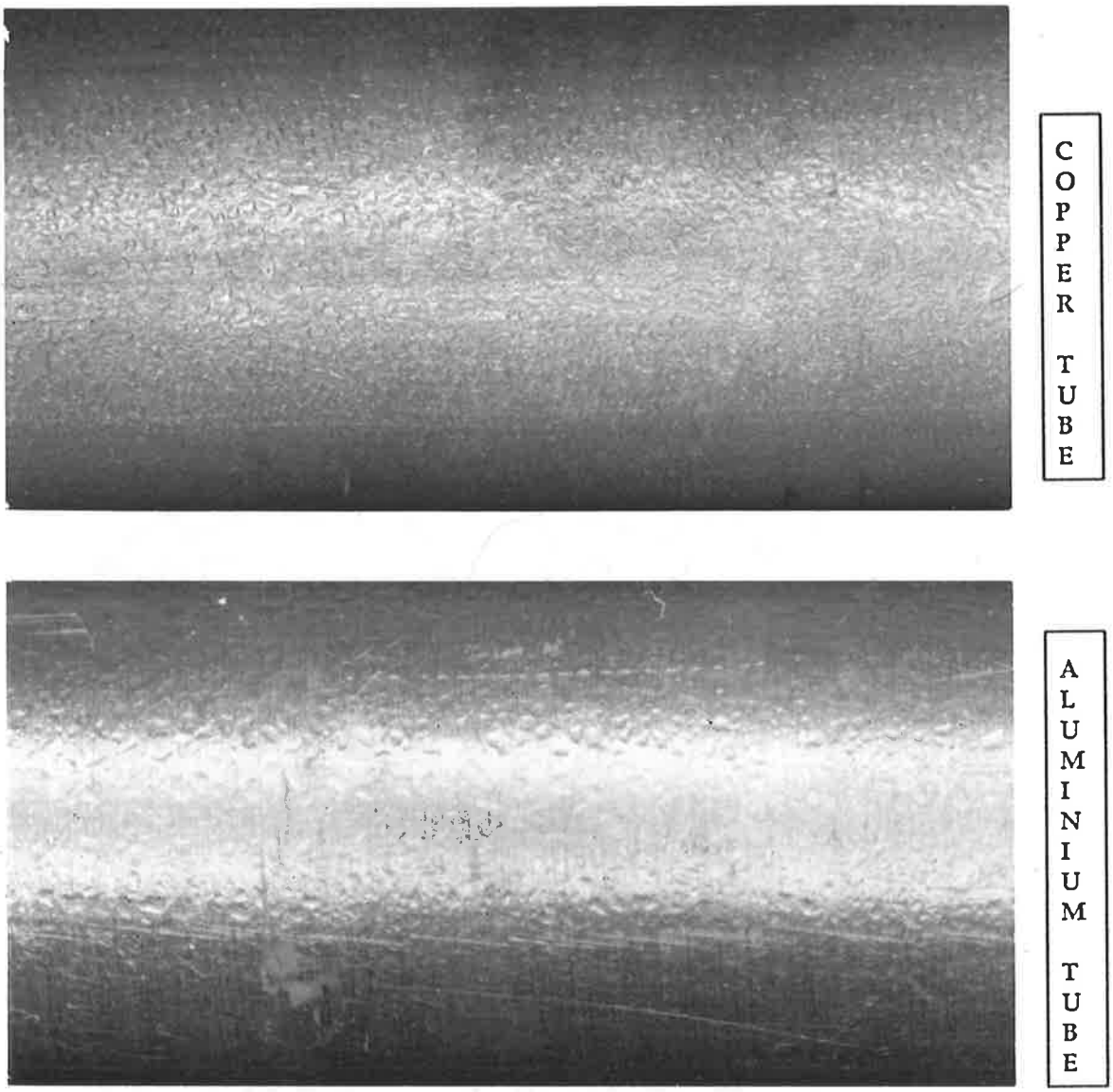

Fig 9.7 : Droplike condensation on copper and aluminium tubes.

Fig 9.8 : Droplike condensation on copper tube (magnified).

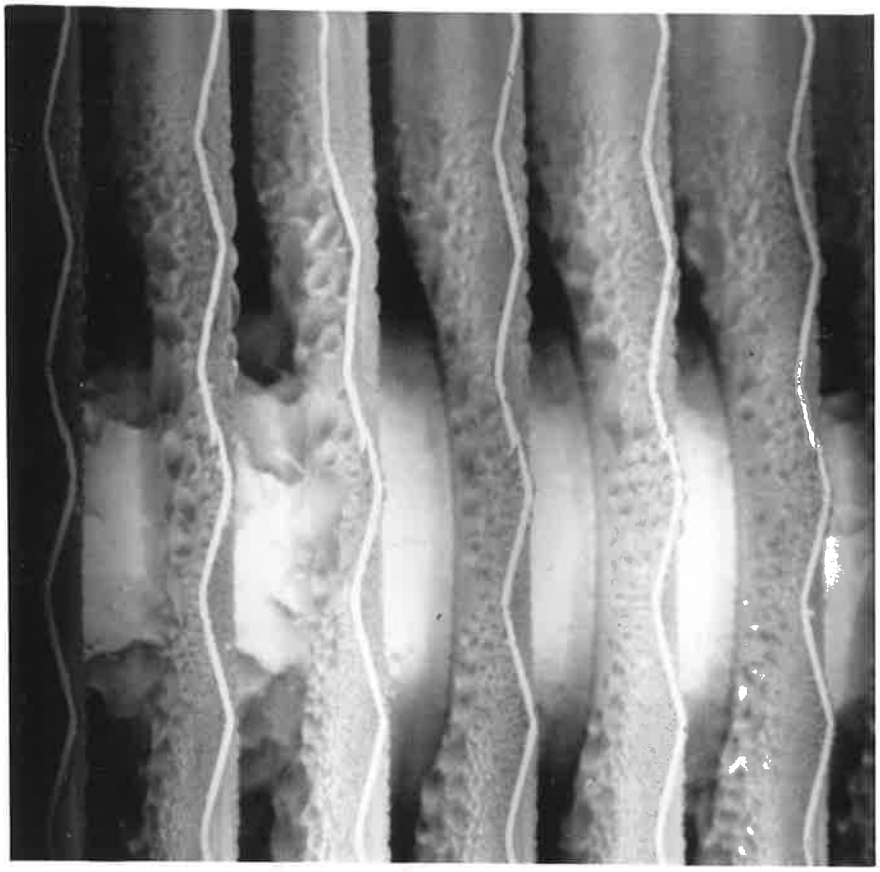

Fig 9.9 : Droplike condensation on a finned-tube coil.

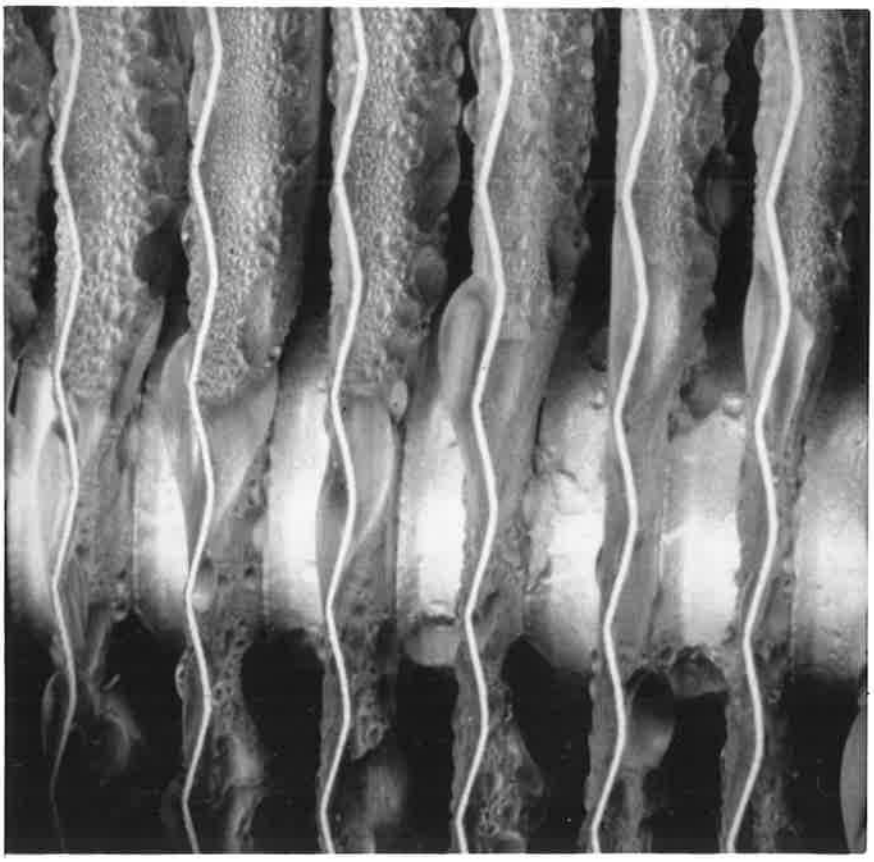

Fig 9.10 : Droplike condensation on a finned-tube coil.

By visual observation of the drops in the photographs, Anne Schroeder-Lanz determined the "maximum drop radius" and obtained a reasonably good correlation for the heat transfer coefficient of the condensate layer using the theory of Rose (1976), which was developed for a pure water vapour system (*i.e.* no inert species). It is important to note that the "maximum drop radius" is not simply the largest possible drop immediately prior to sweeping, since by no means do all drops reach the same size. It is an average value; to be exact, it is the average value of all drops of the oldest generation prior to sweeping. In the process of investigating the "maximum drop radius", it was observed that the condensation on a bare copper tube coil was filmwise, as shown in Fig 9.6. To determine if the effect was due to the different material, the experiment was repeated with two single tubes, one made of copper and the other made of aluminium. Both tubes were placed in the same coolant circuit. The condensation on the aluminium tube had a dimpled character suggesting that it was not filmwise; see photographs Figs 9.7 and 9.8. Thus it was concluded that the copper of the tubes in the bare tube coil has different adhesive properties, which can be due to previous chemical treatment or difference in the composition of the metal.

The literature does not contain many results regarding the influence of vapour velocity. O'Bara *et al* (1967) state the interaction between vapour velocity and heat transfer coefficient for pure steam. With increasing velocity the shear stress between condensate and vapour increases and eventually reaches a critical value at which the drop formation becomes instable and disrupts into a more or less continuous film. This results in a sudden drop in heat transfer coefficient. In the case of moist air flowing horizontally through a dehumidifying coil an increase in the face velocity is likely to have a similar effect on heat transfer by influencing the maximum drop sizes, the shape of the drops and also the vapour-side heat and mass transfer coefficients. Some preliminary photographs, not presented here, show a higher percentage of large drops of more irregular shape for higher face velocities. In the limit a large drop becomes a film. As stated earlier, larger drops represent a higher thermal resistance to conduction within the drops, so their surface temperature is higher than that of smaller drops, and consequently, they contribute less to the condensation process.

9.4 The "Moisture Staircase" Phenomenon

During marginal weather conditions, the transmission of sensible heat to the treated space is reduced or may actually become negative and so cancel part of the internal sensible heat load. However latent heat addition from people, infiltration and other sources, which occurs simultaneously and in conjunction with the sensible transfer, will usually remain the same or may rise. It is quite common, as will be shown in Section 9.5, to have a part load condition where the ambient dry bulb temperature is lower and the dew point temperature higher than at peak design conditions. Thus, there is a decreased sensible heat load and an increased latent heat load. The

dehumidifier must then operate at a reduced Room Sensible Heat Ratio (RSHR) and, hence, the slope of the coil condition curve must be steeper.

During coil selection, if at the required air-off dry bulb temperature (dbt) the nearest approach to the desired air-off condition has a humidity ratio which is too high, two procedures are possible:

1. Conventionally, one or more additional rows are added to the coil to achieve the required moisture ratio by over-cooling the air and then using some means of reheat to correct the sensible temperature. This is not a recommended procedure unless (*a*) the amount of reheat required is sufficiently small to be satisfied by recovery from lights or other sources of waste heat, and (*b*) the amount of overcooling and reheat can be controlled.

2. Track the dynamic process to determine the equilibrium state which will result within the conditioned space; then assess if the condition lies within the comfort zone.

Procedure 2 involves accepting the predicted air-off condition at the required leaving dbt (which is controlled). From this air-off condition the required load ratio line, with a gradient equal to the RSHR, is drawn to intersect with the required room dbt (which is also controlled). This then establishes the room condition after one circuit of the air. From this new condition, allowing for return duct heat gain, a new air-on condition may be determined. The coil simulation is then re-run to obtain the new air-off condition. The sequence is repeated as many times as necessary to converge to the equilibrium balance between the room loads, in their correct ratio, and the coil performance. The equilibrium condition will be at a moisture content greater than that initially desired, and this new condition may, or may not, be within the acceptable comfort zone (< 12 g/kg, as shown in Fig 12.1, Chapter 12).

The "moisture staircase" is a phenomenon which is generally overlooked during coil selection. If the selected coil produces a lower moisture ratio than the target, the "staircase" will be downward and the room will find an equilibrium state at a moisture content lower than that specified. The "moisture staircase" adjusts the driving potential for dehumidification between the air and the coil surface until the amount of moisture removed from the air at the coil equals the amount of moisture added to the air in the conditioned space. When more dehumidification per unit of sensible cooling is required, this driving potential increases and the coil condition curve becomes steeper. The reverse occurs if less dehumidification is required. The phenomenon is of special significance when considering the part-load performance of a dehumidifier. As discussed earlier, internal loads tend not to vary very much and hence part loads are usually the result of a reduction in the transmitted sensible load. Thus the room latent load becomes a larger proportion of the total room load and hence the RSHR is smaller. To satisfy the smaller RSHR requires a coil condition curve which is

steeper than that required at peak conditions. Thus a dehumidifier designed only for peak load conditions must inevitably produce an increase in room moisture content at part load unless overcooling and reheat are used. This increase is more severe for Constant Air Volume (CAV) systems than for Variable Air Volume (VAV) systems.

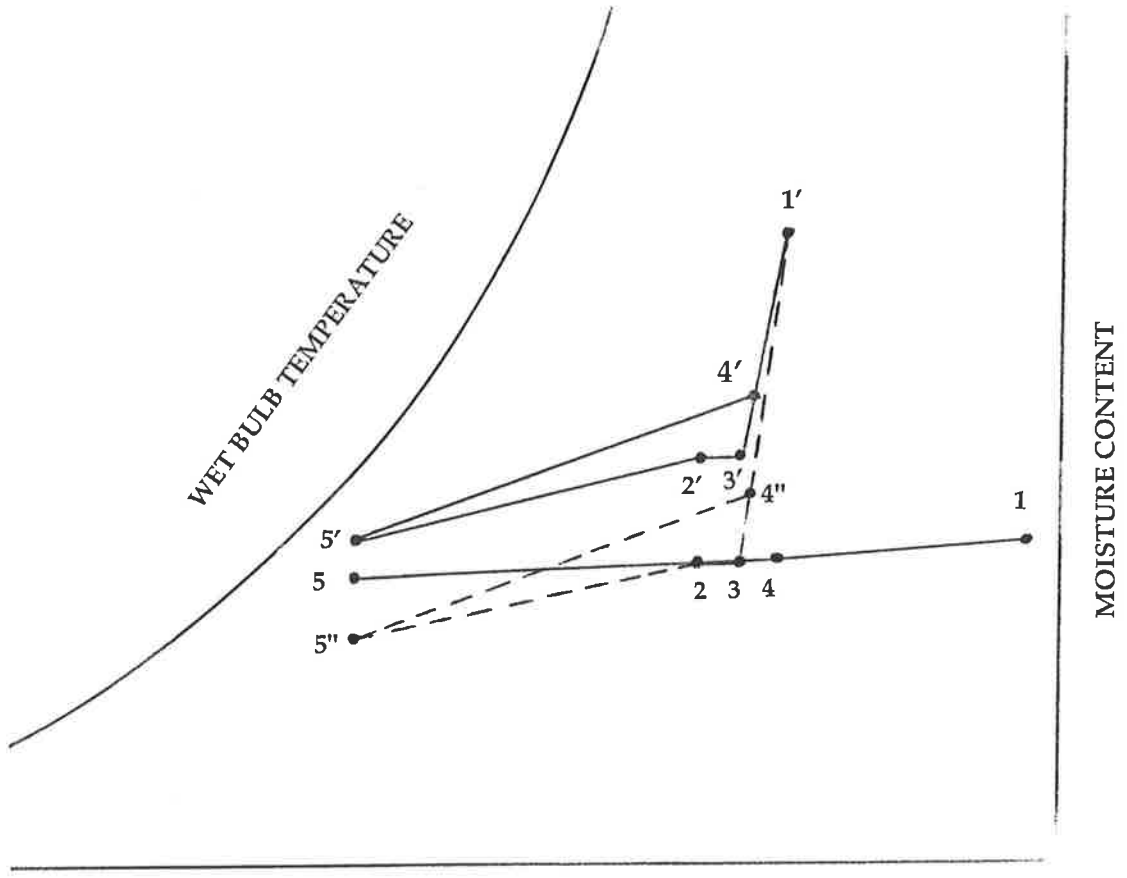

	Peak load	Part load
Outside air condition	1	1′
Room condition	2	2′
Return air condition	3	3′
Air-on condition	4	4′ (4")*
Air-off condition	5	5′ (5")*

* Required conditions if the room condition at part load is to be the same as that at peak load.

Fig 9.11 : Psychrometric process for a VAV system - An illustration of the "moisture staircase" phenomenon.

The dew-point temperature corresponding to 12g/kg moisture content is 16.8 °C. Thus if chilled water entry temperature is 8 °C, for example, and an 8 °C water temperature rise is set as a design requirement, a significant proportion of the coil will be above the maximum dew-point temperature for comfort when allowance is made for the local temperature difference between the coil surface and coolant. Allowing too high a water temperature rise thus leaves negligible driving potential for dehumidification and frequently leads to room conditions which exceed the 12g/kg humidity ratio comfort limit. Experienced designers of conventional air-conditioning plant may be concerned that chilled water quantities with the LFV-HCV system tend to be a little larger than those conventionally used. The difference merely reflects the difference in the ability of the LFV-HCV system to maintain comfort conditions throughout the load range. If the moisture ratio to be achieved is that available from a conventional system, the LFV/HCV system can do this with less water and significantly less energy consumption. But such a condition is frequently unacceptable without reheat; thus water quantity should not be imposed as an immovable constraint but should be one of the factors considered when assessing the economic merits of the various systems.

To illustrate the moisture staircase phenomenon, consider the psychrometric process shown in Fig 9.11 for a VAV system. The room and the supply air dry bulb temperatures are maintained constant. The load ratio line 2-5 would be representative of that at peak load having a RSHR of about 0.9. The peak load coil condition curve (CCC) is represented by 4-5. As discussed in Chapter 10, the RSHR at part load would be lower than that at peak and if the room is required to be maintained at state 2, the new imposed load ratio line 2-5" would require a CCC 4"-5". It is apparent from Fig 9.11 that such a CCC is thermodynamically impossible if capacity control is by means of a reduction in coolant flow as such a reduction must result in a higher average coil surface temperature (Fig 9.3). The dynamic response of the coil and the system therefore causes the room moisture level to rise in order to attain an equilibrium condition at 2′, where the load ratio line 2′-5′ becomes compatible with a thermodynamically possible CCC 4′-5′.

9.5 Specification of Ambient Conditions at Peak and Part Loads

In air-conditioning system design, it is common practice to consider only the summer peak design condition for the outside air. Despite the relatively small percentage of the outside air usually required for ventilation purposes, this air can play an important role in the overall air-conditioning system design. The influence is particularly significant in the case of a VAV system as the minimum ventilation requirement has to be satisfied at all times. Hence the percentage of the outside air at part loads must increase in comparison to the percentage required at peak load.

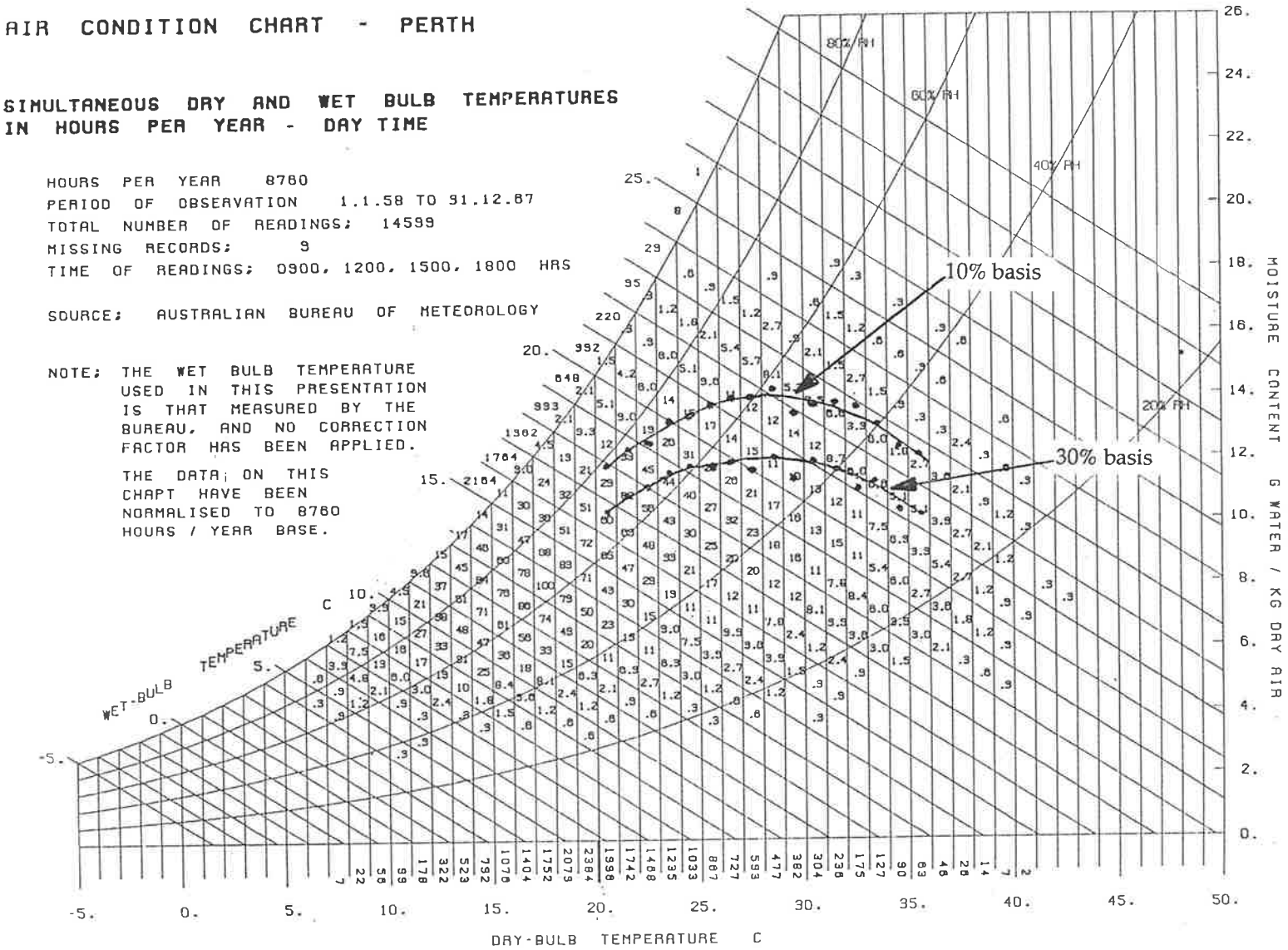

Fig 9.12 : Simultaneous dry and wet bulb temperatures in day-time hours per year for Perth.

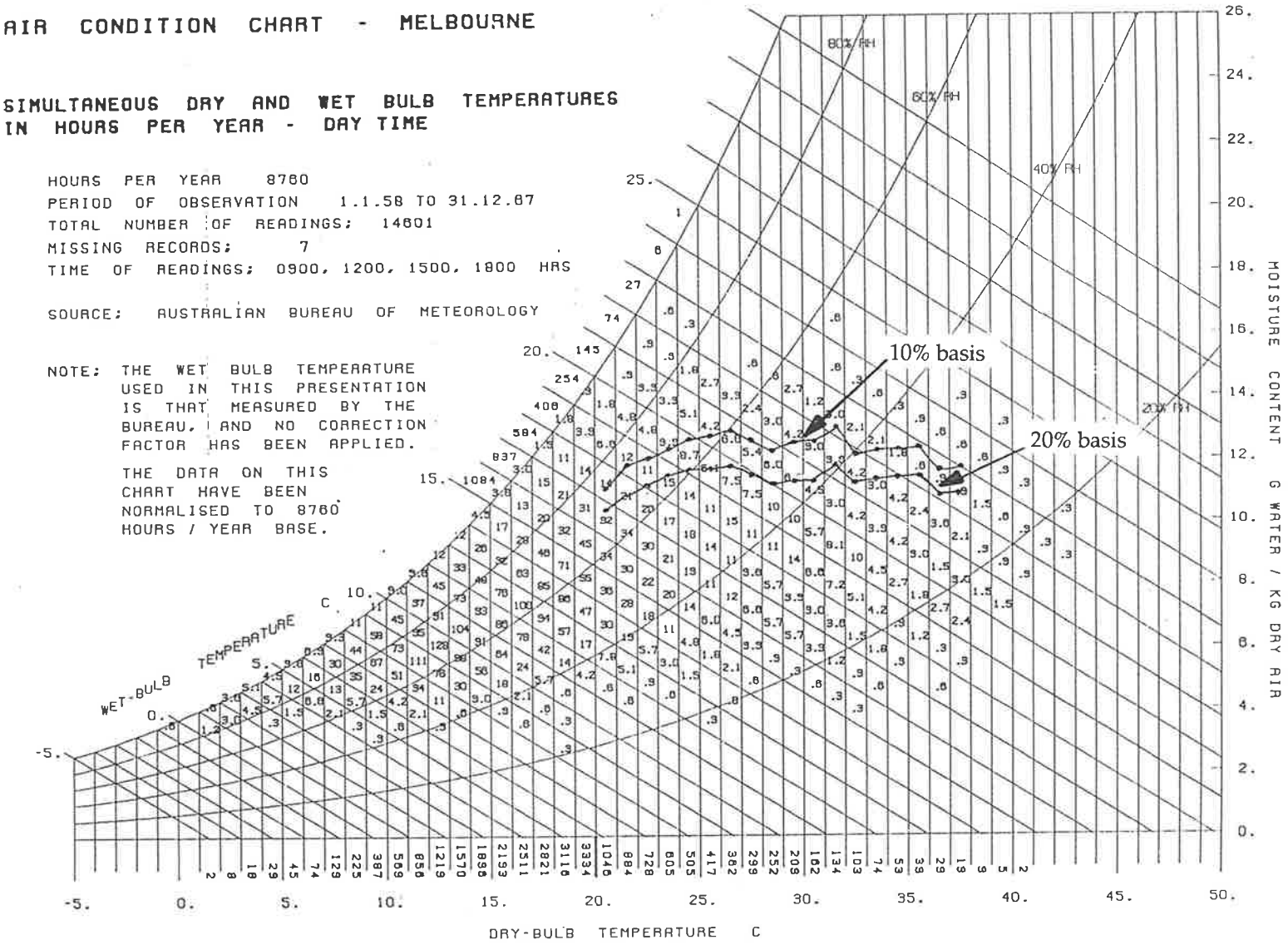

Fig 9.13 : Simultaneous dry and wet bulb temperatures in day-time hours per year for Melbourne.

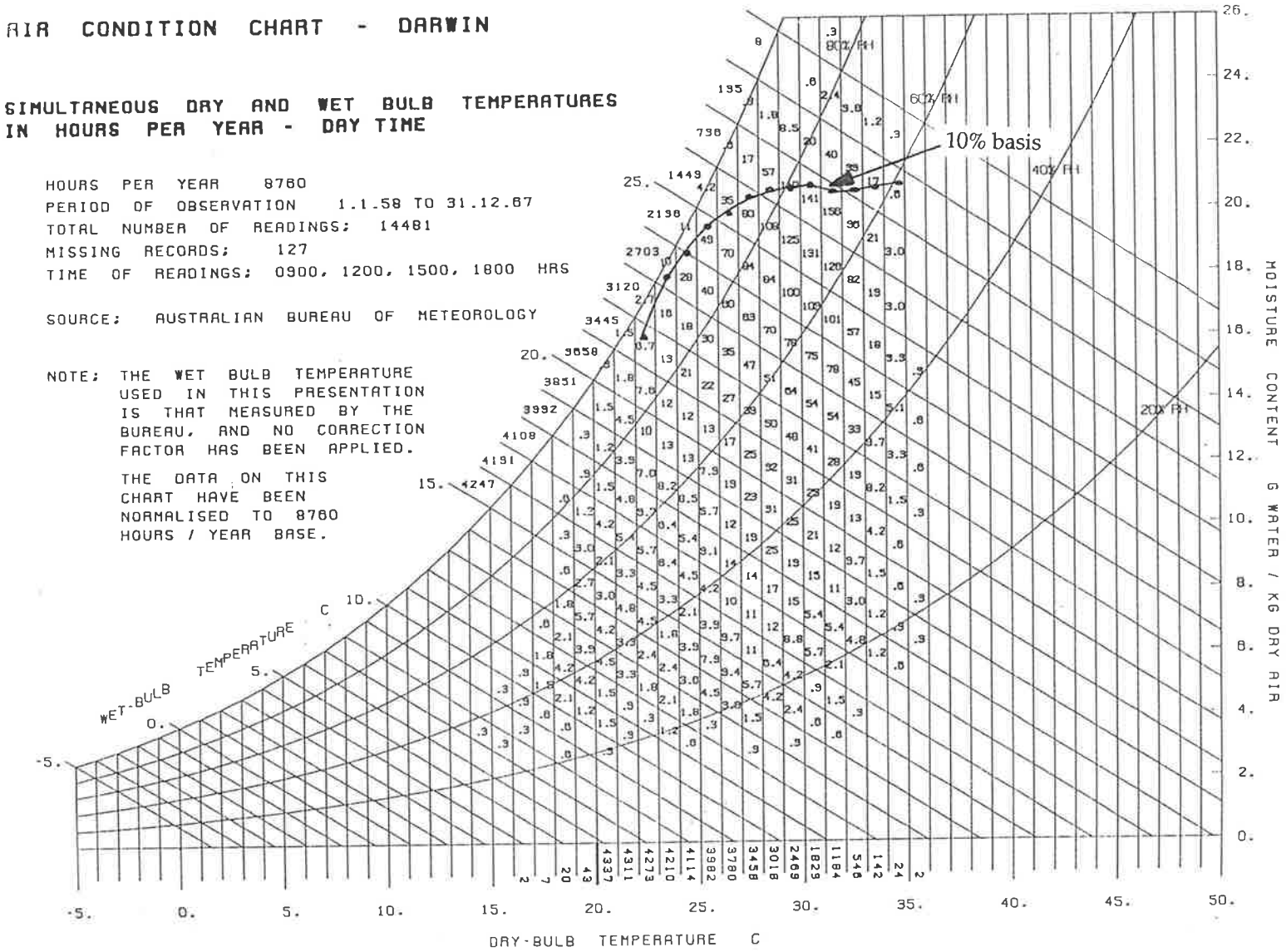

Fig 9.14 : Simultaneous dry and wet bulb temperatures in day-time hours per year for Darwin.

It is necessary to distinguish between part loads and design part loads. Depending on the geographical location, during part load days when the ambient sensible temperature is below the peak design condition there can be many periods during which the ambient humidity ratio is considerably above that for summer peak conditions. In the same way as one specifies a peak load design condition one can specify one or more humid part load design conditions for a given locality. In some cases humid part loads will be associated with hot humid peak loads as in Washington and Singapore. In others humid part loads are associated with hot dry peak loads as in Melbourne and Dallas.

It is apparent that specification of design part load ambient conditions is important. "Design part load conditions" may be taken as high total enthalpy combinations of dry-bulb temperature and humidity ratio which are not exceeded for more than some specified number of hours per year. In the absence of any existing standard specification of part load ambient conditions a method for establishing such conditions has been proposed (Luxton, Shaw and Sekhar, 1989). Reference is made to the Meteorological Weather Charts or tabulations which are available for most major cities in the world. A selection of such charts showing the incidence of simultaneous dry and wet bulb temperatures in day-time hours per year for the Australian cities of Perth, Melbourne and Darwin are reproduced as Figs 9.12, 9.13 and 9.14. At each dry bulb temperature (dbt), spanning the range from peak (summer) dbt to minimum cooling dbt (say 20°C), the high enthalpy condition which corresponds to 10% of the total number of hours of observation of simultaneous dry and wet bulb temperatures at that dbt is located. This is taken as the design humid point at each of the dry bulb temperatures. The outside design condition for any part load then lies on the locus of the design humid points. For less rigorous designs a higher percentage of hours during which a condition is exceeded may be acceptable. For example, a 30% locus is illustrated for Perth in Fig 9.12.

Chapter 10

THE "LFV/HCV" LIFE CYCLE DESIGN METHODOLOGY

In this chapter is described the systematic design procedure (Sekhar *et al*, 1989) used in the LFV/HCV method of air-conditioning. The design encompasses all definable operating conditions likely to be imposed on the system during its life. Although the LFV/HCV design methodology is applicable to both VAV and CAV systems, a VAV system is used in the following sections as the vehicle for discussing the fundamentals and the design procedure.

10.1 Preparing The Way

As with standard practice, it is important to decide initially the overall design strategy for the building air-conditioning system, including number, approximate air capacity and refrigeration capacity of air handlers per floor, zoning, peak design sensible and latent room loads, simultaneous peak loads of all zones to be served by each air handler (*i.e.*, simultaneous design conditions), ventilation air quantities, plant room size, layout and constraints, air distribution and return paths, and any requirement for special psychrometric conditions. Appropriate peak outside air conditions and minimum outside air quantities must also be specified. A prominent feature of the design brief is the specification of all room sensible, latent and total heat loads, with proper reference to present and future functions and both peak and part load conditions. Unless a special condition is specified for the room, as may be a requirement for a laboratory or process, room at all load conditions should normally be specified to remain within the ASHRAE comfort zone (Fig 12.1, Chapter 12) without the use of reheat. Common practice, unfortunately, is to specify that the room is maintained at a fixed dry bulb temperature and relative humidity throughout the cooling season. Such a specification is in almost all cases contrary to the laws of thermodynamics.

Peak outside air conditions may be selected according to ASHRAE recommendations or from Meteorological Bureau tables or charts of simultaneous dbt/wbt, with an appropriate incidence criterion or according to in-house standards. As described in Chapter 9, the outside air design condition for each dry-bulb temperature within the operating range is chosen as that for which the simultaneous day-time dbt/wbt is only exceeded for, say, 10% of the total number of operating hours. Clearly the percentage incidence can be varied depending on the sensitivity of the particular application and, for hotels and hospitals which operate on a 24 hour basis, the 24 hour incidence data would be used.

It must be noted and stressed that at this stage of the design it is inappropriate to specify either the air-off conditions or the precise room conditions to be achieved, except where these constitute "special conditions". A "target" room condition can be specified and used to obtain airflow rates for

each room, so that ducts, dampers and registers can be chosen and air handlers approximately sized. For both VAV and CAV systems the humidity ratio, which becomes a figure of merit for the design, cannot be specified *ab initio*.

10.2 Determining Peak Room Design Condition, Room (ΔT) and Air Volume Flow

From consideration of the functions, ceiling height and type, floor plan, and load distributions within the building spaces, a range of acceptable supply air temperatures is specified. This sets the range of acceptable "Room (ΔT) dbt", where

Room (ΔT) dbt = dbt room - dbt supply air.

Hence the volume flow to each space is determined, and the distribution ducting and VAV mixing boxes may be sized.

From knowledge of peak design loads and the chosen range of Room (ΔT) dbt, the range of supply air quantities for each room and zone between simultaneous peak and economy cycle operation can be determined. It is now necessary to recheck acceptability of the air quantities and refrigeration load for each air handler and of discharge air velocities in relation to the choice of supply air registers. The sizing, type and location of VAV mixing boxes, and the definition of the minimum total air volume to be handled by the air handling unit, should be verified.

Note that the lower the permissible supply temperature, the smaller is the volume of air to be handled, subject to ventilation requirements and the maintenance of air movement, and the smaller also is the face area required for a given air velocity entering the face of the dehumidifier coils. In addition, a low supply air temperature assists the dehumidification process.

For a given dbt off the coil, if a large Room (ΔT) dbt is acceptable both the room design dbt and the moisture content can be higher while remaining within the comfort zone. This is seldom a serious consideration in dry climates for peak load design, but for part-load design and for both peak and part-load design in tropical climates where the RSHR is low, it becomes important.

The load ratio line on a psychrometric chart, which has the gradient of RSHR, is drawn through a selected room peak design condition. It is important to think in terms of the gradient of the RSHR line as this is what is imposed on the system. It is not within the control of the air-conditioning system designer once the room loads have been established. Further, in a basic VAV system in which there is no direct control of moisture content and the prime sensor for control of the dehumidifier is the dbt of the air leaving the air handling unit (AHU), the condition of the air in the room will move up or down along a line of constant dbt as the moisture content varies (Sekhar *et al*

1988). Thus in temperate climates where both load and RSHR reduce significantly during operation, the room condition in a VAV system should be chosen safely within the comfort zone.

It is essential to specify the return air path pressure drop and temperature gain between room and air handler in sufficient detail to allow temperature and pressure conditions at inlet to the air handler to be specified correctly. With the LFV/HCV system, it is not usually necessary to incorporate noise attenuators in the return air path as plant room noise is very low (70 - 72 dBA).

10.3 Determination of Peak Face Velocity

Layout sketches are then prepared of possible AHU arrangements which could be accommodated within the plant room. The objective is not to design the AHU cabinet, but to estimate the largest face area of coil which can be accommodated in a notional air handler within the limitations of plant room floor area, ceiling height, locations of air inlets, pipework, switchboards, access doorways and panels. A face area of coil which allows a peak face velocity of 1 m/s is preferred, and experience suggests that this can usually be achieved, if necessary through minor rearrangement of the plant room. In very confined situations face velocities may have to rise to 1.5 m/s or higher, but the aim in such cases is to achieve the lowest face velocity possible within the constraints.

It is pertinent to mention at this stage that the manufacturer of the AHU must arrange the selected coil within the "box" together with filters, fan and means of removing condensate. Several important elements are listed here :

1. Flow distribution over the face of the coil must be uniform, preferably between ±10% of the desired mean.

2. Every effort must be made to achieve a smooth, unencumbered flow into the inlets of the fan or fans.

3. Filters do not need to be of the deep bed variety, as the velocity through the filters is significantly lower than with a conventional system.

We have undertaken extensive model tests on a range of air handler designs fitted with aerodynamic devices that have resulted in the development of LFV/HCV units which occupy substantially the same floor area as conventional units, have a high uniformity of flow distribution, use less fan power, are almost 20 dBA quieter, and achieve significantly higher fan efficiencies.

10.4 Coil Selection for Peak Load Condition

Having chosen the face velocity and the face dimensions of the coil, a specific coil and circuiting can then be selected for the peak load condition. It is important to obtain a reasonably accurate air-on condition to the coil. In determining this, an allowance for the sensible temperature gain by the return air due to lights and infiltration should be added to the selected room peak design condition discussed earlier. A mixing line may then be drawn from the return air condition to the peak design outside air condition. From the required volume of ventilation air with allowance for infiltration, the volume of return air, the leakage and the spill, the air-on condition may be set off on the mixing line.

A range of acceptable Room ΔT values around the initially assumed value and the imposed RSHR must now be used to determine the range of air-off conditions which could satisfy the RSHR. It is to be noted that the designer cannot use RSHR as an adjustable parameter without changing room function, fenestration and other related parameters, as RSHR is the balance of sensible and latent heat loads to be satisfied by the air-conditioning plant being designed. The air-on condition may be connected on the psychrometric chart to the air-off conditions for each of the range of Room ΔT values explored, and extrapolated to the saturation line. Any line which does not meet the saturation line defines a thermodynamically unobtainable condition. Those lines which meet the saturation line define approximately the range of achievable "apparatus dew points" (ADP). The old-fashioned term ADP is revived here only as a means of describing how the approximate chilled water temperature may be obtained. The chilled water temperature required for each of these possible designs is approximately equal to ADP minus the temperature drop between the coil surface and the coolant. It is a characteristic of LFV coil performance that the coil condition curve approximates a straight line for air face velocities less than about 1 m/s. Thus a preliminary design may be explored by assuming this as an approximation for the coil condition curve.

The designer is now in a position to determine the feasibility of the various acceptable Room ΔT values. Some may be thermodynamically unobtainable for the particular selection of room peak design condition. If none of the required off-conditions can be met, as judged by the nonexistence of an ADP, the standard design procedures, such as increasing the Room ΔT, moving the room to a higher dbt or to a higher humidity ratio, reducing the outside air proportion, or pretreating the outside air, may be followed each within its defined constraints. Pretreatment of outside air can often be beneficial, both functionally and economically, in humid climates. An achievable humidity ratio for a given set of Room dbt, Room ΔT and other conditions may be determined approximately via the "moisture staircase", Chapter 9, by assuming that the CCC is a straight line.

By this point the designer should have established achievable peak load design conditions within the assumption that the coil condition curve is a straight line at low face velocity.

Having specified the air-on condition and quantity, permissible chilled water temperature range, maximum permissible water pressure drop, estimated maximum coil size and desired face velocity, a coil may be selected via the **"AU COIL SELECTION PROGRAM"** to meet as closely as possible the desired air-off condition. The program is used interactively to determine a cost-effective combination of coil size, number of rows, fin spacing, air velocity, coolant temperature, coolant flow rate, circuiting, water pressure drop, and room moisture content to satisfy the prescribed RSHR. The program can also be iterated over the moisture staircase to determine the achievable room moisture condition. This then establishes a good approximation to the peak load design.

10.5 Part-load Conditions

Assuming a satisfactory design has been achieved for peak load operation, the question of part load may be addressed. Specification of design conditions for part loads is straightforward. Outside-air conditions for part loads may be determined as described in Chapter 9 and room conditions from a building load simulation program. As indicated earlier when discussing the fundamental problem, part load dehumidification requirements cannot be met by throttling the coolant flow through the now oversized coil. The LFV-HCV part-load design procedure consists of choosing an outside air dbt which is below the peak condition, as in Chapter 9, finding the corresponding sensible and latent loads, and then finding the fraction of the peak load coil and its associated (high) coolant velocity necessary to offset the sensible and latent loads in their correct ratio. This procedure differs from that at peak load only in that the coil selection is constrained. A row or rows, or parts of rows, of the peak load coil can be isolated to give the coil characteristics required for the particular part load. In this way, the effective size of the dehumidifier coil is staged so that it is at all times compatible with the imposed load; thus the room can always remain within the comfort zone. The accuracy with which the room condition is to be met determines the number of stages. Only two or three stages are needed in normal office buildings. More stages may be needed for specialist laboratories or similar applications.

The first part-load condition addressed during the design procedure is the "minimum range", *i.e.*, that for which the sensible load is, for example, 60% of the peak value. The actual point is that which best represents the point below which supply air temperatures are "naturally" rescheduled upwards. Such rescheduling can be made automatic ("natural") by transferring operating strategy from VAV to CAV (Constant Air Volume) below the chosen point. In this form of the CAV mode, the only control measure is throttling the chilled water flow through the remaining operative sections of the coil. As dehumidification can be very important in this lowest range of operation, it is desirable to enter the range of CAV operation with the highest practicable water velocity through the operating part of the coil. CAV "turn-down" can thereby be maximized. When the "Room"

enthalpy (averaged over all the rooms/zones served by an air handler) becomes less than the outside air enthalpy by a prescribed margin, the "economy cycle" is activated.

It may be surprising that it is in the lowest range of operation of a conventional VAV system that comfort conditions can be most difficult to satisfy. The reason is that, for a building with a constant "population", any decrease in the total load is dominated by the decrease in the sensible load. The latent load changes only marginally, except where outside air at part-load has a higher humidity ratio than at full-load, in which case the latent load can actually increase as total load decreases. Thus the Room SHR decreases as load decreases. To achieve compatibility between the coil condition curve and the load ratio line it is necessary to steepen the coil condition curve; that is, the need for dehumidification relative to sensible cooling increases as load decreases. This situation reaches an extremum in the lowest operating range of the equipment.

The above detailing of the LFV/HCV design procedure suggests the reasons for many of the complaints about the performance of air-conditioning systems, especially where VAV operation is maintained throughout, and why they are most vocal from the low load zones in the building near the low end of the load range. The criticisms addressed by the ASHRAE Forum on VAV, namely "stuffiness", "stickiness", "lack of ventilation", "lack of air motion", and "too cold!" are all consequences of the impossibility of achieving the required level of dehumidification when the whole coil is operating (as conventionally) without overcooling and/or reducing airflow to levels which are inadequate to ensure good air movement and adequate ventilation, especially in the low load zones (Gupta *et al* 1987).

The range of sensible loads between peak and the minimum range is subdivided into a number of stages. The choice of the number of stages to maintain comfort conditions is an iterative process.

If for example three stages are to be used, the sensible load range may be found to divide into stages from 100 to 78%, 82 to 58%, and below 62%, where the overlaps ensure stable operation in the region of a changeover between stages.

The dehumidification performance of the peak load coil may then be computed when the coolant is throttled to satisfy 80% of the peak sensible load, and the resulting room condition determined. If this is within the comfort zone, the combination of coolant velocity and proportion of active coil which will maximize dehumidification within the normal constraints of flow rate and pressure drop at 80% of sensible load is selected.

This second-stage selection is checked when the coolant is throttled to satisfy only 60% of the peak sensible load. If either of the intermediate selections gives unacceptable conditions, additional

stages may be introduced or alternative peak and minimum part-load strategies may be investigated.

Water velocity can be augmented without increasing water quantity by appropriate circuiting. The process of chosing circuiting involves a trade-off between water velocity, water quantity, water pressure drop and dehumidification capacity.

The design process is greatly simplified by use of a personal computer. The "AU COIL SELECTION PROGRAM", discussed in Chapters 6 and 8 enables a number of strategies to be investigated in a short time.

10.6 Piping and Valving Logic Diagram

Once coil proportioning is complete, the means of implementing it must be defined. The first step is to prepare a piping and valving logic diagram to achieve the required switching of coil areas between active and inactive. Only one modulating valve is required. All other valves are of the on/off (open/shut) variety. Some may be simple two-port valves, while multiport valves may be more appropriate in other situations. These valves do not need to seal tightly and inexpensive shoe or butterfly valves are adequate.

Having developed the logic circuit, the number of manifolds required to service the tubes in each coil row is determined. Where one or more complete rows of the coil can be switched as a block between active and inactive states, only one supply and one return manifold are required for that block. However, where only a fraction of a row is to be switched, two supply and two return manifolds may be required. Frequently a return manifold from one row or part row can serve also as the supply manifold for another row or part row. It is important to distribute the active tubes within a row evenly over the face of that row. This requires that the tubes associated with different parts of the row must be interwoven to minimize the adverse effects of bypass. For this same reason it is good practice to configure the coil so that all tubes in the last row are always active. Examples of detailed piping and valving logic diagrams are presented in Chapter 11 as part of the discussions of case studies of LFV/HCV designs.

Chapter 11
CASE STUDIES

11. Case studies

The LFV/HCV design methodology has been applied to the selection of dehumidifiers for buildings in several different climatic regions around Australia. These are presented in the form of case studies in which the LFV/HCV designs are compared with conventional designs. An economic appraisal for one of the case studies is presented to show that the good psychrometric performance of the LFV/HCV system is well within the normal investment guidelines of most clients.

11.1 Perth Building : A Comparison of Conventional with LFV/HCV Design

A VAV system design is considered for a fifty storey building in Perth, Western Australia. It is important to note that the heat generated by the fan motor can form part of the cooling load and can affect the selection and performance of the dehumidifier. Hence three different cases of the VAV system design are discussed :

CASE 1 : The fan and its motor are located downstream of the dehumidifier in which case the heat generated has to be considered as reheat, so requiring an initial overcooling of the air and hence affecting the total cooling capacity of the dehumidifier.

CASE 2 : The fan motor is placed upstream from the dehumidifier in the return air path, for example in the plant room plenum, and thus constitute an additional sensible load on the dehumidifier.

CASE 3 : The fan and its motor are located in a naturally ventilated space in the plant room and is thus isolated from the conditioned air flow path. Hence there is no additional cooling demand on the dehumidifier due to the heat dissipation from the fan.

Perth has a climate ranging from very warm to mild. It is not normally considered to be very humid but examination of the simultaneous dbt/wbt incidence chart, Fig 9.12 of Chapter 9 indicates that the humidity ratio tends to increase as the dbt decreases. This is indicated by the design locus for which the 10% criterion has been adopted for this present example.

* - Water velocity through 2-Row coil with 1/3 circuiting. # - Water velocity through two 1-Row coils with 1/2 circuiting.		CONV : 4Rows, 12FPI, 1/2 Cir			LFV/HCV : 2Rows, 6FPI, 1/3Cir and two 1-Row, 6FPI, 1/2Cir				
		STG 1	STG 2	STG 3	STAGE 1		STAGE 2		STG 3
					TOP	BOT	TOP	BOT	TOP
1.	Total air flow (lps)	5750	3852	2300	5750	3852	3852	2300	2300
2.	Fresh air intake (lps)	520	520	520	520	520	520	520	520
3.	Standard face velocity (m/s)	2.5	1.68	1.0	1.20	0.80	0.80	0.48	0.48
4.	Air pressure drop (Pa)	188	106	48	38	20	20	8	8
5.	Outside design DBT (°C)	36	29	25	36	29	29	25	25
6.	Outside design WBT (°C)	24	22	21	24	22	22	21	21
7.	Return air DBT (°C)	25	25	25	25	25	25	25	25
8.	Room design DBT (°C)	24	24	24	24	24	24	24	24
9.	Room relative humidity (%)	49	58	62	48	58	56	63	59
10.	Room moisture content (g/kg)	9.3	10.8	11.6	9	10.8	10.4	11.5	11
11.	Room ΔT	10.6	10.6	10.6	10.6	10.6	10.6	10.6	10.6
12.	Room sensible heat ratio	0.87	0.67	0.6	0.87	0.67	0.67	0.60	0.60
13.	Chilled water temperature (°C)	7	7	7	7	7	7	7	7
14.	Water temperature rise	6.8	7.5	8.8	6.8	8.4	4.7	7.5	3
15.	Chilled water flow (lps)	4.32	3	1.68	4*	2.55*	4.5*	1.95*	4.7*
					4#	2.55#	4.5#	1.95#	- -
16.	Water velocity (m/s)	1.55	1.07	0.60	1.43*	0.91*	1.61*	0.70*	1.7*
					0.95#	0.61#	1.07#	0.47#	- -
17.	Water pressure drop (kPa)	36	18	6	41.5	19.7	45	11	41.5
18.	Air-on DBT (°C)	26.1	25.6	25	26.0	25.8	25.7	25	25
19.	Air-on WBT (°C)	18.2	19.1	19.6	17.8	19.3	18.8	19.6	19.1
20.	Air-on DPT (°C)	13.9	15.8	16.9	13.2	15.8	15.3	17.0	16.2
21.	Air-off DBT (°C)	12.0	12.0	12.0	12.5	12.5	12.5	12.5	12.5
22.	Air-off WBT (°C)	11.8	11.9	11.9	11.8	12.2	11.9	12.1	11.7
23.	Air-off DPT (°C)	11.8	11.9	11.9	11.3	12.0	11.4	11.9	11.1
24.	Supply air DBT (°C)	13.4	13.4	13.4	13.4	13.4	13.4	13.4	13.4
25.	Supply air DPT (°C)	11.8	11.9	11.9	11.3	12.0	11.4	11.9	11.1
26.	Total refrigerating capacity (kW)	122	94.4	60.8	113.4	89.6	89	57.9	58
27.	Room total load (kW)	86.3	74.7	49.7	86	74.8	74.8	49.83	49.84
28.	Room sensible load (kW)	75	50.2	30	75	50.2	50.2	30	30

Table 11.1a : A summary of conventional and LFV/HCV coil selections for the Perth case study - CASE 1.

11.1.1 CASE 1 - Fan and Motor Downstream of Dehumidifier

The conventional and LFV/HCV coil selections are summarised in Table 11.1a. The "AU COIL SELECTION PROGRAM" has been used to select the LFV/HCV coil, while a standard commercial coil selection program based on ARI Standard 410 has been used to select the conventional coil. The room and the supply air dry bulb temperatures are maintained at 24°C and 13.4°C respectively. In the case of the conventional design the air has to be cooled to a dry bulb temperature of 12°C whereas in the case of the LFV/HCV design the air has to be cooled to only 12.5°C. The lower reheat from the fan in the case of the LFV/HCV design arises from the lower power fan motor which is required because of the lower air pressure drop through the dehumidifier, the casing and the filter.

The conventional coil selection for a face velocity of 2.5 m/s is a 4-row coil with 12 fins per inch and half circuiting. The frontal dimensions of the coil are 1220 mm (32 tubes) high x 1885 mm long. The air pressure drop through the coil at peak is 188 Pa. As the sensible load reduces, the dry bulb temperature of the air leaving the coil is held constant by the control action reducing both the air volume and the coil sensible cooling capacity, the latter by throttling the chilled water flow. Again it is noted that there is no imposed control on the moisture content of the air. As discussed in Chapter 9, it is seen that with reducing loads the "moisture staircase" climbs upward. Table 11.1a indicates that as the water velocity (line 16) is decreased by throttling to balance the sensible load, the water temperature rise through the coil (line 14) increases, the dew point temperature of the air on to the coil (line 20) increases, and the moisture content of the room air (line 10) increases. However it is not until the room sensible load reduces to 41% of the peak value that the room moisture content (11.6 g/kg) approaches the upper limit of the ASHRAE comfort chart (Fig 12.1, Chapter 12). This is because the heat input from the fan motor energy is a source of reheat for the overcooled air. The penalty associated with this apparently desirable result is that the total refrigerating capacity of the dehumidifier in the conventional selection (line 26) is 122 kW compared with 113.4 kW in the LFV/HCV selection. Thus there is an additional 7% energy consumption in the conventional design.

The LFV/HCV coil selection consists of two rows with six fins per inch, 1/3 circuiting and two 1-row coils with six fins per inch, and 1/2 circuiting. The frontal dimensions of the coil are 1830 mm (48 tubes) high x 1885 mm long. The peak face velocity is 1.20 m/s and the air pressure drop through the coil at peak is 38 Pa. The two different circuiting arrangements enable the water consumption and the water pressure drop through the coil to be held within acceptable limits. The combination of a low face velocity, a high coolant velocity and a reducing size of active dehumidifier maintains a low interface temperature at part loads, thus promoting better dehumidification. The LFV/HCV coil selection in Table 11.1a shows that the room moisture content

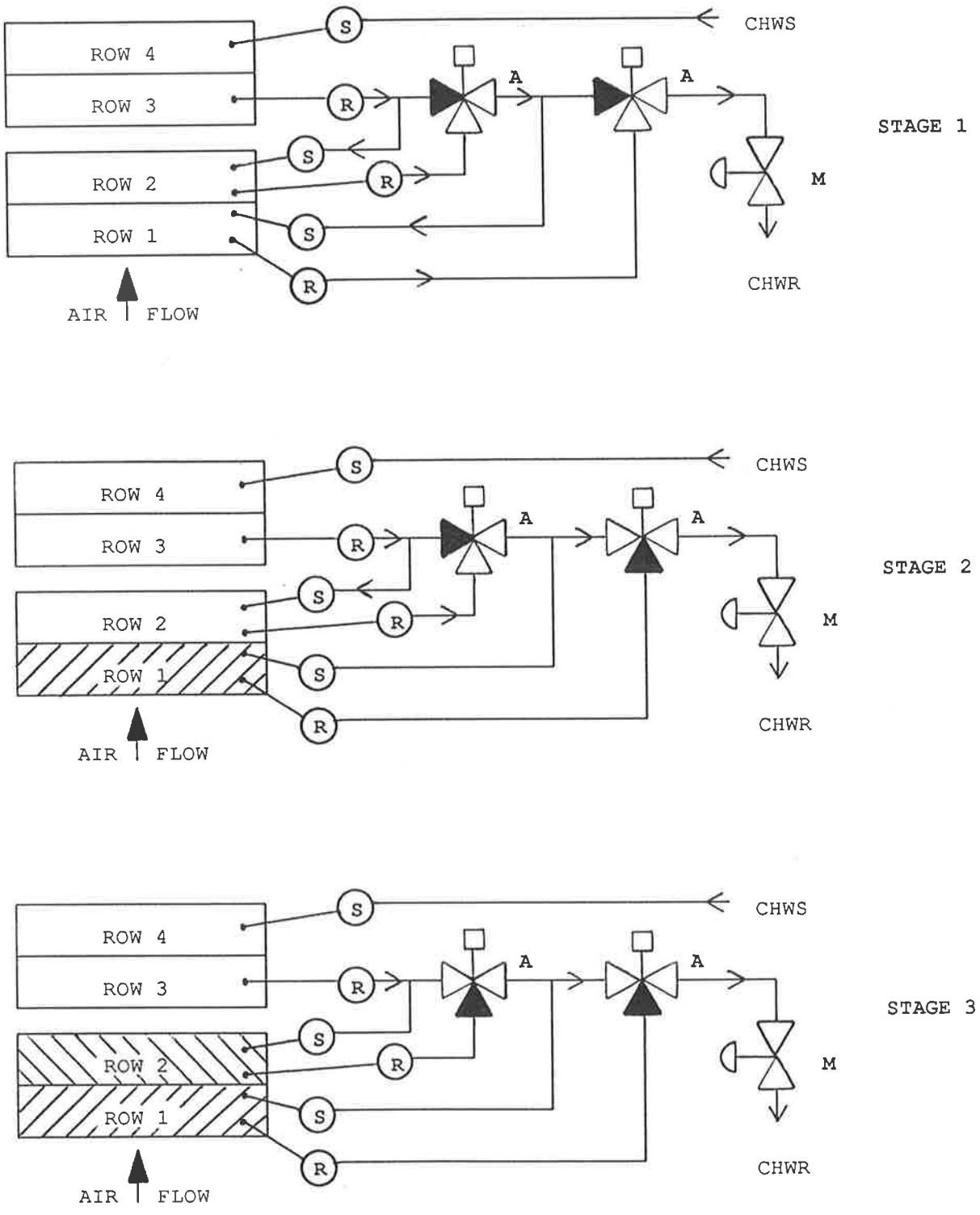

Row 1, 2	:	Two 1-Row, 6FPI, 1/2 Circuiting	M	:	Modulating Valve
Rows 3, 4	:	2-Row, 6FPI, 1/3 Circuiting	A	:	3 Port - 2 Way Valve
CHWS	:	Chilled Water Supply	S	:	Supply Manifold
CHWR	:	Chilled Water Return	R	:	Return Manifold

Fig 11.1a : Sequence of operation of the LFV/HCV coil for the Perth case study - CASE 1.

in stage 3 (41% of peak room sensible load, line 10) is safely below the top of the ASHRAE comfort range and that the room humidity at all other stages is much lower than with a conventional coil.

The results for the LFV/HCV coil are summarised in Table 11.1a and the sequence of operation is explained by the schematic in Fig 11.1a. The coil arrangement consists of a supply and a return manifold to the 2-row coil (rows 3 and 4) with 1/3 circuiting, and a set of supply and return manifolds to each of the 1-row coils (row 1 and row 2) with half circuiting. The flow of chilled water is through the 2-row coil with 1/3 circuiting, followed by row 2 and then row 1. The 3-port/2-way valves enable the chilled water flow through the 2-row coil and the two 1-row coils to be manipulated. In stage 1, all the four rows are active, thus providing the maximum total refrigerating capacity. The modulating valve throttles the water flow in stage 1. It is seen from Fig 11.1a that in stage 2, row 1 is inactive. This coil changeover occurs at a sensible part load of about 67%, and the reduction in effective coil size is accompanied by an increased water flow. The modulating valve then throttles the water flow as the load continues to fall, until the changeover to stage 3 occurs at a sensible part load of about 41%. In stage 3, both the one row coils (rows 1 and 2) are inactive, while the 2-row coil remains active and carries the maximum water flow, giving a high water velocity and low interface temperature. As discussed in Chapter 10, overlaps are provided between stages to ensure stable operation in the region of coil changeover. This is represented as "BOTTOM" in each of the stages 1 and 2 in Table 11.1a. The "TOP" of each stage represents the beginning of that particular stage with the highest water velocity through the coil.

11.1.2 CASE 2- Fan and Motor Upstream of Dehumididier

The conventional and LFV/HCV coil selections are summarised in Table 11.1b. As stated earlier, the fan motor is placed upstream from the dehumidifier and hence the heat generated consitutes an additional sensible load on the dehumidifier. In this case the air-off temperature from the dehumidifier is the supply air temperature.

The conventional coil selection for a face velocity of 2.5 m/s is a 4-row coil with 9 fins per inch and half circuiting. The frontal dimensions of the coil are 1220 mm (32 tubes) high x 1885 mm long. The air pressure drop through the coil at peak is 152 Pa. The control mechanism is the same as described in the previous section and it is seen that the room moisture content at 55% of the peak room sensible load (12.3 g/kg) is out of the range of the ASHRAE comfort chart, indicating that a further reduction in sensible load, unless accompanied by a reduction in latent load, will lead to unacceptably sticky conditions in the room. It is seen that the total refrigerating capacity of the dehumidifier in the conventional selection (line 24) is 117.2 kW compared with 112.8 kW in the LFV/HCV selection.

* - Water velocity through 2-Row coil with 1/3 circuiting. # - Water velocity through 1-Row coil with 1/2 circuiting.		CONV : 4Rows, 9FPI, 1/2Cir			LFV/HCV : 2Rows, 6FPI, 1/3Cir and 1Row, 6FPI, 1/2Cir				
		STG 1	STG 2	STG 3	STAGE 1		STAGE 2		STG 3
					TOP	BOT	TOP	BOT	TOP
1.	Total air flow (lps)	5750	4485	3163	5750	4485	4485	3163	3163
2.	Fresh air intake (lps)	520	520	520	520	520	520	520	520
3.	Standard face velocity (m/s)	2.5	1.95	1.37	0.95	0.74	0.74	0.53	0.53
4.	Air pressure drop (Pa)	152	106	62	20	15	15	7	7
5.	Outside design DBT (°C)	36	31	25	36	31	31	25	25
6.	Outside design WBT (°C)	24	22.5	21	24	22.5	22.5	21	21
7.	Return air DBT (°C)	25	25	25	25	25	25	25	25
8.	Room design DBT (°C)	24	24	24	24	24	24	24	24
9.	Room relative humidity (%)	52	60	65	48	59	57	63	61
10.	Room moisture content (g/kg)	9.6	11.3	12.3	9	11	10.7	11.8	11.4
11.	Room ΔT	10.6	10.6	10.6	10.6	10.6	10.6	10.6	10.6
12.	Room sensible heat ratio	0.88	0.68	0.60	0.88	0.68	0.68	0.60	0.60
13.	Chilled water temperature (°C)	7	7	7	7	7	7	7	7
14.	Water temperature rise	6.7	7	8.2	5.7	6.7	5.3	7.3	3.9
15.	Chilled water flow (lps)	4.2	3.6	2.4	4.8*	3.7*	4.7*	2.6*	4.8*
					4.8#	3.7#	4.7#	2.6#	- -
16.	Water velocity (m/s)	1.5	1.3	0.86	1.53*	1.18*	1.50*	0.83*	1.53*
					1.02#	0.78#	1.42#	0.78#	- -
17.	Water pressure drop (kPa)	34	25.6	12	43	27	46	17	37
18.	Air-on DBT (°C)	27.3	27	26	26.9	26.6	26.6	25.7	25.8
19.	Air-on WBT (°C)	18.8	19.8	20.5	18.3	19.6	19.4	20	19.7
20.	Air-on DPT (°C)	14.3	16.3	18	13.2	16	15.6	17.3	16.7
21.	Air-off DBT (°C)	13.4	13.4	13.4	13.4	13.4	13.4	13.4	13.4
22.	Air-off WBT (°C)	12.8	13.1	13.2	12.2	12.7	12.5	12.8	12.5
23.	Air-off DPT (°C)	12.5	13.0	13.1	11.4	12.3	11.9	12.4	11.9
24.	Total refrigerating capacity (kW)	117.2	106	82.4	112.8	103.5	103.6	78.9	78.5
25.	Room total load (kW)	85.7	85.7	69.1	86	86	86	68.3	68.2
26.	Room sensible load (kW)	75	58.5	41.2	75	58.8	58.5	41.2	41.2

Table 11.1b : A summary of conventional and LFV/HCV coil selections for the Perth case study - CASE 2.

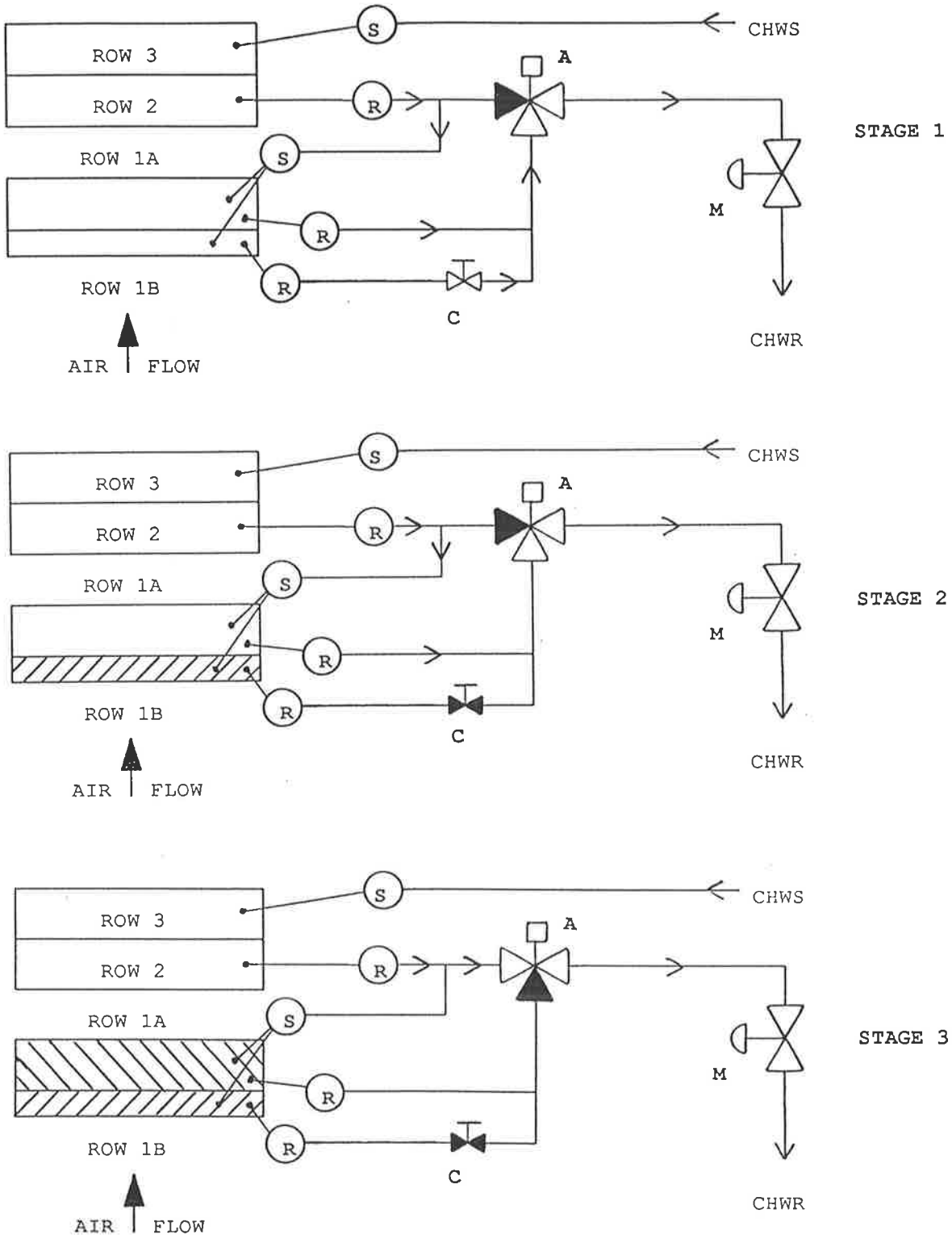

Row 1	:	1-Row, 6FPI, 1/2 Circuiting			
Rows 2, 3	:	2-Row, 6FPI, 1/3 Circuiting	S	:	Supply Manifold
A	:	3 Port - 2 Way Valve	R	:	Return Manifold
M	:	Modulating Valve	CHWS	:	Chilled Water Supply
C	:	ON/OFF Valve	CHWR	:	Chilled Water Return

Fig 11.1b : Sequence of operation of the LFV/HCV coil for the Perth case study - CASE 2 and CASE 3.

The LFV/HCV coil selection consists of two rows with six fins per inch, 1/3 circuiting and 1-row with six fins per inch, 1/2 circuiting. The frontal dimensions of the coil are 2057 mm (54 tubes) high x 2940 mm long. The peak face velocity is 0.95 m/s and the air pressure drop through the coil at peak is 20 Pa. The two different circuiting arrangements enable the water consumption and the water pressure drop through the coil to be held within acceptable limits. As discussed earlier, the combination of a low face velocity, a high coolant velocity and a reducing size of active dehumidifier maintains a low interface temperature at part loads, thus promoting better dehumidification. The LFV/HCV coil selection in Table 11.1b shows that the room moisture content in stage 3 (55% of peak room sensible load, line 10) is safely below the top of the ASHRAE comfort range and that the room humidity at all other stages is much lower than with a conventional coil.

The results for the LFV/HCV coil are summarised in Table 11.1b and the sequence of operation is explained by the schematic in Fig 11.1b. An interwoven circuiting is chosen for the 1-row coil resulting in two unequal portions of the coil - ROW 1A consisting of 38 active tubes and ROW 1B consisting of 16 active tubes. In stage 1, the 2-row coil and both portions of the 1-row coil are active, thus providing the maximum total refrigerating capacity. The flow of chilled water is through the 2-row coil, followed by the 1-row coil. The 3-port/2-way valve and the on/off valve enable the chilled water flow through the 1- and the 2-row coils to be manipulated. The modulating valve throttles the water flow in stage 1. It is seen from Fig 11.1b that in stage 2, the smaller portion of the 1-row coil, ROW 1B is inactive. This coil changeover occurs at a sensible part load of about 78%, and the reduction in effective coil size is accompanied by an increased water flow. The modulating valve then throttles the water flow as the load continues to fall, until the changeover to stage 3 occurs at a sensible part load of about 55%. In stage 3, both portions of the 1-row coil are inactive, while the 2-row coil remains active and carries close to the peak water flow, giving a high water velocity and low interface temperature.

11.1.3 CASE 3 - Fan and Motor isolated from the Conditioned Space

In this case there is no additional load imposed by the fan motor on the dehumidifier and the air-off temperature from the dehumidifier is the supply air temperature. The conventional and LFV/HCV coil selections are summarised in Table 11.1c.

The resulting conventional coil selection for a face velocity of 2.5 m/s is the same as that obtained in CASE 2. However the quantity of chilled water (line 15) required at peak is 3.8 lps compared with 4.2 lps in CASE 2. The control mechanism is the same as described in the previous section and it is seen that the room moisture content at 53% of the peak room sensible load (12.4 g/kg) is out of the range of the ASHRAE comfort chart, indicating that unacceptably sticky conditions will prevail in the room.

* - Water velocity through 2-Row coil with 1/3 circuiting. # - Water velocity through 1-Row coil with 1/2 circuiting.		CONV : 4Rows, 9FPI, 1/2Cir			LFV/HCV : 2Rows, 6FPI, 1/3Cir and 1Row, 6FPI, 1/2Cir				
		STG 1	STG 2	STG 3	STAGE 1		STAGE 2		STG 3
					TOP	BOT	TOP	BOT	TOP
1.	Total air flow (lps)	5750	4427	3050	5750	4427	4427	3050	3050
2.	Fresh air intake (lps)	520	520	520	520	520	520	520	520
3.	Standard face velocity (m/s)	2.5	1.93	1.33	1.05	0.8	0.8	0.55	0.55
4.	Air pressure drop (Pa)	152	105	58	23	15	15	8	8
5.	Outside design DBT (°C)	36	31	25	36	31	31	25	25
6.	Outside design WBT (°C)	24	22.5	21	24	22.5	22.5	21	21
7.	Return air DBT (°C)	25	25	25	25	25	25	25	25
8.	Room design DBT (°C)	24	24	24	24	24	24	24	24
9.	Room relative humidity (%)	52	60	66	48	59	57	63	61
10.	Room moisture content (g/kg)	9.7	11.3	12.4	9	11	10.7	11.8	11.4
11.	Room ΔT	10.6	10.6	10.6	10.6	10.6	10.6	10.6	10.6
12.	Room sensible heat ratio	0.88	0.68	0.60	0.88	0.68	0.68	0.60	0.60
13.	Chilled water temperature (°C)	7	7	7	7	7	7	7	7
14.	Water temperature rise	6.8	7.2	8.3	5.3	6.3	4.9	6.9	3.7
15.	Chilled water flow (lps)	3.8	3.36	2.12	4.7*	3.7*	4.7*	2.5*	4.7*
					4.7#	3.7#	4.7#	2.5#	- -
16.	Water velocity (m/s)	1.36	1.2	0.76	1.50*	1.18*	1.50*	0.80*	1.50*
					1.00#	0.78#	1.50#	0.80#	- -
17.	Water pressure drop (kPa)	28.3	22.6	9.7	40	26	46	14	34.5
18.	Air-on DBT (°C)	26.1	25.9	25	26	25.8	25.8	25	25
19.	Air-on WBT (°C)	18.5	29.6	20.1	17.9	19.3	19	19.7	19.5
20.	Air-on DPT (°C)	14.3	16.5	17.9	13.2	16.1	15.6	17.2	16.8
21.	Air-off DBT (°C)	13.4	13.4	13.4	13.4	13.4	13.4	13.4	13.4
22.	Air-off WBT (°C)	12.9	13.1	13.3	12.3	12.8	12.5	12.8	12.5
23.	Air-off DPT (°C)	12.6	12.9	13.3	11.5	12.4	11.9	12.4	12.0
24.	Total refrigerating capacity (kW)	108.8	100.8	74.4	104.8	98	97	72.4	73.2
25.	Room total load (kW)	85.2	84.7	66.5	85	84.7	84.8	65.9	65.6
26.	Room sensible load (kW)	75	57.7	39.8	75	57.7	57.7	39.8	39.8

Table 11.1c : A summary of conventional and LFV/HCV coil selections for the Perth case study - CASE 3.

The LFV/HCV coil selection consists of two rows with six fins per inch, 1/3 circuiting and 1-row with six fins per inch, 1/2 circuiting. The frontal dimensions of the coil are 2057 mm (54 tubes) high x 2660 mm long. The peak face velocity is 1.05 m/s and the air pressure drop through the coil at peak is 23 Pa. Again the two different circuiting arrangements enable the water consumption and the water pressure drop through the coil to be held within acceptable limits. The LFV/HCV coil selection in Table 11.1c shows that the room moisture content in stage 3 (53% of peak room sensible load, line 10) is safely below the top of the ASHRAE comfort range and that the room humidity at all other stages is much lower than with a conventional coil.

The results for the LFV/HCV coil are summarised in Table 11.1c and the sequence of operation is explained by the schematic in Fig 11.1b. An interwoven circuiting is chosen for the 1-row coil resulting in two unequal portions of the coil - ROW 1A consisting of 36 active tubes and ROW 1B consisting of 18 active tubes. In stage 1, the 2-row coil and both portions of the 1-row coil are active, thus providing the maximum total refrigerating capacity. The flow of chilled water is through the 2-row coil, followed by the 1-row coil. The 3-port/2-way valve and the on/off valve enable the chilled water flow through the 1- and the 2-row coils to be manipulated. The modulating valve throttles the water flow in stage 1. It is seen from Fig 11.1b that in stage 2, the smaller portion of the 1-row coil, ROW 1B is inactive. This coil changeover occurs at a sensible part load of about 77%, and the reduction in effective coil size is accompanied by an increased water flow. The modulating valve then throttles the water flow as the load continues to fall, until the changeover to stage 3 occurs at a sensible part load of about 53%. In stage 3, both portions of the 1-row coil are inactive, while the 2-row coil remains active and carries close to the peak water flow, giving a high water velocity and low interface temperature.

11.2 Darwin Building : A Comparison of Conventional with LFV/HCV Design

This study considers a small air-handling unit forming an element of a basic VAV system design for a multistoried building located in Darwin, capital of the Northern Territory of Australia. Darwin has a humid climate for most of the year. The outside design conditions for peak and part loads are obtained from Fig 9.14 in accordance with the criteria discussed earlier in Chapter 9. The conventional and LFV/HCV coil selection summaries are presented in Table 11.2. The **"AU COIL SELECTION PROGRAM"** is used to select the LFV/HCV coil, while the ARI-based coil selection program is used to select the conventional coil.

The conventional coil selection for a face velocity of 2.5 m/s is a 4-row coil with 9 fins per inch (359 fins per metre) and half circuiting. The frontal dimensions of the coil are 610 mm (16 tubes) high x 1764 mm long. The air pressure drop through the coil at peak is 158 Pa. It is seen again that there is

	* - Water velocity through 2-Row coil with 1/3 circuiting. # - Water velocity through 1-Row coil with 1/4 circuiting.	CONV : 4Rows, 9FPI, 1/2Cir			LFV/HCV : 2Rows, 6FPI, 1/3Cir and 1Row, 6FPI, 1/4Cir				
		STG 1	STG 2	STG 3	STAGE 1		STAGE 2		STG 3
					TOP	BOT	TOP	BOT	TOP
1.	Total air flow (lps)	2690	2018	1345	2690	2018	2018	1345	1345
2.	Fresh air intake (lps)	251	251	251	251	251	251	251	251
3.	Standard face velocity (m/s)	2.5	1.88	1.25	1.00	0.75	0.75	0.50	0.50
4.	Air pressure drop (Pa)	158	99	54	20	12	12	4	4
5.	Outside design DBT (°C)	34.7	30	26	34.7	30	30	26	26
6.	Outside design WBT (°C)	27.8	27	25	27.8	27	27	25	25
7.	Return air DBT (°C)	24.5	24.5	24.5	24.5	24.5	24.5	24.5	24.5
8.	Room design DBT (°C)	24	24	24	24	24	24	24	24
9.	Room relative humidity (%)	54	61	68	52	59	58	63	61
10.	Room moisture content (g/kg)	10	11.4	12.6	9.7	11.0	10.8	11.7	11.4
11.	Room ΔT	10.5	10.5	10.5	10.5	10.5	10.5	10.5	10.5
12.	Room sensible heat ratio	0.83	0.67	0.60	0.80	0.67	0.67	0.60	0.60
13.	Chilled water temperature (°C)	6.5	6.5	6.5	6.5	6.5	6.5	6.5	6.5
14.	Water temperature rise	6.7	7.5	8.9	5.6	6.8	5.2	6.4	3.1
15.	Chilled water flow (lps)	2	1.62	0.96	2.4*	1.7*	2.7*	1.65*	2.7*
					2.4#	1.7#	1.3#	0.75#	- -
16.	Water velocity (m/s)	1.43	1.14	0.70	1.25*	0.90*	1.40*	0.90*	1.40*
					0.53#	1.10#	1.80#	1.10#	- -
17.	Water pressure drop (kPa)	30	19.7	7.7	39	30	45	30	25
18.	Air-on DBT (°C)	25.7	25.3	24.8	25.8	25.3	25.4	24.9	24.8
19.	Air-on WBT (°C)	19	20.2	20.7	19.0	19.9	19.8	20.3	20.1
20.	Air-on DPT (°C)	15.6	17.7	18.8	15.5	17.4	17.3	18.2	18.0
21.	Air-off DBT (°C)	13.5	13.5	13.5	13.5	13.5	13.5	13.5	13.5
22.	Air-off WBT (°C)	13	13.2	13.4	12.6	12.8	12.6	12.7	12.6
23.	Air-off DPT (°C)	12.8	13	13.2	12.0	12.5	12.0	12.1	12.0
24.	Total refrigerating capacity (kW)	56	50	36	57	48	47.4	35.4	35
25.	Room total load (kW)	42	39	31	43.7	38.5	38.5	29	29
26.	Room sensible load (kW)	34.7	26	17.4	34.7	26.0	26.0	17.4	17.4
27.	Additional power to achieve equivalent conditions (kW)	13.4	11.5	9.0	-	-	-	-	-
28.	Additional installed ref.cap. (kW)	8.3	-	-	-	-	-	-	-

Table 11.2 : A summary of conventional and LFV/HCV coil selections for the Darwin case study.

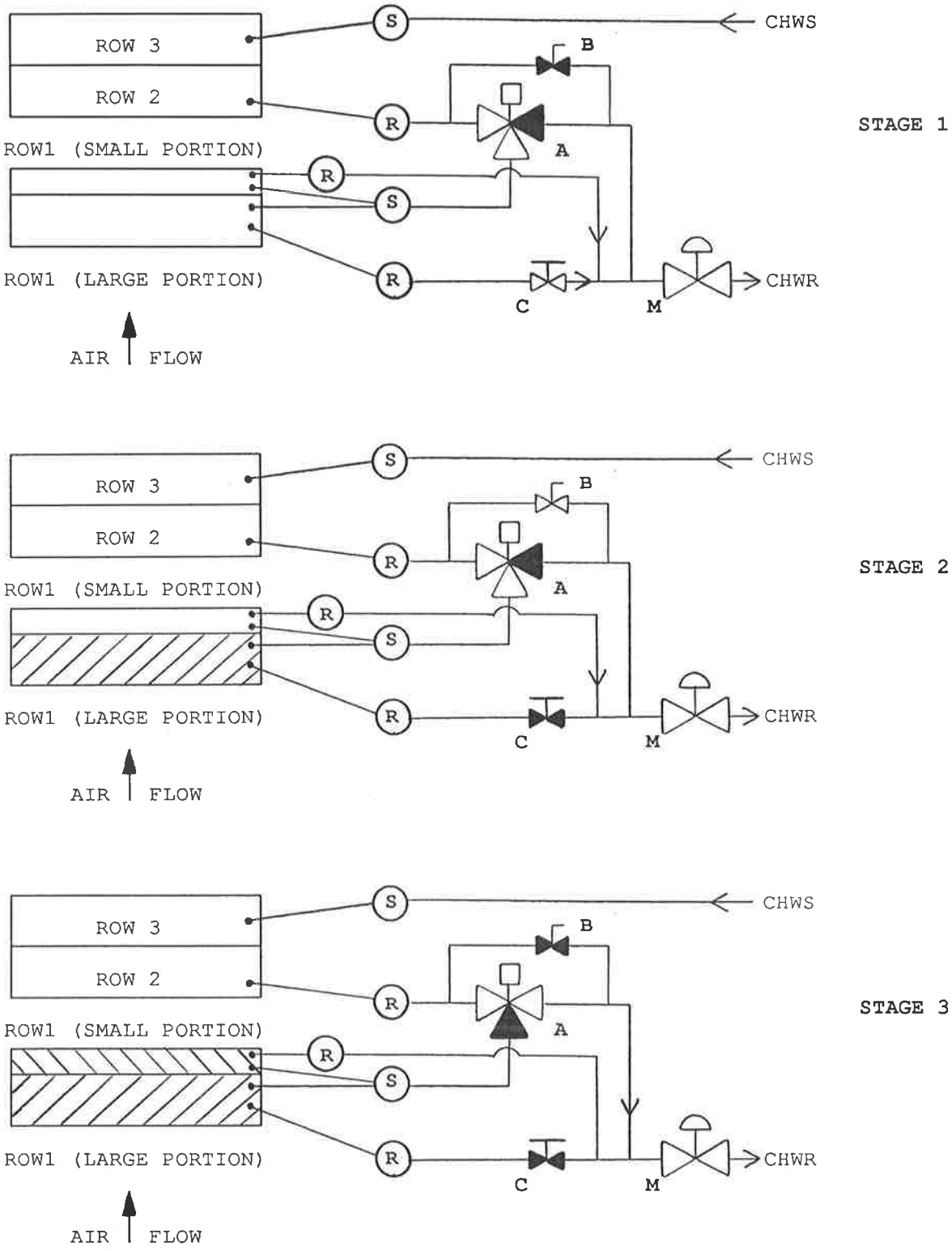

Row 1	:	1-Row, 6FPI, 1/4 Circuiting	M	:	Modulating Valve
Rows 2, 3	:	2-Row, 6FPI, 1/3 Circuiting	S	:	Supply Manifold
A	:	3 Port - 2 Way Valve	R	:	Return Manifold
B	:	By-pass Valve	CHWS	:	Chilled Water Supply
C	:	ON/OFF Valve	CHWR	:	Chilled Water Return

Fig 11.2 : Sequence of operation of the LFV/HCV coil for the Darwin case study.

no imposed control on the moisture content of the air and that the "moisture staircase" climbs upward with reducing loads. As observed in the previous case study, it is seen from Table 11.2 that as the water velocity (line 16) is decreased by throttling to balance a reducing sensible heat load, the water temperature rise through the coil (line 14) increases, the dew-point temperature of the air on to the coil (line 20) increases, and the moisture content of the room air (line 10) increases.

The LFV/HCV coil selection consists of two rows with six fins per inch, 1/3 circuiting and one row with six fins per inch, 1/4 circuiting. The frontal dimensions of the coil are 1372 mm (36 tubes) high x 2000mm long. The air pressure drop through the coil at peak is 20 Pa. The two different circuiting arrangements enable the water consumption and the water pressure drop to be held within acceptable limits. The LFV/HCV coil selection in Table 11.2 shows the room humidity ratio in stage 3 (50% of peak sensible load, line 10) to be safely below the top of the ASHRAE Comfort Range and that the room humidity at all other stages is much lower than with a conventional coil.

The sequence of operation of the LFV/HCV coil is explained by the schematic in Fig 11.2. The one-row coil is divided into two uneven portions. In stage 1, the two-row coil and both portions of the one-row coil are active, thus providing the maximum total refrigerating capacity. The flow of chilled water is through the two-row coil, followed by the one-row coil. The 3-port/2-way valve and the on/off valve enable the chilled water flow through the one- and the two-row coils to be manipulated. The modulating valve throttles the water flow in stage 1. It is seen from Fig 11.2 that in stage 2, the larger portion of the one-row coil is inactive. This coil changeover occurs at a sensible part load of about 75%, and the reduction in effective coil size is accompanied by an increased water flow. The modulating valve then throttles the water flow as the load continues to fall, until the changeover to stage 3 occurs at a sensible part load of about 50%. In stage 3, both portions of the one-row coil are inactive, while the two-row coil remains active and carries close to the peak water flow, giving a high water velocity and low interface temperature.

11.3 Melbourne Building : A Comparison of Conventional with LFV/HCV Design

A VAV system design is considered for a forty storey building in Melbourne, Australia. The outside design conditions for peak and part loads are obtained from Fig 9.13. The conventional and LFV/HCV coil selection summaries are presented in Table 11.3. As in the previous case studies, the **"AU COIL SELECTION PROGRAM"** is used to select the LFV/HCV coil and the ARI-based program is used to select the conventional coil.

The conventional coil for a face velocity of 2.5 m/s is a 4-row deep coil with 9 fins per inch (359 fins per metre) and two-third circuiting. The frontal dimensions of the coil are 608 mm (16 tubes) high x

* - Water velocity through 2-Row coil with 1/3 circuiting. # - Water velocity through 1-Row coil with 1/2 circuiting.		CONV : 4Rows, 9FPI, 2/3Cir			LFV/HCV : 2Rows, 6FPI, 1/3Cir and 1Row, 6FPI, 1/2Cir				
		STG 1	STG 2	STG 3	STAGE 1		STAGE 2		STG 3
					TOP	BOT	TOP	BOT	TOP
1.	Total air flow (lps)	4070	3052	2120	4070	3052	3052	2120	2120
2.	Fresh air intake (lps)	407	407	407	407	407	407	407	407
3.	Standard face velocity (m/s)	2.5	1.9	1.3	1.05	0.8	0.8	0.55	0.55
4.	Air pressure drop (Pa)	148	98	55	23	14	14	8	8
5.	Outside design DBT (°C)	37	31.5	26	37	31.5	31.5	26	26
6.	Outside design WBT (°C)	23	22	20.5	23	22	22	20.5	20.5
7.	Return air DBT (°C)	25	25	25	25	25	25	25	25
8.	Room design DBT (°C)	24.5	24.5	24.5	24.5	24.5	24.5	24.5	24.5
9.	Room relative humidity (%)	48	57	64	46	55	53	61	59
10.	Room moisture content (g/kg)	9.5	11	12.3	8.8	10.6	10.2	11.7	11.4
11.	Room ΔT	11.1	11.1	11.1	11.1	11.1	11.1	11.1	11.1
12.	Room sensible heat ratio	0.92	0.72	0.62	0.91	0.73	0.73	0.63	0.62
13.	Chilled water temperature (°C)	7.5	7.5	7.5	7.5	7.5	7.5	7.5	7.5
14.	Water temperature rise	6.8	6.9	8	4.4	5.5	4	6	3
15.	Chilled water flow (lps)	2.6	2.33	1.53	4.0*	2.9*	3.9*	2.0*	4.0*
					4.0#	2.9#	3.9#	2.0#	- -
16.	Water velocity (m/s)	1.4	1.25	0.82	1.64*	1.20*	1.70*	0.80*	1.64*
					1.09#	0.80#	1.60#	0.90#	- -
17.	Water pressure drop (kPa)	31	25.4	11.7	44	24.6	49	15	38
18.	Air-on DBT (°C)	26.5	26.2	25.3	26.4	26.1	26.1	25.2	25.3
19.	Air-on WBT (°C)	18.3	19.4	20	17.8	19.1	18.8	19.6	19.5
20.	Air-on DPT (°C)	14	16	17.5	12.8	15.6	15	17	16.8
21.	Air-off DBT (°C)	13.4	13.4	13.4	13.4	13.4	13.4	13.4	13.4
22.	Air-off WBT (°C)	12.9	13.1	13.3	12.2	12.7	12.4	12.8	12.6
23.	Air-off DPT (°C)	12.6	12.9	13.3	11.4	12.3	11.8	12.4	12.0
24.	Total refrigerating capacity (kW)	74.2	67.3	51	73.7	66.6	64.7	50	51.2
25.	Room total load (kW)	60.5	58.2	46.5	60.5	57.1	57.2	46	46.5
26.	Room sensible load (kW)	55.6	41.7	29	55.3	41.7	41.7	29	28.8

Table 11.3 : A summary of conventional and LFV/HCV coil selections for the Melbourne case study.

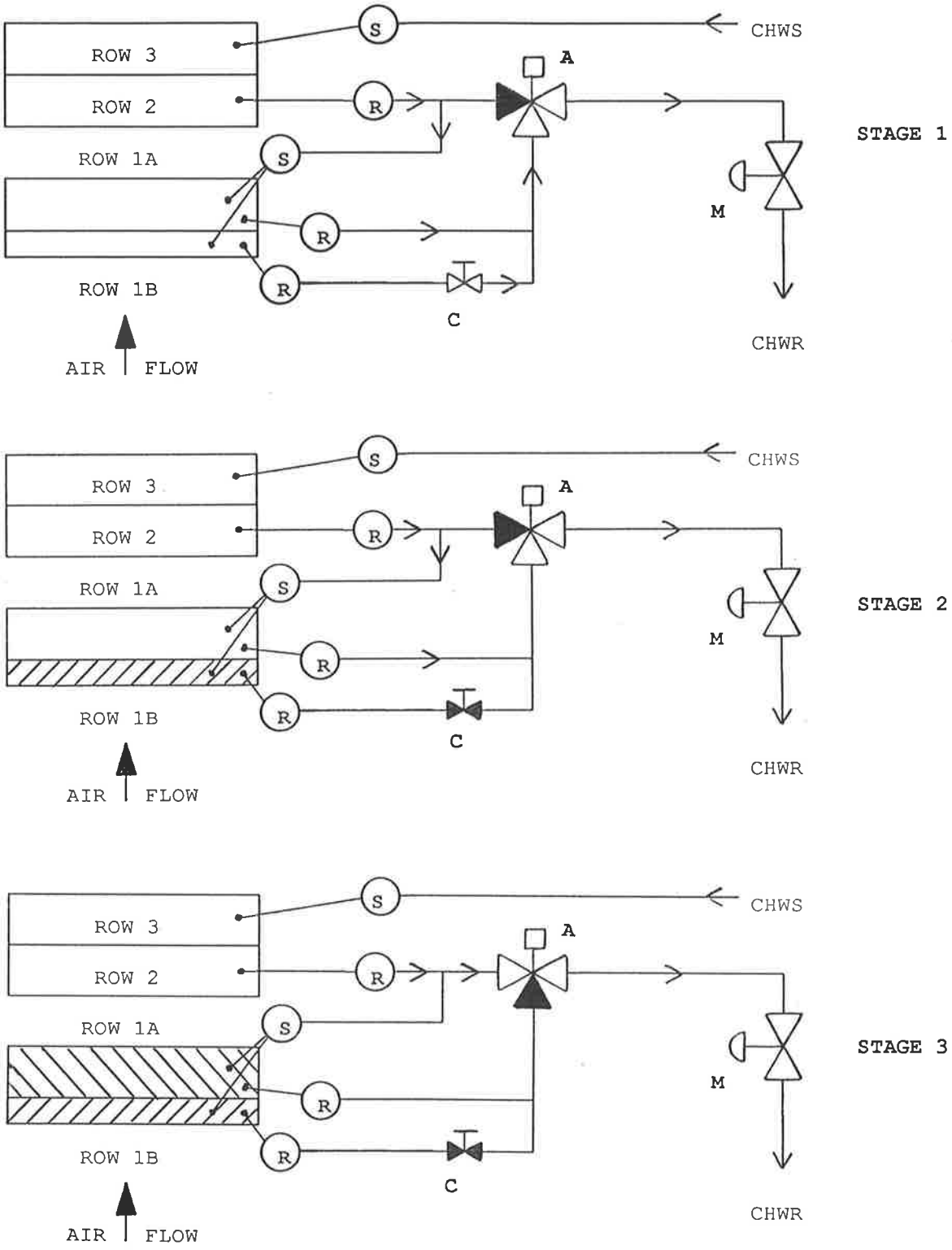

Row 1	:	1-Row, 6FPI, 1/2 Circuiting			
Rows 2, 3	:	2-Row, 6FPI, 1/3 Circuiting	S	:	Supply Manifold
A	:	3 Port - 2 Way Valve	R	:	Return Manifold
M	:	Modulating Valve	CHWS	:	Chilled Water Supply
C	:	ON/OFF Valve	CHWR	:	Chilled Water Return

Fig 11.3 : Sequence of operation of the LFV/HCV coil for the Melbourne case study.

2700 mm long. The air pressure drop through the coil at peak is 148 Pa. It is seen again that the "moisture staircase" climbs upward with reducing loads and the moisture content of the room air at 52% of peak room sensible load is 12.3 g/kg, which is above the top humidity limit of the ASHRAE comfort chart.

The LFV/HCV coil selection for a peak face velocity of 1.05 m/s consists of two rows with 6 fins per inch, one-third circuiting and one row with 6 fins per inch, half circuiting. The frontal dimensions of the coil are 1600 mm (42 tubes) high x 2420 mm long. The air pressure drop through the coil at peak is 23 Pa. The two different circuiting arrangements enable the water consumption and the water pressure drop to be held within acceptable limits. It is seen from the LFV/HCV coil selection in Table 11.3 that the room humidity ratio in stage 3 (52% of peak room sensible load, line 10) is safely below the top of the ASHRAE comfort chart and that the room humidity at all other stages is much lower than with a conventional coil.

The sequence of operation of the LFV/HCV coil is similar to that described in the previous section for the case study in Darwin and is schematically presented in Fig 11.3. An interwoven circuiting is chosen for the one-row coil resulting in two unequal portions of the coil - ROW 1A consisting of 26 active tubes and ROW 1B consisting of 16 active tubes. In stage 1, the two-row coil and both portions of the one-row coil are active, thus providing the maximum total refrigerating capacity. The flow of chilled water is through the two-row coil, followed by the one-row coil. The 3-port/2-way valve and the on/off valve enable the chilled water flow through the one- and the two-row coils to be manipulated. The modulating valve throttles the water flow in stage 1. It is seen from Fig 11.3 that in stage 2 the smaller portion of the one-row coil, ROW 1B, is inactive. This coil changeover occurs at a sensible part load of about 75%, and the reduction in effective coil size is accompanied by an increased water flow. The modulating valve then throttles the water flow as the load continues to fall until the changeover to stage 3 occurs at a sensible part load of about 52%. In stage 3, both portions of the one-row coil are inactive, while the two-row coil remains active and carries close to the peak water flow, giving a high water velocity and low interface temperature.

11.4 Economic Appraisal

Sekhar *et al.* (1989) presented an economic appraisal for the Darwin case study which is discussed here. In an earlier paper, Luxton *et al.* (1987) assessed in general terms the energy cost savings achievable with the LFV technology. They showed, *inter alia*, that the return on LFV investment for large plants is significantly greater than that on small plants. The present example is a small plant, only 2690 lps and 56 kW refrigeration capacity. Thus the economic comparison for the present case study is particularly severe.

Two comparisons are made. The first is "direct" in the sense that the poor psychrometric performance achieved by the conventional unit without the aid of reheat is accepted by the client. The second is on an equity basis, in that it includes the cost of the overcooling and reheat required by the conventional system to achieve the same psychrometric conditions in the room as those achieved by the LFV/HCV system.

A capital cost differential of $1,500 exists between the LFV/HCV air handler and the conventional unit without reheat. With reheat on the conventional system, this premium reduces to $1,400. No allowance has been made for the capital saving due to the LFV/HCV system not requiring acoustic isolation of the plant room, and no allowance has been made for the capital cost differences in the refrigeration capacity required to overcool with the conventional system.

In terms of running costs, there is a saving in fan power of 656 W averaged over the operating cycle. Against this, the average penalty in pumping power (including riser overheads) is 55 W, giving an average net power saving of 601 W and an operating cost saving (at 15 cents per kWh for electricity) of 9 cents per operating hour.

The economic evaluations for an office which operates for 3000 hours per year, and for an hotel or hospital which operates for 8760 hours per year are shown in Table 11.4. On the "direct" comparison for unequal psychrometric conditions, the application of such a small unit in an office building is a marginal investment proposition. This comparison places no premium on the quality of the environment achieved by the LFV/HCV unit. On the basis of United States figures, the total cost of losing a tenant from a building can exceed the tenant's annual rental, which would be many times the incremental cost of the LFV/HCV unit (Custer 1988). Custer quotes a survey of the Dallas rental market, which showed that about half the tenants who were relocating believed comfort conditions were important in deciding whether to stay or to leave a property, and three-quarters of all tenants believed comfort was important in choosing a new building. Against these factors the premium for the LFV/HCV system becomes trivial.

Again using the uneven basis of the "direct" comparison, there is no question of the value of investing in LFV/HCV when plant is required to operate continuously, as in humid climates. Furthermore, as the size of plant increases, so too does the economic worth of the investment. For example, for a 10,000 lps unit the capital investment recovery period is approximately half that for the small 2690 lps plant of the case study.

Turning now to the more realistic "equity" comparison, the true worth of the LFV/HCV system is apparent. Even the office application becomes a spectacular investment opportunity, a result dominated by the huge and often undeclared cost of overcooling and reheating. The use of

overcooling and terminal reheat is common practice in quality buildings, and especially in major hotels, in tropical areas. The twin penalties of overcooling and reheat are more severe than is revealed in the present example as both hotels and hospitals are required to use very much higher proportions of outside air. Payback of the LFV/HCV premium is measured in weeks or months rather than years, and the discounted present value of the operating cost savings is several times the total cost of the complete air handling unit.

	Office Application		Hotel/Hospital Application	
	Unequal Conditions No Reheat	Equal Conditions Reheat	Unequal Conditions No Reheat	Equal Conditions (Reheat)
Capital cost premium for LFV/HCV, $	1,500	1,400	1,500	1,400
Annual operating hours	3,000	3,000	8,760	8,760
Plant life, years	15	15	15	15
Discount rate, %	10	10	10	10
Net annual savings, $	270	5,873	790	6,393
Present worth factor	7.6	7.6	7.6	7.6
Present value of savings, $	2,054	44,671	6,009	48,626
Benefit/Cost ratio	1.34	31.9	4.0	34.7
Simple payback, years	5.6	0.24	1.9	0.22
Return on investment, %	11	413	46	450
Capital investment recovery, years	8.7	0.25	2.2	0.23
Internal rate of return, %	15.7	420	53	457
Assessment	Marginal	Excellent	Favourable	Excellent

(Prices in Australian Dollars)

Table 11.4 : Economic evaluation of LFV/HCV premium investment for the Darwin case study.

Chapter 12

COMFORT INTEGRATED "LFV/HCV" SYSTEMS[1]

12.1 Introduction

It has been widely accepted for a long time that the thermal comfort of a human being is a function of environmental and personal parameters. The important environmental parameters are air-temperature, radiation, humidity and air-movement, while the important personal parameters are clothing and activity. However, the combined influence of all the parameters was only quantified with the introduction of the "Comfort Equation" (Fanger, 1973). Comfort in an environment can be defined as the range of combinations of these parameters for which at least 80% of the occupants find conditions thermally acceptable. The ASHRAE comfort chart (ASHRAE Standard 55 - 1981), reproduced as Fig 12.1, is frequently assumed to provide a basis for the design of comfort air-conditioning systems. However this ASHRAE comfort chart pertains to a particular combination of parameters within the comfort equation, namely the activity level is light such as in an office building, the occupants are clothed in typical summer or winter clothing, the air temperature is equal to the mean radiant temperature and the air velocities relative to the occupants are low. Although a room condition may lie within the comfort area of the ASHRAE comfort chart, a more detailed examination indicates that conditions in the room may not be thermally comfortable. Thus it is a misconception to assume that the comfort area of the ASHRAE comfort chart is a sufficient requirement. It will be shown in this chapter that there is a much smaller band, determined by the various environmental and personal parameters described earlier, in which the prime comfort criterion is satisfied. Being multi-dimensional in nature, the comfort equation is comprehensive and complex and therefore ill suited to manual calculation. But it has been solved for a range of conditions by computer and has been plotted as a series of two-dimensional cuts through the multidimensional equation to give 28 comfort diagrams (Fanger, 1973). In each case, the comfort equation has been reduced to a two dimensional model and comfort lines have been drawn. These lines are curves through various combinations of two variables which will create comfort providing the values of the other variables are held constant. Some of these comfort diagrams are used in the present discussion to illustrate the concept of COMFORT INTEGRATED LFV/HCV SYSTEMS, but it should be noted that such systems are not constrained to the "two-dimensional" situations.

1/ The concepts described in this chapter have been formulated by Shaw and Luxton (1989). The candidate's contribution has been in the exploration of the concepts and the computation of variations in the loads and power consumption resulting from hypothetical applications.

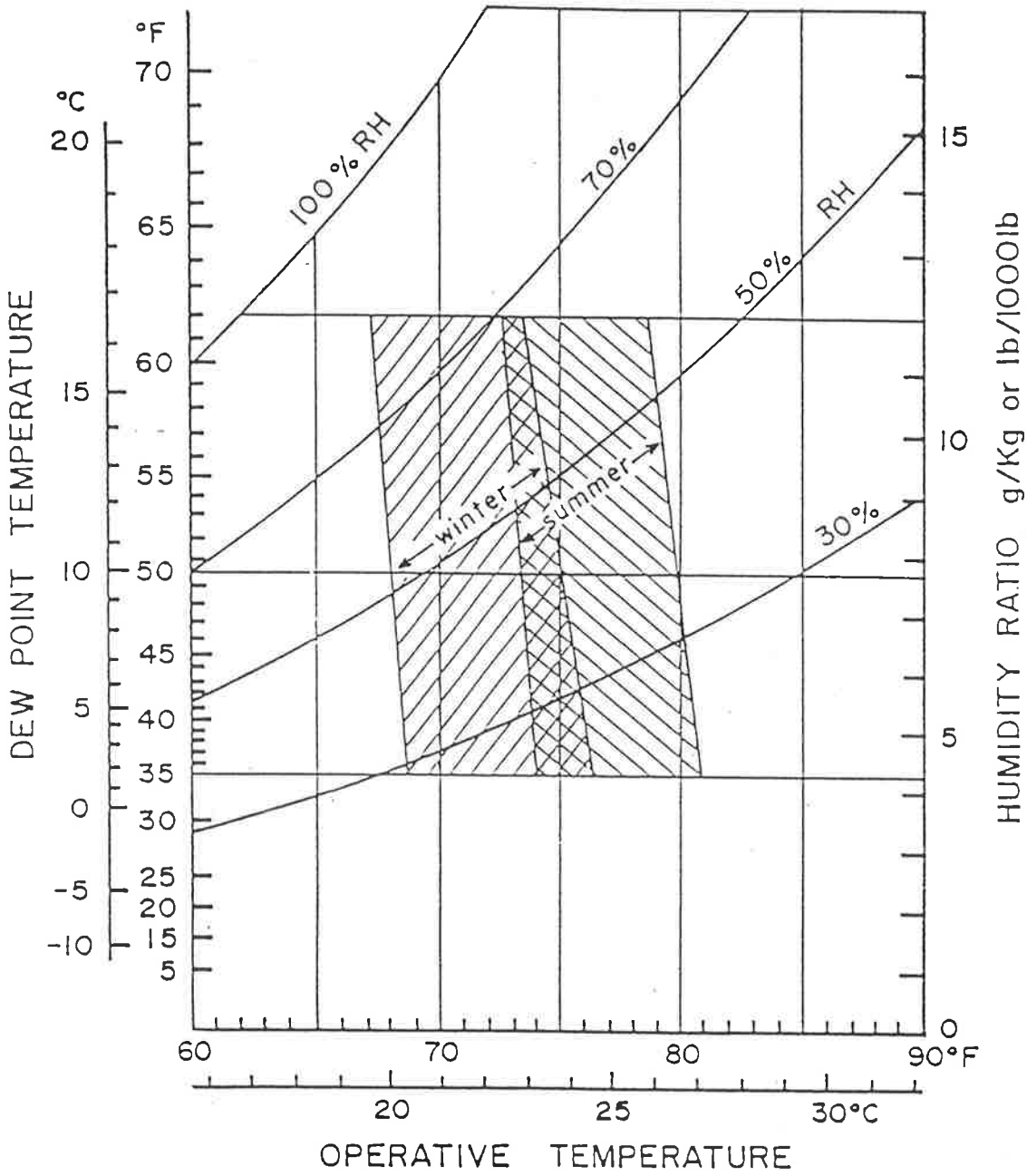

Fig 12.1 : ASHRAE comfort chart

12.2 Comfort Diagram - Air Temperature vs Wet Bulb Temperature with Relative Air Velocity as Parameter

This comfort diagram is presented in Fig 12.2 and has been reproduced from ASHRAE Fundamentals (ASHRAE 1985). The comfort lines are curves through different combinations of ambient temperature and humidity that provide optimum thermal comfort. The six charts apply to six different combinations of activity and clothing, where air temperature equals mean radiant temperature. The top two charts relate to sedentary activity such as in an office, the middle two relate to medium activity and the bottom two relate to high activity such as in a gymnasium or the stage of a theatre. The charts on the left-hand side pertain to light clothing with a clothing insulation value of about 0.5 clo, as would be worn in summer or peak load conditions, while the charts on the right-hand side pertain to medium clothing of about 1.0 clo, as would be worn in marginal weather or part load conditions. An important observation is the relative shift of the comfort lines in these charts.

It must be noted that in the preparation of the comfort charts of Fig 12.2 the dimensionality of the problem had to be reduced by assuming that the air temperature equals the mean radiant temperature. The ASHRAE chart in Fig 12.1 is in terms of the operative temperature, which for the thermal environmental range for human comfort is defined approximately as the simple average of the air and mean radiant temperatures. Thus, if the air temperature does equal the mean radiant temperature, as in an interior zone with low temperature lighting, this condition would be satisfied. Since often they will not be equal as in the perimeter zone of glass curtain wall building, the conclusions drawn from Fig 12.2 can only be regarded as qualitative. More detailed analysis based on the use of the full comfort equation suggests that these qualitative conclusions are nevertheless indicative for practical situations in which the mean radiant temperature differs from the dry bulb temperature.

12.2.1 Relative Velocity

It is apparent from all the six charts in Fig 12.2 that the relative velocity of air is an important variable which restricts the available area of optimum comfort. The ASHRAE standard on thermal comfort (ASHRAE - 55, 1981) specifies an average summer air movement in the occupied zone not exceeding 0.25 m/s and an average winter air movement in the occupied zone not exceeding 0.15 m/s. The ASHRAE comfort chart in Fig 12.1 is based on the above maximum velocities. The ASHRAE standard does not specify any minimum air movement for thermal comfort.

In normal air-conditioning practice it is unlikely that zone air temperatures higher than 26°C would be considered acceptable, although the ASHRAE standard on thermal comfort does allow the temperature to increase to 28°C if accompanied by an increase in air movement of 0.275 m/s for each degree Celsius increase in zone temperature. The increase in air movement increases the rate

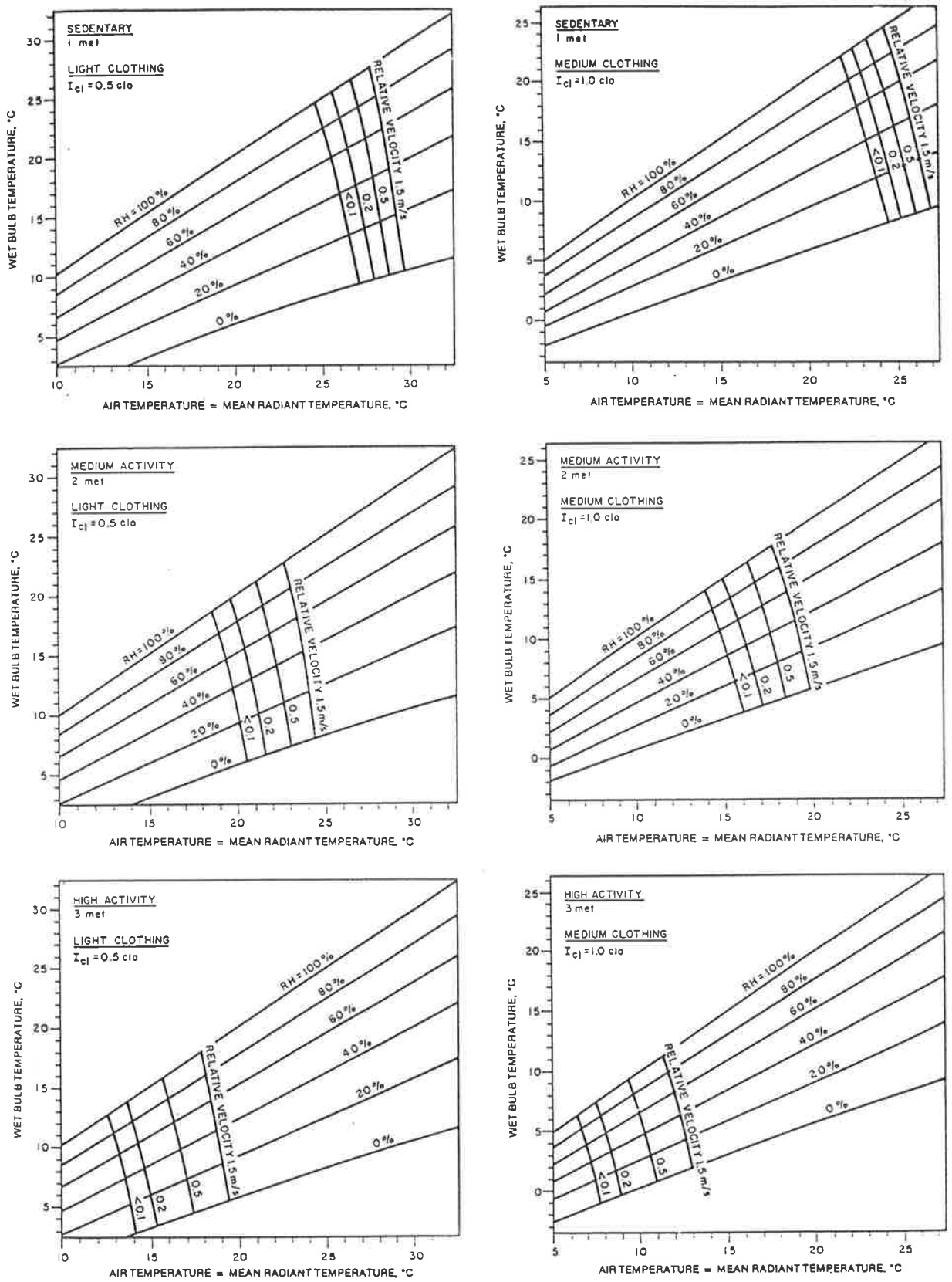

Fig 12.2 : Relative velocity comfort lines as function of attire, activity and relative humidity.

of heat transfer and transpiration from the occupants to compensate for the higher temperature of air in the room, so maintaining comfortable skin temperatures.

The specification of maximum acceptable relative velocities is to avoid draughty conditions in the occupied zone. Thus it is vital in air-conditioning system design to ensure that supply air registers and diffusers are designed to deliver air to the occupied zone in such manner that the relative velocities in the micro environments of the occupants lie within the range specified by the ASHRAE Standard (ASHRAE - 55, 1981) or its equivalent.

12.3 Comfort Evaluation

The objective of this section is to evaluate the extent to which existing air conditioning systems adhere to human comfort principles. The procedure is illustrated by reference to the performance of the actual system design developed in Chapter 11, Section 11.1 for a high-rise office building in Perth, Western Australia. The ability of the LFV/HCV system to maintain sensible temperatures and humidity ratios which are always within the bounds of comfort of the ASHRAE comfort chart has already been established in Tables 11.1a - 11.1c. The results of the LFV/HCV system of Table 11.1c are used in the present discussion of comfort evaluation. A quick review of this Table reveals the following salient features :

- The room dry bulb temperature is held constant throughout at 24°C.

- At peak load the selection provided a room condition of 24°C with 48% relative humidity (9 g/kg) and offsets the room sensible heat ratio of 0.88 for the Perth climatic design condition.

- At 77% of the room sensible load the selection provides a room condition of 24°C and 57% relative humidity (10.7 g/kg) and offsets the room sensible heat ratio of 0.68 for a Perth mild but humid part-load design condition.

A system capable of maintaining each of these room conditions would be considered good when compared with that which could be expected from the competing conventional VAV system as shown in Table 11.1c.

The top two comfort charts of Fig 12.2 in which the above room conditions are located are enlarged and presented as Fig 12.3. It has already been mentioned earlier that these two charts are applicable for an office building with mainly sedentary type activity. The left chart represents peak load conditions and the right chart represents part load conditions. It is seen from Fig 12.3 that the peak

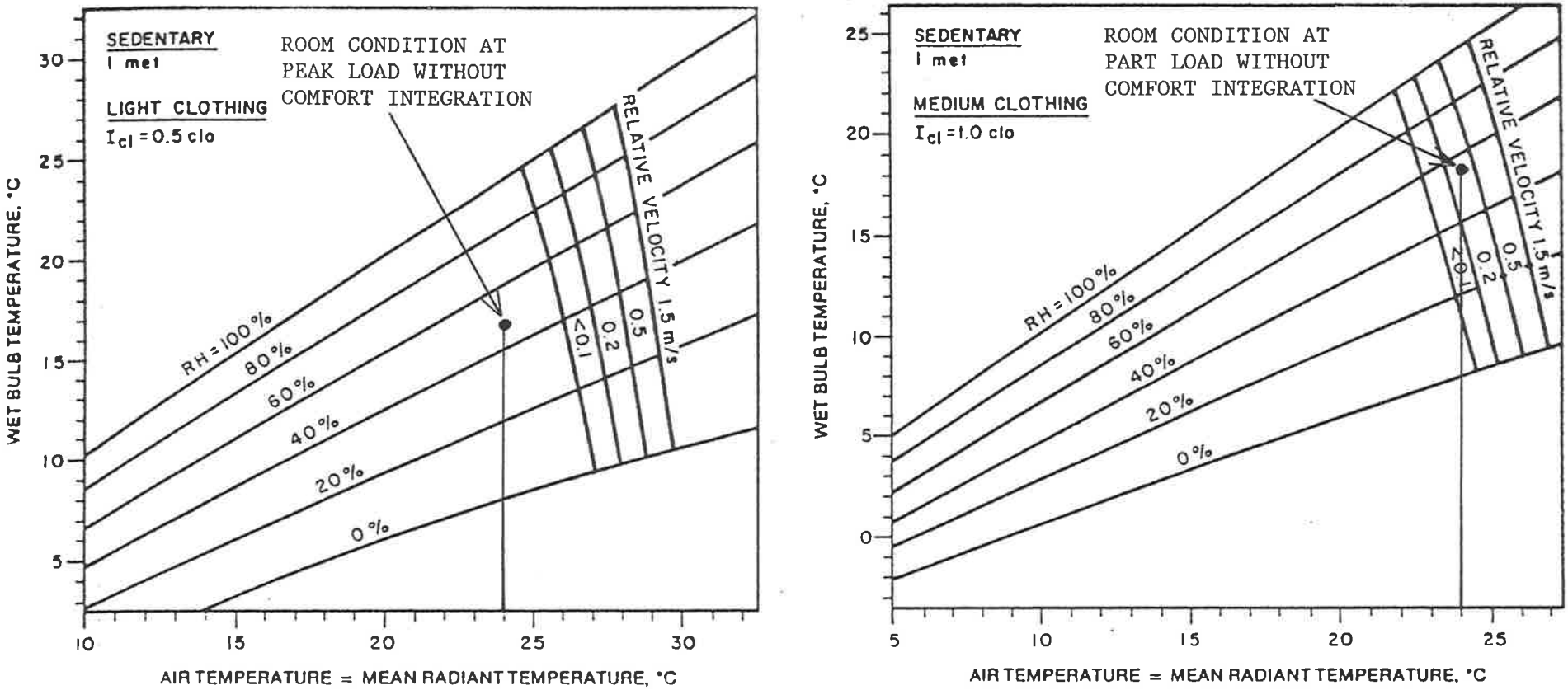

Fig 12.3 : Case study of an LFV/HCV system without comfort integration.

load room condition of 24°C and 48% relative humidity lies significantly below the "<0.1 m/s" relative velocity comfort line. Since there is no minimum air movement specified as being necessary for thermal comfort, it could be an acceptable point, provided the air distribution system can achieve this low velocity. However, it is not practical to achieve such low air movement yet also to offset the peak load and satisfy the ventilation requirement. Besides, the air movement would be further decreased during part load operation since a VAV system is employed. It may be concluded that 24°C is not a practical room dry bulb temperature for peak load operation from the point of view of thermal comfort.

It is also seen from Fig 12.3 that the room condition of 24°C, 57% relative humidity achieved during humid part load operation lies around the "0.4 m/s" relative velocity comfort line which is well above the maximum relative velocity recommended by ASHRAE. It is also incompatible with the peak load condition in that less air is supplied to the room but air motion required is several times greater. Thus at part load, although the system properly offsets the required room sensible heat ratio while maintaining a comfortable humidity ratio in the room, it fails to maintain an acceptable relative velocity. It may again be concluded that 24°C is not a practical room dry bulb temperature for humid part load operation from the point of view of thermal comfort.

The air distribution system is identical for both peak and humid part load operation, with the latter requiring only 67% of the air flow volume required by the former. Thus it would be impossible to provide the performances indicated on Fig 12.3 as being required for comfort at both peak and humid, or indeed any other part load conditions. The air required to offset part loads could not possibly be delivered in a way which results in a higher relative velocity than that at peak load through the same supply air system.

12.4 Design of LFV/HCV System with Comfort Integration

A critical examination of the left and right hand charts of Fig 12.2 reveals that the operative temperature in the conditioned space should not be constrained to a constant value, but should be allowed to vary as a function of the particular room loads of the moment and the appropriate clothing. It is evident from Fig 12.3 that the room temperature of 24°C was too low for peak load and too high for part load for comfort to be achieved in a practical design.

The same LFV/HCV system that was selected for the high-rise office building in Perth will now be considered with the inclusion of comfort integration within the control strategy. To satisfy both the air conditioning thermal design requirements and the comfort standards it is essential that the peak and part load conditions are achieved at compatible relative velocities within the ASHRAE range of <0.1 to 0.25 m/s during the entire operating season. The additional constraint imposed by relative

* - Water velocity through 2-Row coil with 1/3 circuiting. # - Water velocity through 1-Row coil with 1/2 circuiting.		WITH COMFORT INTEGRATION					WITHOUT COMFORT INTEGRATION				
		LFV/HCV : 2Rows, 6FPI, 1/3Cir and 1Row, 6FPI, 1/2Cir					LFV/HCV : 2Rows, 6FPI, 1/3Cir and 1Row, 6FPI, 1/2Cir				
		STAGE 1		STAGE 2		STG 3	STAGE 1		STAGE 2		STG 3
		TOP	BOT	TOP	BOT	TOP	TOP	BOT	TOP	BOT	TOP
1.	Total air flow (lps)	4535	4535	4535	3039	3039	5750	4427	4427	3050	3050
2.	Fresh air intake (lps)	520	520	520	520	520	520	520	520	520	520
3.	Standard face velocity (m/s)	0.90	0.90	0.90	0.60	0.60	1.05	0.8	0.8	0.55	0.55
4.	Air pressure drop (Pa)	19	19	19	9	9	23	15	15	8	8
5.	Outside design DBT (°C)	36	31	31	25	25	36	31	31	25	25
6.	Outside design WBT (°C)	24	22.5	22.5	21	21	24	22.5	22.5	21	21
7.	Return air DBT (°C)	27	24	24	23.8	23.8	25	25	25	25	25
8.	Room design DBT (°C)	26	23	23	22.8	22.8	24	24	24	24	24
9.	Room relative humidity (%)	44	60	59	66	64	48	59	57	63	61
10.	Room moisture content (g/kg)	9.2	10.7	10.4	11.6	11.1	9	11	10.7	11.8	11.4
11.	Room ΔT	12.6	9.6	9.6	9.4	9.46	10.6	10.6	10.6	10.6	10.6
12.	Room sensible heat ratio	0.88	0.68	0.68	0.60	0.60	0.88	0.68	0.68	0.60	0.60
13.	Chilled water temperature (°C)	7	7	7	7	7	7	7	7	7	7
14.	Water temperature rise	5.1	5.9	4.6	6.6	3.5	5.3	6.3	4.9	6.9	3.7
15.	Chilled water flow (lps)	4.7*	3.7*	4.7*	2.5*	4.7*	4.7*	3.7*	4.7*	2.5*	4.7*
		4.7#	3.7#	4.7#	2.5#	- -	4.7#	3.7#	4.7#	2.5#	- -
16.	Water velocity (m/s)	1.50*	1.18*	1.50*	0.80*	1.50*	1.50*	1.18*	1.50*	0.80*	1.50*
		1.00#	0.78#	1.50#	0.80#	- -	1.00#	0.78#	1.50#	0.80#	- -
17.	Water pressure drop (kPa)	37.5	24	42.5	12.5	32.2	40	26	46	14	34.5
18.	Air-on DBT (°C)	28.1	24.9	24.9	24.2	24.1	26	25.8	25.8	25	25
19.	Air-on WBT (°C)	18.8	18.8	18.6	19.4	19	17.9	19.3	19	19.7	19.5
20.	Air-on DPT (°C)	13.8	15.6	15.2	17.1	16.5	13.2	16.1	15.6	17.2	16.8
21.	Air-off DBT (°C)	13.4	13.4	13.4	13.4	13.4	13.4	13.4	13.4	13.4	13.4
22.	Air-off WBT (°C)	12.3	12.6	12.5	12.8	12.5	12.3	12.8	12.5	12.8	12.5
23.	Air-off DPT (°C)	11.5	12.3	11.9	12.5	11.9	11.5	12.4	11.9	12.4	12.0
24.	Total refrigerating capacity (kW)	100	91.2	91.3	68.6	67.9	104.8	98	97	72.4	73.2
25.	Room total load (kW)	79.9	79	78.5	58.5	57.7	85	84.7	84.8	65.9	65.6
26.	Room sensible load (kW)	70.3	53.55	53.55	35.14	35.14	75	57.7	57.7	39.8	39.8

The LFV/HCV coil selection is reproduced from Table 11.1c, Chapter 11.

Table 12.1 : "Comfort Integrated LFV/HCV System" compared with a LFV/HCV system without comfort integration for the Perth case study.

velocity results in the narrow hatched areas of the comfort charts in Fig 12.4 within which the room condition must be maintained. It is shown here that a room dry bulb temperature of 26°C at peak load and 23°C at part load are wholly consistent with comfort standards and with the LFV/HCV system selection. Both peak and part load conditions fall within the hatched areas in the left and right hand charts respectively. Thus the required peak relative velocity is higher than the part load relative velocity. The inconsistent performance achieved by requiring a fixed room temperature of 24°C, from Fig 12.3, is also indicated.

Further advantages accrue from the comfort integration, as discussed in the following paragraphs and the final comfort integrated LFV/HCV coil selection is summarised in Table 12.1. The results of the LFV/HCV coil selection without comfort integration, tabulated in Table 11.1c are also included in Table 12.1 for simplicity of comparison. The frontal dimensions of the coil are 2057 mm (54 tubes) high x 2450 mm long which is smaller than that required for the coil without comfort integration. The basic sequence of operation of this coil is similar to that discussed in Chapter 11 and is described by referring to the schematic in Fig 11.1b. The two row coil with 1/3 circuiting remains active at all times. However, an interwoven circuiting is adopted for the one row coil with half circuiting such that any of the following three options are possible for this coil :

- Stage 1 : All the 54 tubes in the height of the coil are active.
- Stage 2 : Only 36 tubes in the height of the coil are active.
- Stage 3 : The entire one row coil is inactive.

The flow of chilled water is through the 2-row coil with 1/3 circuiting [Row 3 and Row 2], followed by the 1-row coil with half circuiting [Row 1A and Row 1B]. The 3-port/2-way valve and the ON/OFF valve enable the chilled water flow through the coils to be manipulated.

The fundamental difference between the two realizations lies in the specification of the system design. It is seen from Table 12.1 that the room dry bulb temperature with comfort integration is allowed to swing from 26°C at peak load to about 22.8°C at the minimum part load conditions. It is also seen that the supply air quantity required with comfort integration is 4535 lps compared with the 5750 lps which was required in the original LFV/HCV coil selection without comfort integration. The reduced supply air quantity results from the increased temperature difference across the room and a reduction in heat transmission to the room due to the smaller temperature difference between ambient and indoor conditions. It is seen from Table 12.1 that the Room ΔT rises from 10.6 to 12.6 which is accompanied by a reduction in the supply air quantity from 5750 lps to (10.6/12.6)x5750 = 4837 lps. Conservatively the transmission load accounts for 25% of the cooling load and the transmission temperature difference due to the higher 26°C room temperature is

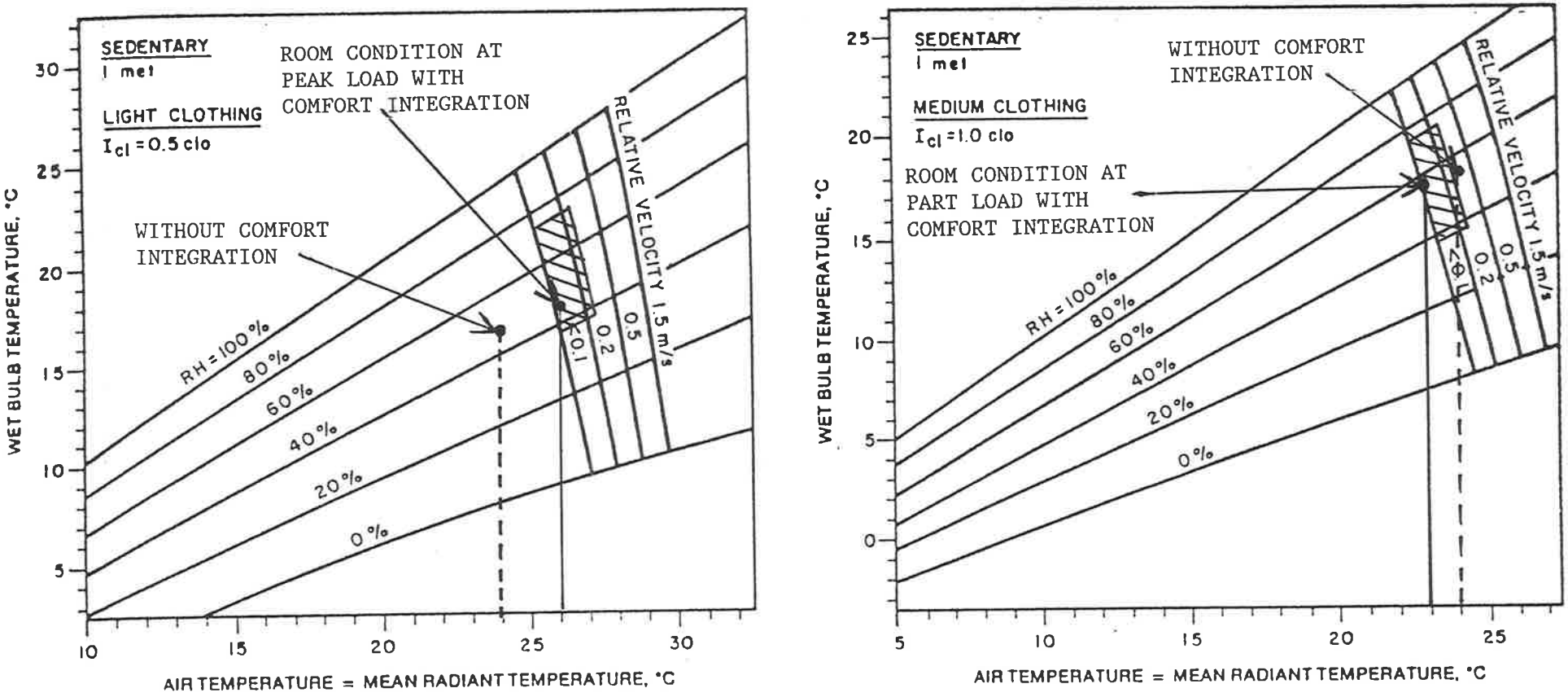

Result from Fig 12.3 is included for comparison.
Target velocity/humidity according to ASHRAE Standard 55 - 1981 is shown cross-hatched.

Fig 12.4 : Case study of an LFV/HCV system with comfort integration.

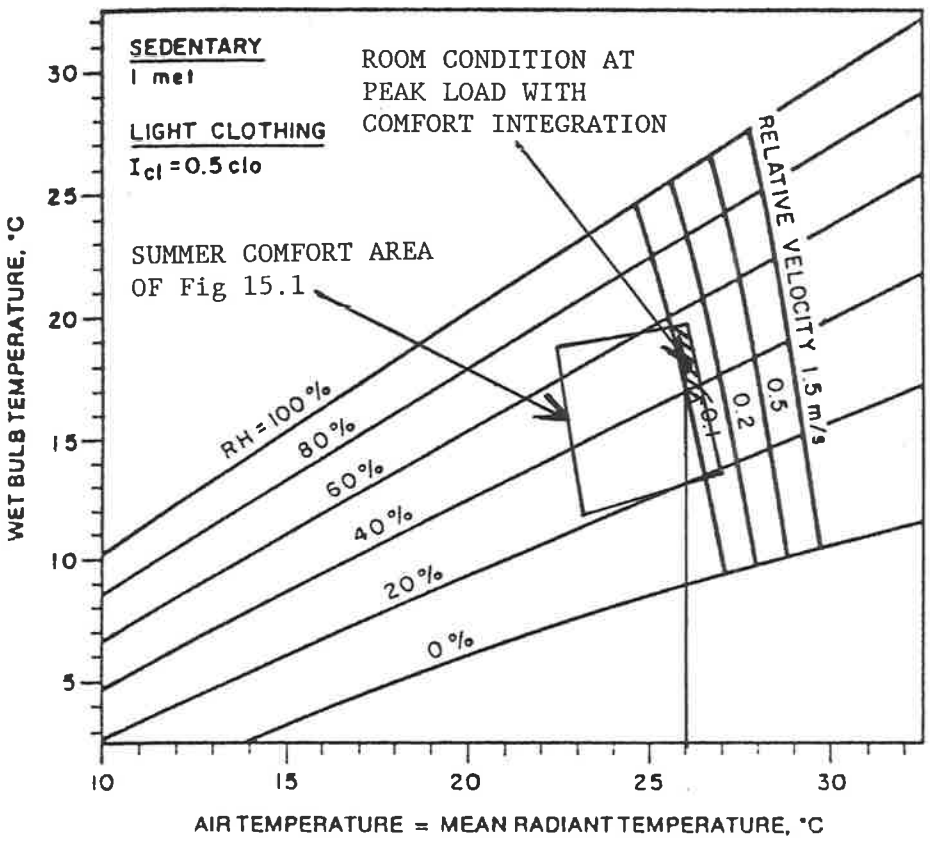

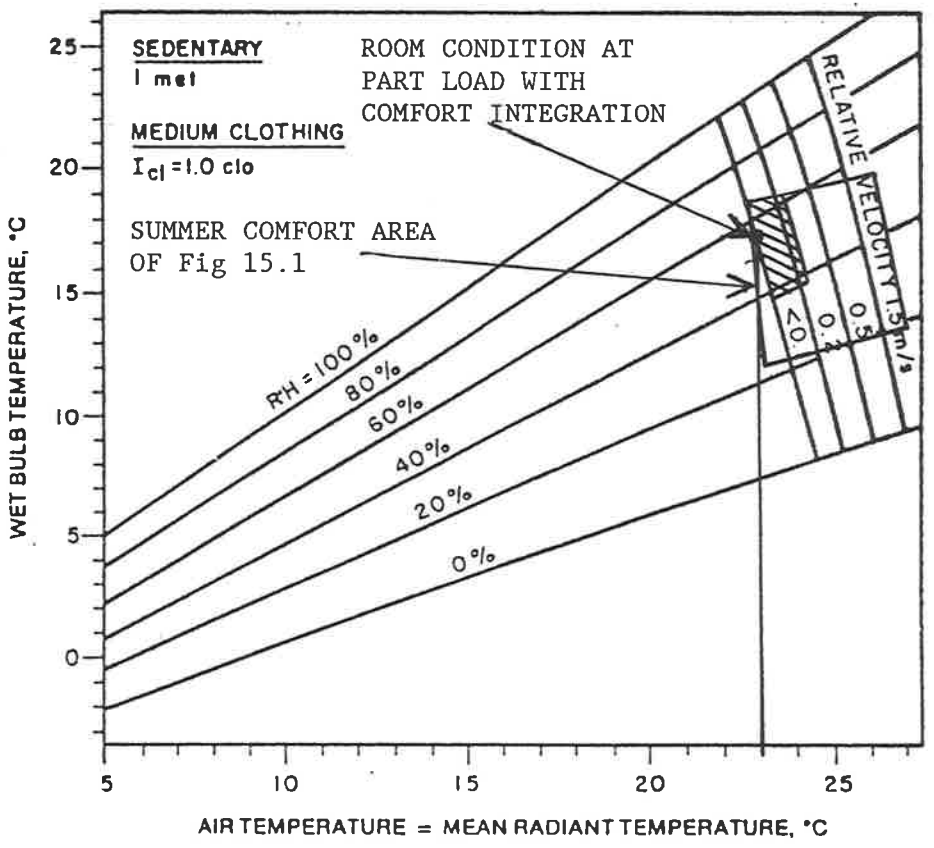

Fig 12.5 : The case study LFV/HCV system with comfort integration shown in relation to both comfort area of ASHRAE comfort chart (Fig 12.1) and relative velocity comfort diagram (Fig 12.2). Common target regions are cross-hatched.

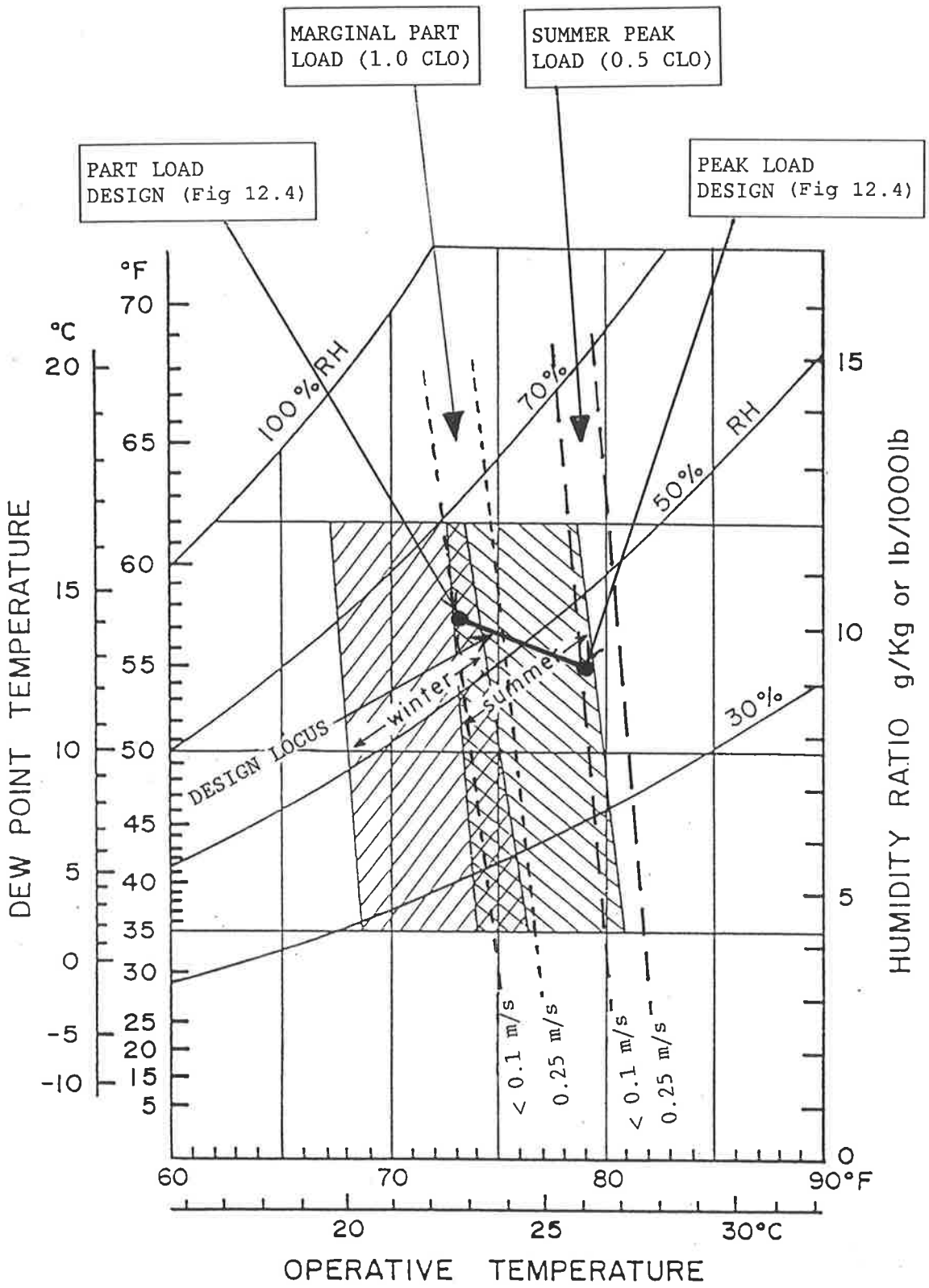

Fig 12.6 : Movement of required range of relative velocities with load and change of clothing weight as seasons change from peak to part load.

reduced by 25%. Thus, (0.25x0.25) or 6.25% of the sensible load is eliminated. Therefore at peak load the air volume flow can be further reduced to (1 - 0.0625)x4837 = 4535lps.

The large summer comfort area of the ASHRAE comfort chart in Fig 12.1 is mapped on to Fig 12.5 to indicate the relative positions of the peak and the part load conditions on the overall ASHRAE comfort chart. Alternatively, allowing for variations in occupant attire, the relative velocity requirements for summer and for marginal weather conditions could be mapped on to the comfort area of the ASHRAE comfort chart as shown in Fig 12.6. It is seen that the relative velocity ranges specified by ASHRAE Standard (ASHRAE - 55, 1981) narrow the comfort zone for a given weight of clothing to a slender band only within the seemingly broad target area indicated by the ASHRAE comfort chart. As the season changes and the typical clothing changes from light to medium weight, the room operating condition must track along a locus as the comfort slot moves towards lower operative temperatures.

12.5 The Control System

The successful operation of any air conditioning system depends, to a large extent, on the associated control system. A typical control logic diagram for the comfort integrated LFV/HCV-VAV system is illustrated in Fig 12.7 and is described in the subsequent parts of this section. The control hardware differs little from that used conventionally, the main differences being in the software algorithms.

Each zone served by an air handling unit has a local controller, preferably but not essentially of the programmable type. At the minimum level of control a manually adjustable zone thermostat is required. The following description relates the use of a programmable controller. The environmental and personal factors discussed earlier are required as inputs to the control system. The environmental factors may be sensed by conventional means while the personal factors relating to the occupants may be deduced with acceptable accuracy from knowledge of the season, and perhaps also the daily weather forecast, with the aid of tabulated data.

The local zone control functions embodied in the control logic diagram of Fig 12.7 are described below.

12.5.1 Estimation of the Zone Sensible Load

The zone sensible load may be obtained from measurements of the volume flow rate Q_{sa} of the supply air (obtained either from the measurement of the pressure difference across some known constriction or from knowledge of the flow characteristic as a function of supply air damper angle

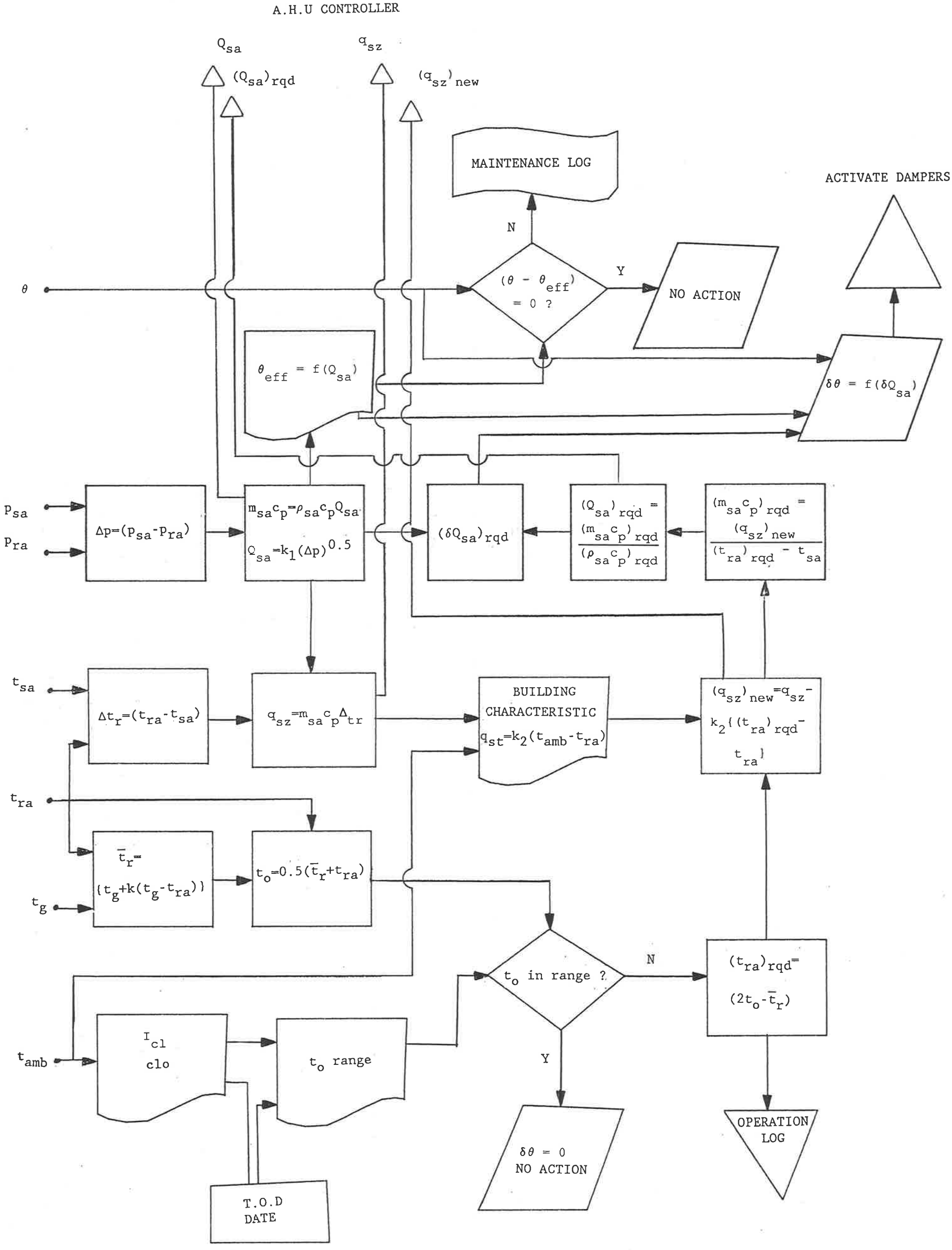

Fig 12.7 : Control strategy for "Comfort Integrated LFV/HCV System".

for a measured supply air pressure) and measurement of the rise in temperature of the supply air between inlet to and outlet from the zone. The zone sensible load is then calculated by

$$q_{sz} = \rho_{sa} Q_{sa} c_p (t_{ra} - t_{sa}) \quad . \qquad (12.1)$$

12.5.2 Estimation of the Actual Operative Temperature in the Zone As mentioned earlier the actual operative temperature t_o is approximately equal to the average of the mean radiant temperature $\bar{t}_r$ and the temperature of air in the room t_a. A room thermocouple or thermistor may be used to measure the room air temperature. The mean radiant temperature $\bar{t}_r$ is the uniform temperature of the surface of a radiantly black enclosure in which the occupant would exchange the same amount of heat by radiation as in the actual non-uniform room. It can be calculated if the room geometry and the temperatures of all surfaces are known. Such information is seldom adequately defined and hence approximations are necessary.

The mean radiant temperature can, however, be derived from measurements of the air temperature, the relative velocity of air movement and the "globe temperature". The latter is the temperature measured at the centre of a six inch (0.15m) diameter thin walled non-reflective sphere. The mean radiant temperature is then calculated from

$$\bar{t}_r = t_g + k \sqrt{v_{rv}} (t_g - t_a) . \qquad (12.2)$$

where k = 2.2 for a standard six inch diameter sphere.

If the diameter of the globe thermometer sphere differs from 0.15m, the value of k is adjusted according to the equation

$$k_d = k \left(\frac{0.15}{d} \right)^{0.4} . \qquad (12.3)$$

ASHRAE Standard 55 - 1981 specifies the locations at which measurements should be made.

12.5.3 Computation of the Optimum and the Acceptable Range of Operative Temperature

The optimum operative temperature is that operative temperature which satisfies the greatest number of similarly clad occupants in a given room for a given relative velocity and relative humidity. The acceptable range of operative temperatures for these subjects is variously defined

but ASHRAE Standard 55 - 1981 specifies acceptability as being the band of conditions within which 80% of occupants are slightly cool, neutral or slightly warm. It is possible to determine this band by calculation from the comfort equation and reference to statistical data derived from the responses of many volunteers who participated in tests.

12.5.4 Determination of the "offset" between (12.5.2) and (12.5.3) The "offset" between the calculated and the optimum operative temperature is obtained by simple difference. This difference is then compared with the acceptable range of operative temperatures.

12.5.5 Initiation of Action to bring the "offset" within the Acceptable Range

If the "offset" is not within the acceptable range the control system then initiates corrective action. Typically this would involve an increase or decrease of the air flow to the room which could be achieved by the opening or closing of the supply air damper in the duct leading to the particular room.

It is apparent that the determination of optimum temperature requires a knowledge of the insulating values of the range of clothing most likely to be being worn by the occupants of the building or of a particular room or zone in the building. Several means of determining or estimating this value may be envisaged. For example, in some zones within a building the occupants may all be required to wear a particular uniform or protective clothing at all times. The insulation value measured in the units of clo where 1 clo = 0.155 m^2 K/W, can be accurately measured and then becomes a unique value in the calculations. For such a circumstance the range of acceptable temperature is a maximum.

By contrast, in a typical building or department store the range of clothing worn by the occupants is usually diverse. It would be possible for a doorman with a trained eye to assess the range of clothing being worn as employees arrive at work. This information could then be translated into a range of clo values. The wider the range of clo values to be accommodated, the narrower is the range of temperatures which are acceptable.

An alternative to use of the observing skills of a doorman would be to estimate the most probable range of clothing being worn. The choice of clothing depends on the local culture, on the time of year and on the early morning weather forecast. Within a given culture, the time of year can be determined from the clock within the controller and the likely variation about the clothing typical of that time of the year is dependent largely on the outside ambient temperature, which can be measured directly. Thus, an estimate of the range of clo values for that particular day may be made.

In addition to the local zone controls, the Air Handling Unit operation is also supervised by a controller. At the simplest level this controller is an air-off thermostat, which actuates a valve or valves to adjust the effective size of and flow of coolant through the dehumidifier coil to maintain the air-off temperature constant, and the conventional means of measuring and controlling the supply air volume. Ideally the controller is a programmable one which receives data from each of the zone controllers and, from a pre-programmed performance map for that particular system, determines the optimum combination of operating point for the air flow fan, active coil area and coolant flow rate.

Chapter 13
CONCLUSIONS AND RECOMMENDATIONS

13.1 Conclusions

In this thesis is documented a different approach to the life cycle design of dehumidifiers in air conditioning. Backed by adequate experimental investigations, the new method is found to deliver a dehumidifier performance which is aimed to achieve the twin objectives of "comfortable indoor environment" and "minimum energy consumption". The major aspects of the project and the findings are briefly summarised below.

1. The first step towards a good design of dehumidifier systems is to be able to "generalise" *i.e.* predict the performance of dehumidifying coils at operating conditions other than those tested. A detailed review of the literature revealed a dearth of information in this area and the ARI Standard - 410 (1981) was found to be the most informative. Owing to its limitations, the ARI method could not be directly used for the LFV/HCV design methodology and there was, therefore, a need to develop an alternative method. This is offered as the AU method, which is discussed in detail in Chapter 6. The **"AU COIL SELECTION PROGRAM"**, developed according to the AU method is a useful tool in the selection of dehumidifying coils via the LFV/HCV design methodology.

2. In view of the lack of information in the regime of low face velocities, an exhaustive testing program was adopted. This led to the creation of the DATABASE and the subsequent development of the **"AU COIL SELECTION PROGRAM"**. The testing facility is discussed in Chapter 7 and the DATABASE and the **"AU COIL SELECTION PROGRAM"** are discussed in Chapter 8.

3. Some of the salient features of the AU method include the determination of Tie Line Slope (TLS) by an iterative process and the determination of the empirical constant, $(R_m + R_{ow})$. This is discussed in Chapters 6 and 8. The AU method, which is essentially developed for wet coil performance, avoids the use of fin efficiency and surface effectiveness.

4. In the process of the development of the AU method, the ARI method has been analysed in some detail (Chapters 5 and 8). As discussed in Chapter 4, the validity of using Gardner's computations of fin efficiency is suspect and this is believed to be a weak point in the ARI method. Gardner's (1945) assumption of constant heat transfer coefficient over all the fin surface appears to be in contradiction to a recent finding by Gilbert (1987) of three distinctly different regions of heat transfer coefficient. This is discussed in Chapters 4 and 9.

5. The nature of the condensate layer on the primary and the secondary surfaces of a dehumidifier is being investigated and preliminary photographs (Anne Schroeder-Lanz, 1989) clearly reveal that "Droplike" condensation occurs at low face velocities (Chapter 9). This observation is in contrast to the conventional assumption of "Filmwise" condensation. It is apparent that the "Droplike" nature of condensation enhances dehumidification, which is the key feature of the LFV/HCV concept.

6. It is normal practice to design an air conditioning system on the basis of peak load alone without due consideration of part loads. As a result designs often fail to satisfy comfort conditions at part loads. One reason for this is the "Moisture Staircase" (Sekhar *et al*, 1988), which is the thermodynamic phenomenon by which the driving potential for dehumidification between the air and the coil surface is adjusted until the amount of moisture removed from the air at the coil surface equals the amount of moisture added to the air in the conditioned space. The "Moisture Staircase" is discussed in detail in Chapters 9 and 10.

7. A solution to the inherent problem of the "Moisture Staircase" is provided in Chapters 9 and 10 in the form of the LFV/HCV design methodology. The twin objectives of the LFV/HCV design methodology are to maintain comfort conditions in the room throughout the operating range at the expense of the minimum energy. The ASHRAE Comfort Zone (ASHRAE Standard 55 - 1981) is regarded as the basis for evaluating the comfort conditions in the room resulting from a particular dehumidifier selection. The LFV/HCV design methodology is not limited to the existing shape of the ASHRAE comfort zone (Fig 12.1, Chapter 12) but is easily adaptable to any comfort design criterion. As discussed in Chapter 10 the important feature of the LFV/HCV design methodology lies in reducing the effective dehumidifier size at part loads so that it is compatible with the actual requirement of a smaller dehumidifier at the reduced part loads.

8. It is shown in Chapter 9 that the combination of a low face velocity and a high coolant velocity enables a low interface temperature to be maintained and, thereby, enhances dehumidification. In the LFV/HCV design methodology, the progressive reduction of effective dehumidifier size enables the high coolant velocity to be sustained throughout the operating range and so maintain a low interface temperature which is necessary for better dehumidification. This is in direct contrast to conventional dehumidifier designs in which the coolant velocity is reduced continuously with reducing loads. This results in a higher interface temperature at part loads which is counter to the requirement of a low interface temperature.

9. It is normal practice in conventional designs to choose a "design day" for the outside air condition and this is usually the hottest summer day, having a high dry bulb temperature. It is shown in Chapter 9 that the "design day" basis would be acceptable for peak load but unacceptable for part load which is usually accompanied by a lower dry bulb temperature and a higher moisture content than the "design day". A means of specifying the outside air condition at part loads (Luxton, Shaw and Sekhar, 1989) is discussed in Chapter 9.

10. The application of the LFV/HCV design methodology is discussed in Chapters 11 and 12 via case studies. It is demonstrated in the case studies that the LFV/HCV design system maintains the room moisture levels safely within the ASHRAE Comfort Zone at peak and part loads, whereas at part loads the conventional system often allows the room moisture levels to rise beyond the top humidity limit of the ASHRAE comfort range. The air handling units for VAV system for the fifty storeyed building in Perth, designed according to the LFV/HCV design methodology, was selected in a competitive tender. The initial lot of one hundred air handling units are being manufactured at the time of writing this thesis.

11. In addition to the fan power savings and the advantage of high quality performance, the LFV/HCV system reduces the need for costly changes in conventional VAV systems to overcome the shortcomings discussed by Gupta *et al* (1987). Modifications which are being implemented by building owners who experience rapid tenant turn-over include the addition of more air-handling units each with separate supply duct runs to satisfy problem zones, the introduction of overcooling and reheat and a significant increase in outside air quantities all of which strategies increase energy consumption. With comfort integration, the LFV/HCV system can solve the VAV part load and multi-zone problems and in addition offers further advantages :

- For a given duty the air handling unit supply air fan is smaller.

- The reduced peak load results in a smaller chiller, cooling tower, piping and ductwork.

- There is a greater flexibility in operating the system as occupants of each zone can choose their desired operative temperature and relative velocity and this can be changed simply with change of tenancy.

- Energy consumption in inefficient fan assisted VAV boxes, used to increase the supply air quantity at low loads by recirculating a proportion

of the return air, are eliminated and the cost of the VAV control boxes is thereby reduced.

- There is improved ventilation to low load rooms without necessarily higher energy consumption.

- Air conditioning performance is improved over those systems which decrease dehumidifier effectiveness by resetting their supply air temperatures upwards during marginal weather to increase the supply air volume to low load rooms.

13.2 Recommendations

While significant progress has been achieved in improving dehumidifier performance, much further research and development remains to be done. The following topics relating to dehumidifiers are suggested :

1. Finite element analysis of dry heat transfer and fluid flow in a tube and plate-fin heat exchanger and comparison with a tube and helical fin heat exchanger. This project would include a definitive numerical examination of the validity of Gardner's fin efficiency and fin effectivenes analysis.

2. Extension of the above finite element analysis to include phase change processes. As a first step the experimentally observed statistical form of the condensate droplets could be input as a boundary condition. Ultimately solutions could be sought which maintain that statistical form as the boundary condition is relaxed to a surface tension and gravity maintained volume of condensate stored on the surface.

3. Endoscopic examination of condensate form and behaviour in operating coils with varying degrees of surface fouling and surface "promotors".

4. The shearing effect of air flow on droplike condensation on a vertical surface.

5. Parametric examination of the effect on dehumidifier performance of pitch distances of the tubes in a row and between rows, of fin density, of tube diameter and of other physical geometric parameters of the dehumidifier such as the shape of the fins and fin discontinuities. These data will give a measure of the accuracy of the finite element procedures (1) and (2).

6. Development of an optimisation package that would include the effects of all the parameters indicated in (5), via experimental data correlations or via finite element analysis or a simplification of same. The optimisation should involve total system economics based on the client's required objective function which may be minimum capital cost, minimum operating cost or a combination of both such as annual owning and operating cost.

APPENDIX 1

The equations to obtain the various physical parameters such as A_p, A_s and A_i of a dehumidifier of a given geometry are derived in this chapter. The geometrical parameters of a coil with staggered tubes and continuous plate fins are shown in Figs A1.1 and A1.2.

A1.1 Primary Surface Area

The net primary surface area consists of the exposed external tube area (if any) plus the external fin collar area, if used, less the area under the fins corresponding to the fin root thickness.

A_P = [External finned tube surface area less the fin collar length area] -[External surface area of the tube under the fin root thickness] + [External surface area of the finned collar length *i.e.* the area over the diameter of $(D_o + 2Y_f)$ for a collar length of L_c].

$$A_P = \pi D_o (L_t - L_c N_{fT}) N_t - \pi D_o Y_f N_{fT} N_t + \pi (D_o + 2Y_f) L_c N_{fT} N_t$$

$$= \frac{\left[N_t D_o L_t - N_{fT} N_t Y_f (D_o - 2L_c) \right]}{1/\pi} \qquad [mm^2] \quad ,$$

where D_o, L_t, Y_f and L_c are expressed in millimetres.

Substituting $\pi = 3.14159$ in the above equation and dividing by 10^6, A_p is expressed in m^2 as

$$A_P = \frac{\left[N_t D_o L_t - N_{fT} N_t Y_f (D_o - 2L_c) \right]}{0.318310 \times 10^6} \qquad [m^2]$$

$$= \frac{\left[N_t D_o L_t - N_t N_{fT} Y_f (D_o - 2L_c) \right]}{318310} \qquad [m^2] \quad . \qquad \text{(A1.1)}$$

A1.2 Secondary Surface Area

The net secondary fin surface area is the sum of the areas of the fin sheets minus the areas of the tube holes, which leads to

A_s = [Total area of both sides of the fin sheets] - [Total area of tube holes over a diameter of $(D_o + 2Y_f)$. A factor of 2 is used for both sides of the fins] + [Area of the fin collar length of the fin tube holes not occupied by tubes *i.e.* for staggered arrangement, $N_h \neq N_t$ because of a few partial holes as shown in Fig A1.1. Two half holes are treated as one full hole].

Thus,

$$A_s = 2(L_f L_d)N_{fT} - 2\left[\frac{\pi}{4}(D_o+2Y_f)^2 N_{fT} N_h\right] + \pi(D_o+2Y_f)L_c(N_h-N_t) \quad [mm^2] ,$$

where D_o, L_t, Y_f and L_c are expressed in millimetres.

Substituting $\pi = 3.14159$ in the above equation and dividing by 10^6, A_s is expressed in m^2 as

$$A_s = N_{fT}\left[\frac{(L_f L_d)}{5000000} - \frac{N_h(D_o+2Y_f)^2}{636620} + \frac{(D_o+2Y_f)(N_h-N_t)L_c}{318310}\right] [m^2] . \quad (A1.2)$$

The total external surface area is given by

$$A_o = A_p + A_s \quad (A1.3)$$

A1.3 Total Internal Surface Area

The total internal surface area is given by

$$A_i = \pi D_i N_t L_t \quad [mm^2] ,$$

where D_i and L_t are expressed in millimetres.

Substituting $\pi = 3.14159$ in the above equation and dividing by 10^6, A_i is expressed in m^2 as

$$A_i = \frac{D_i N_t L_t}{318310} \quad [m^2] . \quad (A1.4)$$

A1.4 Surface Ratio

The surface ratio, B, is defined as the ratio of the total external surface area to the total internal surface area and is given by

$$B = \frac{A_o}{A_i} . \quad (A1.5)$$

TOTAL NUMBER OF TUBE HOLES PER FIN = N_h

[Two partial tube holes to be treated as one complete hole]

[For staggered arrangement, $N_h \neq N_t$]

Coil Casing

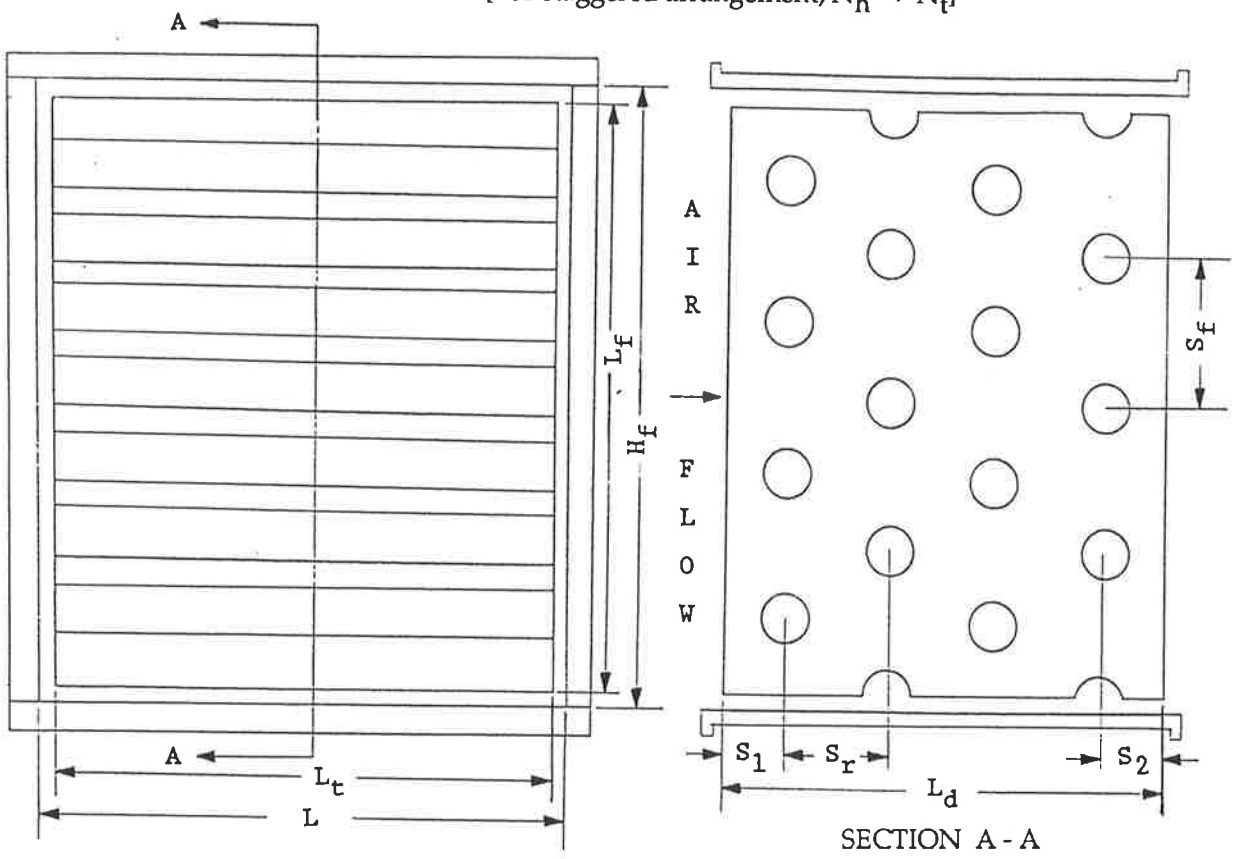

Fig A1.1 : Geometrical parameters of a coil with staggered tubes and continuous plate fins.

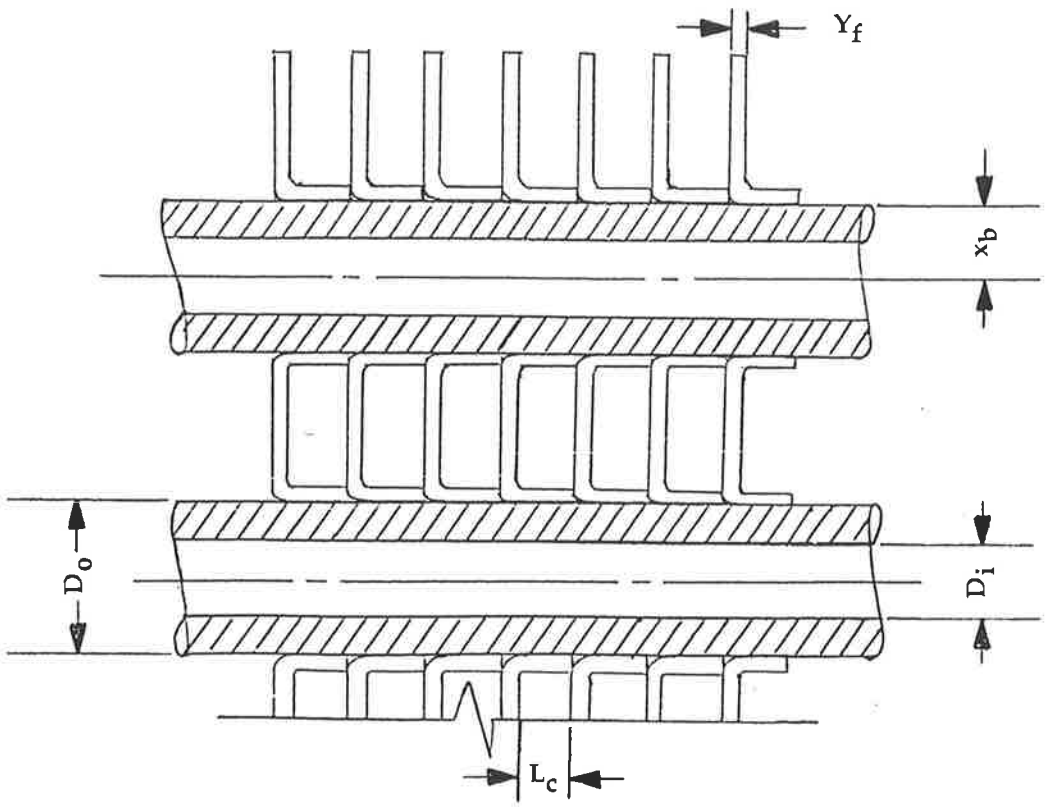

Fig A1.2 : Details of fin and tube geometry.

APPENDIX 2

The detailed development of the equivalent hydraulic diameter, the mass velocity, Reynolds number and the product $St.(Pr)^{2/3}$ is presented in this Appendix.

The experimental program described in this thesis employed a family of coils manufactured by F.Muller and Sons Pty. Limited. The relevant data for the six fins per inch coils are as follows :

Tube outside diameter, D_o = 5/8" = 0.625" (15.875mm);
Tube thickness = 0.0189" (0.48mm);
Tube inside diameter, D_i = 0.5872" (14.915mm);
Fin thickness, Y_f = 0.0075" (0.19mm);
Number of fins per inch, N_f = 6.18;
Ratio of secondary to primary surface area = 11.26;
Ratio of total external surface area to internal surface area, B = 12.73;
Ratio of total external surface area per row to face area = 15.66;
Ratio of secondary surface area to internal surface area = 11.71;
Ratio of secondary surface area per row to face area = 14.38;
Tube spacing in the plane of the fins, S_f = 1.5" (38.1mm);
Tube spacing between coil rows, S_r = 1.38" (35.05mm);

A2.1 Equivalent Hydraulic Diameter - Gunter and Shaw Method

According to Gunter and Shaw (1945), the equivalent hydraulic diameter is defined as

$$D_e = \frac{4\ (\text{Free volume of tube bundle})}{(\text{Outside surface area of the tubes})} \quad . \qquad (A2.1)$$

Before determining D_e, we have to obtain an equivalent outer diameter of a flat circular plate fin of equal area to that of a rectangular plate fin used in the MULLER (thesis) coils. For continuous plate fin of uniform thickness commonly used in finned coils, Carrier and Anderson (1940) showed that an adequate approximation is to assume that the fin area served by each tube is equivalent in performance to a flat circular plate fin of equal area. This is also used in ARI Standard 410-81 for fin efficiency calculations. Fig A2.1 shows the method where the equivalent outer radius of the circular fin, r_c, is determined. The area of a fin surrounding a tube = $S_f.S_r$ where S_f is the tube spacing in the plane of the fins and S_r is the tube spacing between rows. For MULLER coil configuration S_f = 1.5" (38.1mm) and S_r = 1.38" (35.05mm). Using the above approximation we have

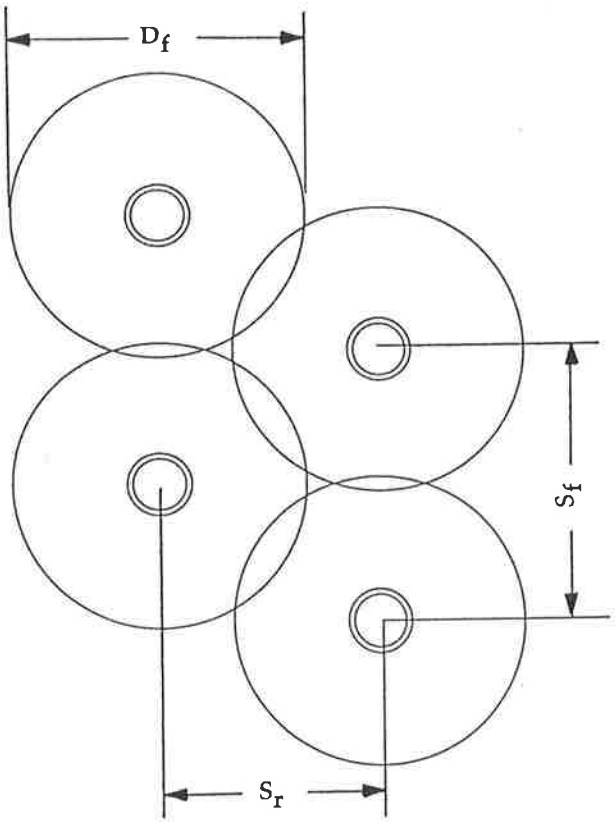

Fig A2.1 : Approximate method for relating a rectangular plate fin of uniform thickness to a flat circular plate fin of equal area.

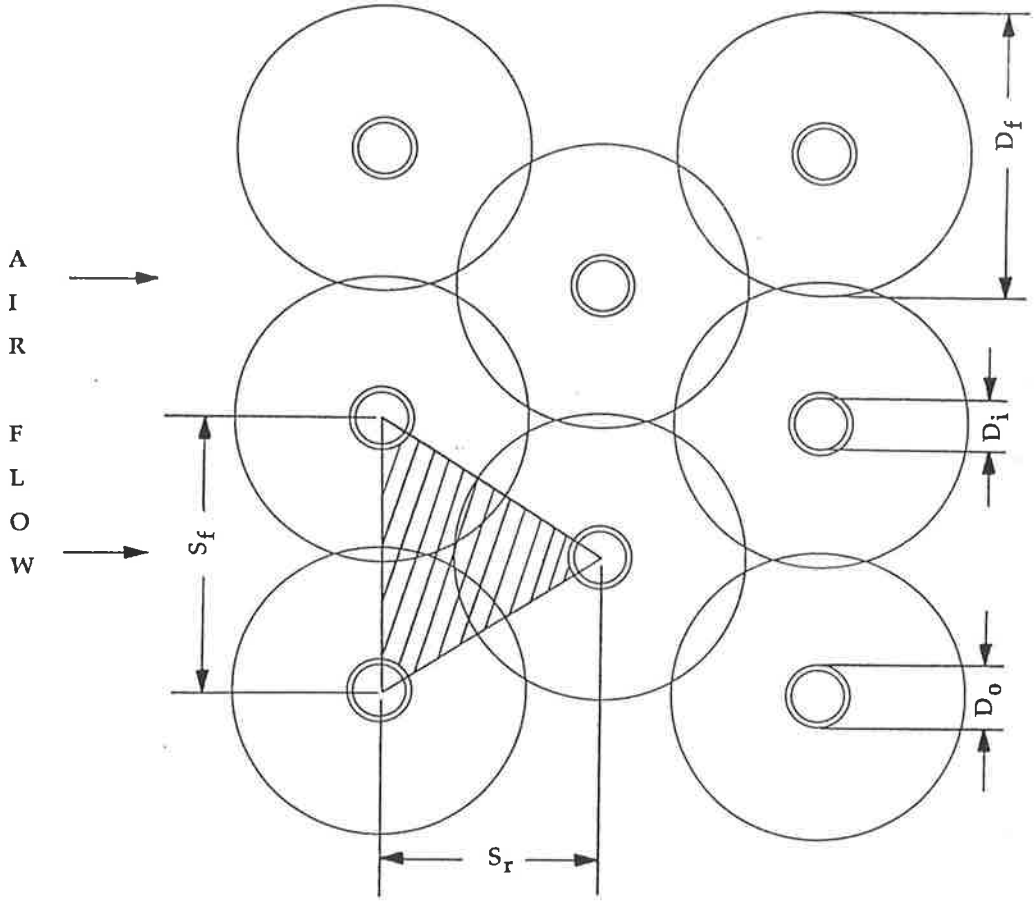

Fig A2.2 : A schematic fin and staggered-tube arrangement considered in the determination of free volume of tube bundles and outside friction surface area of tubes.

$$\pi r_c^2 = S_f \cdot S_r$$

$$\therefore \quad r_c = \sqrt{\frac{S_f \cdot S_r}{\pi}} \qquad \text{(A2.2)}$$

$$= 0.81"$$

and $D_f = 2 r_c = 1.62"$

where D_f is the equivalent outer diameter of the circular fin.

Fig A2.2 shows a schematic fin and staggered-tube arrangement where the rectangular plate fin has been replaced by a flat circular plate fin of equivalent outer diameter, D_f. The three tubes forming the vertices of an isoscles triangle, as shown in Fig A2.2, is considered in the determination of the equivalent hydraulic diameter.

Free volume of the tube bundle per inch = (Volume of 1 inch length prism) - 0.5x(Volume of 1 inch of finned tube length).

Approximating the isoscles triangled prism to an equilateral triangled prism (Fig A2.2), the volume of the unshaded portion of the prism, consisting only of the tube, is given by

Volume = 0.5x(Volume of the tube with outside diameter, D_o)

$$= 0.5 \frac{\pi}{4} D_o^2 \text{ x 1 per inch of the finned tube .} \qquad \text{(A2.3)}$$

Similarly, the volume occupied by the equivalent circular fins of outer diameter, D_f is given by

Volume = Annular volume between D_f and D_o .

Sum of annular volumes of 3 finned tubes, constituting a prism, is given by

$$\text{Volume} = 0.5 \frac{\pi}{4} (D_f^2 - D_o^2) Y_f N_f \quad . \qquad \text{(A2.4)}$$

Thus, the free volume of the tube bundle per inch, derived directly from the geometry is

$$\text{Free volume} = 0.5 S_r S_f \text{ x 1} - 0.5\left[(\frac{\pi}{4} D_o^2 \text{x1}) + \frac{\pi}{4} (D_f^2 - D_o^2) Y_f N_f\right]. \qquad \text{(A2.5)}$$

Fig: 10-92 Finned circular tubes, surface 7.75–5/8T.

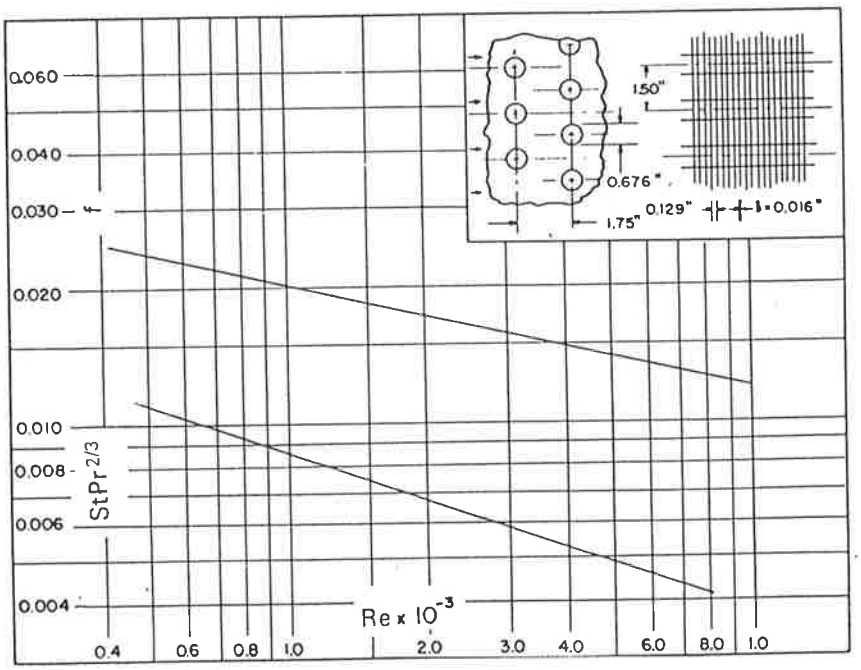

Tube outside diameter = 0.676 in = 17.17 x 10^{-3} m

Fin pitch = 7.75 per in = 305 per m

Flow passage hydraulic diameter, $4r_h$ = 0.0114 ft = 3.48 x 10^{-3} m

Fin-flow area/frontal area, σ = 0.481

Heat transfer area/total volume, α = 169 ft^2/ft^3 = 554 m^2/m^3

Fin area/total area = 0.950

Note: Minimum free-flow area in spaces transverse to flow.

Fig A2.3 : Data quoted by Kays and London (Reproduced from "Compact Heat Exchangers - Kays and London, 1984).

Substituting the various values in the above equation, the free volume of the tube bundle per inch for the coil being considered is found to be 0.843 in^3.

The outside friction surface area is given by

$$0.5\left[\frac{\pi}{4}\left(D_f^2 - D_o^2\right) N_f x2\right] + 0.5\left[\pi D_f Y_f N_f\right] + 0.5\left[\pi D_o \left(1 - N_f Y_f\right)\right] \quad \text{(A2.6)}$$

A factor of 2 is included in the first bracketed term of the above equation to consider both sides of the fin surface.

Substituting the various values in equation (A2.6), the outside friction surface area for the coil being considered is 11.5814in^2. Thus from equation (A2.1)

$$D_e = \frac{4 \text{ (Free volume of tube bundle)}}{\text{(Outside surface area of the tubes)}}$$

$$= \frac{4 \times 0.843}{11.5814} = 0.2912" = 0.02426 \text{ ft.} = 7.396 \times 10^{-3} \text{ m.}$$

The above value of D_e has been obtained by considering a multiple row coil. If a single row coil is considered, then the isoscles triangled prism discussed earlier reduces to a rectangular prism having the dimensions of S_f x (0.5 S_r). A rectangular prism with the dimensions of S_f x (0.5 S_r) is the same as the equilateral triangled prism considered earlier in the case of a multiple row coil. It is thus apparent that the free volume of the tube bundle and the friction surface area for a single row coil can be expressed by the same equations that were developed for a multiple row coil, that is, equations (A2.5) and (A2.6) respectively. Hence the equivalent hydraulic diameter for a single row coil would be the same as that determined for a multiple row coil.

The above value of D_e for the MULLER (thesis) coil is compared with the equivalent diameter of Fig 10.92 in Kays and London (1984) which is reproduced as Fig A2.3. The finned circular tube of Fig A2.3 has a higher fin density but appears to be the closest to the Muller coils used in the present research project. The determination of hydraulic diameter according to the definition of Kays and London and their comparison with those determined by the Gunter and Shaw method are discussed in the next section.

A2.2 Equivalent Hydraulic Diameter - Kays and London Method

Kays and London define a hydraulic diameter D_h as

$$D_h = 4 \frac{A_c}{A_o} L \quad , \qquad (A2.7)$$

where A_c = Minimum free flow area

L = Flow length of the heat exchanger

A_o = Total heat transfer area.

The information provided in Fig A2.3 will be used to obtain the value of D_h for the coil quoted by Kays and London. Let us consider the coil in Fig A2.3 to be two rows deep and having a frontal area, A_f of 1"x1.5". The flow length of the coil is then L = 2x1.75" = 3.5" = 0.2917ft. The ratio of the free flow area to the frontal area is 0.481 and the ratio of the heat transfer area to the total volume is 169 ft^2/ft^3. Therefore

$$A_c = 0.481\, A_f = 0.481\left[\frac{1 \times 1.5}{12 \times 12}\right] = 0.00501 ft^2$$

and $$A_o = 169\, V_{tot} = 169\left[\frac{1 \times 1.5 \times 3.5}{12 \times 12 \times 12}\right] = 0.5135 ft^2,$$

where V_{tot} = total volume of the coil being considered.

The hydraulic diameter, D_h is then obtained from equation (A2.3) and is

$$D_h = \frac{4 \times 0.00501 \times 0.2917}{0.5135} = 0.0114ft = 3.48 \times 10^{-3} m.$$

This is the same as that indicated in Fig A2.3.

We shall now obtain the hydraulic diameter, D_h for the MULLER coil. An exaggerated view of a fin and tube section of a MULLER coil is shown in Fig A2.4. Let us consider a two row deep coil having the frontal dimensions of 1" long and 1.5" high. The flow length of the coil is then L=2x1.38"=2.76".

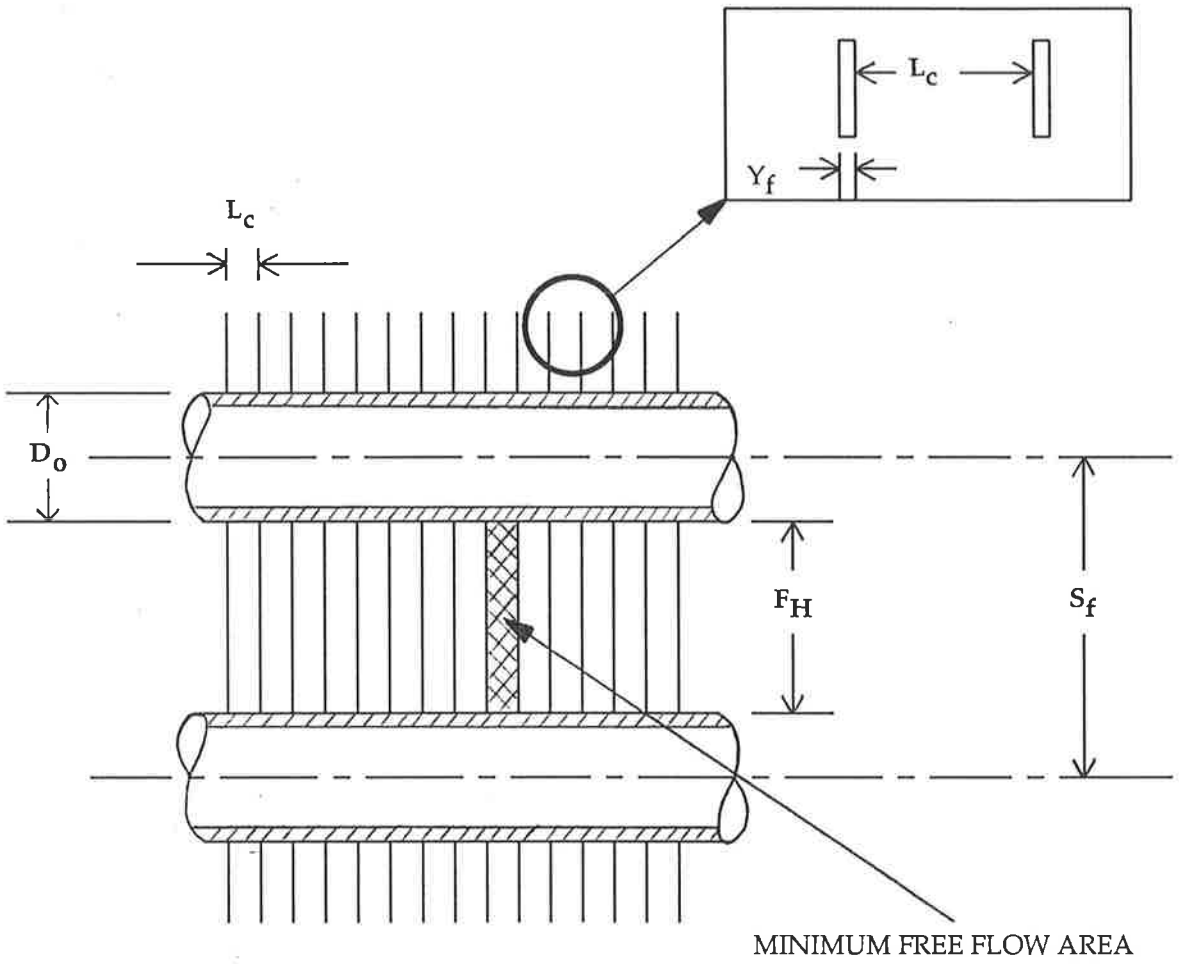

D_o	15.875 mm
F_H	22.2 mm
S_f	38.1 mm
L_c	4 mm
Y_f	0.19 mm

Fig A2.4 : Details of the fin and tube section of a MULLER coil. An exaggerated view of the fin spacing and the fin thickness is shown in the insert.

Total metal cross sectional area across the face in a direction normal to the air flow is

$$A_{metal} = [(D_o L_t) + N_{fT} (F_H Y_f)] N_{tr} \quad , \qquad (A2.8)$$

where

N_{fT} = Total number of fins,

N_{tr} = Number of tubes per row,

F_H = $S_f - D_o$.

Minimum free flow area, A_{min} = Face area - Total metal cross sectional area across the face.

Thus

$$A_{min} = L_f L_t - A_{metal} \quad . \qquad (A2.9)$$

In the coil being considered D_o=0.625", L_t=1", N_{fT}=6.18, S_f=1.5", Y_f=0.0075" and N_{tr}=1. Therefore

$$A_{metal} = [(0.625x1) + 6.18x(1.5 - 0.625)x0.0075x1] = 0.6656in^2$$

and $A_{min} = 1x1.5 - 0.6656 = 0.8344in^2$.

Since the ratio of total external surface area per row to face area is 15.66, the total external surface area, A_o for the two row deep coil under consideration is 15.66x(1x1.5)x2 = 46.98in^2.

The hydraulic diameter for the MULLER coil is then obtained from equation (A2.7) and is

$$D_h \text{ for MULLER coil} = \frac{4 \times 0.8344 \times 2.76}{46.98}$$

$$= 0.1961" = 0.0163ft = 4.98x10^{-3}m.$$

Note that the same value of D_h would have been obtained if a single row coil had been considered in the above example. In the case of a single row coil the flow length, L and the total heat transfer area, A_o would each be halved resulting in the same value of D_h as obtained above for a multiple row coil.

A comparison of D_e and D_h for the MULLER coil as obtained by the Gunter/Shaw and the Kays/London methods respectively and D_h as quoted by Kays and London for their coil (K&L coil) is summarised in Table A2.1.

	Muller coil (Gunter/Shaw) D_e	Muller coil (Kays/London) D_h	K & L coil (Kays/London) D_h
Tube outside diameter	0.625" (15.875mm)	0.625" (15.875mm)	0.676" (17.17mm)
Fin density	6.18 per inch (243 per m)	6.18 per inch (243 per m)	7.75 per inch (305 per m)
Tube spacing in the plane of the fins	1.5" (38.1mm)	1.5" (38.1mm)	1.5" (38.1mm)
Tube spacing between coil rows	1.38" (35.05mm)	1.38" (35.05mm)	1.75" (44.45mm)
Equivalent hydraulic diameter	0.02426ft (7.396×10^{-3}m)	0.0163ft (4.98×10^{-3}m)	0.0114ft (3.48×10^{-3}m)

Table A2.1 : Comparison of equivalent hydraulic diameter

A2.3 Mass Velocity

The mass velocity, sometimes referred to as the cut-off velocity, is given by

$$G = \frac{\text{Mass flow rate}}{\text{Minimum flow area}} ,$$

$$\text{i.e. } G = \frac{m_a}{A_{min}} . \qquad \text{(A2.10)}$$

The mass velocity is then

$$G = \frac{m_a}{(L_f L_t - A_{metal})} . \qquad \text{(A2.10a)}$$

A2.4 Reynolds Number

The Reynolds number is given by

$$Re = \frac{D_h \, G}{\mu} \quad , \qquad \text{(A2.11)}$$

where $\mu = 0.018 \times 10^{-3}$ Pa.s.

Substituting for D_h and G, we have

$$Re = \frac{4.98 \times 10^{-3} \, m_a}{0.018 \times 10^{-3} \, (L_f \, L_t - A_{metal}) \times 10^{-6}} \quad .$$

Hence,

$$Re = \frac{276.67 \times 10^{6} \, m_a}{(L_f \, L_t - A_{metal})} \quad . \qquad \text{(A2.11)}$$

In equation (A2.11) m_a is in kg/s and L_f and L_t are in mm.

A2.4.1 Effect of Fin Spacing Variation on Reynolds Number

The total number of flow passages per tube spacing = $N_f \times L_t$,

where N_f = Number of fins per inch and

L_t = Length of the tube in inches.

The total area of flow passages (Fig A2.4) = $N_f \, L_t \, (L_c - Y_f) \, F_H \, N_{tr}$,

where N_{tr} is the number of tubes per row.

The total flow through the face of the coil, $Q = G \, N_f \, L_t \, (L_c - Y_f) \, F_H \, N_{tr}$,

where G is the mass velocity.

Thus Reynolds number based on fin spacing is

$$(Re)_{fp} = \frac{G \, (L_c - Y_f)}{\mu} = \frac{Q}{\mu \, N_f \, L_t \, F_H \, N_{tr}} \quad . \qquad \text{(A2.12)}$$

For a fixed Q and fixed face velocity, it is apparent from equation (A2.12) that the effective Reynolds number, $(Re)_{fp}$ varies inversely with the number of fins per unit length. Thus an <u>increase</u> in the number of fins <u>decreases</u> the Reynolds number by <u>decreasing</u> the fin spacing.

The argument is not as simple if we consider variation of the face velocity as well. For example, consider two coils with same Q but face velocities V_{a1} and V_{a2}.

Now $Q = V_a\ A_f$ and $A_f = L_t\ N_{tr}\ S_f$,

where A_f = Face area of the coil and S_f = Tube spacing in the plane of the fins.

Thus for fixed tube spacing $A_f \propto (L_t\ N_{tr})$.

$\therefore\ Q \propto (V_a L_t N_{tr})$ or $V_a \propto Q/(L_t N_{tr})$.

Comparing the effective Reynolds numbers then gives

$$\frac{(Re)_{fp2}}{(Re)_{fp1}} = \frac{Q}{\mu\ N_{f2}\ L_{t2}\ N_{tr2}\ F_H} \quad \frac{\mu\ N_{f1}\ L_{t1}\ N_{tr1}\ F_H}{Q}$$

$$= \frac{N_{f1}\ L_{t1}\ N_{tr1}}{N_{f2}\ L_{t2}\ N_{tr2}} \quad . \qquad \text{(A2.13)}$$

But V_a is inversely proportional to the product of $(L_t\ N_{tr})$ for fixed Q and thus

$$\frac{(Re)_{fp2}}{(Re)_{fp1}} = \frac{N_{f1}\ V_{a2}}{N_{f2}\ V_{a1}} \quad . \qquad \text{(A2.14)}$$

If fin density is kept constant ($N_{f1} = N_{f2}$)

$$(Re)_{fp2} = \frac{V_{a2}}{V_{a1}}\ (Re)_{fp1} \quad . \qquad \text{(A2.14a)}$$

That is, if we reduce the face velocity for constant Q and constant fin spacing, we reduce the effective Reynolds number in proportion.

Alternatively, if we keep face velocity constant and vary fin density

$$(Re)_{fp2} = \frac{N_{f1}}{N_{f2}} (Re)_{fp1} \quad . \qquad (A2.14b)$$

That is, by decreasing fin density we increase Reynolds number proportionally.

By halving the face velocity and halving the fin density, Reynolds number is kept constant.

A2.5 Stanton.(Prandtl)$^{2/3}$ Number

The product St.(Pr)$^{2/3}$ is given by

$$St.(Pr)^{2/3} = \left[\frac{h_{cow}}{G\, c_p} \right] \left[\frac{\mu\, c_p}{k} \right]^{2/3} \quad . \qquad (A2.15)$$

For consistency the following properties of air in the range of 20°C - 30°C are extracted from Table A-1 of Kays and London (1984) :

μ = 0.01817×10^{-3} Pa.s

c_p = 1.018 kJ/(kg.K)

k = 25.63×10^{-6} kW/(mK) .

Substituting the various values in consistent units in the equations for the Stanton and Prandtl numbers, we have

$$Pr = \frac{\mu\, c_p}{k} = \frac{0.01817 \times 10^{-3} \times 1.018}{25.63 \times 10^{-6}} = 0.7217 \quad ,$$

and, with G from equation (A2.10a) equation (A2.12) becomes

$$St.(Pr)^{2/3} = \left[\frac{h_{cow} \times 10^{-3} \, (L_f\, L_t - A_{metal}) \times 10^{-6}}{1.018\, m_a} \right] \times (0.7217)^{2/3}$$

$$= \frac{0.79035 \times 10^{-9} \, [\, h_{cow} \, (L_f\, L_t - A_{metal}) \,]}{m_a} \quad . \qquad (A2.15a)$$

The units of m_a are kg/s and L_f and L_t are in mm.

APPENDIX 3

A summary of the equations involved in the **"TESTP"** program to evaluate the basic psychrometric properties is presented below (ASHRAE, 1985). The saturation pressure over liquid water for the temperature range of 0 - 200 °C is given by:

$$\ln(p_{ws}) = \frac{C_8}{t} + C_9 + C_{10}\, t + C_{11}\, t^2 + C_{12}\, t^3 + C_{13} \ln(t) \quad , \quad (A3.1)$$

where

C_8 = - 5800.2206

C_9 = 1.3914993

C_{10} = - 0.04860239

C_{11} = $0.41764768 \times 10^{-4}$

C_{12} = - $0.14452093 \times 10^{-7}$

C_{13} = 6.5459763

ln = $\log_e$

p_{ws} = saturation pressure in Pa

t = absolute temperature in K = °C + 273.15

The humidity ratio, W, at any temperature and pressure is

$$W = 0.62198 \frac{p_w}{P - p_w} \quad , \quad (A3.2)$$

where

P = total pressure

p_w = partial pressure of water vapour

and the coefficient is the ratio of molecular masses of water vapour to dry air.

The humidity ratio at saturation, W_s, is obtained by replacing p_w with p_{ws} in equation (A3.2).

It is apparent from the perfect gas equation of state and Dalton's law of partial pressures that the specific volume, v, of moist air is

$$v = \frac{R_a\, t}{P - p_w}$$

and substituting for p_w from equation (A3.2), we have

$$v = \frac{R_a\ t}{P} \left[1 + 1.6078W \right] \quad . \qquad \text{(A3.3)}$$

The enthalpy of moist air in kJ/kg dry air is a function of the air temperature and the humidity ratio. Thus

$$h = t + W(2501 + 1.805t) \quad , \qquad \text{(A3.4)}$$

where t is the dry bulb temperature in °C and the coefficients are empirical constants of a straight line fitted to a plot of enthalpy versus temperature.[1]

The mass flow rate is given by

$$m_a = (Q_a)_{act}\ \rho_{act} \quad . \qquad \text{(A3.5)}$$

The sensible heat capacity is given by

$$q_s = m_a\ c_p\ (t_1 - t_2) \quad , \qquad \text{(A3.6)}$$

where t_1 and t_2 are the entering and the leaving air dry bulb temperatures respectively and c_p is the specific heat of the moist air.

The total heat capacity is given by

$$q_t = m_a\ (H_1 - H_2) \quad , \qquad \text{(A3.7)}$$

where H_1 and H_2 are the entering and the leaving air enthalpies respectively.

The sensible heat factor is the ratio of the sensible to the total heat capacities *i.e.* q_s/q_t.

1The plotted values were taken from Keenan and Keyes' Thermodynamic Properties of Steam.

The water-side cooling capacity, q_{tw} is given by

$$q_{tw} = W_w \, c_{pw} \, (t_{w2} - t_{w1}) \quad , \qquad \text{(A3.8)}$$

where W_w = chilled water flow rate, c_{pw} = specific heat capacity of water and t_{w1} and t_{w2} are the "measured" entering and leaving water temperatures.

As discussed earlier in Chapter 8, the "measured" water temperature rise was found to be less accurate due to difficulties encountered in measuring low water temperature rises, inherent in the tests described in this thesis. Therefore, a "corrected" water temperature rise was computed by using the air-side total heat capacity and this is

$$\text{Corrected water temperature rise} = \frac{q_t}{W_w \, c_{pw}} \quad . \qquad \text{(A3.9)}$$

The theoretical amount of moisture, m_c', condensed from the moist air stream is given by

$$m_c' = m_a \, (W_1 - W_2) \quad , \qquad \text{(A3.10)}$$

where W_1 and W_2 are the entering and the leaving air humidity ratios.

APPENDIX 4

Samples of the archive of 450 tests of dehumidifying coil is presented here. Tables A4.1 and A4.2 are respectively samples of the data sheet and the Digistrip recording. Typical backup data such as Honeywell recorder charts and the hygrothermograph chart, with annotations made at the time of the actual test, are illustrated in Figs A4.1 - A4.3. A brief discussion of these Tables and Figures can be found in Chapter 8.

16:26:00	778.9M	697.2M	3358.8M	2281.9M	1708.7M	2024.6M	3473.4M	120.4M
16:27:00	778.4M	696.6M	3359.4M	2282.0M	1715.4M	2015.0M	3473.3M	119.2M
16:28:00	778.6M	696.4M	3360.9M	2281.3M	1710.6M	2022.1M	3502.3M	119.4M
16:29:00	779.5M	697.3M	3361.1M	2282.4M	1715.2M	2014.5M	3502.5M	120.2M
16:30:00	779.5M	697.7M	3361.2M	2281.9M	1713.3M	2021.7M	3516.8M	119.3M
16:31:00	779.8M	699.1M	3363.1M	2283.6M	1716.8M	2028.1M	3473.3M	121.4M
16:32:00	780.6M	698.7M	3361.5M	2284.3M	1717.3M	2023.2M	3482.0M	120.7M
16:32:46	781.4M	699.3M	3361.5M	2285.0M	1712.4M	2014.9M	3473.3M	120.5M
16:33:00	781.6M	699.4M	3362.0M	2285.7M	1721.1M	2020.3M	3473.3M	120.2M
16:33:44	781.9M	699.7M	3358.8M	2285.8M	1716.1M	2022.9M	3473.3M	120.8M
16:34:00	782.0M	699.6M	3359.5M	2286.0M	1721.9M	2021.5M	3473.5M	120.7M

1 LOW FACE VELOCITY COOLING COILS 13

0395	01	02	03	04	05	06	07	08	09	10
100	NA	CHW OUT	CHW IN	NA	AIR ON	AIR OFF	DWPT OFF	DWPT ON	WTR FLF	AIR FL
16:34:44		781.2M	698.7M		3359.5M	2284.5M	1714.9M	2011.4M	3473.4M	119.8M
16:35:00		780.9M	698.7M		3359.9M	2284.2M	1716.4M	2022.2M	3473.5M	119.6M
16:35:43		781.0M	700.3M		3359.2M	2283.7M	1711.4M	2023.9M	3516.8M	118.7M
16:36:00		781.6M	700.4M		3359.6M	2283.5M	1718.1M	2020.7M	3473.3M	119.4M
16:36:42		781.6M	700.2M		3359.8M	2282.1M	1709.6M	2011.9M	3473.4M	119.3M
16:37:00		782.2M	700.0M		3359.7M	2281.8M	1719.9M	2023.8M	3516.8M	118.5M
16:37:41		782.0M	700.2M		3359.3M	2283.0M	1716.4M	2018.7M	3473.3M	119.9M
16:38:00		782.1M	701.0M		3360.1M	2283.3M	1719.4M	2019.2M	3517.0M	120.3M
16:38:41		782.1M	700.7M		3360.5M	2284.3M	1714.0M	2028.3M	3475.4M	120.3M
16:39:00		781.9M	699.9M		3360.9M	2284.5M	1719.0M	2003.6M	3485.6M	120.4M
16:39:40		781.4M	699.8M		3360.8M	2284.2M	1717.7M	2032.6M	3473.5M	120.1M
16:40:00		781.6M	699.8M		3360.7M	2284.5M	1719.1M	2015.1M	3473.3M	120.9M
16:40:39		781.7M	699.8M		3360.4M	2285.3M	1716.1M	2025.8M	3473.3M	120.8M
16:41:00		782.5M	700.6M		3359.8M	2285.0M	1722.5M	2016.0M	3516.9M	120.1M
16:41:38		782.5M	700.4M		3360.8M	2285.0M	1716.4M	2022.5M	3473.3M	120.2M
16:42:00		782.5M	699.9M		3360.3M	2284.4M	1714.9M	2021.1M	3473.3M	119.9M
16:42:38		782.9M	699.8M		3360.7M	2284.4M	1723.8M	2026.4M	3473.3M	119.0M
16:43:00		783.1M	700.3M		3360.9M	2284.6M	1717.6M	2019.8M	3473.3M	118.3M
16:43:36		782.7M	700.7M		3361.1M	2283.6M	1717.1M	2023.4M	3517.0M	118.3M
16:44:00		782.3M	700.8M		3360.8M	2283.2M	1718.4M	2020.4M	3475.1M	119.1M
16:44:36		782.5M	700.6M		3361.2M	2282.9M	1717.7M	2025.3M	3473.3M	119.7M
16:45:00		782.9M	701.1M		3360.9M	2282.5M	1709.7M	2018.4M	3473.3M	119.6M
16:45:35		783.7M	702.2M		3361.6M	2282.0M	1720.3M	2017.0M	3473.3M	118.3M
16:46:00		783.7M	702.8M		3361.3M	2281.7M	1718.0M	2028.6M	3473.3M	119.5M
16:46:34		783.0M	702.0M		3361.4M	2282.7M	1718.3M	2021.5M	3516.8M	120.1M
16:47:00		782.6M	701.6M		3360.7M	2282.4M	1722.6M	2030.2M	3484.9M	120.1M
16:47:32		782.4M	701.2M		3361.4M	2283.2M	1718.6M	2029.3M	3473.2M	119.7M
16:48:00		782.5M	701.4M		3361.7M	2284.0M	1722.1M	2027.3M	3473.3M	121.6M
16:48:31		782.5M	701.2M		3360.8M	2284.4M	1720.5M	2031.0M	3516.8M	121.1M
16:49:00		783.3M	703.7M		3360.9M	2284.6M	1724.9M	2028.2M	3473.3M	121.2M
16:49:30		783.5M	703.0M		3361.4M	2285.1M	1723.9M	2025.2M	3473.3M	120.2M

Table A4.1 : Digistrip recording.

DATA SHEET

Test Attempted:

FACE VELOCITY	- 0.6	M/S	DATE	: 30-1-87
WATER VELOCITY	- 1.0	M/S	TIME	: 16.30
ENT.AIR DRY BULB TEMP.	- 33.6°	C	TEST CODE	: H726:W3953
ENT.AIR WET BULB TEMP.	- 24.1°	C	COIL DIMENSION	: 457×760mm
ENT.AIR DEW POINT TEMP.	- 20.3°	C	MAKE	: Muller
ENT.WATER TEMP.	- 7°	C	ROWS	: 1
ENT.ENTHALPY	- 72	kJ/kg	FPI	: 6
			CIRCUITING	: Half
			NUMBER OF TUBES/ROW	: 12
			NUMBER OF TUBES FED/ROW	: 6

Control Settings:

COMP.RPM	- 478		
FAN RPM	- 630		
HUMID SETTING	- 21% (Manual)		
REHEAT SETTING	- 45 (Automatic)	AMBIENT PRESSURE	: 30.166"
HEAD PRESSURE	- 91.5	AMBIENT TEMPERATURE	: 76°F
NO.OF FIXED HEATERS	- -		
NO.OF FIXED HUM.HEATERS	- -		

Refrigeration side readings:

UPSTREAM EVAPORATOR PRESSURE REGULATOR	- 210	KPa
DOWNSTREAM EVAPORATOR (BY-PASSES EV.PR.REG.)	- 180	KPa
LIQUID UPSTREAM (LIQUID SUCTION HEAT EXCHANGER)	- 920	KPa
LIQUID DOWNSTREAM CONDENSER	- 920	KPa
VAPOUR DOWNSTREAM (LIQUID SUCTION HEAT EXCHANGER) (UPSTREAM COMPRESSOR)	- 210	KPa
DOWNSTREAM EVAPORATOR PRESSURE REGULATOR	- 190	KPa
UPSTREAM TX VALVE	- 930	KPa
COMPRESSOR SUCTION	- 170	KPa
COMPRESSOR-DISCHARGE	- 840	KPa

DATA A

		1	2	3	4
Time	:	16.39			
GAPMETER	lpm -	65			
COND.WATER FLOWMETER	lpm -	-			
FREON FLOWMETER	lpm -	-			
INCLINE MANOMETER ("of water)		- 0.175"			

DATA B: ASSMAN RECORDINGS

		1	2	3	4
Air On	Time :	16.39			
EDB	-	33.6			
EWB	-	24.2			
EDP(From Psych.Chart)	-	20.4			
Air Off					
LDB	-	22.8			
LWB	-	19.1			
LDP(From Psych.Chart)	-	17.3			

DATA C: CONDENSATE MASS RECORDINGS

		1	2	3	4
Time	:	16.30	16.42	16.52	
WT.OF BEAKER	-	83	83	83	
TOTAL MASS(BEAKER+COND.)	-	456.5	426	338	
COND.MASS	-	373.5	343	255	
TIME PERIOD	-	9m13.33s	8m36.44s	6m17.51s	
TIME IN SECONDS	-	553.33s	516.44s	377.51s	
COND.MASS/SEC g/s	-	0.675	0.664	0.675	
AVERAGE g/s	-		0.665 g/s		

Table A4.2 : Data sheet.

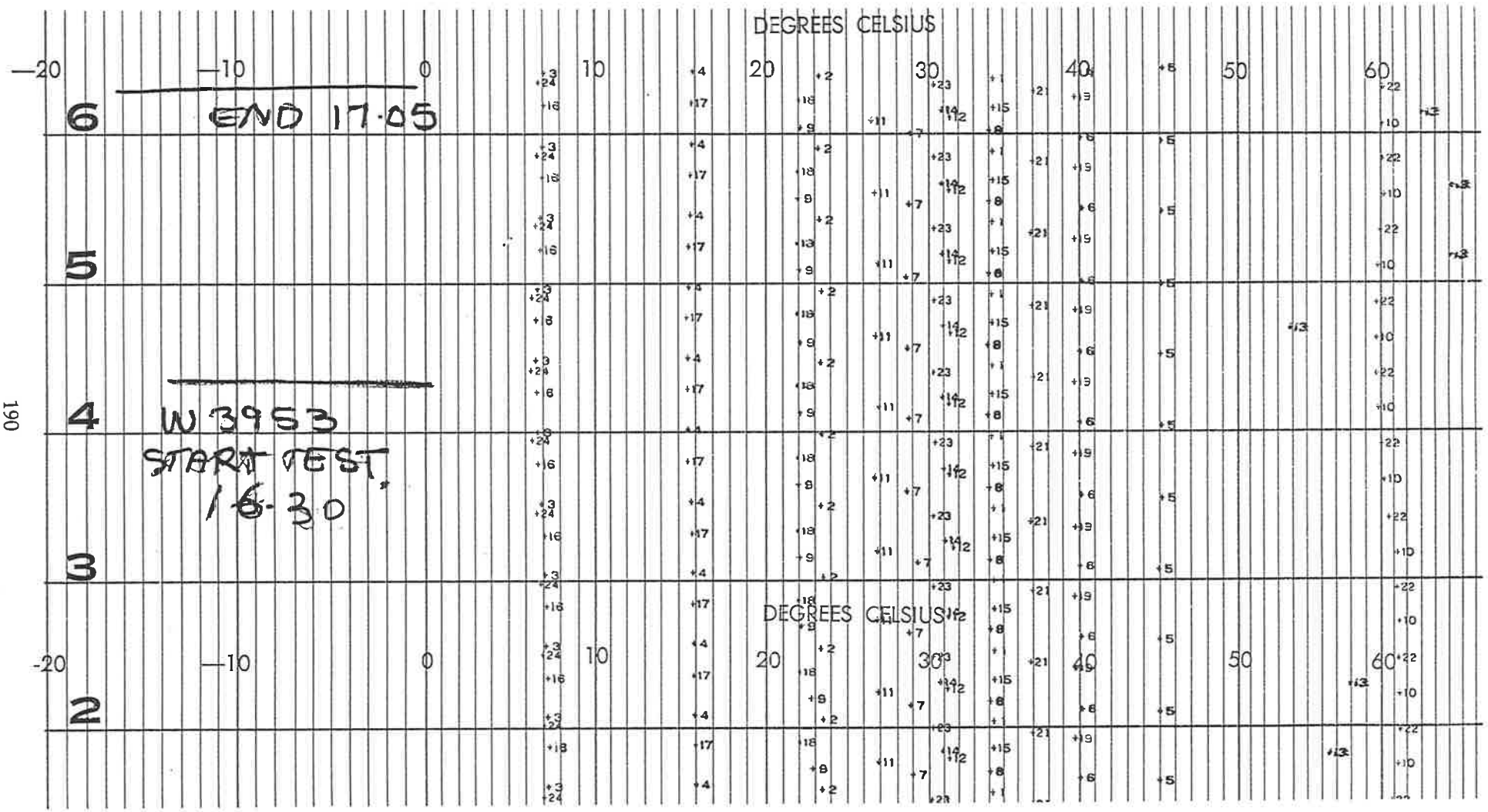

Fig A4.1 : Honeywell recorder chart - 1.

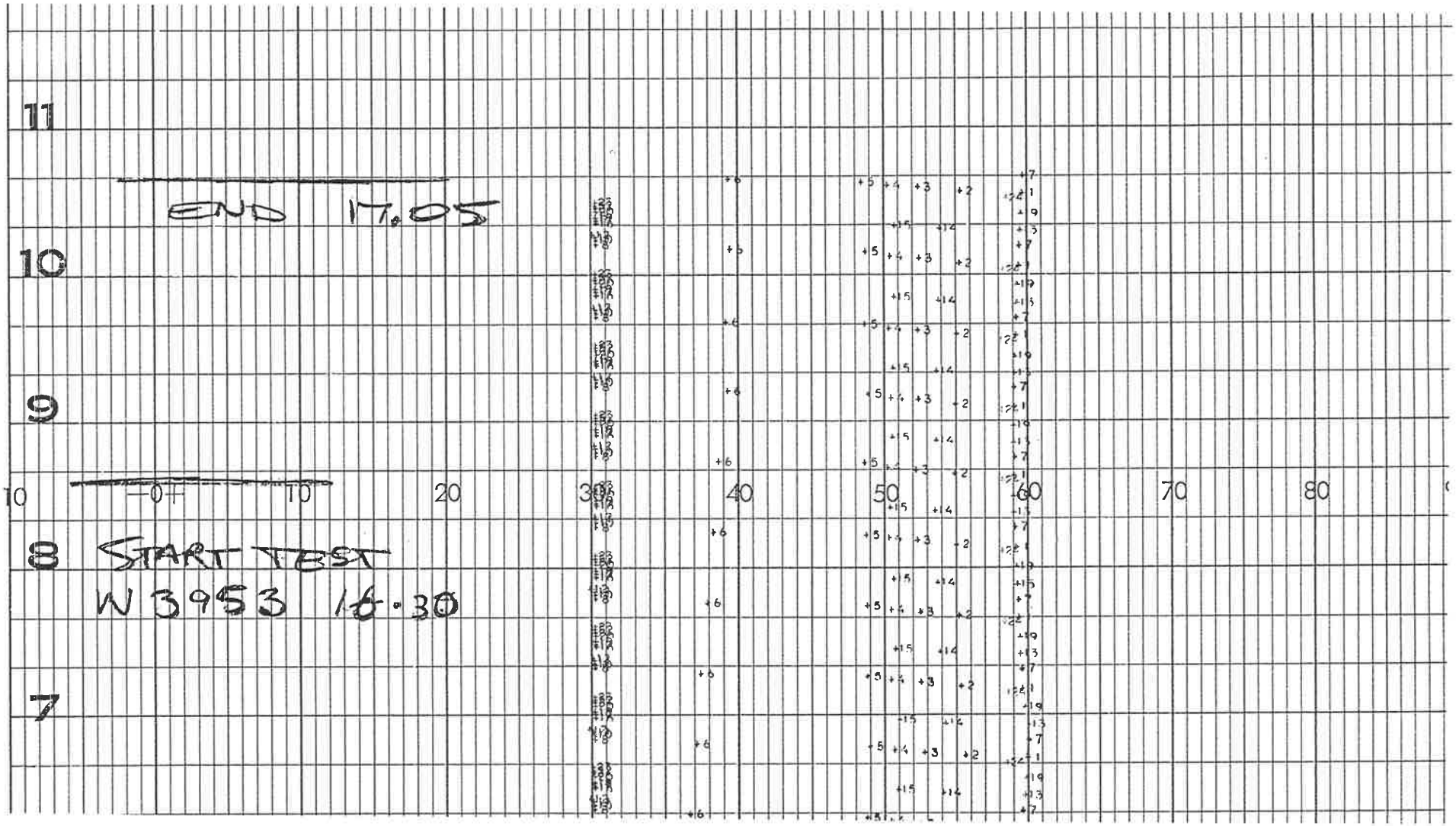

Fig A4.2 : Honeywell recorder chart - 2.

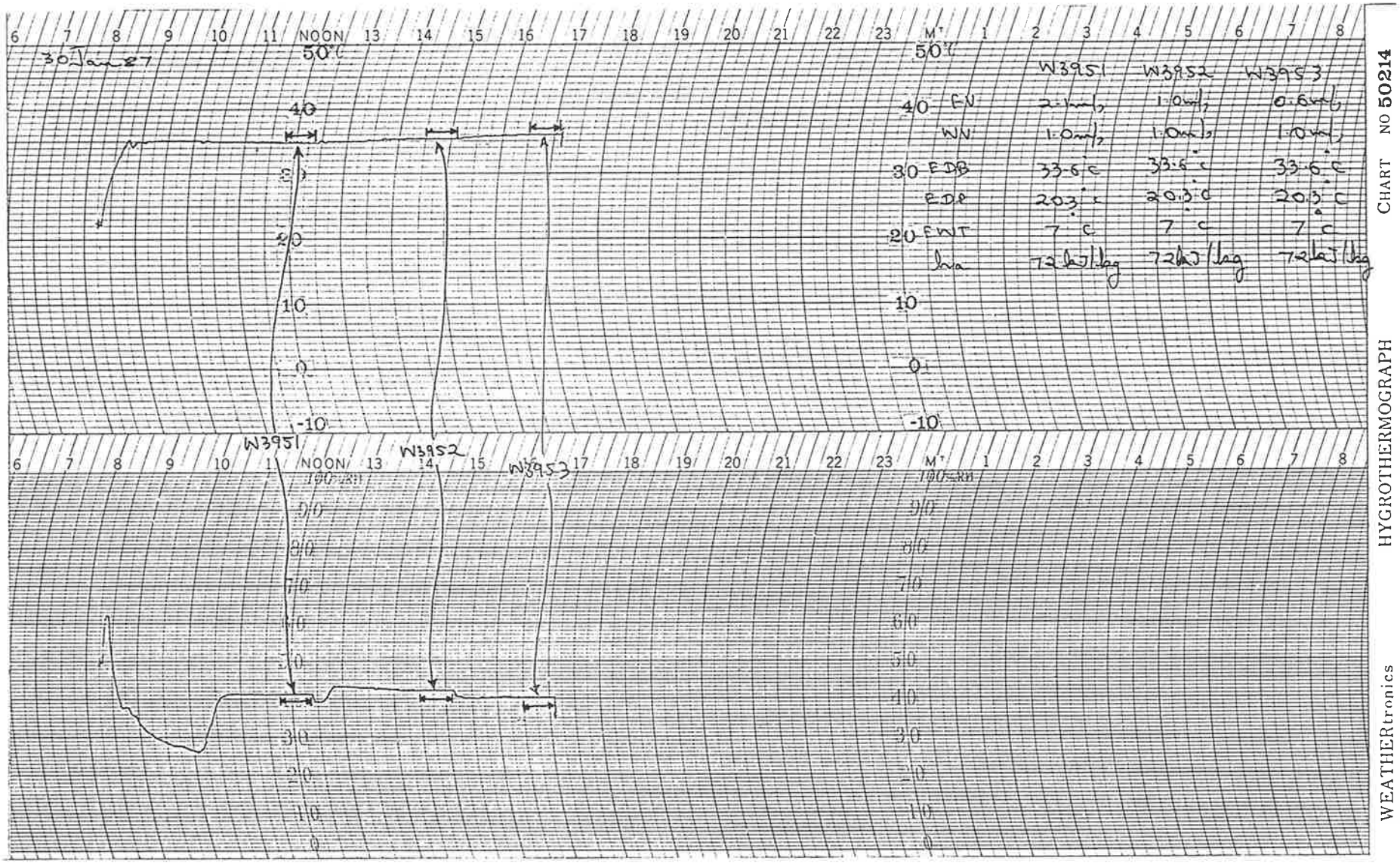

Fig A4.3 : Hygrothermograph.

APPENDIX 5

The theories on which the ARI and the AU methods of generalisation are based have been discussed in Chapters 5 and 6 respectively and as already stated earlier the **"ARI GENERALISATION PROGRAM"** and the **"AU COIL SELECTION PROGRAM"** have been developed to predict the performance of coils by the two methods. Examples of the computer printouts of these two programs are presented in Tables A5.1 through A5.5 and A5.1a through A5.5a in this Appendix. Tables A5.1 - A5.5 consist of the output of the **"AU COIL SELECTION PROGRAM"** followed by the corresponding output of the **"TESTP"** program. Tables A5.1a - A5.5a consist of the output of the **"ARI GENERALISATION PROGRAM"** followed by the corresponding output of the **"TESTP"** program. Thus a direct comparison of the predictions of coil performance by the ARI and the AU methods with the actual test results is obtained. For example, Tables A5.1 and A5.1a give a comparison of the AU and the ARI predictions of the same series of tests with actual test results.

Tables A5.1 - A5.3 and A5.1a - A5.3a give a comparison of the performance prediction with the actual results for the 1-row coil. Tables A5.4 and A5.4a pertain to the 2-row coil and Tables A5.5 and A5.5a pertain to the 4-row coil. Table A5.5 also involves a coil with a different circuiting arrangement from that actually tested.

Results of AU (ADELAIDE UNIVERSITY)
coil selection program. Suitable for
1, 2 or 4 Row, 6 fpi, half circuiting.

INPUT DATA :										
Title :	H66B:W4261	H66B:W4271	H66B:W4361	H66B:W4362	H66B:W4363	H72B:W3991	H72B:W3953	H72B:W3952	H72B:W3942	H72B:W3951
ent dbt (°C) :	31.03	31.04	31.05	31.00	30.96	33.63	33.61	33.64	33.62	33.66
ent dpt (°C) :	18.81	18.84	18.72	18.95	18.89	20.30	20.27	20.34	20.27	20.36
ent water temp (°C) :	7.02	7.04	7.00	7.00	7.02	7.02	7.01	7.04	7.01	7.07
act air vol (cms) :	0.136	0.202	0.350	0.548	0.730	0.137	0.212	0.346	0.557	0.731
water flow (lps) :	2.35	2.35	2.35	2.36	2.352	1.05	1.06	1.05	1.052	1.05
coil height (m) :	0.457	0.457	0.457	0.457	0.457	0.457	0.457	0.457	0.457	0.457
coil length (m) :	0.760	0.760	0.760	0.760	0.760	0.760	0.760	0.760	0.760	0.760
rows :	1	1	1	1	1	1	1	1	1	1
no. of tubes high :	12	12	12	12	12	12	12	12	12	12
OUTPUT :										
face area (sq.m) :	0.35	0.35	0.35	0.35	0.35	0.35	0.35	0.35	0.35	0.35
actual fv (m/s) :	0.39	0.58	1.01	1.58	2.10	0.39	0.61	1.00	1.60	2.10
water vel (m/s) :	2.24	2.24	2.24	2.25	2.24	1.01	1.01	1.01	1.00	1.01
water temp rise :	0.33	0.41	0.52	0.64	0.71	0.78	0.97	1.18	1.41	1.53
ent enth (kJ/kg) :	65.87	65.94	65.69	66.15	65.97	72.00	71.91	72.11	71.92	72.18
lvg enth (kJ/kg) :	45.11	48.64	52.87	56.13	57.65	49.80	54.18	58.85	62.13	64.04
lvg dbt (°C) :	18.71	20.45	22.63	24.12	24.92	20.62	22.71	24.88	26.52	27.39
lvg dpt (°C) :	14.50	15.48	16.54	17.41	17.75	16.01	17.16	18.34	19.06	19.50
cooling cap (kw) :	3.25	4.02	5.17	6.32	7.00	3.47	4.29	5.23	6.22	6.78

Results of TEST-P analysis

INPUT DATA :										
Title :	H66B:W4261	H66B:W4271	H66B:W4361	H66B:W4362	H66B:W4363	H72B:W3991	H72B:W3953	H72B:W3952	H72B:W3942	H72B:W3951
edb (°C) :	31.03	31.04	31.05	31.00	30.96	33.63	33.61	33.64	33.62	33.66
edp (°C) :	18.81	18.84	18.72	18.95	18.89	20.30	20.27	20.34	20.27	20.36
ldb (°C) :	19.14	20.98	23.13	24.41	25.08	20.54	22.85	24.99	26.56	27.34
ldp (°C) :	14.65	15.65	16.70	17.67	17.98	15.96	17.22	18.41	19.18	19.57
ewt (°C) :	7.02	7.04	7.00	7.00	7.02	7.02	7.01	7.04	7.01	7.07
lwt (°C) :	7.41	7.50	7.56	7.70	7.79	7.68	7.83	8.09	8.31	8.54
digistrip water (volts) :	3.870	3.870	3.880	3.890	3.880	1.740	1.745	1.740	1.735	1.740
digistrip air (volts) :	0.050	0.110	0.330	0.810	1.440	0.050	0.120	0.320	0.830	1.430
barometric pressure ("Hg) :	30.14	29.78	30.12	30.12	30.12	30.13	30.17	30.17	30.10	30.17
actual condensate (g/s) :	0.53	0.62	0.70	0.73	0.70	0.59	0.67	0.74	0.71	0.65
height of face (m) :	0.457	0.457	0.457	0.457	0.457	0.457	0.457	0.457	0.457	0.457
length of face (m) :	0.760	0.760	0.760	0.760	0.760	0.760	0.760	0.760	0.760	0.760
rows :	1	1	1	1	1	1	1	1	1	1
No. of tubes high :	12	12	12	12	12	12	12	12	12	12
No. of tubes fed :	6	6	6	6	6	6	6	6	6	6
OUTPUT :										
air volume flow (cms) :	0.136	0.202	0.350	0.548	0.730	0.137	0.212	0.346	0.557	0.731
air mass flow (kg/s) :	0.157	0.232	0.403	0.631	0.841	0.156	0.242	0.395	0.635	0.834
water flow rate (lps) :	2.35	2.35	2.35	2.36	2.35	1.05	1.06	1.05	1.05	1.05
entering enthalpy (kJ/kg) :	65.87	65.94	65.69	66.15	65.97	72.00	71.91	72.11	71.92	72.18
leaving enthalpy (kJ/kg) :	45.53	49.19	53.38	56.64	57.97	49.31	54.12	58.80	62.12	63.81
specific volume (m^3/kg) :	0.881	0.881	0.881	0.881	0.881	0.890	0.890	0.890	0.890	0.890
delta (H1 - H2) :	20.34	16.76	12.31	9.51	8.00	22.68	17.78	13.30	9.80	8.37
water side capacity (kw) :	3.831	4.518	5.515	6.911	7.583	2.915	3.632	4.637	5.725	6.492
air side capacity (kw) :	3.188	3.895	4.957	5.997	6.727	3.539	4.297	5.250	6.227	6.976
sensible heat factor :	0.60	0.61	0.66	0.71	0.75	0.59	0.62	0.66	0.74	0.77
ratio of water/air cap. :	1.20	1.16	1.11	1.15	1.13	0.82	0.85	0.88	0.92	0.93
est. condensate (g/kg) :	0.50	0.59	0.66	0.68	0.65	0.57	0.64	0.69	0.64	0.61
act/est condensate :	1.05	1.05	1.05	1.07	1.07	1.04	1.05	1.08	1.12	1.06
coil face area (sq.m) :	0.347	0.347	0.347	0.347	0.347	0.347	0.347	0.347	0.347	0.347
face velocity (m/s) :	0.39	0.58	1.01	1.58	2.10	0.39	0.61	1.00	1.60	2.11
water velocity (m/s) :	2.24	2.24	2.24	2.25	2.24	1.01	1.01	1.01	1.00	1.01
measured water temp.rise :	0.39	0.46	0.56	0.70	0.77	0.66	0.82	1.05	1.30	1.47
corrected water temp.rise :	0.32	0.40	0.50	0.61	0.68	0.80	0.97	1.19	1.41	1.58

Table A5.1 : Comparison of a one row coil performance predicted by "AU COIL SELECTION PROGRAM" with actual test results.

Results of ARI generalisation program. Suitable for 1, 2 or 4 Row, 6FPI, half circuiting.

INPUT :										
TEST CODE :	H66B:W4261	H66B:W4271	H66B:W4361	H66B:W4362	H66B:W4363	H72B:W3991	H72B:W3953	H72B:W3952	H72B:W3942	H72B:W3951
Ent dry bulb temp (°C) :	31.03	31.04	31.05	31.00	30.96	33.63	33.61	33.64	33.62	33.66
Ent dew point temp (°C) :	18.81	18.84	18.72	18.95	18.89	20.30	20.27	20.34	20.27	20.36
Ent water temp (°C) :	7.00	7.04	7.00	7.00	7.00	7.00	7.00	7.04	7.00	7.00
Actual air flow (lps) :	136.0	202.0	350.0	548.0	730.0	137.0	212.0	346.0	557.0	731.0
Water velocity (m/s) :	2.24	2.24	2.24	2.25	2.24	1.00	1.00	1.00	1.00	1.00
Number of tubes fed :	6	6	6	6	6	6	6	6	6	6
Coil height (mm) :	457.0	457.0	457.0	457.0	457.0	457.0	457.0	457.0	457.0	457.0
Coil length (mm) :	760.0	760.0	760.0	760.0	760.0	760.0	760.0	760.0	760.0	760.0
Number of rows :	1	1	1	1	1	1	1	1	1	1
OUTPUT :										
Coil face area (sq.m) :	0.35	0.35	0.35	0.35	0.35	0.35	0.35	0.35	0.35	0.35
Standard air flow (lps) :	130.45	193.75	335.71	525.65	700.34	130.19	201.48	328.79	529.35	694.59
Std face velocity (m/s) :	0.38	0.56	0.97	1.51	2.02	0.37	0.58	0.95	1.52	2.00
Water flow (lps) :	2.35	2.35	2.35	2.36	2.35	1.05	1.05	1.05	1.05	1.05
Water temperature rise :	0.33	0.41	0.53	0.64	0.71	0.80	0.98	1.21	1.43	1.56
Ent enthalpy (kJ/kg) :	65.87	65.94	65.69	66.15	65.97	72.00	71.91	72.11	71.92	72.18
Lvg enthalpy (kJ/kg) :	45.01	48.66	52.84	56.19	57.70	49.60	54.09	58.69	62.07	63.96
Lvg dry bulb temp (°C) :	19.03	20.96	23.30	24.91	25.76	20.96	23.27	25.60	27.41	28.33
Lvg dew point temp (°C) :	14.26	15.21	16.18	17.04	17.36	15.73	16.83	17.92	18.62	19.04
Cooling capacity (kw) :	3.26	4.02	5.17	6.28	6.95	3.50	4.31	5.29	6.26	6.85

Results of TEST-P analysis

INPUT DATA :										
Title :	H66B:W4261	H66B:W4271	H66B:W4361	H66B:W4362	H66B:W4363	H72B:W3991	H72B:W3953	H72B:W3952	H72B:W3942	H72B:W3951
edb (°C) :	31.03	31.04	31.05	31.00	30.96	33.63	33.61	33.64	33.62	33.66
edp (°C) :	18.81	18.84	18.72	18.95	18.89	20.30	20.27	20.34	20.27	20.36
ldb (°C) :	19.14	20.98	23.13	24.41	25.08	20.54	22.85	24.99	26.56	27.34
ldp (°C) :	14.65	15.65	16.70	17.67	17.98	15.96	17.22	18.41	19.18	19.57
ewt (°C) :	7.02	7.04	7.00	7.00	7.02	7.02	7.01	7.04	7.01	7.07
lwt (°C) :	7.41	7.50	7.56	7.70	7.79	7.68	7.83	8.09	8.31	8.54
digistrip water (volts) :	3.870	3.870	3.880	3.890	3.880	1.740	1.745	1.740	1.735	1.740
digistrip air (volts) :	0.050	0.110	0.330	0.810	1.440	0.050	0.120	0.320	0.830	1.430
barometric pressure ("Hg) :	30.14	29.78	30.12	30.12	30.12	30.13	30.17	30.17	30.10	30.17
actual condensate (g/s) :	0.53	0.62	0.70	0.73	0.70	0.59	0.67	0.74	0.71	0.65
height of face (m) :	0.457	0.457	0.457	0.457	0.457	0.457	0.457	0.457	0.457	0.457
length of face (m) :	0.760	0.760	0.760	0.760	0.760	0.760	0.760	0.760	0.760	0.760
rows :	1	1	1	1	1	1	1	1	1	1
No. of tubes high :	12	12	12	12	12	12	12	12	12	12
No. of tubes fed :	6	6	6	6	6	6	6	6	6	6
OUTPUT :										
air volume flow (cms) :	0.136	0.202	0.350	0.548	0.730	0.137	0.212	0.346	0.557	0.731
air mass flow (kg/s) :	0.157	0.232	0.403	0.631	0.841	0.156	0.242	0.395	0.635	0.834
water flow rate (lps) :	2.35	2.35	2.35	2.36	2.35	1.05	1.06	1.05	1.05	1.05
entering enthalpy (kJ/kg) :	65.87	65.94	65.69	66.15	65.97	72.00	71.91	72.11	71.92	72.18
leaving enthalpy (kJ/kg) :	45.53	49.19	53.38	56.64	57.97	49.31	54.12	58.80	62.12	63.81
specific volume (m^3/kg) :	0.881	0.881	0.881	0.881	0.881	0.890	0.890	0.890	0.890	0.890
delta (H1 - H2) :	20.34	16.76	12.31	9.51	8.00	22.68	17.78	13.30	9.80	8.37
water side capacity (kw) :	3.831	4.518	5.515	6.911	7.583	2.915	3.632	4.637	5.725	6.492
air side capacity (kw) :	3.188	3.895	4.957	5.997	6.727	3.539	4.297	5.250	6.227	6.976
sensible heat factor :	0.60	0.61	0.66	0.71	0.75	0.59	0.62	0.66	0.74	0.77
ratio of water/air cap. :	1.20	1.16	1.11	1.15	1.13	0.82	0.85	0.88	0.92	0.93
est. condensate (g/kg) :	0.50	0.59	0.66	0.68	0.65	0.57	0.64	0.69	0.64	0.61
act/est condensate :	1.05	1.05	1.05	1.07	1.07	1.04	1.05	1.08	1.12	1.06
coil face area (sq.m) :	0.347	0.347	0.347	0.347	0.347	0.347	0.347	0.347	0.347	0.347
face velocity (m/s) :	0.39	0.58	1.01	1.58	2.10	0.39	0.61	1.00	1.60	2.11
water velocity (m/s) :	2.24	2.24	2.24	2.25	2.24	1.01	1.01	1.01	1.00	1.01
measured water temp.rise :	0.39	0.46	0.56	0.70	0.77	0.66	0.82	1.05	1.30	1.47
corrected water temp.rise :	0.32	0.40	0.50	0.61	0.68	0.80	0.97	1.19	1.41	1.58

Table A5.1a : Comparison of a one row coil performance predicted by "ARI GENERALISATION PROGRAM" with actual test results.

Results of AU (ADELAIDE UNIVERSITY)
coil selection program. Suitable for
1, 2 or 4 Row, 6 fpi, half circuiting.

INPUT DATA :										
Title :	H78B:W4021	H78B:W4022	H78B:W4023	H78B:W2831	H78B:W2832	H66A:W4211	H66A:W4213	H66A:W4231	H78A:W4151	H78A:W4152
ent dbt (°C) :	35.41	35.27	35.53	35.54	35.35	26.00	26.00	26.00	29.01	29.04
ent dpt (°C) :	21.89	22.06	22.02	22.00	22.08	21.00	20.94	20.94	24.30	24.30
ent water temp (°C) :	7.02	6.96	7.05	7.09	6.95	7.03	7.00	7.02	6.98	7.17
act air vol (cms) :	0.141	0.205	0.354	0.556	0.734	0.348	0.550	0.723	0.345	0.551
water flow (lps) :	1.04	1.04	1.05	1.07	1.067	2.35	2.35	2.34	2.340	2.34
coil height (m) :	0.457	0.457	0.457	0.457	0.457	0.457	0.457	0.457	0.457	0.457
coil length (m) :	0.760	0.760	0.760	0.760	0.760	0.760	0.760	0.760	0.760	0.760
rows :	1	1	1	1	1	1	1	1	1	1
no. of tubes high :	12	12	12	12	12	12	12	12	12	12
OUTPUT :										
face area (sq.m) :	0.35	0.35	0.35	0.35	0.35	0.35	0.35	0.35	0.35	0.35
actual fv (m/s) :	0.41	0.59	1.02	1.60	2.11	1.00	1.58	2.08	0.99	1.59
water vel (m/s) :	0.99	0.99	1.00	1.02	1.02	2.24	2.24	2.23	2.23	2.23
water temp rise :	0.89	1.08	1.34	1.54	1.69	0.53	0.64	0.71	0.66	0.80
ent enth (kJ/kg) :	77.87	78.18	78.34	78.30	78.32	65.89	65.74	65.74	78.12	78.15
lvg enth (kJ/kg) :	53.43	57.89	63.75	67.34	69.22	53.10	55.92	57.49	61.77	65.82
lvg dbt (°C) :	21.85	23.75	26.43	28.10	28.87	20.19	21.38	22.01	22.60	24.07
lvg dpt (°C) :	17.22	18.42	19.80	20.58	21.02	17.89	18.63	19.05	20.61	21.62
cooling cap (kw) :	3.90	4.72	5.85	6.90	7.57	5.20	6.31	6.97	6.51	7.85

Results of TEST-P analysis

INPUT DATA :										
Title :	H78B:W4021	H78B:W4022	H78B:W4023	H78B:W2831	H78B:W2832	H66A:W4211	H66A:W4213	H66A:W4231	H78A:W4151	H78A:W4152
edb (°C) :	35.41	35.27	35.53	35.54	35.35	26.01	26.00	26.00	29.01	29.04
edp (°C) :	21.89	22.06	22.02	22.00	22.08	21.00	20.94	20.94	24.30	24.30
ldb (°C) :	21.65	23.88	26.50	28.33	29.17	20.40	21.56	22.08	22.98	24.27
ldp (°C) :	17.13	18.44	19.74	20.74	21.18	18.03	18.84	19.24	20.81	21.82
ewt (°C) :	7.02	6.96	7.05	7.09	6.95	7.03	7.00	7.02	6.98	7.17
lwt (°C) :	7.77	7.88	8.25	8.70	8.73	7.60	7.70	7.80	7.70	8.04
digistrip water (volts) :	1.720	1.720	1.725	1.760	1.760	3.870	3.870	3.860	3.860	3.860
digistrip air (volts) :	0.053	0.112	0.332	0.820	1.430	0.332	0.830	1.434	0.322	0.822
barometric pressure ("Hg) :	29.74	29.74	29.74	29.88	29.88	30.26	30.26	30.16	30.50	30.50
actual condensate (g/s) :	0.72	0.84	0.92	0.86	0.80	1.14	1.35	1.44	1.58	1.90
height of face (m) :	0.457	0.457	0.457	0.457	0.457	0.457	0.457	0.457	0.457	0.457
length of face (m) :	0.760	0.760	0.760	0.760	0.760	0.760	0.760	0.760	0.760	0.760
rows :	1	1	1	1	1	1	1	1	1	1
No. of tubes high :	12	12	12	12	12	12	12	12	12	12
No. of tubes fed :	6	6	6	6	6	6	6	6	6	6
OUTPUT :										
air volume flow (cms) :	0.141	0.205	0.354	0.556	0.734	0.348	0.550	0.723	0.345	0.551
air mass flow (kg/s) :	0.160	0.233	0.401	0.629	0.831	0.407	0.643	0.846	0.398	0.636
water flow rate (lps) :	1.04	1.04	1.05	1.07	1.07	2.35	2.35	2.34	2.34	2.34
entering enthalpy (kJ/kg) :	77.87	78.18	78.34	78.30	78.32	65.90	65.74	65.74	78.12	78.15
leaving enthalpy (kJ/kg) :	52.72	57.73	63.34	67.63	69.60	53.29	56.23	57.66	62.31	66.22
specific volume (m^3/kg) :	0.897	0.897	0.898	0.898	0.898	0.869	0.869	0.869	0.882	0.883
delta (H1 - H2) :	25.16	20.45	15.00	10.67	8.72	12.61	9.51	8.08	15.81	11.94
water side capacity (kw) :	3.274	4.016	5.254	7.192	7.952	5.599	6.876	7.642	7.054	8.524
air side capacity (kw) :	4.027	4.760	6.007	6.714	7.246	5.131	6.117	6.831	6.299	7.596
sensible heat factor :	0.56	0.57	0.62	0.69	0.72	0.45	0.48	0.50	0.39	0.41
ratio of water/air cap. :	0.81	0.84	0.87	1.07	1.10	1.09	1.12	1.12	1.12	1.12
est. condensate (g/kg) :	0.69	0.80	0.90	0.80	0.76	1.10	1.25	1.35	1.50	1.75
act/est condensate :	1.04	1.05	1.03	1.08	1.05	1.04	1.08	1.07	1.05	1.09
coil face area (sq.m) :	0.347	0.347	0.347	0.347	0.347	0.347	0.347	0.347	0.347	0.347
face velocity (m/s) :	0.41	0.59	1.02	1.60	2.11	1.00	1.58	2.08	0.99	1.59
water velocity (m/s) :	0.99	0.99	1.00	1.02	1.02	2.24	2.24	2.23	2.23	2.23
measured water temp.rise :	0.75	0.92	1.20	1.61	1.78	0.57	0.70	0.78	0.72	0.87
corrected water temp.rise :	0.92	1.09	1.37	1.50	1.62	0.52	0.62	0.70	0.64	0.78

Table A5.2 : Comparison of a one row coil performance predicted by "AU COIL SELECTION PROGRAM" with actual test results.

Results of ARI generalisation program. Suitable for 1, 2 or 4 Row, 6FPI, half circuiting.

INPUT :										
TEST CODE :	H78B:W4021	H78B:W4022	H78B:W4023	H78B:W2831	H78B:W2832	H66A:W4211	H66A:W4213	H66A:W4231	H78A:W4151	H78A:W4152
Ent dry bulb temp (°C) :	35.41	35.27	35.53	35.54	35.35	26.00	26.00	26.00	29.00	29.04
Ent dew point temp (°C) :	21.89	22.06	22.02	22.00	22.08	21.00	20.94	20.94	24.30	24.30
Ent water temp (°C) :	7.02	6.96	7.05	7.09	6.95	7.00	7.00	7.00	7.00	7.17
Actual air flow (lps) :	141.0	205.0	354.0	556.0	734.0	348.0	550.0	723.0	345.0	551.0
Water velocity (m/s) :	1.00	1.00	1.00	1.00	1.00	2.24	2.24	2.24	2.23	2.23
Number of tubes fed :	6	6	6	6	6	6	6	6	6	6
Coil height (mm) :	457.0	457.0	457.0	457.0	457.0	457.0	457.0	457.0	457.0	457.0
Coil length (mm) :	760.0	760.0	760.0	760.0	760.0	760.0	760.0	760.0	760.0	760.0
Number of rows :	1	1	1	1	1	1	1	1	1	1
OUTPUT :										
Coil face area (sq.m) :	0.35	0.35	0.35	0.35	0.35	0.35	0.35	0.35	0.35	0.35
Standard air flow (lps) :	133.10	193.58	334.01	524.58	692.92	339.01	535.81	704.34	332.06	530.26
Std face velocity (m/s) :	0.38	0.56	0.96	1.51	2.00	0.98	1.54	2.03	0.96	1.53
Water flow (lps) :	1.05	1.05	1.05	1.05	1.05	2.35	2.35	2.35	2.34	2.34
Water temperature rise :	0.90	1.09	1.36	1.59	1.74	0.53	0.64	0.71	0.67	0.81
Ent enthalpy (kJ/kg) :	77.87	78.18	78.34	78.30	78.32	65.89	65.74	65.74	78.11	78.15
Lvg enthalpy (kJ/kg) :	53.16	57.69	63.47	67.24	69.13	53.06	55.99	57.54	61.58	65.74
Lvg dry bulb temp (°C) :	22.17	24.24	27.13	29.00	29.81	20.36	21.65	22.31	22.63	24.23
Lvg dew point temp (°C) :	16.93	18.10	19.37	20.16	20.59	17.79	18.54	18.93	20.52	21.52
Cooling capacity (kw) :	3.95	4.76	5.96	6.97	7.64	5.22	6.27	6.93	6.59	7.90

Results of TEST-P analysis

INPUT DATA :										
Title :	H78B:W4021	H78B:W4022	H78B:W4023	H78B:W2831	H78B:W2832	H66A:W4211	H66A:W4213	H66A:W4231	H78A:W4151	H78A:W4152
edb (°C) :	35.41	35.27	35.53	35.54	35.35	26.01	26.00	26.00	29.01	29.04
edp (°C) :	21.89	22.06	22.02	22.00	22.08	21.00	20.94	20.94	24.30	24.30
ldb (°C) :	21.65	23.88	26.50	28.33	29.17	20.40	21.56	22.08	22.98	24.27
ldp (°C) :	17.13	18.44	19.74	20.74	21.18	18.03	18.84	19.24	20.81	21.82
ewt (°C) :	7.02	6.96	7.05	7.09	6.95	7.03	7.00	7.02	6.98	7.17
lwt (°C) :	7.77	7.88	8.25	8.70	8.73	7.60	7.70	7.80	7.70	8.04
digistrip water (volts) :	1.720	1.720	1.725	1.760	1.760	3.870	3.870	3.860	3.860	3.860
digistrip air (volts) :	0.053	0.112	0.332	0.820	1.430	0.332	0.830	1.434	0.322	0.822
barometric pressure ("Hg) :	29.74	29.74	29.74	29.88	29.88	30.26	30.26	30.16	30.50	30.50
actual condensate (g/s) :	0.72	0.84	0.92	0.86	0.80	1.14	1.35	1.44	1.58	1.90
height of face (m) :	0.457	0.457	0.457	0.457	0.457	0.457	0.457	0.457	0.457	0.457
length of face (m) :	0.760	0.760	0.760	0.760	0.760	0.760	0.760	0.760	0.760	0.760
rows :	1	1	1	1	1	1	1	1	1	1
No. of tubes high :	12	12	12	12	12	12	12	12	12	12
No. of tubes fed :	6	6	6	6	6	6	6	6	6	6
OUTPUT :										
air volume flow (cms) :	0.141	0.205	0.354	0.556	0.734	0.348	0.550	0.723	0.345	0.551
air mass flow (kg/s) :	0.160	0.233	0.401	0.629	0.831	0.407	0.643	0.846	0.398	0.636
water flow rate (lps) :	1.04	1.04	1.05	1.07	1.07	2.35	2.35	2.34	2.34	2.34
entering enthalpy (kJ/kg) :	77.87	78.18	78.34	78.30	78.32	65.90	65.74	65.74	78.12	78.15
leaving enthalpy (kJ/kg) :	52.72	57.73	63.34	67.63	69.60	53.29	56.23	57.66	62.31	66.22
specific volume (m^3/kg) :	0.897	0.897	0.898	0.898	0.898	0.869	0.869	0.869	0.882	0.883
delta (H1 - H2) :	25.16	20.45	15.00	10.67	8.72	12.61	9.51	8.08	15.81	11.94
water side capacity (kw) :	3.274	4.016	5.254	7.192	7.952	5.599	6.876	7.642	7.054	8.524
air side capacity (kw) :	4.027	4.760	6.007	6.714	7.246	5.131	6.117	6.831	6.299	7.596
sensible heat factor :	0.56	0.57	0.62	0.69	0.72	0.45	0.48	0.50	0.39	0.41
ratio of water/air cap. :	0.81	0.84	0.87	1.07	1.10	1.09	1.12	1.12	1.12	1.12
est. condensate (g/kg) :	0.69	0.80	0.90	0.80	0.76	1.10	1.25	1.35	1.50	1.75
act/est condensate :	1.04	1.05	1.03	1.08	1.05	1.04	1.08	1.07	1.05	1.09
coil face area (sq.m) :	0.347	0.347	0.347	0.347	0.347	0.347	0.347	0.347	0.347	0.347
face velocity (m/s) :	0.41	0.59	1.02	1.60	2.11	1.00	1.58	2.08	0.99	1.59
water velocity (m/s) :	0.99	0.99	1.00	1.02	1.02	2.24	2.24	2.23	2.23	2.23
measured water temp.rise :	0.75	0.92	1.20	1.61	1.78	0.57	0.70	0.78	0.72	0.87
corrected water temp.rise :	0.92	1.09	1.37	1.50	1.62	0.52	0.62	0.70	0.64	0.78

Table A5.2a : Comparison of a one row coil performance predicted by "ARI GENERALISATION PROGRAM" with actual test results.

Results of AU (ADELAIDE UNIVERSITY)
coil selection program. Suitable for
1, 2 or 4 Row, 6 fpi, half circuiting.

INPUT DATA :										
Title :	H72A:W3774	H72A:W3814	H72A:W3813	H78A:W3762	H78A:W3802	H66A:W4053	H66A:W4121	H72A:W4002	H72A:W4003	H72A:W4004
ent dbt (°C) :	27.35	27.60	27.65	28.92	28.98	26.03	26.06	27.63	27.62	27.62
ent dpt (°C) :	22.75	22.85	22.76	24.21	24.30	21.00	21.03	22.65	22.69	22.72
ent water temp (°C) :	7.08	6.96	7.02	7.02	7.05	7.00	7.00	7.02	7.02	7.00
act air vol (cms) :	0.349	0.550	0.723	0.351	0.550	0.348	0.550	0.350	0.549	0.725
water flow (lps) :	1.72	1.72	1.71	1.71	1.706	1.06	1.05	1.06	1.058	1.06
coil height (m) :	0.457	0.457	0.457	0.457	0.457	0.457	0.457	0.457	0.457	0.457
coil length (m) :	0.760	0.760	0.760	0.760	0.760	0.760	0.760	0.760	0.760	0.760
rows :	1	1	1	1	1	1	1	1	1	1
no. of tubes high :	12	12	12	12	12	12	12	12	12	12
OUTPUT :										
face area (sq.m) :	0.35	0.35	0.35	0.35	0.35	0.35	0.35	0.35	0.35	0.35
actual fv (m/s) :	1.00	1.58	2.08	1.01	1.58	1.00	1.58	1.01	1.58	2.09
water vel (m/s) :	1.64	1.64	1.63	1.63	1.63	1.01	1.01	1.01	1.01	1.01
water temp rise :	0.79	0.96	1.05	0.88	1.05	1.06	1.26	1.19	1.41	1.54
ent enth (kJ/kg) :	71.90	72.44	72.24	77.76	78.09	65.92	66.02	71.92	72.02	72.10
lvg enth (kJ/kg) :	57.97	61.64	63.28	62.26	66.23	54.38	57.35	58.92	62.23	64.00
lvg dbt (°C) :	21.54	22.95	23.63	22.79	24.18	20.66	21.85	22.00	23.22	23.87
lvg dpt (°C) :	19.47	20.42	20.80	20.73	21.73	18.26	19.06	19.68	20.54	20.99
cooling cap (kw) :	5.65	6.90	7.53	6.28	7.54	4.69	5.57	5.28	6.24	6.82

Results of TEST-P analysis

INPUT DATA :										
Title :	H72A:W3774	H72A:W3814	H72A:W3813	H78A:W3762	H78A:W3802	H66A:W4053	H66A:W4121	H72A:W4002	H72A:W4003	H72A:W4004
edb (°C) :	27.35	27.60	27.65	28.92	28.98	26.03	26.06	27.63	27.62	27.62
edp (°C) :	22.75	22.85	22.76	24.21	24.30	21.00	21.03	22.65	22.69	22.72
ldb (°C) :	21.74	23.06	23.63	22.92	24.22	20.87	21.93	22.11	23.33	23.89
ldp (°C) :	19.52	20.54	20.91	20.71	21.79	18.31	19.22	19.69	20.69	21.11
ewt (°C) :	7.08	6.96	7.02	7.02	7.05	7.01	7.00	7.02	7.02	7.01
lwt (°C) :	7.72	7.78	7.95	7.76	8.00	7.87	8.02	8.08	8.32	8.46
digistrip water (volts) :	2.830	2.835	2.825	2.815	2.815	1.745	0.565	1.745	1.745	1.745
digistrip air (volts) :	0.332	0.823	1.422	0.333	0.820	0.332	1.050	0.333	0.820	1.430
barometric pressure ("Hg) :	30.06	30.08	30.08	30.13	30.14	29.98	1.17	30.14	30.14	30.14
actual condensate (g/s) :	1.38	1.64	1.70	1.57	1.87	1.04	0.46	1.22	1.40	1.50
height of face (m) :	0.457	0.457	0.457	0.457	0.457	0.457	0.760	0.457	0.457	0.457
length of face (m) :	0.760	0.760	0.760	0.760	0.760	0.760	6.000	0.760	0.760	0.760
rows :	1	1	1	1	1	1	1	1	1	1
No. of tubes high :	12	12	12	12	12	12	20	12	12	12
No. of tubes fed :	6	6	6	6	6	6	1	6	6	6
OUTPUT :										
air volume flow (cms) :	0.349	0.550	0.723	0.351	0.550	0.348	0.616	0.350	0.549	0.725
air mass flow (kg/s) :	0.406	0.639	0.839	0.405	0.636	0.407	0.720	0.406	0.637	0.842
water flow rate (lps) :	1.72	1.72	1.71	1.71	1.71	1.06	0.34	1.06	1.06	1.06
entering enthalpy (kJ/kg) :	71.90	72.44	72.24	77.76	78.09	65.92	66.02	71.92	72.02	72.10
leaving enthalpy (kJ/kg) :	57.95	61.73	63.23	62.00	66.09	54.37	57.46	58.72	62.37	63.99
specific volume (m^3/kg) :	0.875	0.876	0.876	0.882	0.882	0.869	0.869	0.876	0.876	0.876
delta (H1 - H2) :	13.95	10.72	9.02	15.76	12.00	11.55	8.56	13.19	9.65	8.10
water side capacity (kw) :	4.597	5.900	6.668	5.287	6.788	3.809	1.463	4.695	5.758	6.422
air side capacity (kw) :	5.663	6.843	7.567	6.384	7.631	4.700	6.167	5.360	6.149	6.822
sensible heat factor :	0.41	0.43	0.46	0.39	0.41	0.46	0.49	0.43	0.45	0.47
ratio of water/air cap. :	0.81	0.86	0.88	0.83	0.89	0.81	0.24	0.88	0.94	0.94
est. condensate (g/kg) :	1.30	1.51	1.61	1.52	1.77	1.00	1.22	1.20	1.31	1.41
act/est condensate :	1.06	1.08	1.06	1.03	1.06	1.04	0.37	1.02	1.07	1.06
coil face area (sq.m) :	0.347	0.347	0.347	0.347	0.347	0.347	4.560	0.347	0.347	0.347
face velocity (m/s) :	1.01	1.58	2.08	1.01	1.58	1.00	0.14	1.01	1.58	2.09
water velocity (m/s) :	1.64	1.64	1.63	1.63	1.63	1.01	1.96	1.01	1.01	1.01
measured water temp.rise :	0.64	0.82	0.93	0.74	0.95	0.86	1.02	1.06	1.30	1.45
corrected water temp.rise :	0.79	0.95	1.06	0.89	1.07	1.06	1.25	1.21	1.39	1.54

Table A5.3 : Comparison of a one row coil performance predicted by "AU COIL SELECTION PROGRAM" with actual test results.

Results of ARI generalisation program. Suitable for 1, 2 or 4 Row, 6FPI, half circuiting.

INPUT :										
TEST CODE :	H72A:W3774	H72A:W3814	H72A:W3813	H78A:W3762	H78A:W3802	H66A:W4053	H66A:W4121	H72A:W4002	H72A:W4003	H72A:W4004
Ent dry bulb temp (°C) :	27.35	27.60	27.65	28.92	28.98	26.00	26.06	27.63	27.60	27.60
Ent dew point temp (°C) :	22.75	22.85	22.76	24.21	24.30	21.00	21.00	22.65	22.70	22.70
Ent water temp (°C) :	7.08	7.00	7.00	7.00	7.05	7.00	7.00	7.00	7.00	7.00
Actual air flow (lps) :	349.0	550.0	723.0	351.0	550.0	348.0	550.0	350.0	549.0	725.0
Water velocity (m/s) :	1.64	1.64	1.63	1.63	1.63	1.00	1.00	1.00	1.00	1.00
Number of tubes fed :	6	6	6	6	6	6	6	6	6	6
Coil height (mm) :	457.0	457.0	457.0	457.0	457.0	457.0	457.0	457.0	457.0	457.0
Coil length (mm) :	760.0	760.0	760.0	760.0	760.0	760.0	760.0	760.0	760.0	760.0
Number of rows :	1	1	1	1	1	1	1	1	1	1
OUTPUT :										
Coil face area (sq.m) :	0.35	0.35	0.35	0.35	0.35	0.35	0.35	0.35	0.35	0.35
Standard air flow (lps) :	338.10	532.34	699.71	337.94	529.40	339.01	535.68	338.77	531.42	701.79
Std face velocity (m/s) :	0.97	1.53	2.01	0.97	1.52	0.98	1.54	0.98	1.53	2.02
Water flow (lps) :	1.72	1.72	1.71	1.71	1.71	1.05	1.05	1.05	1.05	1.05
Water temperature rise :	0.79	0.96	1.06	0.89	1.06	1.07	1.27	1.22	1.43	1.56
Ent enthalpy (kJ/kg) :	71.90	72.44	72.24	77.76	78.09	65.89	65.95	71.92	72.02	72.02
Lvg enthalpy (kJ/kg) :	57.84	61.64	63.25	62.03	66.12	54.29	57.30	58.77	62.18	63.89
Lvg dry bulb temp (°C) :	21.63	23.16	23.89	22.83	24.34	20.84	22.13	22.15	23.45	24.13
Lvg dew point temp (°C) :	19.37	20.32	20.68	20.62	21.63	18.14	18.91	19.55	20.42	20.84
Cooling capacity (kw) :	5.71	6.90	7.55	6.38	7.60	4.72	5.56	5.34	6.28	6.85

Results of TEST-P analysis

INPUT DATA :										
Title :	H72A:W3774	H72A:W3814	H72A:W3813	H78A:W3762	H78A:W3802	H66A:W4053	H66A:W4121	H72A:W4002	H72A:W4003	H72A:W4004
edb (°C) :	27.35	27.60	27.65	28.92	28.98	26.03	26.06	27.63	27.62	27.62
edp (°C) :	22.75	22.85	22.76	24.21	24.30	21.00	21.03	22.65	22.69	22.72
ldb (°C) :	21.74	23.06	23.63	22.92	24.22	20.87	21.93	22.11	23.33	23.89
ldp (°C) :	19.52	20.54	20.91	20.71	21.79	18.31	19.22	19.69	20.69	21.11
ewt (°C) :	7.08	6.96	7.02	7.02	7.05	7.01	7.00	7.02	7.02	7.01
lwt (°C) :	7.72	7.78	7.95	7.76	8.00	7.87	8.02	8.08	8.32	8.46
digistrip water (volts) :	2.830	2.835	2.825	2.815	2.815	1.745	0.565	1.745	1.745	1.745
digistrip air (volts) :	0.332	0.823	1.422	0.333	0.820	0.332	1.050	0.333	0.820	1.430
barometric pressure ("Hg) :	30.06	30.08	30.08	30.13	30.14	29.98	1.17	30.14	30.14	30.14
actual condensate (g/s) :	1.38	1.64	1.70	1.57	1.87	1.04	0.46	1.22	1.40	1.50
height of face (m) :	0.457	0.457	0.457	0.457	0.457	0.457	0.760	0.457	0.457	0.457
length of face (m) :	0.760	0.760	0.760	0.760	0.760	0.760	6.000	0.760	0.760	0.760
rows :	1	1	1	1	1	1	1	1	1	1
No. of tubes high :	12	12	12	12	12	12	20	12	12	12
No. of tubes fed :	6	6	6	6	6	6	1	6	6	6
OUTPUT :										
air volume flow (cms) :	0.349	0.550	0.723	0.351	0.550	0.348	0.616	0.350	0.549	0.725
air mass flow (kg/s) :	0.406	0.639	0.839	0.405	0.636	0.407	0.720	0.406	0.637	0.842
water flow rate (lps) :	1.72	1.72	1.71	1.71	1.71	1.06	0.34	1.06	1.06	1.06
entering enthalpy (kJ/kg) :	71.90	72.44	72.24	77.76	78.09	65.92	66.02	71.92	72.02	72.10
leaving enthalpy (kJ/kg) :	57.95	61.73	63.23	62.00	66.09	54.37	57.46	58.72	62.37	63.99
specific volume (m^3/kg) :	0.875	0.876	0.876	0.882	0.882	0.869	0.869	0.876	0.876	0.876
delta (H1 - H2) :	13.95	10.72	9.02	15.76	12.00	11.55	8.56	13.19	9.65	8.10
water side capacity (kw) :	4.597	5.900	6.668	5.287	6.788	3.809	1.463	4.695	5.758	6.422
air side capacity (kw) :	5.663	6.843	7.567	6.384	7.631	4.700	6.167	5.360	6.149	6.822
sensible heat factor :	0.41	0.43	0.46	0.39	0.41	0.46	0.49	0.43	0.45	0.47
ratio of water/air cap. :	0.81	0.86	0.88	0.83	0.89	0.81	0.24	0.88	0.94	0.94
est. condensate (g/kg) :	1.30	1.51	1.61	1.52	1.77	1.00	1.22	1.20	1.31	1.41
act/est condensate :	1.06	1.08	1.06	1.03	1.06	1.04	0.37	1.02	1.07	1.06
coil face area (sq.m) :	0.347	0.347	0.347	0.347	0.347	0.347	4.560	0.347	0.347	0.347
face velocity (m/s) :	1.01	1.58	2.08	1.01	1.58	1.00	0.14	1.01	1.58	2.09
water velocity (m/s) :	1.64	1.64	1.63	1.63	1.63	1.01	1.96	1.01	1.01	1.01
measured water temp.rise :	0.64	0.82	0.93	0.74	0.95	0.86	1.02	1.06	1.30	1.45
corrected water temp.rise :	0.79	0.95	1.06	0.89	1.07	1.06	1.25	1.21	1.39	1.54

Table A5.3a : Comparison of a one row coil performance predicted by "ARI GENERALISATION PROGRAM" with actual test results.

Results of AU (ADELAIDE UNIVERSITY)
coil selection program. Suitable for
1, 2 or 4 Row, 6 fpi, half circuiting.

INPUT DATA :								
Title :	H66D:W5472	H66D:W5201	H66A:W6031	H60A:W5461	H60B:W5431	H78A:W5641	H78C:W6092	H78C:W5601
ent dbt (°C) :	33.99	34.09	25.96	26.04	30.00	29.03	32.05	31.82
ent dpt (°C) :	17.41	17.42	20.98	18.53	16.36	24.35	23.28	23.27
ent water temp (°C) :	6.98	6.98	6.99	6.99	7.00	7.04	6.94	7.00
act air vol (cms) :	0.203	0.346	0.270	0.209	0.210	0.272	0.106	0.273
water flow (lps) :	1.68	1.69	0.85	1.68	1.691	0.84	0.84	0.84
coil height (m) :	0.457	0.457	0.229	0.457	0.457	0.229	0.229	0.229
coil length (m) :	0.760	0.760	0.760	0.760	0.760	0.760	0.760	0.760
rows :	2	2	2	2	2	2	2	2
no. of tubes high :	12	12	6	12	12	6	6	6
OUTPUT :								
face area (sq.m) :	0.35	0.35	0.17	0.35	0.35	0.17	0.17	0.17
actual fv (m/s) :	0.58	1.00	1.55	0.60	0.60	1.56	0.61	1.57
water vel (m/s) :	1.61	1.61	1.62	1.61	1.61	1.61	1.60	1.61
water temp rise :	0.94	1.30	1.62	0.84	0.82	2.05	1.24	2.04
ent enth (kJ/kg) :	65.90	66.02	65.80	60.14	59.73	78.29	78.25	77.99
lvg enth (kJ/kg) :	37.34	42.75	47.52	35.88	35.66	55.20	42.41	54.90
lvg dbt (°C) :	14.96	17.56	17.64	13.36	14.03	19.98	15.79	20.64
lvg dpt (°C) :	12.06	13.80	16.41	12.16	11.56	18.95	14.66	18.51
cooling cap (kw) :	6.61	9.18	5.77	5.93	5.84	7.26	4.35	7.22

Results of TEST-P analysis

INPUT DATA :								
Title :	H66D:W5472	H66D:W5201	H66A:W6031	H60A:W5461	H60B:W5431	H78A:W5641	H78C:W6092	H78C:W5601
edb (°C) :	33.99	34.09	25.96	26.04	30.00	29.03	32.05	31.82
edp (°C) :	17.41	17.42	20.98	18.53	16.36	24.35	23.28	23.27
ldb (°C) :	14.65	17.46	17.59	13.33	13.85	19.72	15.76	20.32
ldp (°C) :	12.10	14.06	16.52	12.02	11.55	18.91	14.62	18.54
ewt (°C) :	6.98	6.98	6.99	6.99	7.00	7.04	6.94	7.00
lwt (°C) :	7.84	8.21	8.52	7.78	7.78	8.88	8.14	8.83
digistrip water (volts) :	2.780	2.790	1.400	2.780	2.790	1.390	1.380	1.390
digistrip air (volts) :	0.110	0.320	0.200	0.120	0.120	0.200	0.030	0.200
barometric pressure ("Hg) :	30.25	30.44	29.92	30.09	31.60	29.84	30.15	29.84
actual condensate (g/s) :	0.84	0.96	1.19	1.13	0.77	1.71	0.92	1.43
height of face (m) :	0.457	0.457	0.229	0.457	0.457	0.229	0.229	0.229
length of face (m) :	0.760	0.760	0.760	0.760	0.760	0.760	0.760	0.760
rows :	2	2	2	2	2	2	2	2
No. of tubes high :	12	12	6	12	12	6	6	6
No. of tubes fed :	6	6	3	6	6	3	3	3
OUTPUT :								
air volume flow (cms) :	0.203	0.346	0.270	0.209	0.210	0.272	0.106	0.273
air mass flow (kg/s) :	0.231	0.395	0.316	0.245	0.243	0.314	0.121	0.313
water flow rate (lps) :	1.69	1.69	0.85	1.69	1.69	0.84	0.84	0.84
entering enthalpy (kJ/kg) :	65.90	66.02	65.80	60.14	59.73	78.29	78.25	77.99
leaving enthalpy (kJ/kg) :	36.86	42.81	47.37	35.40	35.25	54.50	42.03	54.30
specific volume (m^3/kg) :	0.888	0.888	0.869	0.866	0.875	0.883	0.890	0.889
delta (H1 - H2) :	29.04	23.21	18.43	24.73	24.48	23.79	36.22	23.68
water side capacity (kw) :	6.068	8.710	5.437	5.574	5.524	6.492	4.203	6.456
air side capacity (kw) :	6.719	9.160	5.822	6.055	5.957	7.470	4.384	7.404
sensible heat factor :	0.68	0.73	0.46	0.53	0.67	0.40	0.46	0.50
ratio of water/air cap. :	0.90	0.95	0.93	0.92	0.93	0.87	0.96	0.87
est. condensate (g/kg) :	0.85	0.97	1.23	1.14	0.77	1.75	0.93	1.45
act/est condensate :	0.99	0.99	0.97	0.99	1.00	0.98	0.99	0.98
coil face area (sq.m) :	0.347	0.347	0.174	0.347	0.347	0.174	0.174	0.174
face velocity (m/s) :	0.58	1.00	1.55	0.60	0.61	1.56	0.61	1.57
water velocity (m/s) :	1.61	1.61	1.62	1.61	1.61	1.61	1.60	1.61
measured water temp.rise :	0.86	1.23	1.53	0.79	0.78	1.84	1.20	1.83
corrected water temp.rise :	0.95	1.29	1.64	0.86	0.84	2.12	1.25	2.10

Table A5.4 : Comparison of a two row coil performance predicted by "AU COIL SELECTION PROGRAM" with actual test results.

Results of ARI generalisation program. Suitable for 1, 2 or 4 Row, 6FPI, half circuiting.

INPUT :								
TEST CODE :	H66D:W5472	H66D:W5201	H66A:W6031	H60A:W5461	H60B:W5431	H78A:W5641	H78C:W6092	H78C:W5601
Ent dry bulb temp (°C) :	33.99	34.09	25.96	26.04	30.00	29.03	32.05	31.82
Ent dew point temp (°C) :	17.40	17.42	20.98	18.53	16.36	24.35	23.28	23.27
Ent water temp (°C) :	6.98	6.98	6.99	6.99	7.00	7.04	6.94	7.00
Actual air flow (lps) :	203.0	346.0	270.0	209.0	210.0	272.0	106.0	273.0
Water velocity (m/s) :	1.61	1.61	1.62	1.61	1.61	1.61	1.60	1.61
Number of tubes fed :	6	6	3	6	6	3	3	3
Coil height (mm) :	457.0	457.0	229.0	457.0	457.0	229.0	229.0	229.0
Coil length (mm) :	760.0	760.0	760.0	760.0	760.0	760.0	760.0	760.0
Number of rows :	2	2	2	2	2	2	2	2
OUTPUT :								
Coil face area (sq.m) :	0.35	0.35	0.17	0.35	0.35	0.17	0.17	0.17
Standard air flow (lps) :	192.97	328.80	263.06	203.84	202.35	261.76	101.07	260.51
Std face velocity (m/s) :	0.56	0.95	1.51	0.59	0.58	1.50	0.58	1.50
Water flow (lps) :	1.69	1.69	0.85	1.69	1.69	0.84	0.84	0.84
Water temperature rise :	0.96	1.31	1.63	0.86	0.85	2.08	1.27	2.06
Ent enthalpy (kJ/kg) :	65.88	66.02	65.80	60.14	59.73	78.29	78.25	77.99
Lvg enthalpy (kJ/kg) :	36.64	42.58	47.47	35.25	35.06	54.95	41.41	54.66
Lvg dry bulb temp (°C) :	14.67	17.90	17.80	13.11	13.80	20.02	15.39	20.92
Lvg dew point temp (°C) :	11.79	13.49	16.30	11.92	11.31	18.83	14.32	18.27
Cooling capacity (kw) :	6.77	9.25	5.78	6.09	5.99	7.33	4.47	7.29

Results of TEST-P analysis

INPUT DATA :								
Title :	H66D:W5472	H66D:W5201	H66A:W6031	H60A:W5461	H60B:W5431	H78A:W5641	H78C:W6092	H78C:W5601
edb (°C) :	33.99	34.09	25.96	26.04	30.00	29.03	32.05	31.82
edp (°C) :	17.41	17.42	20.98	18.53	16.36	24.35	23.28	23.27
ldb (°C) :	14.65	17.46	17.59	13.33	13.85	19.72	15.76	20.32
ldp (°C) :	12.10	14.06	16.52	12.02	11.55	18.91	14.62	18.54
ewt (°C) :	6.98	6.98	6.99	6.99	7.00	7.04	6.94	7.00
lwt (°C) :	7.84	8.21	8.52	7.78	7.78	8.88	8.14	8.83
digistrip water (volts) :	2.780	2.790	1.400	2.780	2.790	1.390	1.380	1.390
digistrip air (volts) :	0.110	0.320	0.200	0.120	0.120	0.200	0.030	0.200
barometric pressure ("Hg) :	30.25	30.44	29.92	30.09	31.60	29.84	30.15	29.84
actual condensate (g/s) :	0.84	0.96	1.19	1.13	0.77	1.71	0.92	1.43
height of face (m) :	0.457	0.457	0.229	0.457	0.457	0.229	0.229	0.229
length of face (m) :	0.760	0.760	0.760	0.760	0.760	0.760	0.760	0.760
rows :	2	2	2	2	2	2	2	2
No. of tubes high :	12	12	6	12	12	6	6	6
No. of tubes fed :	6	6	3	6	6	3	3	3
OUTPUT :								
air volume flow (cms) :	0.203	0.346	0.270	0.209	0.210	0.272	0.106	0.273
air mass flow (kg/s) :	0.231	0.395	0.316	0.245	0.243	0.314	0.121	0.313
water flow rate (lps) :	1.69	1.69	0.85	1.69	1.69	0.84	0.84	0.84
entering enthalpy (kJ/kg) :	65.90	66.02	65.80	60.14	59.73	78.29	78.25	77.99
leaving enthalpy (kJ/kg) :	36.86	42.81	47.37	35.40	35.25	54.50	42.03	54.30
specific volume (m^3/kg) :	0.888	0.888	0.869	0.866	0.875	0.883	0.890	0.889
delta (H1 - H2) :	29.04	23.21	18.43	24.73	24.48	23.79	36.22	23.68
water side capacity (kw) :	6.068	8.710	5.437	5.574	5.524	6.492	4.203	6.456
air side capacity (kw) :	6.719	9.160	5.822	6.055	5.957	7.470	4.384	7.404
sensible heat factor :	0.68	0.73	0.46	0.53	0.67	0.40	0.46	0.50
ratio of water/air cap. :	0.90	0.95	0.93	0.92	0.93	0.87	0.96	0.87
est. condensate (g/kg) :	0.85	0.97	1.23	1.14	0.77	1.75	0.93	1.45
act/est condensate :	0.99	0.99	0.97	0.99	1.00	0.98	0.99	0.98
coil face area (sq.m) :	0.347	0.347	0.174	0.347	0.347	0.174	0.174	0.174
face velocity (m/s) :	0.58	1.00	1.55	0.60	0.61	1.56	0.61	1.57
water velocity (m/s) :	1.61	1.61	1.62	1.61	1.61	1.61	1.60	1.61
measured water temp.rise :	0.86	1.23	1.53	0.79	0.78	1.84	1.20	1.83
corrected water temp.rise :	0.95	1.29	1.64	0.86	0.84	2.12	1.25	2.10

Table A5.4a : Comparison of a two row coil performance predicted by "ARI GENERALISATION PROGRAM" with actual test results.

Results of AU (ADELAIDE UNIVERSITY)
coil selection program. Suitable for
1, 2 or 4 Row, 6 fpi, half circuiting.

INPUT DATA :								
Title :	H60B:W6451	H60C:W6511	W6681	W6671	W6613	W6611	W6672	W6661
ent dbt (°C) :	29.99	26.02	31.06	31.00	29.04	28.99	31.02	31.00
ent dpt (°C) :	16.48	18.34	18.78	18.70	19.75	19.68	18.90	18.73
ent water temp (°C) :	7.07	7.02	10.80	9.70	10.70	7.03	11.94	7.00
act air vol (cms) :	0.265	0.165	0.105	0.265	0.170	0.165	0.265	0.265
water flow (lps) :	1.69	1.69	0.85	0.85	0.849	0.85	0.85	0.85
coil height (m) :	0.457	0.457	0.229	0.229	0.229	0.229	0.229	0.229
coil length (m) :	0.373	0.373	0.746	0.746	0.746	0.746	0.746	0.746
rows :	4	4	4	4	4	4	4	4
no. of tubes high :	12	12	6	6	6	6	6	6
OUTPUT :								
face area (sq.m) :	0.17	0.17	0.17	0.17	0.17	0.17	0.17	0.17
actual fv (m/s) :	1.55	0.97	0.61	1.55	1.00	0.97	1.55	1.55
water vel (m/s) :	1.61	1.61	1.62	1.62	1.62	1.62	1.62	1.62
water temp rise :	1.13	0.81	1.01	2.14	1.49	1.82	1.82	2.53
ent enth (kJ/kg) :	59.95	59.70	65.83	65.59	65.97	65.76	66.06	65.66
lvg enth (kJ/kg) :	33.71	30.06	36.24	40.65	39.03	31.80	44.79	36.13
lvg dbt (°C) :	12.38	10.51	13.12	15.03	14.20	11.27	16.53	13.27
lvg dpt (°C) :	11.37	10.11	12.56	14.09	13.62	10.81	15.57	12.38
cooling cap (kw) :	8.04	5.73	3.58	7.61	5.30	6.49	6.49	9.01

Results of TEST-P analysis

INPUT DATA :								
Title :	H60B:W6451	H60C:W6511	W6681	W6671	W6613	W6611	W6672	W6661
edb (°C) :	29.99	26.02	31.06	31.00	29.04	28.99	31.02	31.00
edp (°C) :	16.48	18.34	18.78	18.70	19.75	19.68	18.90	18.73
ldb (°C) :	12.06	10.40	13.48	15.00	14.11	11.32	16.50	13.25
ldp (°C) :	11.89	10.32	12.49	14.28	13.26	10.39	15.76	12.51
ewt (°C) :	7.07	7.02	10.80	9.70	10.70	7.03	11.94	7.00
lwt (°C) :	7.88	7.53	11.89	11.93	12.26	8.99	13.85	9.66
digistrip water (volts) :	2.790	2.790	1.400	1.400	1.400	1.400	1.400	1.400
digistrip air (volts) :	0.190	0.074	0.030	0.190	0.078	0.074	0.190	0.190
barometric pressure ("Hg) :	29.92	30.02	30.13	30.21	30.00	29.98	30.13	30.15
actual condensate (g/s) :	1.00	1.09	0.54	1.03	0.90	1.21	0.78	1.36
height of face (m) :	0.457	0.457	0.457	0.457	0.457	0.457	0.457	0.457
length of face (m) :	0.373	0.373	0.373	0.373	0.373	0.373	0.373	0.373
rows :	4	4	4	4	4	4	4	4
No. of tubes high :	12	12	12	12	12	12	12	12
No. of tubes fed :	6	6	3	3	3	3	3	3
OUTPUT :								
air volume flow (cms) :	0.265	0.165	0.105	0.265	0.170	0.165	0.265	0.265
air mass flow (kg/s) :	0.306	0.193	0.121	0.306	0.196	0.191	0.305	0.306
water flow rate (lps) :	1.69	1.69	0.85	0.85	0.85	0.85	0.85	0.85
entering enthalpy (kJ/kg) :	59.95	59.70	65.83	65.59	65.97	65.76	66.06	65.66
leaving enthalpy (kJ/kg) :	33.92	30.05	36.26	40.68	38.10	31.07	44.82	36.06
specific volume (m^3/kg) :	0.875	0.866	0.881	0.880	0.876	0.876	0.881	0.880
delta (H1 - H2) :	26.03	29.66	29.57	24.92	27.88	34.68	21.24	29.60
water side capacity (kw) :	5.736	3.612	3.873	7.924	5.543	6.965	6.787	9.452
air side capacity (kw) :	7.970	5.718	3.590	7.612	5.473	6.634	6.488	9.044
sensible heat factor :	0.70	0.54	0.61	0.66	0.55	0.52	0.70	0.61
ratio of water/air cap. :	0.72	0.63	1.08	1.04	1.01	1.05	1.05	1.05
est. condensate (g/kg) :	0.94	1.05	0.56	1.03	0.98	1.26	0.77	1.38
act/est condensate :	1.07	1.04	0.97	1.00	0.92	0.96	1.02	0.98
coil face area (sq.m) :	0.170	0.170	0.170	0.170	0.170	0.170	0.170	0.170
face velocity (m/s) :	1.55	0.97	0.62	1.56	0.99	0.97	1.56	1.56
water velocity (m/s) :	1.61	1.61	1.62	1.62	1.62	1.62	1.62	1.62
measured water temp.rise :	0.81	0.51	1.09	2.23	1.56	1.96	1.91	2.66
corrected water temp.rise :	1.13	0.81	1.01	2.14	1.54	1.87	1.83	2.55

Table A5.5 : Comparison of a four row coil performance predicted by "AU COIL SELECTION PROGRAM" with actual test results.

Results of ARI generalisation program. Suitable for 1, 2 or 4 Row, 6FPI, half circuiting.

INPUT :								
TEST CODE :	H60B:W6451	H60C:W6511	W6681	W6671	W6613	W6611	W6672	W6661
Ent dry bulb temp (°C) :	30.00	26.02	31.06	31.00	29.04	29.00	31.02	31.00
Ent dew point temp (°C) :	16.50	18.34	18.78	18.70	19.75	19.68	18.90	18.73
Ent water temp (°C) :	7.07	7.02	10.80	9.70	10.70	7.03	11.94	7.00
Actual air flow (lps) :	265.0	165.0	105.0	265.0	170.0	165.0	265.0	265.0
Water velocity (m/s) :	1.61	1.61	1.62	1.62	1.62	1.62	1.62	1.62
Number of tubes fed :	6	6	3	3	3	3	3	3
Coil height (mm) :	457.0	457.0	457.0	457.0	457.0	457.0	457.0	457.0
Coil length (mm) :	373.0	373.0	373.0	373.0	373.0	373.0	373.0	373.0
Number of rows :	4	4	4	4	4	4	4	4
OUTPUT :								
Coil face area (sq.m) :	0.17	0.17	0.17	0.17	0.17	0.17	0.17	0.17
Standard air flow (lps) :	255.33	160.96	100.71	254.23	164.06	159.26	254.18	254.22
Std face velocity (m/s) :	1.50	0.94	0.59	1.49	0.96	0.93	1.49	1.49
Water flow (lps) :	1.69	1.69	0.85	0.85	0.85	0.85	0.85	0.85
Water temperature rise :	1.14	0.81	1.01	2.15	1.50	1.83	1.84	2.54
Ent enthalpy (kJ/kg) :	60.00	59.70	65.83	65.59	65.97	65.77	66.06	65.66
Lvg enthalpy (kJ/kg) :	33.69	30.03	36.07	40.52	38.90	31.73	44.63	36.04
Lvg dry bulb temp (°C) :	12.49	10.53	13.11	15.11	14.21	11.29	16.60	13.35
Lvg dew point temp (°C) :	11.27	10.07	12.45	13.96	13.54	10.75	15.44	12.28
Cooling capacity (kw) :	8.06	5.73	3.6	7.65	5.33	6.51	6.54	9.04

Results of TEST-P analysis

INPUT DATA :								
Title :	H60B:W6451	H60C:W6511	W6681	W6671	W6613	W6611	W6672	W6661
edb (°C) :	29.99	26.02	31.06	31.00	29.04	28.99	31.02	31.00
edp (°C) :	16.48	18.34	18.78	18.70	19.75	19.68	18.90	18.73
ldb (°C) :	12.06	10.40	13.48	15.00	14.11	11.32	16.50	13.25
ldp (°C) :	11.89	10.32	12.49	14.28	13.26	10.39	15.76	12.51
ewt (°C) :	7.07	7.02	10.80	9.70	10.70	7.03	11.94	7.00
lwt (°C) :	7.88	7.53	11.89	11.93	12.26	8.99	13.85	9.66
digistrip water (volts) :	2.790	2.790	1.400	1.400	1.400	1.400	1.400	1.400
digistrip air (volts) :	0.190	0.074	0.030	0.190	0.078	0.074	0.190	0.190
barometric pressure ("Hg) :	29.92	30.02	30.13	30.21	30.00	29.98	30.13	30.15
actual condensate (g/s) :	1.00	1.09	0.54	1.03	0.90	1.21	0.78	1.36
height of face (m) :	0.457	0.457	0.457	0.457	0.457	0.457	0.457	0.457
length of face (m) :	0.373	0.373	0.373	0.373	0.373	0.373	0.373	0.373
rows :	4	4	4	4	4	4	4	4
No. of tubes high :	12	12	12	12	12	12	12	12
No. of tubes fed :	6	6	3	3	3	3	3	3
OUTPUT :								
air volume flow (cms) :	0.265	0.165	0.105	0.265	0.170	0.165	0.265	0.265
air mass flow (kg/s) :	0.306	0.193	0.121	0.306	0.196	0.191	0.305	0.306
water flow rate (lps) :	1.69	1.69	0.85	0.85	0.85	0.85	0.85	0.85
entering enthalpy (kJ/kg) :	59.95	59.70	65.83	65.59	65.97	65.76	66.06	65.66
leaving enthalpy (kJ/kg) :	33.92	30.05	36.26	40.68	38.10	31.07	44.82	36.06
specific volume (m^3/kg) :	0.875	0.866	0.881	0.880	0.876	0.876	0.881	0.880
delta (H1 - H2) :	26.03	29.66	29.57	24.92	27.88	34.68	21.24	29.60
water side capacity (kw) :	5.736	3.612	3.873	7.924	5.543	6.965	6.787	9.452
air side capacity (kw) :	7.970	5.718	3.590	7.612	5.473	6.634	6.488	9.044
sensible heat factor :	0.70	0.54	0.61	0.66	0.55	0.52	0.70	0.61
ratio of water/air cap. :	0.72	0.63	1.08	1.04	1.01	1.05	1.05	1.05
est. condensate (g/kg) :	0.94	1.05	0.56	1.03	0.98	1.26	0.77	1.38
act/est condensate :	1.07	1.04	0.97	1.00	0.92	0.96	1.02	0.98
coil face area (sq.m) :	0.170	0.170	0.170	0.170	0.170	0.170	0.170	0.170
face velocity (m/s) :	1.55	0.97	0.62	1.56	0.99	0.97	1.56	1.56
water velocity (m/s) :	1.61	1.61	1.62	1.62	1.62	1.62	1.62	1.62
measured water temp.rise :	0.81	0.51	1.09	2.23	1.56	1.96	1.91	2.66
corrected water temp.rise :	1.13	0.81	1.01	2.14	1.54	1.87	1.83	2.55

Table A5.5a : Comparison of a four row coil performance predicted by "ARI GENERALISATION PROGRAM" with actual test results.

REFERENCES

Anne-Katrin Schroeder-Lanz (1989) : *Investigation of the heat transfer coefficient of the condensate layer on dehumidifying coils.* A report. Department of Mechanical Engineering, The University of Adelaide.

ARI Standard 410 (1981) : *Standard for forced-circulation air-cooling and air-heating coils.* Air Conditioning and Refrigeration Institute, American National Standard.

ASHRAE (1985) : *Handbook of fundamentals.* American Society of Heating, Refrigerating, and Air Conditioning Engineers, Inc., Atlanta, Georgia.

ASHRAE Standard 33 (1978) : *Methods of testing forced-circulation air-cooling and air-heating coils.* American Society of Heating, Refrigerating, and Air Conditioning Engineers, Inc., Atlanta, Georgia.

ASHRAE Standard 55 (1981) : *Thermal environmental conditions for human occupancy.* American Society of Heating, Refrigerating, and Air Conditioning Engineers, Inc., Atlanta, Georgia.

Brown, Gosta (1954) : *Theory of moist air heat exchangers.* Trans. Royal Institute of Technology, Stockholm, Sweden, Number 77.

Carrier W.H. and Anderson S.W. (1944) : *The resistance to heat flow through finned tubing.* Heating, Piping and Air Conditioning - ASHVE Journal Section, Page 304.

Custer J.B. (1988) : *The economics and marketing of tenant comfort.* The Australian Institute of Refrigeration, Air Conditioning and Heating, AIRAHFAIR-88, Sydney.

Fanger P.O. (1973) : *Thermal comfort.* McGraw - Hill Book Company, New York.

Gardner K.A. (1945) : *Efficiency of extended surface.* ASME Transactions, Vol. 67.

Gilbert G.P. (1987) : *Flow through a model fin and tube heat exchanger and its influence on mass and heat transfer.* Thesis for the degree of Master of Engineering Science, The University of Adelaide.

Goodman W. (1938-39) : *Performance of coils for dehumidifying air.* Heating, Piping and Air Conditioning, Vol.10 and 11.

Gunter A.Y. and Shaw W.A. (1945) : *A general correlation of friction factors for various types of surfaces in crossflow.* ASME Transactions, Vol. 67.

Gupta V.K., Int-Out D., Roberts M.M., Wessel D.J., Brickman H. and Waeldner W. (1987) : *A forum on variable air volume.* ASHRAE Journal, Volume 29, No.8.

Kays W.M. and London A.L. (1984) : *Compact heat exchangers.* 3rd Edition, McGraw-Hill Inc., New York.

Kern D.Q. and Kraus A.D. (1972) : *Extended surface heat transfer.* McGraw-Hill Inc., New York

Kays W.M. and London A.L. (1950) : *Heat transfer and flow friction characteristics of some compact heat exchanger surfaces.* ASME Transactions.

Kusuda T. (1957) : *Graphical method simplifies determination of air coil wet surface temperature.* Refrigerating Engineering.

Lewis W.K. (1922) : *The evaporation of a liquid into a gas.* Transactions of the American Society of Mechanical Engineers, Volume 44, Page 325.

Luxton R.E., Brown M.R. and Shaw A. (1987) : *An assessment of achievable air conditioning energy.* Proceedings of Fourth ASEAN energy Conference - Energy Technology, Singapore.

Luxton R.E., Shaw A. and Sekhar S.C. (1989) : *Specification and achievement of part load conditions for air-conditioning systems with minimum energy penalty.* Proceedings of CLIMA 2000, Second World Congress on Heating, Ventilating, Refrigerating and Air Conditioning, Sarajevo, Yugoslavia, Vol. III, pp 333 - 338.

McAdams W.H. (1954) : *Heat Transmission.* 3rd Edition.

McElgin J. and Wiley D.C. (1940) : *Calculation of coil surface areas for air cooling and dehumidification.* Heating, Piping and Air Conditioning, Page 195.

McQuiston F.C. (1976) : *Heat, mass and momentum transfer in a parallel plate dehumidifying exchanger.* ASHRAE Transactions, Vol. 82, Part 2.

Myers R.J. (1967) : *The effect of dehumidification on the air side heat transfer coefficient for a finned-tube coil.* Master's Thesis, University of Minnesota.

O'Bara J.T., Killian E.S. and Roblee Jr L.H.S. (1967) : *Dropwise condensation of steam at atmospheric and above atmospheric pressures.* Chemical Engineering Science, Vol. 22, pp. 1305 - 1314.

Rose J.W. (1976) : *Further aspects of dropwise condensation theory.* Int. Journal of Heat Mass Transfer, Vol. 19, pp. 1363 - 1370.

Sekhar S.C. (1987) : *Investigation of gross heat and mass transfer coefficients in cooling coils at low air face velocities.* An interim report. Department of Mechanical Engineering, The University of Adelaide.

Sekhar S.C., Shaw A. and Luxton R.E. (1987) : *A unique testing facility for the investigation of heat and mass transfer coefficients.* Proceedings of the Indian Chemical Engineering Congress, Sindri, India.

Sekhar S.C., Luxton R.E. and Shaw A. (1988) : *Some problems in the rating of cooling coils - ARI Standard 410 revisited.* Proceedings of the International Congress of International Institute of Refrigeration, Brisbane.

Sekhar S.C., Luxton R.E. and Shaw A. (1989) : *Design methodology for cost-effective air conditioning in humid climates.* Proceedings of ASHRAE Far East Conference on Air Conditioning in Hot Climates, Kuala Lumpur, Malaysia, pp 57 - 65.

Shaw A. (1979a) : *A unified approach to the design of climate simulators.* Ph.D. Thesis, University of Adelaide.

Shaw A. and The University of Adelaide (1979b) : *Method of air conditioning.* Patent No.49875/79 (Commonwealth of Australia).

Shaw A. (1982a) : *Exploration of air velocity across air conditioning system dehumidifiers - an energy conservation project.* ASHRAE Transactions, 88, Part 2.

Shaw A. (1982b) : *Airstream velocity across dehumidifiers.* Proceedings of seventh international heat transfer conference. Munich, F.D.R.

Shaw A. and Luxton R.E. (1985) : *Latest findings on airstream velocity effects in heat and mass transfer through dehumidifier coils.* Proceedings of Third Australasian Conference on Heat and Mass Transfer, Melbourne University.

Shaw A., Luxton R.E. and Harrland P. (1987) : *High quality tropical air conditioning with low energy consumption.* Proceedings of ASHRAE Far East Conference on Air Conditioning in hot climates, Singapore.

Shaw A. and Luxton R.E. (1988a) : *A comprehensive method of improving part-load air conditioning performance.* ASHRAE Transactions, Vol 94, Part1.

Shaw A. and Luxton R.E. (1988b) : *An over-view of low face velocity air conditioning.* Australian Refrigeration, Air Conditioning and Heating (AIRAH) Journal.

Shaw A and Luxton R.E. (1989) : *Comfort integration and energy efficient method of air conditioning.* Commonwealth of Australia Provisional Patent Application No.PJ6035, Filed 30th August 1989.

Stoecker W.F. and Jones J.W. (1982) : *Refrigeration and Air Conditioning.* 2nd Edition, McGraw-Hill Book Co., Singapore.

Threlkeld J.L. (1970) : *Thermal Environmental Engineering.* 2nd Edition, Prentice-Hall Inc., New Jersey.

Trane (1977) : *Application and selection data for Trane cooling and heating coils.* The Trane Company, La Crosse, Wisconsin.

Tree D.R. and Helmer W.A. (1976) : *Experimental heat and mass transfer data for condensing flow in a parallel plate heat exchanger.* ASHRAE Transactions, Vol. 82, Part 1.

Ware C.D. and Hacha T.H. (1960) : *Heat transfer from humid air to fin and tube extended surface cooling coils.* ASME Paper No. 60-HT-17.

Wooldridge M.J. (1979) : *Simultaneous dry bulb and wet bulb temperature data for 14 Australian locations.* Technical report No. TR22, CSIRO Division of Mechanical Engineering.